Entwicklung und Anwendung von Methoden zur metabolischen Phänotypisierung von Formalin-fixiertem, Paraffin-eingebettetem Gewebe und Tumor-Organoiden

Dissertation

der Mathematisch-Naturwissenschaftlichen Fakultät
der Eberhard Karls Universität Tübingen
zur Erlangung des Grades eines
Doktors der Naturwissenschaften
(Dr. rer. nat.)

vorgelegt von
Diplom-Lebensmittelchemikerin Sylvia Karin Neef
aus Esslingen am Neckar

Tübingen
2021

Gedruckt mit Genehmigung der Mathematisch-Naturwissenschaftlichen Fakultät der Eberhard Karls Universität Tübingen.

Tag der mündlichen Qualifikation:	12.05.2021
Dekan:	Prof. Dr. Thilo Stehle
1. Berichterstatter:	Prof. Dr. Matthias Schwab
2. Berichterstatter:	Prof. Dr. Michael Lämmerhofer

Inhaltsverzeichnis

Abkürzungen

5-FU	5-Fluorouracil
AC	Acylcarnitin
ACN	Acetonitril
AS	Aminosäure
ASC	Adulte Stammzelle (engl.: *adult stem cell*)
CapLC	Kapillar-Flüssigkeitschromatographie (engl.: *capillary liquid chromatography*)
ccRCC	Klarzelliges Nierenzellkarzinom (engl.: *clear cell renal cell carcinoma*)
Cer	Ceramid
CF	Mukoviszidose (engl.: *cystic fibrosis*)
CRC	Kolorektales Karzinom (engl.: *colorectal cancer*)
CV	Variationskoeffizient (engl.: *coefficient of variation*)
DNA	Desoxyribonukleinsäure (engl.: *desoxyribonucleic acid*)
ECM	Extrazelluläre Matrix
EIC	Extrahiertes Ionenchromatogramm (engl.: *extracted ion chromatogram*)
ESI	Elektrosprayionisation
et al.	und andere (lat.: *et alii)*
FC	Quotient (engl.: *fold change*)
FDA	US-Behörde für Lebens- und Arzneimittel (engl.: *U.S. food and drug administration*)
FF	(Frisch) gefroren (engl.: *fresh frozen*)
FFPE	Formalin-fixiert und Paraffin-eingebettet
GC	Gaschromatographie
GCA	Glycocholsäure (engl.: glycocholic acid)
GLCA	Taurocholsäure (engl.: *glycolithocholic acid*)
GSL	Glycosphingolipid
HER2	Humaner epidermaler Wachstumsfaktor-Rezeptor Typ 2 (engl.: *human epidermal growth factor receptor 2*)
HexCer	Hexosylceramid

HILIC	Hydrophile Interaktionschromatographie (engl.: *hydrophilic interaction liquid chromatography*)
HPLC	Hochleistungsflüssigkeitschromatographie (engl.: *high performance liquid chromatography*)
i.D.	Innendurchmesser (engl.: *inner diameter*)
IPA	Isopropanol
LC	Flüssigkeitschromatographie *(engl.: liquid chromatography*)
LoA	Niveau der Zuordnung (engl.: *level of assignement*)
MALDI-FT-ICR MS	Matrix-unterstützte Laser-Desorption/Ionisation Fourier-Transform Ionenzyklotronresonanz Massenspektrometrie (engl.: *Matrix-assisted laser desorption/ionization Fourier transform ion cyclotron resonance mass spectrometry*)
MeOH	Methanol
mRNA	Boten-Ribonukleinsäure (engl.: *messenger ribonucleic acid*)
MS	Massenspektrometrie
MS/MS	Tandem-Massenspektrometrie
MSI	Initiative zur Standardisierung im Bereich Metabolomics (engl.: *Metabolomics Standard Initiative*)
MTBE	Methyl-tert-butylether
na	Nicht zugeordnet (engl.: *not assigned*)
NMe	N-methyliert (am Stickstoffmolekül methyliert)
NMR	Kernspinresonanz (engl.: *nuclear magnetic resonance*)
PBS	Phosphatgepufferte Salzlösung (engl.: *phosphate buffered saline*)
PC	Phosphocholin
PCA	Hauptkomponentenanalyse (engl.: *principal component analysis*)
PE	Phosphatidylethanolamin
PI	Phosphatidylinositol
PS	Phosphatidylserin
PSC	Pluripotente Stammzelle (engl.: *pluripotent stem cell*)
QC	Qualitätskontrolle (engl.: *quality control)*
QTOF-MS	Quadrupol-Flugzeit-Massenspektrometer (engl.: *quadrupole time-of-flight mass spectrometer*)

RPLC	Umkehrphasen-Chromatographie (engl.: *reversed-phase liquid chromatography*)
RT	Retentionszeit (engl.: *retention time*)
S/N	Signal/Rausch-Verhältnis (engl.: *signal/noise ratio*)
SM	Sphingomyelin
TAG	Triglycerid (engl.: *triacylglycerol*)
TCA	Glycolithocholsäure (engl.: *taurocholic acid*)
TIC	Gesamtionenchromatogramm (engl.: *total ion chromatogram*)
TLCA	Taurolithocholsäure (engl.: *taurolithocholic acid*)
TMA	Gewebemikroarrays (engl.: *tissue microarray*)

Formelzeichen und Symbole

m/z	Masse-zu-Ladungs-Verhältnis; hier dimensionslos verwendet
n	Anzahl der (unabhängig) durchgeführten Experimente
r_S	Spearman-Korrelationskoeffizient
t_R	Retentionszeit [min]
V	Volumen [L]

Zusammenfassung

Metabolomics ist die möglichst umfassende Analyse der Stoffwechsel-Intermediate (Metaboliten) eines biologischen Systems. In der klinisch-pharmakologischen Forschung wird dieser innovative Ansatz zunehmend genutzt, um Erkenntnisse über die Pathophysiologie komplexer Erkrankungen zu erlangen und mögliche Therapiewege zu finden.

Da sich die meisten Krebszellen durch charakteristische Stoffwechselveränderungen auszeichnen, stellt Metabolomics auch in der Erforschung von Tumorerkrankungen ein vielversprechendes Mittel zur Identifizierung potenzieller Biomarker und therapeutischer Targets dar. In diesem Zusammenhang gewinnt besonders der nicht zielgerichtete Ansatz „*non-targeted* Metabolomics“ an Bedeutung. Dieser zielt darauf ab, mit einer einzelnen Analyse den Stoffwechselzustand der untersuchten Matrix komplett zu erfassen und eignet sich daher besonders zur Generierung neuer Hypothesen. Hierfür wurden im Rahmen der vorliegenden Arbeit Methoden zur Extraktion und Analyse des Metaboloms und Lipidoms aus (I.) Formalin-fixiertem Paraffin-eingebettetem (FFPE) Gewebe und (II.) Tumor-Organoiden des kolorektalen Karzinoms entwickelt. Die analytische Messung der Extrakte erfolgte mittels Flüssigchromatographie-Quadrupol-Flugzeitmassenspektrometrie (LC-QTOF-MS) und die erarbeiteten Extraktionsmethoden wurden hinsichtlich der Signalintensität sowie der analytischen und methodischen Präzision und der Wiederholbarkeit optimiert und validiert. Des Weiteren (III.) erfolgte die vorläufige Evaluierung eines Mikrofluss-Chromatographie-Systems, betrieben mit Kapillarchromatographie Flussraten (< 10 µL/min) und Säulendimensionen (< 500 µm), hinsichtlich seiner Leistungsfähigkeit für *non-targeted* Metabolomics-Analysen. Hierfür wurde die analytische Präzision, die Anzahl detektierbarer Signale sowie das Signal-Rausch-Verhältnis und die Signalintensität von 16 annotierten Metaboliten in Extrakten von FFPE Schweinenierengewebe bewertet.

I. Die Herstellung von FFPE Gewebe zur Konservierung und anschließenden histopathologischen Untersuchung ist ein Standardprozess in der klinischen Diagnostik. FFPE Gewebeproben werden weltweit in Archiven gelagert und stellen eine wertvolle Ressource für retrospektive Studien dar. Die wenigen bislang etablierten Protokolle zur Analyse des Metaboloms von FFPE Gewebe sind vor allem auf das Erfassen polarer Metaboliten ausgerichtet, während

Lipide nicht im Fokus stehen. In der vorliegenden Arbeit wurde über einen umfangreichen Methodenvergleich ein optimiertes Extraktionsprotokoll zur Analyse des Metaboloms und Lipidoms von FFPE Nierengewebe etabliert. Das Protokoll wurde auf der Basis von strukturell annotierten Metaboliten validiert und seine Anwendbarkeit durch die Unterscheidung von FFPE Proben des klarzelligen Nierenzellkarzinoms (ccRCC) von korrespondierendem Normalgewebe, auf Grundlage differenzieller Metaboliten-Profile, demonstriert. Des Weiteren wurde das Protokoll eingesetzt, um den Einfluss der Fixierzeit (Verweildauer des Gewebes in Formalin) auf die Metabolitenprofile in FFPE Gewebe zu untersuchen. Hierbei konnten Metaboliten identifiziert werden, deren Signale durch die Fixierzeit nicht beeinflusst wurden. Um deren Eignung für weiterführende Experimente zu prüfen, erfolgte die Detektion ausgewählter Metaboliten über bildgebende Matrix-unterstützte Laser-Desorption/Ionisation Fourier-Transform Ionenzyklotronresonanz Massenspektrometrie in einer unabhängigen ccRCC Kohorte.

II. Organoide sind innovative 3D Organmodelle, die *in vitro* aus Stammzellen generiert werden und die die Komplexität und Funktionalität eines Organs wesentlich präziser widerspiegeln als herkömmliche 2D Zellkulturen. Durch die Möglichkeit aus Tumorbiopsien Organoide zu kultivieren, deren genetisches Profil dem Ausgangsgewebe weitgehend entspricht, spielt diese Zellkulturtechnik mittlerweile eine zentrale Rolle in der personalisierten Medizin und im Medikamentenscreening. In der vorliegenden Arbeit wurden Extraktionsprotokolle zur Charakterisierung des Metaboloms von in extrazellulärer Matrix (ECM) kultivierten Organoiden des kolorektalen Karzinoms (CRC) mittels *non-targeted* LC-QTOF-MS evaluiert. Zur präzisen Normalisierung und statistischen Analyse wurde ein Filterprozess zum Entfernen von Hintergrundsignalen eingeführt, der auf statistischer Signifikanz (*p*-Wert, Welch's Test) und *fold change*-Grenzwerten (biologisches Signal/ECM Blanksignal) beruht. Die optimierte Methode wurde durch die Analyse der dosisabhängigen metabolischen Antwort von CRC Organoiden auf die Behandlung mit 5-Fluorouracil (5-FU), über drei unabhängige Experimente hinweg, auf ihre Wiederholbarkeit validiert. In Übereinstimmung mit dem Wirkungsmechanismus von 5-FU wurden wiederholt signifikante metabolische Veränderungen detektiert (erhöhte Spiegel an 2'-Deoxyuridin, 2'-O-

Methylcytidin, Inosin und 1-Methyladenosin sowie eine Verminderung von 2'-Deoxyadenosin und bestimmten Phospholipid-Spezies), was die Qualität der etablierten Methode demonstriert und den Weg zur Anwendung in größer angelegten Studien ebnet.

III. *Non-targeted* Metabolomics-Untersuchungen zur Findung diagnostischer oder prognostischer Biomarker basieren häufig auf Proben, die nur in limitierter Menge vorhanden sind (z.B. Biopsien oder Metastasen). Da die Empfindlichkeit der massenspektrometrischen Detektion durch eine Reduzierung des Säuleninnendurchmessers und durch den Einsatz niedriger Flussraten erheblich gesteigert werden kann, empfiehlt sich die Nutzung von Nano- und Mikrofluss-LC-Systemen zur Untersuchung seltener klinischer Proben. In der vorliegenden Arbeit wurde eine vorläufige Evaluierung des Zirconium™ Ultra Nano- und Micro-UHPLC Systems (Prolab), betrieben im Kapillarchromatographie Modus (CapLC, Flussrate: 5 µL/min, Säuleninnendurchmesser: 0,3 mm), in Kombination mit einem Zirconium™ CUBE Autosampler (Prolab) und einem speziellen Micro-ESI-Interface Prototypen (Prolab) durchgeführt. Die Ergebnisse wurden mit einer im Haus etablierten Plattform für *non-targeted* Metabolomics-Analysen, welche auf analytischen Flussraten (400 µL/min) und Säulendimensionen (2.1 mm, sogenannte *narrow bore* LC) basiert, verglichen. Im Hinblick auf die Anzahl der detektierten Signale (*Features*) konnte hierbei kein nennenswerter Unterschied zwischen den Systemen beobachtet werden. Während bei den Signalflächen unter Verwendung der CapLC eine Verbesserung bei allen 16 Metaboliten festgestellt wurde, war das Signal-Rausch-Verhältnis für nur 50 % der Metaboliten verbessert. Darüber hinaus war die analytische Präzision unter Verwendung des CapLC-Systems (median CV = 11,8 %), verglichen mit dem *narrow-bore* LC-System (median CV = 2,9 %), geringer. Ein unabhängiges Experiment, durchgeführt mit Gallensäure-Referenzsubstanzen (ohne biologische Matrix), ergab jedoch eine bis zu 80-fache Erhöhung der Peakfläche (für Taurocholsäure) und eine zufriedenstellende Messpräzision. Die Ergebnisse des Plattformvergleichs deuten darauf hin, dass die beobachteten Effekte von der Art der analysierten Metaboliten abhängig sind. In diesem Kontext sind weitere Versuche nötig um zu überprüfen, ob die sehr guten

Ergebnisse für Gallensäure-Reinsubstanzen in biologischer Matrix reproduziert werden können und ob die getestete CapLC-Plattform unter Umständen besser für spezielle *targeted* Metabolomics-Ansätze geeignet ist, als für *non-targeted* Metabolomics seltener klinischer Proben.

Abstract

Metabolomics is the comprehensive analysis of the metabolic intermediates (metabolites) in a biological system and an innovative approach in clinical and pharmaceutical research. As most tumor cells are characterized by specific metabolic reprogramming, metabolomics is a promising tool for the identification of potential biomarkers and therapeutic targets. In this context, non-targeted metabolomics is gaining increasing importance in cancer research.

Within the scope of the present work, extraction methods for non-targeted metabolomic and lipidomic profiling via liquid chromatography quadrupole time-of-flight mass spectrometry (LC-QTOF-MS) from (I.) formalin-fixed paraffin-embedded (FFPE) tissue and (II.) organoids have been established. The extraction methods developed have been optimized and validated in terms of signal intensity as well as analytical and methodical precision and repeatability. Further (III.) a preliminary evaluation of the performance of a new microfluidic chromatography system for non-targeted metabolic profiling by LC-QTOF-MS was carried out, using flow rates (<10 µL/min) and column dimensions (<500 µm) in the capillary liquid chromatography (CapLC) range. The quality of analysis was assessed based on the number of detectable features as well as the analytical repeatability, the signal intensity and the signal-to-noise ratio of 16 annotated metabolites in extracts from porcine FFPE kidney tissue.

I. The preparation of FFPE tissue for preservation and subsequent histopathological examination is a standard format in clinical diagnostics. The fixed and embedded samples are stored in archives worldwide and represent a valuable resource for retrospective studies. With respect to mass spectrometry based metabolomics, only a limited number of protocols for FFPE tissue are currently available with most of them focusing on the profiling of small, polar molecules while lipids have been considered only scarcely. In the present study, an optimized extraction protocol for metabolomics and lipidomics from clinical FFPE kidney tissue was established. The protocol was validated on the basis of annotated metabolites and its applicability was demonstrated by differentiating FFPE samples of clear cell renal cell carcinoma (ccRCC) from corresponding normal tissue, based on differential metabolite profiles. Furthermore, the protocol was used to investigate the influence of formalin fixation time on metabolite profiles in FFPE tissue. Thereby metabolites were identified whose

signals were not influenced by the fixation time. In order to validate their suitability for further experiments, selected metabolites were detected by matrix-assisted laser desorption/ionization Fourier transform ion cyclotron resonance mass spectrometry imaging in an independent ccRCC cohort.

II. Organoids are innovative stem cell derived 3D organ models and reflect the complexity of an organ more precisely than conventional 2D cell cultures. Since the genetic profile of organoids grown from tumor biopsies corresponds to the genetic profile of the original tissue, this cell culture technology now plays a central role in personalized medicine and drug screening. In the present work, extraction protocols for the metabolic characterization of colorectal carcinoma (CRC) organoids cultivated in extracellular matrix (ECM) by non-targeted LC-QTOF-MS were evaluated. For precise normalization and statistical analysis, a filter procedure to remove background signal, based on *p*-value (Welch's test) and fold change cut-offs (biological signal/ECM blank signal), was introduced. The optimized method was validated for repeatability by analyzing the dose-dependent metabolic response of CRC organoids to treatment with 5-fluorouracil (5-FU) over three independent experiments. In accordance with the mechanism of action of 5-FU, highly specific metabolic changes were repeatedly detected (elevated levels of 2'-deoxyuridine, 2'-O-methylcytidine, inosine and 1-methyladenosine and depletion of 2'-deoxyadenosine and specific phospholipids), demonstrating the quality of the established method and paving the way for further application in larger studies.

III. Non-targeted metabolomics investigations often rely on samples that are available in limited quantities (e.g. metastases or biopsies). Since the sensitivity of MS detection can be significantly increased by reducing the column inner diameter and flow rates, the use of microfluidic systems is recommended for the investigation of rare clinical samples. In the present work, a preliminary evaluation of the Zirconium™ Ultra Nano- and Micro-UHPLC system (Prolab), operated in capillary chromatography mode (CapLC, flow rate: 5 µL/min, column inner diameter: 0.3 mm), in combination with a Zirconium™ CUBE autosampler (Prolab) and a customized micro-ESI interface prototype (Prolab), was performed. The results were compared with a well established LC system that is based on an analytical flow rate (400 µL/min) and column inner diameter (2.1 mm, ≙ narrow-*bore* LC). No meaningful difference in the number of

detected features could be observed between the systems when injecting the same sample volume (1 µL). Further, while the signal area of all evaluated metabolites was increased by using CapLC, the signal-to-noise ratio was only improved in 50 % of the metabolites. In addition, the analytical repeatability (median CV = 11.8%) was poor for the CapLC system compared to narrow-bore LC (median CV = 2.9%) when FFPE tissue extracts were analyzed. In contrast, significantly better reproducibility (median CV = 5.2%) and up to 80-fold increase in signal intensity were observed in independent experiments when pure bile acid standard solutions were analyzed. The results further suggest that the observed effects are dependent on the type of metabolites analyzed. Even if the observed improvement for specific bile acids must be evaluated in biological matrix, the platform comparison indicate, that the tested CapLC system is more suitable for specific targeted analyses than for non-targeted metabolomics of rare clinical samples.

Liste der Publikationen der Dissertation

Akzeptierte Publikation 1:

Optimized protocol for metabolomic and lipidomic profiling in formalin-fixed paraffin-embedded kidney tissue by LC-MS

Sylvia K. Neef [a], Stefan Winter [a], Ute Hofmann [a], Thomas E. Muerdter [a], Elke Schaeffeler [a,g], Heike Horn [a], Achim Buck [d], Axel Walch [d], Jörg Hennenlotter [e], German Ott [a,b], Falko Fend [e,f], Jens Bedke [e], Matthias Schwab[a,c,g] and Mathias Haag[a,*]

[a] *Dr. Margarete Fischer-Bosch-Institute of Clinical Pharmacology, Stuttgart, Germany and University of Tübingen, Tübingen, Germany*
[b] *Department of Clinical Pathology, Robert-Bosch Hospital, Stuttgart, Germany*
[c] *Departments of Clinical Pharmacology, Pharmacy and Biochemistry University Tübingen, Tübingen, Germany*
[d] *Research Unit Analytical Pathology, Helmholtz Zentrum München, Neuherberg, Germany*
[e] *Department of Urology, University Hospital Tübingen, Tübingen, Germany*
[f] *Institute of Pathology and Neuropathology, University Hospital Tübingen, Tübingen, Germany*
[g] *iFIT Cluster of Excellence (EXC2180) "Image Guided and Functionally Instructed Tumor Therapies", University of Tübingen, Tübingen, Germany*

Analytica Chimica Acta **2020**,1134, 125–135; doi: 10.1016/j.aca.2020.08.005

Akzeptierte Publikation 2:

Metabolic Drug Response Phenotyping in Colorectal Cancer Organoids by LC-QTOF-MS

Sylvia K. Neef [1,#], Nicole Janssen [1,#], Stefan Winter [1], Svenja K. Wallisch [1], Ute Hofmann [1], Marc H. Dahlke [1,2], Matthias Schwab [1,3,4], Thomas E. Mürdter [1,#] and Mathias Haag [1,#]

[1] *Dr. Margarete Fischer-Bosch-Institute of Clinical Pharmacology, Stuttgart, Germany and University of Tuebingen, Tuebingen, Germany*
[2] *Department of Surgery, Robert-Bosch Hospital, Stuttgart, Germany*
[3] *Departments of Clinical Pharmacology, and of Pharmacy and Biochemistry, University of Tuebingen, Tuebingen, Germany*
[4] *Cluster of Excellence iFIT (EXC 2180) „Image-Guided and Functionally Instructed Tumor Therapies", University of Tuebingen, Germany*
[#] *contributed equally*

Metabolites **2020**, 10, 494; doi: 10.3390/metabo10120494

Manuskript in Vorbereitung:

Performance comparison of narrow-bore and capillary liquid-chromatography for non-targeted metabolomics profiling of small sample amounts by LC-QTOF-MS

Sylvia K. Neef [1], Stefan Winter [1], Ute Hofmann [1], Thomas E. Mürdter [1], Matthias Schwab [1,2,3] and Mathias Haag [1]

[1] *Dr. Margarete Fischer-Bosch-Institute of Clinical Pharmacology, Stuttgart, Germany and University of Tuebingen, Tuebingen, Germany*
[2] *Departments of Clinical Pharmacology, and of Pharmacy and Biochemistry, University of Tuebingen, Tuebingen, Germany*
[3] *Cluster of Excellence iFIT (EXC 2180) „Image-Guided and Functionally Instructed Tumor Therapies“, University of Tuebingen, Germany*

Eigenanteil

Akzeptierte Publikation 1:

Die Erstautorin **Sylvia Karin Neef** hat die beschriebenen Versuche sowie die getesteten Methoden weitgehend eigenständig geplant und alle im Artikel beschriebenen LC-QTOF-MS-basierten Experimente selbstständig durchgeführt. Die Ergebnisse wurden von ihr unter Anwendung statistischer Techniken und Programme ausgewertet, interpretiert und visualisiert. Die Erstellung des veröffentlichten Werkes, insbesondere das Verfassen und Korrigieren des ursprünglichen Entwurfs, erfolgte durch die Erstautorin und **Mathias Haag.**

Akzeptierte Publikation 2:

Das Projekt zur Entwicklung einer *non-targeted* Organoid Metabolomics-Methode wurde in Eigeninitiative von **Sylvia Karin Neef** und **Nicole Janssen** initiiert. Die in der Arbeit beschriebenen Experimente zur Evaluierung und Validierung einer Extraktionsmethode für *non-targeted* LC-QTOF-MS Organoid Metabolomics wurde von der Erstautorin Sylvia Neef weitestgehend eigenständig geplant und durchgeführt. Hierbei wurde die Kultivierung der analysierten Organoide von Nicole Janssen durchgeführt. Die Ergebnisse wurden von Sylvia Neef unter Anwendung statistischer Techniken und Programme ausgewertet, interpretiert und visualisiert. Die Erstellung des veröffentlichten Werkes, insbesondere das Verfassen und Korrigieren des ursprünglichen Entwurfs, erfolgte durch die Erstautorin, **Mathias Haag** und **Thomas Mürdter,** unterstützt durch Nicole Janssen.

Manuskript in Vorbereitung:

Die in der Arbeit beschriebenen Experimente zur Evaluierung der Eignung eines neuen CapLC-Systems zur Metabolomics-Analyse geringer Probenmengen mittels *non-targeted* LC-QTOF-MS wurden von der Erstautorin **Sylvia Karin Neef** eigenständig geplant und durchgeführt. Die Ergebnisse wurden von Sylvia Neef ausgewertet, interpretiert und visualisiert. Die Erstellung des Manuskripts, insbesondere das Verfassen und Korrigieren des vorläufigen Entwurfs, erfolgte durch die Erstautorin und **Mathias Haag**.

1. Einleitung

1.1. Das Metabolom und dessen Erforschung: Metabolomics

Die Gesamtheit aller niedermolekularer Stoffwechselverbindungen (Metaboliten < 1.5 kDa)[1,2] in einem biologischen System (z.B. Gewebe, Plasma oder Urin) wird als Metabolom bezeichnet. Es besteht aus Intermediaten und Produkten des endogenen Stoffwechsels (Metabolismus), sowie aus exogenen Stoffen und deren Metaboliten. Das Metabolom ist der Endpunkt der sogenannten „Omics"-Kaskade (siehe Abb.1) und resultiert aus dem Genom[a], dem Transkriptom[b] und dem Proteom[c].[1] Seine Zusammensetzung wurzelt somit einerseits im genetischen Code, wird andererseits jedoch stark durch extrinsische Faktoren wie die Ernährung, die Umwelt und durch die Einnahme von Medikamenten beeinflusst.[3] Somit ist das Metabolom Endprodukt aller regulatorischen Prozesse einer Zelle.

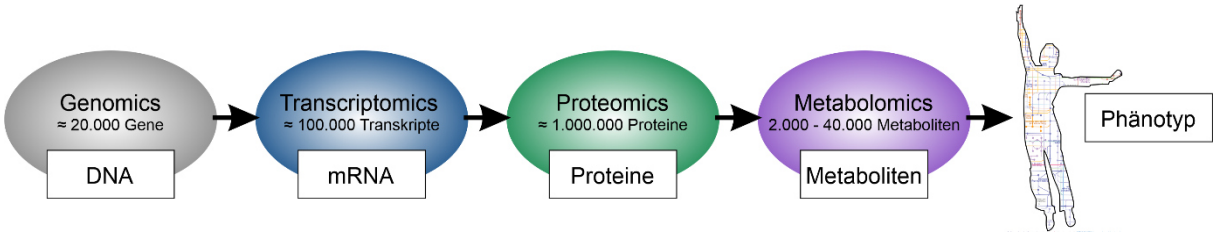

Abbildung 1 Die „Omics"-Kaskade beschreibt das Ineinandergreifen der verschiedenen „Omics"-Disziplinen. Das Vereinen von Informationen aus allen Disziplinen ermöglicht das Verstehen von biologischen Vorgängen in einem Organismus. Metabolomics ist die Disziplin, die hierbei den Phänotyp eines Individuums am genausten zu charakterisieren vermag. DNA (Desoxyribonukleinsäure, engl.: *desoxyribonucleic acid*); mRNA (Boten-Ribonukleinsäure, engl.: *messenger ribonucleic acid*).
Modifiziert nach Cortes *et al*. 2017

Die Zahl der unterschiedlichen Metaboliten, die das Metabolom des menschlichen Körpers umfassen, ist zum jetzigen Zeitpunkt nicht vollständig beschrieben, wird jedoch auf 2.000 bis 40.000 geschätzt.[1,3] Eine absolute quantitative Bestimmung wird durch die starken strukturellen Unterschiede der Metaboliten sowie durch die Tatsache erschwert, dass sich das Metabolom zwischen den einzelnen biologischen Systemen

---

[a] Die Gesamtheit aller Gene

[b] Die Gesamtheit aller Transkripte (mRNA)

[c] Die Gesamtheit aller Proteine

stark unterscheidet. So wird beispielsweise das Metabolom des menschlichen Urins auf ~3.100 vorwiegend hochpolare Verbindungen[4] geschätzt, während das Metabolom des Humanserums schätzungsweise aus ~4.600 Metaboliten[5] besteht, von denen über die Hälfte verschiedenen Lipid-Spezies zugeordnet werden. Hinzu kommt, dass das Metabolom aufgrund von sich ständig ändernden extrinsischen Faktoren (z.B. aufgenommene Nahrung) einer permanenten Dynamik unterliegt. Seine exakte Komposition kann als unmittelbare Antwort des Organismus auf alle einwirkenden genetischen und extrinsischen Faktoren angesehen werden[6] und spiegelt den physiologischen, oder auch pathologischen, Status eines biologischen Systems zum Zeitpunkt der Probennahme wieder.[3]

Der Begriff „Metabolomics“ beschreibt die möglichst umfassende Analyse der Metaboliten eines biologischen Systems und ist ein neuartiger Forschungsansatz in vielen Bereichen der Lebenswissenschaften. Im Bereich Metabolomics hat sich die umfassende Analyse der Gesamtheit der Lipide (das Lipidom) als die weitgehend eigenständige Teildisziplin „Lipidomics“ etabliert.[7] Lipide spielen in vielen Stoffwechselwegen eine zentrale Rolle und werden mit der Entstehung eines weiten Spektrums an Erkrankungen, unter anderem Krebs,[8–11] assoziiert. Im Folgenden wird jedoch nicht zwischen Metabolomics und Lipidomics unterschieden.

Gängige Methoden zur Analyse des Metaboloms sind die Kernspinresonanzspektroskopie (NMR-Spektroskopie) und die Massenspektrometrie (MS) beziehungsweise Tandem-Massenspektrometrie (MS/MS). Letztere beiden werden in der Regel mit chromatographischen Verfahren wie der Hochleistungsflüssigkeitschromatographie (*high performance liquid chromatography*, HPLC bzw. LC) oder der Gaschromatographie (GC) gekoppelt. Dabei ist die LC-MS mit Elektrospray-Ionisation (LC-ESI-MS) besonders weit verbreitet. Die Vorschaltung einer Chromatographie-Methode erleichtert insbesondere die Analyse komplexer Proben. Beispielsweise können isobare Moleküle (z.B. die Aminosäuren L-Leucin und L-Isoleucin) getrennt werden, da ihre strukturellen Unterschiede zu verschiedenen Elutionseigenschaften führen. Zudem werden durch eine chromatographische Auftrennung potentielle Matrixeffekte, die vor allem beim Einsatz von ESI-Quellen zu einer beträchtlichen Abnahme der Signalintensität führen können, verringert.[12] Für Metabolomics-Analysen sind die am häufigsten eingesetzten Trennprinzipien die Umkehrphasen-Chromatographie (*reversed-phase liquid chromatography*, RPLC) und

die hydrophile Interaktionschromatographie (*hydrophilic interaction liquid chromatography*, HILIC). Im Bereich der Chromatographie-Technik werden in den letzten Jahrzehnten vermehrt miniaturisierte Systeme entwickelt, die hauptsächlich in Kombination mit ESI-MS eingesetzt werden.[13] Durch die Reduzierung des Innendurchmessers (i.D.) der chromatographischen Säule wird für die mobile Phase eine geringere Flussrate benötigt. Dies führt zu einer reduzierten Verdünnung der injizierten Probenbande, wodurch unter anderem die Konzentration in der Ionenquelle des MS und somit auch die Empfindlichkeit gesteigert werden kann.[14,15] Daher sind LC-Anwendungen mit reduzierten Flussraten ein wertvolles Werkzeug für Anwendungen im Spurenbereich oder wenn nur sehr geringe Probenmengen zur Verfügung stehen. Weitere Vorteile sind eine mögliche Verbesserung der chromatographischen Effizienz und Auflösung[14,16] sowie der wesentlich geringere Verbrauch an Lösemitteln, wodurch die Kosten für deren Anschaffung und Entsorgung gesenkt werden.

In der Literatur findet sich eine Vielzahl von Nomenklaturen für die eingesetzten Systeme, die sich teilweise stark unterscheiden und/oder überlappen.[15–17] In Tabelle 1 sind die in der vorliegenden Arbeit genutzten Definitionen aufgeführt.

Tabelle 1: Nomenklatur für Flüssigkeitschromatographie-Systeme modifiziert nach Rapp *et al*. 2003

Anwendung	**Säulen-Typ**	**Säulen-Innendurchmesser (i.D.)**	**Flussrate**
Analytical LC	*normal-bore* Säulen	5,0 mm – 3.9 mm	5–1,5 mL/min
Narrow-bore LC	*narrow-bore* Säulen	3,9 mm – 2.1 mm	1,5–0,2 mL/min
Micro LC	*micro-bore* Säulen	2,1 mm – 500 µm	300–10 µL/min
Capillary LC	gepackte Kapillaren	500 µm – 150 µm	15–1 µL/min
Nano LC	gepackte Kapillaren	< 150 µm	< 1 µL/min

LC, Flüssigkeitschromatographie (*liquid chromatography*); i.D., Innendurchmesser

Grundsätzlich kommen, je nach biologischer Fragestellung, zwei verschiedene Metabolomics-Ansätze zum Einsatz: *targeted* Metabolomics und *non-targeted* Metabolomics. In *targeted* Metabolomics-Studien werden vor der Analyse Metaboliten ausgewählt, die dann gezielt detektiert und quantitativ erfasst werden. Ein solcher Studienaufbau basiert in der Regel auf einer bereits existierenden Hypothese. Im Gegensatz hierzu zielt der *non-targeted* Metabolomics-Ansatz auf die möglichst vollständige Analyse aller in der Probe enthaltenen Metaboliten ab. Hierbei kommen häufig hochauflösende Massenspektrometer (z.B. *quadrupole time-of-flight mass spectrometer*, QTOF-MS) zum Einsatz. Die detektierten Signale (sogenannte

metabolic features) werden nach der Messung statistisch analysiert und durch strukturelle Charakterisierung bekannten, aber auch unbekannten Metaboliten zugeordnet. In diesem Schritt spielt der Abgleich der analysierten Daten (exakte Molekülmasse und MS/MS-Fragmentspektren) mit Datenbanken und Bibliotheken eine wichtige Rolle.

Non-targeted Metabolomics-Analysen ermöglichen einen umfassenden Blick auf den metabolischen Status der untersuchten Probenmatrix. Dabei können sich unerwartete Zusammenhänge oder Erkenntnisse, wie beispielsweise Hinweise auf bisher unbekannte Wirkmechanismen von Medikamenten, ergeben.[18,19] Aus diesem Grund wird diese ungezielte Herangehensweise auch als hypothesengenerierender Ansatz bezeichnet. Hierbei ist zu beachten, dass die Ergebnisse von *non-targeted* Metabolomics-Analysen häufig semiquantitativ sind und nur relative Rückschlüsse auf die mengenmäßige Veränderung der Metaboliten zulassen. Daher bedarf es stets einer eingehenden Validierung der Ergebnisse, wobei vor allem *targeted* Metabolomics-Methoden eingesetzt werden.

1.1.1. **Metabolomics in der klinisch-pharmakologischen Forschung**

Ändern sich die Faktoren, die auf einen Organismus wirken, verändert sich unmittelbar und zeitnah auch die Zusammensetzung des Metaboloms. Daher erlaubt Metabolomics einen detaillierten Blick auf den klinischen Phänotypen eines Individuums. In Bezug auf Erkrankungen sind die Veränderungen häufig sehr spezifisch und können auf die Zu- oder Abnahme eines, oder einiger weniger, Metaboliten im Metabolom reduziert werden. Diese Moleküle werden als Biomarker bezeichnet und können zur klinischen Diagnose oder zur Überprüfung des Krankheitsverlaufs eingesetzt werden. Als wohl bekanntestes diagnostisches Verfahren ist in diesem Zusammenhang das Neugeborenenscreening[20] zu erwähnen. Diese bereits seit Jahren in der klinischen Chemie etablierte Routinediagnostik ermöglicht, unter anderem durch die massenspektrometrische Analyse[21] von Blutmetaboliten, die Diagnose zahlreicher Erkrankungen (z.B. Phenylketourie durch die Analyse des Gehalts an Phenylalanin)[20,22] bereits in den ersten Lebenstagen von Neugeborenen.

Auch in der Krebsforschung gewinnen Metabolomics-Analysen zunehmend an Bedeutung. Bereits in den 1950er Jahren beschrieb Otto Warburg, dass sich die Energiegewinnung in Krebszellen, auch unter aeroben Bedingungen, zur ansonsten

unter anaeroben Bedingungen ablaufenden Milchsäuregärung hin verschiebt, was einen erhöhten Glukoseverbrauch und eine vermehrte Bildung von Lactat zur Folge hat.[23] Die Beobachtung dieser sogenannten Warburg-Hypothese wurde inzwischen für eine Vielzahl verschiedener Krebszelltypen beschrieben.[24–26] Da sich der Metabolismus einer Krebszelle nicht nur in Hinblick auf die Glykolyse ändert,[9,27] wird Krebs in der Literatur vermehrt als metabolische Erkrankung betrachtet.[24,28] Metabolomics-Studien liefern in diesem Kontext wichtige Hinweise zur Identifikation diagnostischer und prognostischer Biomarker und tragen zum allgemeinen Verständnis der Karzinogenese bei.[27] Dabei gewinnen auch Lipide zunehmend an Bedeutung. Sie werden, neben ihrer Rolle als Energiespeicher und Membranbestandteil von Zellen, zunehmend als wichtige inter- und intrazelluläre Signalmoleküle erkannt und Störungen des Lipidstoffwechsels werden mit der Entstehung und Progression von Krebs assoziiert.[10,11,29]

Ein weiteres Fachgebiet in dem Metabolomics zunehmend an Bedeutung gewinnt, ist die personalisierte Medizin. Ihr Ziel ist es, interindividuellen Variationen in der Disposition und der Wirksamkeit von Medikamenten begegnen zu können, und für jeden Patienten die richtige Therapie zum richtigen Zeitpunkt in der richtigen Dosis zu finden.[30] Um beobachtete Variationen in der Wirksamkeit von Medikamenten durch genetische Polymorphismen zu erklären, wurden in den letzten Jahrzehnten große Anstrengungen im Bereich Pharmacogenomics unternommen.[31,32] Dabei können extrinsische Faktoren wie Umwelteinflüsse oder das individuelle Microbiom[d] jedoch nicht mit einbezogen werden.[31] Metabolomics ist in dieser Hinsicht vorteilhaft und neue klinische Studien zeigen, dass metabolische Biomarker genutzt werden können, um Voraussagen in den Bereichen der Pharmakokinetik, der Medikamentenwirksamkeit, dem Auftreten von Nebenwirkungen und der individuellen Disposition zu treffen.[31] Ein Beispiel hierfür ist die quantitative Analyse von Gallensäuren mittels LC-QTOF-MS[33] zur Unterstützung der Abschätzung der Sicherheit und Wirksamkeit von Myrcludex B, einem neuen Wirkstoff zur Behandlung von chronischen Hepatitis B und D Infektionen, in klinischen Studien.[34–36]

[d] Die Gesamtheit aller, hauptsächlich im Darm angesiedelter, Mikroorganismen

1.1.2. **Entwicklung und Validierung von LC-MS-basierten *non-targeted* Metabolomics-Methoden**

Non-targeted Metabolomics-Methoden zielen darauf ab, die Gesamtheit der Stoffwechselprodukte einer Probenmatrix zu erfassen. Eine für solche Zwecke geeignete Extraktionsmethode sollte daher möglichst effektiv, aber wenig selektiv ein breites Spektrum an Metaboliten aus der Probenmatrix freisetzen und dabei etwaige Störstoffe ausschließen (z.B. Fällung von Proteinen). Zur Untersuchung von Gewebe oder adhärenten Zellen wird hierfür häufig die Extraktion mit Lösemitteln oder Lösemittelgemischen gegensätzlicher Polarität genutzt. Diese kann in einem Extraktionsschritt (biphasisch oder monophasisch mit anschließender Phasentrennung)[37,38] oder sequentiell (z.B. erst mit polarem Lösemittel und dann mit unpolarem Lösemittel)[8,37,39] durchgeführt werden. Aufgrund der großen physikalischen und chemischen Diversität der durch die Extraktion freigesetzten Metaboliten (z. B. molare Masse, Ladung, Dampfdruck oder Polarität) ist die Erfassung des gesamten Proben-Metaboloms durch den Einsatz einer einzelnen Analysenmethode jedoch nicht möglich. Um ein möglichst weites Spektrum an Verbindungen zu erfassen empfiehlt sich daher die Kombination verschiedener analytischer Verfahren, wie beispielsweise LC- mit GC-MS[40,41] oder, bei Einsatz einer einzelnen chromatographischen Trenntechnik, die Verwendung komplementärer Chromatographiesäulen.[8,39,42]

Ein Schlüsselelement jeder analytischen Methodenentwicklung ist deren Validierung. Diese belegt die Richtigkeit der Ergebnisse und die Zuverlässigkeit der Methode. Während für *targeted* LC-MS-Methoden seit Jahren offizielle Validierungsanforderungen definiert sind (z.B. in den Richtlinien der US-amerikanischen Behörde für Lebens- und Arzneimittel: *FDA Guidance on bioanalytical method validation*), gibt es für die Validierung von *non-targeted* Metabolomics-Methoden derzeit keine offiziellen Vorschriften. Naz *et al*.[43] formulierten Empfehlungen im Hinblick auf die Probenauswahl, die Probenaufarbeitung und –analyse, sowie bezüglich der Validierung der analytischen Methode auf Präzision, Richtigkeit und Linearität der Ergebnisse. Aufgrund des hypothesengenerierenden und semiquantitativen Charakters von *non-targeted* Metabolomics-Studien verlieren die beiden letzten Punkte im Vergleich zu *targeted* Metabolomics-Methoden jedoch an Gewicht. Die Validierung einer neuen Methode in Hinblick auf deren Präzision in kurzen, aber auch längeren Zeitabständen, ist hingegen von hoher Relevanz. Als Maß

für die Präzision wird im Allgemeinen der Variationskoeffizient (*coefficient of variation*, CV) von nicht zugeordneten *Features* oder annotierten Metaboliten angegeben.

Eine empfohlene[43,44] und vielfach angewandte[8,39,42] Praxis ist die Bestimmung der Messpräzision (Maß für die Schwankungen, die durch das Analysengerät verursacht werden, auch analytische Präzision genannt)[45] über die wiederholte Analyse sogenannter Qualitätskontrollproben (*quality control samples*, QC *samples*). QC Proben werden in der Regel durch Mischen definierter Aliquote (gleiche Volumina) aller Probenextrakte einer Messreihe hergestellt. Damit repräsentieren sie die gemittelte Zusammensetzung aller im Rahmen einer *non-targeted* Metabolomics-Studie analysierten Proben mit identischer Probenmatrix. Sie werden am Anfang (oft bereits zum Äquilibrieren des Systems), am Ende und in regelmäßigen Abständen zwischen den Proben vermessen. So ermöglichen sie die Kontrolle der analytischen Leistung über den Zeitraum der gesamten Analyse. Besteht diese aus verschiedenen Serien, kann die selbe QC Probe über alle Messungen mitgeführt werden. Dadurch können auftretende Schwankungen in der Signalintensität über eine einzelne Analysenserie hinweg, aber auch zwischen verschiedenen Analysetagen, nachträglich mathematisch korrigiert werden.

Auch die Methodenpräzision wird vermehrt zur Bewertung der Qualität neu entwickelter oder optimierter *non-targeted* Metabolomics-Methoden ermittelt.[8,39,46–48] Sie ist das Maß für die Ergebnisschwankungen, die durch alle Schritte der Methode verursacht werden[45] und wird über Replikate einer Probe (wiederholte Aufarbeitung) hinweg bestimmt.

Ein weiterer wichtiger Validierungsparameter ist die Wiederholbarkeit (Wiederholpräzision). Sie ist die Präzision einer Methode unter Wiederholbedingungen (kurze Zeitabstände, mit demselben Verfahren, an identischen Proben, im selben Labor, durch den selben Bearbeiter, mit derselben Geräteausrüstung)[45] und daher von Bedeutung, wenn eine Methode in größer angelegten Studien eingesetzt werden soll. Angaben bezüglich der Wiederholbarkeit von *non-targeted* Metabolomics-Methoden finden sich, im Gegensatz zur Mess- und Methodenpräzision, in der Literatur jedoch nur selten.

1.2. **Formalin-fixiertes, Paraffin-eingebettetes Gewebe**

Formalin-fixierte, Paraffin-eingebettete (FFPE) Gewebeproben werden seit Jahrzehnten routinemäßig zur histopathologischen Untersuchung von gesundem und krankem Gewebe verwendet. Klinisch archiviertes FFPE Gewebe kann problemlos bei Raumtemperatur gelagert werden,[49] was einen erheblichen Platz- als auch Kostenvorteil (z.B. im Vergleich zur Lagerung von Frischgewebe) mit sich bringt. Die Herstellung von FFPE Gewebe in der klinischen Pathologie ist nicht standardisiert, folgt jedoch gewissen Grundprinzipien, die im Folgenden beschrieben werden.

Wird im Rahmen einer Operation Gewebe entnommen (z.B. als Biopsie oder Teilresektion), wird es zunächst zur Fixierung in 4–10 %ige, wässrige Formaldehydlösung gegeben. Formaldehyd hydratisiert in wässriger Lösung (= Formalin) großteils zu Methylenglycol und polymerisiert bei längeren Stehzeiten weiter zu Polyoxymethylen.[50] In neutraler Umgebung, wie im Gewebe, ist die Reaktion reversibel und Formaldehyd wird freigesetzt.[51] Die reaktiven Moleküle Methylenglycol und freies Formaldehyd dringen ins Gewebe ein und reagieren in einer additiven und quervernetzenden Art und Weise.[50] Die Fixierung des Gewebes erfolgt im Wesentlichen durch die Reaktion von Formaldehyd mit reaktiven Endgruppen proteingebundener Aminosäuren. Bevorzugte Reaktionspartner sind primäre Amine (z.B. Lysin) und Thiole (z.B. Cystein). Nach der Addition von Formaldehyd an die reaktiven Gruppen erfolgt eine Quervernetzung mit weniger reaktiven Gruppen wie Amiden (z.B. Glutamin, Asparagin), Guanidingruppen (z.B. Arginin) und aromatischen Ringen (z.B. Tyrosin).[50,52] Das Gewebe wird von Formaldehyd, in Form von Methylenglycol, schnell durchdrungen (ca. 1 mm/h) aber langsam quervernetzt (fixiert).[49,50] Die benötigte Zeit zur vollständigen Fixierung ist somit unter anderem von der Struktur und der Größe des Gewebes abhängig und unterliegt daher einer großen Variation (z.B. 6–72 h empfohlen für Proben zur Rezeptorstatus-Testung des humanen epidermalen Wachstumsfaktor-Rezeptor Typ 2 [HER2] bei Brustkrebspatientinnen).[53]

Im Anschluss an die Gewebefixierung erfolgt die Einbettung in Paraffin. Um die Infiltration des unpolaren Paraffins in die Gewebeporen zu ermöglichen wird das fixierte Gewebe zunächst dehydriert. Hierzu werden Alkoholreihen in aufsteigender Konzentration und absteigender Polarität (z.B. 50%–70%–96%–100% Ethanol, 100% Isopropanol, 100% Xylol) genutzt, die im Gewebe vorhandenes Wasser verdrängen.[49] Im Anschluss erfolgt die Infiltration und Einbettung mit flüssigem Paraffin. Der gesamte

Prozess wird in der Regel vollautomatisch und unter Einwirkung von erhöhter Temperatur (Dehydrierung: ca. 40 °C, Infiltration/Einbettung: ca. 60 °C) sowie vermindertem Druck (Vakuum) vollzogen.[49] Die Temperaturerhöhung wirkt sich vorteilhaft auf die Viskosität und Diffusionsrate der Lösemittel aus, während bei vermindertem Druck eingeschlossene Luft besser entfernt wird und durch herabgesetzte Siedepunkte die eingesetzten Reagenzien schneller abdampfen.[49] Dennoch nimmt der Prozess üblicherweise >12 h (Dehydrierung und Infiltration/Einbettung ohne vorangegangene Fixierzeit) in Anspruch.[49]

1.2.1. **FFPE Gewebe-Metabolomics**

Aufgrund der routinemäßigen Herstellung, Haltbarkeit und der einfachen Lagerbedingungen von FFPE Gewebe existieren weltweit umfangreiche Archive mit gesammeltem Probenmaterial. Häufig liegen für die Blöcke detaillierte Informationen zur Krankheitsgeschichte des Patienten vor. Diese Tatsachen machen FFPE Gewebe zu einer wertvollen Ressource für retrospektive Studien, die in den vergangenen Jahrzenten vielfach für die Genomics-, Transkriptomics- und Proteomics-basierte Biomarkerforschung erschlossen wurde.[54–56] Im Gegensatz hierzu finden sich in der Literatur nur wenig Metabolomics-Analysen auf der Basis von FFPE Gewebeproben.
Die erste Machbarkeitsstudie zur Verwendung von FFPE Gewebe als Probenmatrix für *targeted* Metabolomics via LC-MS/MS wurde 2011 von Kelly *et al*.[57] veröffentlicht. Die Arbeitsgruppe demonstrierte die reproduzierbare Analyse von bis zu 143 polaren Metaboliten nach deren methanolischer Extraktion aus FFPE Weichteilsarkom-Proben. Dabei wurde in der Hauptkomponentenanalyse (*principal component analysis*, PCA) auf Basis der gemessenen Metabolitenprofile eine phänotypische Differenzierung zwischen Sarkom-Proben und gepaarten Normalgewebe-Proben erzielt.[57]
Das von Kelly *et al*.[57] publizierte Protokoll wurde in darauffolgenden LC-MS basierten *non-targeted* Metabolomics-Studien geringfügig modifiziert[40,58–60] und zur Untersuchung von FFPE Zelllinien[40] sowie FFPE Gewebe des Prostata-,[40] Pankreas-[59] und Kolorektalkarzinoms[60] genutzt. Für GC-MS/(MS)-basierte Studien an murinem FFPE Nierengewebe und humanem FFPE Gewebe von Lymphom und Prostatakrebs, wurden zweistufige Extraktionsprotokolle etabliert, in denen die Proben zunächst durch Waschen mit Xylol entparaffiniert und im Anschluss mit Methanol:Wasser (1:1, *v*/*v*) gefolgt von Chlorofom:Methanol (3:1, *v*/*v*) extrahiert wurden.[61–63]

Neben den Chromatographie-basierten Verfahren zur Analyse des Metaboloms ermöglichte die hochauflösende Matrix-unterstützte Laser-Desorption/Ionisation Fourier-Transform Ionenzyklotronresonanz Massenspektrometrie (MALDI-FT-ICR MS)[2,64] die bildgebende Messung von Metaboliten in FFPE Gewebe. Solche innovativen Verfahren liefern räumlich aufgelöste Informationen über die Verteilung von Metaboliten im Gewebe, was in heterogenen Tumorproben von großem Vorteil sein kann und die Korrelation der Daten mit histologischen Befunden ermöglicht.[2,64] Limitiert ist diese Technik jedoch in der Unterscheidung und Annotation isobarer Verbindungen, die ohne chromatographische Trennung deutlich erschwert ist.[65]

1.3. **Organoide**

Organoide sind kleine, dreidimensionale Zellverbände, die sich im Hinblick auf ihre Architektur und zelluläre Zusammensetzung *in vitro* analog zu einem *in vivo* Organ organisieren. Sie gehören zu den vielversprechendsten Neuentwicklungen im Bereich der Lebenswissenschaften und gewinnen als Modellsystem in zahlreichen Forschungsgebieten zunehmend an Bedeutung. Der Einsatz von Organoiden birgt großes Potential für die Erforschung von organspezifischen Erkrankungen und deren Therapie. Auch wenn ihnen wichtige Strukturen wie Nervenbahnen, Blutgefäße oder Immunzellen fehlen, spiegeln sie die Komplexität und Physiologie eines menschlichen Organs besser wider als bisherige 2D-Zellkulturen und könnten daher zur Reduzierung und Komplementierung von Tierversuchen beitragen.[66,67]

Die Entwicklung der heute etablierten Organoid-Modellsysteme wurde in erster Linie durch die Arbeitsgruppen von Hans Clevers[68] und Yoshiki Sasai[69] vorangetrieben, die unabhängig voneinander an adulten Stammzellen (ASC), beziehungsweise pluripotenten Stammzellen (PSC), forschten. Organoide können aus beiden Zelltypen gebildet werden. PSC sind embryonale Stammzellen, die sich zu jeder im Körper vorkommenden Zelle ausdifferenzieren können.[67] Im Gegensatz hierzu können sich ASC nur in bestimmte, organspezifische Zellen umwandeln, die in ihrem Ursprungsgewebe vorkommen.[67] Durch Zugabe von zellspezifischen Transkriptionsfaktoren (z.B. Oct3/4, Sox2, Klf4 und c-Myc bei humanen Fibroblasten)[70] können ASC jedoch reprogrammiert werden, und die Eigenschaften von embryonalen Zellen zurück gewinnen. Diese Zellen werden dann als induzierte pluripotente Stammzellen bezeichnet.[70]

Die Zellkultur-Bedingungen, die zur Bildung von Organoiden führen, variieren stark in Abhängigkeit der Ausgangszellen und der angestrebten Entität. Häufig ist die Einbettung in eine extrazelluläre Matrix (ECM) erforderlich, die unter anderem das Zellwachstum unterstützt und die Adhäsion der Zellen ermöglicht.[66,67] Zudem müssen die Ausgangszellen häufig gewebespezifisch stimuliert werden, um eine Ausdifferenzierung zum gewünschten Organoid zu erzielen. Dies geschieht durch den Einfluss von Morphogenen (z.B. Transkriptionsfaktoren oder Wachstumsfaktoren), die entweder von der Zelle selbst gebildet (endogene Signale) oder in das Zellkulturmedium zugegeben werden (exogene Signale).[67]

In den vergangenen Jahren wurde eine Vielzahl von Organoid-Modellen etabliert, die unter anderem die Untersuchung von genetischen Defekten,[71,72] Wirt-Erreger-Wechselwirkungen[73,74] und Krebserkrankungen[29,73,75] in verschiedenen Entitäten ermöglichen. Besonders im Bereich der personalisierten Medizin wurden beachtenswerte Erfolge erzielt. So wurden beispielsweise in einer Machbarkeitsstudie Organoide aus intestinalen Stammzellen zweier Mukoviszidose (*cystic fibrosis*, CF) Patienten mit seltenem Genotyp (G1249R/F508del) genutzt, um deren Ansprechen auf Ivacaftor (KALYDECO, ursprünglich registriert für G551D, S1251N und sieben weitere Mutationen) zu testen.[71] Die Wirksamkeit von Ivacaftor konnte durch die Behandlung der Organoide *in vitro* bestätigt werden und ermöglichte die Therapie der Patienten *in vivo*.[71]

Ein großer Vorteil von PSC oder ASC basierten Organoid-Kulturen ist zudem, dass sie sich zur Langzeitkultivierung eignen.[76] So können Organoid-Biobanken, die ein weites Spektrum einer Erkrankung (verschiedene Subtypen oder genetische Varianten) abdecken, etabliert und zur Entwicklung neuer Arzneimittel genutzt werden. Solche Biobanken stellen insbesondere hinsichtlich der Entwicklung neuer Krebstherapien eine große Hoffnung dar, da Tumorerkrankungen oft auf einer Vielzahl genetischer Mutationsvarianten beruhen.

1.3.1. **Organoid-Metabolomics**

Die Anzahl von Veröffentlichungen im Bereich Zellkultur-Metabolomics steigt in den vergangenen Jahren ebenso wie die Verwendung von Organoiden als *in vitro* Modellsystem stetig an.[76,77] Dennoch existiert zum jetzigen Zeitpunkt nur eine begrenzte Zahl an Studien, die Metabolomics- bzw. Lipidomics-Analysen in Organoiden durchgeführt haben. Eingesetzt wurden hierzu NMR, *targeted*[29] und *non-*

targeted[75,78,79] LC-MS-Methoden. Letztere basierten auf biphasischer Extraktion mit Methanol und Chloroform (Folch-Extraktion)[78,79] oder monophasischer Extraktion mit Methanol:Acetonitril:Wasser (5:3:2, *v*/*v*/*v*).[75] In Übereinstimmung mit etablierten Protokollen zur Kultivierung intestinaler Organoide,[80] nutzten die *non-targeted* Metabolomics-Studien basalmembranartige Matrices als ECM (Cultrex® BME und Matrigel®). Dieser ECM-Typ ist eine komplexe biologische Matrix, die aus gereinigten Extrakten des murinen *Engelbreth-Holm-Swarm*-Sarkoms gewonnen wird und in erster Linie aus Proteinen (unter anderem Laminin und Kollagen) sowie Wachstumsfaktoren besteht.[81] In den beschriebenen Protokollen wurde die ECM vor der Extraktion entweder durch Waschen und Trypsinieren entfernt[78] oder mitextrahiert.[75] Über eine systematische Optimierung der Extraktion von Organoiden für *non-targeted* LC-MS-Metabolomics wird in den in den vorliegenden Arbeiten jedoch nicht berichtet und die Wahl der genutzten Protokolle wird nicht diskutiert. Zudem wurden keine Angaben bezüglich der Überprüfung gängiger Validierungsparameter (z.B. analytische und methodische Präzision) und der eingesetzten Probenmenge (Zellzahl) gemacht. Für beide Extraktionsvarianten sind jedoch Vor- und Nachteile denkbar. So könnte eine Isolierung von Organoiden aus der ECM die Metabolomics-Analyse sowohl positiv (z.B. Vermeidung störender Hintergrundsignale) als auch negativ (z.B. Verluste von Metaboliten während der Lyse der ECM) beeinflussen. Die Mitextraktion der ECM würde die Aufarbeitung hingegen vereinfachen und beschleunigen, könnte jedoch durch die Anwesenheit von Signalen nicht Organoid-abgeleiteter Moleküle unter anderem die angeschlossene statistische Analyse erschweren.

2. Zielsetzung

Die Ergebnisse der vorangegangenen Studien im Bereich FFPE Gewebe-Metabolomics deuten darauf hin, dass in FFPE Gewebe neben polaren Metaboliten auch ein großer Teil an unpolaren Metaboliten (Lipiden) konserviert ist.[40,61] Die bereits etablierten Extraktionsprotokolle zielen jedoch in erster Linie auf die Detektion kleiner polarer Moleküle ab. Da Veränderungen des Lipidstoffwechsels in vielen Erkrankungen, unter anderem bei Krebs, eine wichtige Rolle spielen,[9,10] empfiehlt sich eine Optimierung der existierenden Protokolle in Hinsicht auf die Erfassung von Lipiden, unter Beibehaltung der Detektion von polaren Metaboliten.
Zudem könnte die Organoid-basierte Biomarkerforschung von einer verlässlichen *non-targeted* Metabolomics-Methode, die sich problemlos auf eine hohe Probenanzahl mit geringen Zellzahlen anwenden lässt, erheblich profitieren. Die gewonnenen Metabolomics-Daten könnten, auch durch Korrelation mit Ergebnissen aus anderen Omics-Disziplinen, einen großen Beitrag zum Verständnis metabolischer Erkrankungen, wie beispielsweise Krebs, leisten und die personalisierte Medizin weiter voranbringen.

Primäres Ziel dieser Arbeit war daher die Entwicklung von Methoden zur Extraktion des Metaboloms und Lipidoms aus

(1) FFPE Gewebe und

(2) Organoiden

die dessen Erfassung mittels *non-targeted* LC-QTOF-MS ermöglichen.
Als Grundlage hierfür diente die im Rahmen einer vorangegangenen Dissertationsarbeit etablierte analytische Plattform für *non-targeted* Metabolomics und Lipidomics via RPLC- und HILIC-QTOF-MS.[8] Die erarbeiteten Extraktionsmethoden sollten hinsichtlich der Signalintensität (bedingt durch die Extraktionseffizienz und die Empfindlichkeit der Methode), der analytischen und methodischen Präzision und der Wiederholbarkeit optimiert und validiert werden.

Ein weiteres Ziel war die Demonstration der Qualität der etablierten Methoden durch deren Anwendung.
Im Rahmen einer Machbarkeitsstudie sollten hierfür die metabolischen Profile von FFPE Gewebe des klarzelligen Nierenzellkarzinoms und korrespondierendem FFPE Normalgewebe analysiert und die Proben auf deren Grundlage unterschieden werden.

Des Weiteren war die Untersuchung des Einflusses der Fixierzeit auf die Konservierung von Metaboliten in tierischem FFPE Gewebe (Schwein) geplant.
Die Qualität der entwickelten Organoid-Metabolomics-Methode sollte durch Analyse der metabolischen Reaktion von Organoiden des kolorektalen Karzinoms auf Behandlung mit 5-Fluorouracil geprüft werden. Hierzu sollte das Metabolom einer mit unterschiedlichen Dosen behandelten Organoid-Linie analysiert und Metaboliten mit dosisabhängig verändertem Gehalt identifiziert werden. Die Ergebnisse sollten in drei unabhängig durchgeführten Experimenten validiert werden.

Einhergehend mit der Entwicklung und Validierung der analytischen Methoden war zudem die Etablierung eines umfassenden Workflows zur Vorprozessierung und statistischen Analyse der Metabolomics-Daten, basierend auf der freien Programmiersprache R, einschließlich der grafischen Darstellung der Ergebnisse sowie der Annotation unbekannter Metaboliten geplantes Ziel der Arbeit.

In einem anknüpfenden Projekt sollte zudem die Eignung eines neuen CapLC-Systems für die Metabolomics-Analyse geringer Probenmengen mittels *non-targeted* CapLC-QTOF-MS überprüft werden. Hierbei war die Inbetriebnahme des neuen Geräts, die Etablierung erster Methoden und die Überprüfung der Leistungsfähigkeit des Systems hinsichtlich der Anzahl detektierbarer *Features*, der Sensitivität, der Signalerhöhung und der Messpräzision bei Messung kleiner Mengen an FFPE Gewebeextrakten Teil der Arbeit. Die Ergebnisse sollten mit einem im Haus etablierten System für *non-targeted* LC-QTOF-MS verglichen werden.

3. Ergebnisse und Diskussion

3.1. Publikation 1: Optimized protocol for metabolomic and lipidomic profiling in formalin-fixed paraffin-embedded kidney tissue by LC-MS

Die vorliegende Arbeit beschreibt die Evaluierung von Extraktionsprotokollen zur metabolischen Phänotypisierung von FFPE Nierengewebeproben mittels *non-targeted* LC-QTOF-MS. Die Qualität der optimierten Methode wurde im Rahmen einer Machbarkeitsstudie zur Unterscheidung von normalem und tumorösem Gewebe des klarzelligen Nierenzellkarzinoms (*clear cell renal cell carcinoma*, ccRCC) demonstriert. Des Weiteren wurde der Einfluss der Fixierzeit (Verweildauer des Gewebes in Formalin) auf die Metaboliten-Profile von FFPE Gewebe untersucht. Hierbei wurden einzelne Metabolit-Spezies identifiziert, die gegenüber dem Einfluss der Fixierung in Formalin resistent zu sein scheinen. Um die Eignung dieser Metaboliten für weiterführende Experimente zu prüfen, erfolgte die Detektion ausgewählter Metaboliten via MALDI-FT-ICR MS *imaging* in einer unabhängigen ccRCC Kohorte.

3.1.1. Methodenoptimierung

Zur Auswahl eines Extraktionsprotokolls, das die umfassende und präzise Analyse des Metaboloms und Lipidoms von FFPE Nierengewebeproben mittels *non-targeted* LC-QTOF-MS ermöglicht, wurden zehn verschiedene Protokolle getestet (siehe Tabelle 2). Diese basierten auf der methanolischen Extraktion des Gewebes (mit 80 % oder 50 % Methanol in Wasser, *v*/*v*) in Kombination mit mechanischer Bearbeitung (Hochgeschwindigkeitshomogenisierung mit Lysematrix-Kügelchen) und/oder Inkubation (70 °C). Zur Verbesserung der Extraktionsausbeute unpolarer Lipide wurde in die Protokolle B1–B3, C1–C3 und D1, im Anschluss an die methanolische Extraktion, eine erneute Extraktion des FFPE Gewebes mit Isopropanol (IPA) oder Methyl-tert-butylether/Methanol (MTBE/MeOH, 3:1, *v*/*v*) integriert (siehe Extraktionsmittel 2 in Tabelle 2). Die resultierenden Extrakte aller Protokolle wurden jeweils im positiven und negativen Ionisationsmodus, sowohl über HILIC- als auch über RPLC-QTOF-MS analysiert (es ergeben sich vier unterschiedliche Analysenmodi). Im Falle der Protokolle mit einem Extraktionsschritt (Protokolle A1–A3, siehe Tabelle 2) wurde das finale Extrakt für alle vier Modi eingesetzt. In den

zweistufigen Protokollen (Protokolle B1–B3, C1–C3 und D1, siehe Tabelle 2) wurde das methanolische Extrakt (erstes Extrakt) zur Analyse der polaren Metaboliten mittels HILIC und das zweite Extrakt zur Analyse der Lipide mittels RPLC genutzt. Die Methodenqualität wurde über die Signalintensität, die analytische und methodische Präzision sowie über das Signal/Rausch-Verhältnis annotierter Metaboliten bewertet. Von 273 Metaboliten, die zuvor in einer unabhängigen Arbeit[8] in humanem Nierengewebe (gefrorenes Frischgewebe, FF Gewebe*, fresh frozen tissue*) annotiert wurden, konnte ein Anteil > 80 % in FFPE Schweinenierengewebe detektiert werden. Die niedrigsten median CVs (beste Methodenpräzision, ermittelt über alle Modi der Analyse) wurden über das einstufige Extraktionsprotokoll A2 (CV = 19,5 %) und über die zweistufigen Extraktionsprotokolle B1 (CV = 14.1 %) und B3 (CV = 16 %) erzielt. Diese drei Protokolle zeichneten sich zudem durch die höchsten Gesamtsignalintensitäten für polare Metaboliten und Lipide aus.

Tabelle 2: Getestete Extraktionsmethoden zur Erfassung des Metaboloms und Lipidoms von FFPE Nierengewebeproben mittels *non-targeted* LC-QTOF-MS

Protokoll	**Extraktionsmittel 1**	**Extraktionsmittel 2**	**Extraktionsbedingung**
A1	80 % MeOH	-	Inkubation
A2			Homogenisierung + Inkubation
A3			Homogenisierung
B1	50 % MeOH	IPA	Inkubation
B2			Homogenisierung + Inkubation
B3			Homogenisierung
C1	50 % MeOH	MTBE/MeOH (3:1, *v*/*v*)	Inkubation
C2			Homogenisierung + Inkubation
C3			Homogenisierung
D1	80 % MeOH	IPA	Inkubation

In Bezug auf die Lipid-Analytik resultierten die Protokolle B1 und B3 zudem in einer 1,5- bis 3-fach höheren Gesamtsignalintensität verglichen mit den MTBE:MeOH-basierten Zweistufenprotokollen C1–C3, deren niedrige Gesamtsignalintensität sich auch in einer vergleichsweise niedrigen Methodenpräzision widerspiegelte (median CVs >25 %). An dieser Stelle ist anzumerken, dass die organischen Extrakte der

Protokolle C1–C3 zur Trockene eingeengt werden mussten, um sie im passenden Lösemittel für die RPLC-Analytik (IPA:MeOH, 2:1, *v*/*v*) rücklösen zu können. Im Gegensatz hierzu wurden die isopropanolischen Extrakte der Protokolle B1 und B3, ohne Trocknungsschritt, direkt mit MeOH auf das entsprechende Verhältnis (2:1, IPA:MeOH, *v*/*v*) verdünnt. Inwieweit das Eindampfen und Rücklösen der Extrakte die Ergebnisse der Lipidanalytik beeinflusst, bleibt zu untersuchen.

Beruhend auf den Ergebnissen der Methodenpräzision und der Gesamtsignalintensität wurden die Protokolle A2, B1 und B3 als besonders geeignet erachtet. Zur Ergebnisfindung wurde für diese drei Protokolle zusätzlich das Signal/Rausch (S/N)-Verhältnis der annotierten Metaboliten untersucht.
Während einige polare Metaboliten (z.B. Hexose, bestimmte Acylcarnitin-Spezies und Aminosäuren wie Arginin, Asparagin und Serin) mit keinem der Protokolle detektiert wurden (S/N < 3), führte die zweistufige Extraktion mit IPA zu einer verbesserten Detektion (S/N > 10) bestimmter Lipidklassen wie z.B. den Ceramiden (Cer), den Hexosylceramide (HexCer) und den Triglyceriden (TAGs). Protokoll B1 resultierte in der höchsten Anzahl detektierbarer Metaboliten (220 Metaboliten mit S/N > 3). Auf Grundlage dieses Ergebnisses und der Resultate bezüglich Signalintensität und Methodenpräzision wurde von den drei favorisierten Protokollen (A2, B1 und B3) die Methode B1 für weiterführende Experimente ausgewählt.
Des Weiteren wurde die Wiederholpräzision des Protokolls B1 in einem unabhängigen Experiment evaluiert. Da vorausgegangene Studien[40,57–60] großteils 80 % MeOH zur Extraktion nutzten, wurde zudem der Einfluss eines erhöhten MeOH-Anteils im ersten Extraktionsschritt auf die Extraktion und Analyse von Lipiden im zweiten Extraktionsschritt untersucht (siehe Tabelle 2, Protokoll D1).
Als Resultat der Experimente zur Wiederholpräzision konnten die sehr guten Ergebnisse bezüglich der Methodenpräzision (median CV der Metaboliten detektiert in HILIC ESI (+)/ESI (−) bzw. RPLC ESI (+)/ESI (−) jeweils < 20 %, n = 5 technische Replikate) reproduziert werden. Der darin enthaltene Anteil der analytischen Präzision betrug < 10 %. Auch mit Blick auf die wiederholbare Detektion von Metaboliten erwies sich die Methode B1 als äußerst geeignet. So konnten in zwei unabhängigen und an verschiedenen Tagen durchgeführten Experimenten 220 (Experiment 1) und 234 Metaboliten (Experiment 2) detektiert werden. Dabei ergab sich eine äußerst zufriedenstellende Überlappung von 216 Metaboliten zwischen den Experimenten. Die

minimale Differenz der Anzahl detektierter Metaboliten zwischen den Experimenten lässt sich durch die natürliche Inhomogenität des Gewebes (Aufarbeitung verschiedener Gewebestücke des Nierenkortex für Experiment 1 und 2) und durch messtägliche Schwankungen der Gerätesensitivität erklären.

Wurde der erste Extraktionsschritt mit 80 % MeOH statt 50 % MeOH durchgeführt (Protokoll D1, siehe Tabelle 2), sank die Gesamtsignalintensität der detektierten Lipide (analysiert im Extrakt des zweiten Extraktionsschritts mittels RPLC). Diese Beobachtung lässt sich über die unterschiedliche chemische Zusammensetzung der Lösemittel im ersten Extraktionsschritt erklären. Bei Verwendung eines erhöhten Anteils an organischem Lösemittel (80 % MeOH verglichen mit 50 % MeOH) sinkt die Polarität des Lösemittels, was eine verbesserte Extraktion eher unpolarer Moleküle (z.B. bestimmte Lipid-Spezies) mit sich führt, die dann im zweiten Extraktionsschritt nicht mehr zur Verfügung stehen.

Hierbei sei anzumerken, dass die Reproduzierbarkeit der Analytik von Lipiden, trotz der verminderten Gesamtsignalintensität, nicht beeinträchtigt war (median CV der Metaboliten detektiert in RPLC ESI (+)/ESI (−) < 16 %, n = 5 technische Replikate). Daher wäre die Integration des hier evaluierten zweiten Extraktionsschritts mit IPA in bereits etablierte Protokolle,[57] die auf einer einstufigen Extraktion mit 80 % MeOH basieren, möglich.

Zusammenfassend lässt sich feststellen, dass eine Extraktion durch Inkubation in 50 % Methanol gefolgt von einem zweiten Extraktionsschritt mittels IPA (Protokoll B1) zu den besten Resultaten bezüglich der Reproduzierbarkeit und Signalintensität von polaren Metaboliten und Lipiden in FFPE Schweinenierengewebe führte.

3.1.2. **Machbarkeitsstudie: Unterscheidung von Tumor- und Normal-Gewebe des klarzelligen Nierenzellkarzinoms**

Um die Anwendbarkeit des optimierten Protokolls B1 zur Unterscheidung zwischen tumorösem und korrespondierendem gesunden FFPE Nierengewebe aufzuzeigen, wurden Proben von vier ccRCC Patienten untersucht. In der PCA zeigte sich in allen Analysemodi eine klare Trennung zwischen ccRCC und angrenzendem Normalgewebe. Durch statistische Analyse der Daten wurden Metaboliten identifiziert, die in ccRCC-Gewebe im Vergleich zu normalem Gewebe signifikant (p-Wert < 0,05) und relevant (absoluter log2 *fold change* > 1) reduziert oder erhöht waren. Die Ergebnisse stimmten in Bezug auf 18 signifikant veränderte Metaboliten mit den

Resultaten einer unabhängigen Metabolomuntersuchung[8] in gesundem und korrespondierendem ccRCC FF Gewebe überein. In beiden Studien waren die relativen Gehalte von Trigonellin, Hippursäure, Pantothensäure, 1-Methyladenosin, Hydroxyisovalerylcarnitin und bestimmten Phospholipiden (hauptsächlich Phosphatidylethanolamin-Spezies) in ccRCC Gewebe im Vergleich zu normalem Gewebe reduziert, sowie in Bezug auf Kreatinin und L-Glutamin erhöht.

Somit konnte die Anwendbarkeit der etablierten Methode zur Unterscheidung von tumorösem und normalem FFPE Nierengewebe (ccRCC) gezeigt werden. Des Weiteren wurden durch den Vergleich der Metabolitenprofile (Tumor vs. Normalgewebe) differenzielle Metaboliten identifiziert, die zuvor bereits in einer auf FF Gewebe basierenden Metabolomics-Studie[8] beschrieben wurden. Diese Übereinstimmung deutet auf eine gute Konservierung charakteristischer, relativer Unterschiede des Metaboloms in FFPE Gewebeproben hin.

Des Weiteren wurden durch die Auswertung von Fragmentspektren im FFPE Gewebe N-methylierte Derivate[82] von Phosphatidylethanolaminen (PE) und Phosphatidylserinen (PS; z.B. PE-NMe 16:0/18:2 und PS-NMe 18:0/20:4) annotiert. Eine besondere Beobachtung hierbei war, dass diese Derivate in gleicher Weise zwischen Tumor- und Normalgewebe verändert waren wie ihre nicht-modifizierten Muttersubstanzen (PE 16:0/18:2 und PS 18:0/20:4). Des Weiteren war die Art der Regulierung (relative Zu- oder Abnahme), trotz der chemischen Modifikation, mit zuvor in FF Gewebe beschriebenen Ergebnissen[8] vergleichbar (z.B. PE (16:0/20:4) und PE (16:0/18:2)). Diese Beobachtung deutet darauf hin, dass biologische Veränderungen der Lipidprofile auch dann erhalten bleiben, wenn die Substanzen während der Konservierung mit Formaldehyd reagieren und ebenfalls durch die entstehenden Lipid-Derivate im FFPE Gewebe widergespiegelt werden.

Eine weitere erwähnenswerte Beobachtung war der Nachweis verringerter relativer Gehalte bestimmter Xenobiotika wie Propofol-Glucuronid und 4-Hydroxy-3,5bis(1-methylethyl)phenylglucuronid/4-Hydroxy-2,6-bis(1methylethyl)phenylglucuronid (zwei bekannte Metaboliten des Narkosemittels Propofol) sowie 5-Acetylamino-6-amino-3-methyluracil/6-Amino-5[N-methylformylamino]-1-methyluracil (bekannt als Metaboliten des Koffeins) in FFPE ccRCC Gewebe. Die reduzierten Gehalte dieser Substanzen könnten auf den Verlust der normalen Nierenfunktion im Tumorgewebe zurückzuführen sein. Darüber hinaus zeigt die Detektion dieser Biotransformationsprodukte auf, dass es möglich ist, sowohl den endogenen

Metabolismus als auch den Metabolismus von Xenobiotika auf der Basis von FFPE Gewebe zu untersuchen. Beispielsweise könnten archivierte FFPE Gewebeproben zur Untersuchung des Beitrags der Niere zum extrahepatischen Metabolismus von Propofol[83–87] herangezogen werden.

3.1.3. **Anwendung der Methode zur Untersuchung des Einflusses der Fixierzeit auf die Metaboliten-Profile von FFPE Gewebe**

Zur Evaluierung des Einflusses der Fixierzeit (Verweildauer des Gewebes in Formalin) auf die detektierbaren Metabolit- und Lipid-Profile von FFPE Gewebe wurden FFPE Schweinenierengewebeproben, die unterschiedlichen Fixierzeiten ausgesetzt waren (6 h, 30 h und 54 h), untersucht. In der PCA zeigte sich durch eine ausgeprägte Trennung (>70 % der Variabilität erklärt durch PC1) der Probengruppen, dass die Gewebefixierzeit einen starken Einfluss auf die Profile der Lipide und der kleinen Moleküle hat. Um eine Abschätzung zu ermöglichen welche Metabolit-Spezies am stärksten zur Auftrennung der Gruppen beitragen, wurden zwischen den Gruppen die CVs annotierter Metaboliten bestimmt. Von den 381 Metaboliten wurden 78 durch die Fixierzeit wenig beeinflusst (CV < 20 %, maximaler log2 *fold change*: 0.06-0.75) während 48 eine hohe Variabilität zwischen den Gruppen zeigten (CV > 80%, maximaler log2 *fold change*: 1.9-5.4).

Während sich bestimmte Klassen von Phospholipiden (Phosphatidylcholine [PCs], PSs und PEs) durch eine hohe Variabilität auszeichneten (CV 20-80 %), zeigte die Mehrheit der Phosphatidylinositol (PIs)-Spezies (höchster CV = 24.6% für PI 16:0/18:2) sowie der zu den Glycosphingolipiden (GSLs) gehörenden HexCers (höchster CV = 31.15 % für HexCer d18:1/24:1) eine vergleichsweise geringe Variabilität. Diese von uns beobachtete „Stabilität" von PIs und GSLs wurde bereits in früheren Publikationen[88] an Formalin-fixiertem Hirngewebe beschrieben. Die ausgeprägte Variabilität von Lipiden mit primären Aminogruppen (PEs und PSs) lässt sich wiederum durch deren hohe Reaktivität gegenüber Formaldehyd erklären.[82] Diese spiegelte sich zudem in einer starken Variation der relativen Verteilung von gebildeten PE-Derivaten (monomethylierte, dimethylierte und formylierte Species) zwischen den Probengruppen wider.

Der Einfluss der Fixierzeit auf die relativen Gehalte von Aminosäuren (AS) war uneinheitlich. Während bestimmte AS wie Glutaminsäure, Glutamin und Tryptophan stärker variierten (CVs > 30 %), waren die Signale anderer AS wie L-Tyrosin, L-Leucin

oder L-Phenylalanin zwischen den FFPE Gewebe-Gruppen besser vergleichbar (CVs < 20 %), was möglicherweise auf deren strukturelle Vielfalt und die Vielzahl möglicher Reaktionen mit Formaldehyd zurückzuführen ist.[89] Auch Taurin, Kreatinin, verschiedene Acylcarnitin (AC)-Spezies (AC 6:0, AC 12:0, AC 14:1, AC 16:1, AC 18:0, AC 18:1), Lyso-Lipide mit gesättigten Fettsäureresten (z.B. LysoPE 16:0 und 18:0) sowie die gesättigten Fettsäuren C16:0 und C18:0 zeigten eine geringe Variabilität (CVs < 20 %). Die letztgenannten Beobachtungen könnten auf die Reaktivität von Formaldehyd gegenüber ungesättigten Fettsäuren[90] und im Umkehrschluss auf eine Reaktionsträgheit gegenüber gesättigten Acylresten zurückzuführen sein.

Ein weiterer Einflussparameter auf die beobachteten Unterschiede zwischen den Gruppen könnte, neben der Fixierzeit, die unterschiedliche Größe der in Formalin fixierten Nierengewebestücke (z.B. ca. 1 cm^3 bei 6 h vs. komplettes Organ für 30 h und 54 h) sein. Beispielsweise könnten verschieden große Gewebestücke unterschiedlich stark von der Auswaschung von Metaboliten in das wässrige Fixiermedium[91] betroffen sein. Da jedoch auch zwischen den 30 h und 54 h fixierten Proben deutliche Unterschiede in den Signalintensitäten bestimmter Metaboliten (z.B. Cer-Spezies) beobachtet wurden, scheint die Fixierzeit einen größeren Einfluss auf die Metaboliten-Profile zu haben, als die Größe der Gewebeproben. Insbesondere für eine Fixierzeit von > 54 h sollte jedoch eine genauere Untersuchung eines möglichen Einflusses der Überfixierung[92] vorgenommen werden, da auch längere Fixierzeiten (z.B. bis zu 72 h zur Untersuchung von FFPE Brustkrebsgewebe)[53,93] in der Histologie empfohlen werden.

Neben den bereits erwähnten Möglichkeiten gibt es noch eine Vielzahl weiterer Faktoren, die Auswirkungen auf die Konservierung von Metaboliten in FFPE Gewebe haben könnten. Dazu gehört unter anderem die Zeit zwischen der Gewebeentnahme und dem Eintauchen des Gewebes in Formalin (in unserer Kohorte < 1 h). Je nach Dauer dieser Zeitspanne könnte z.B. Hypoxie-bedingter Stress die metabolischen Profile in FFPE Gewebe verändern. Als weitere Einflussmöglichkeiten können z.B. wenig standardisierte Behandlungsschritte, wie die alkoholische Dehydrierung des Gewebes vor der Paraffineinbettung, genannt werden. Zur Untersuchung dieser Faktoren wären einheitliche Gewebstücke, wie beispielsweise komplette, murine Nieren,[61] ein geeignetes experimentelles System, da hierdurch ein möglicher Effekt durch Variationen in der Größe der Gewebestücke minimiert werden könnte.

Da die klinischen Abläufe zur Erstellung von FFPE Gewebeproben jedoch wenig standardisiert sind[94,95] und sich vor allem zwischen einzelnen pathologischen Instituten unterscheiden können, ist eine Nutzung von gepaarten Proben (z.B. Tumor- und Normalgewebe desselben Patienten, am selben Tag entnommen und zeitgleich fixiert und eingebettet) empfehlenswert. Hierdurch ließe sich ein möglicher Einfluss der oben genannten Parameter auf die Ergebnisse der Untersuchung reduzieren.

3.1.4. **Bildgebende Analyse von Metaboliten, die durch die Fixierzeit nicht beeinflusst werden**

Je nach klinischer Fragestellung ist die Verwendung von gepaarten Proben nicht möglich. So werden beispielsweise bildgebende MALDI-FT-ICR-MS-Analysen, deren Vorteile unter anderem eine einfache Probenhandhabung und die Eignung für Hochdurchsatz-Analysen sind,[64] auf der Basis von Gewebemikroarrays (*tissue microarray*, TMA) durchgeführt. TMAs sind in der Regel Multi-Patienten-Arrays, die aus Gewebekernen von verschiedenen FFPE Blöcken stammen. Diese waren wiederum häufig unterschiedlichen Herstellungsbedingungen ausgesetzt und wurden oft über einen längeren Zeitraum (mehrere Jahre) gesammelt. In dieser Hinsicht wäre die Detektion von „stabilen“ Metaboliten wünschenswert, da diese eine verlässliche Basis zur Findung neuer prognostischer und diagnostischer Biomarker darstellen könnten.

In einem weiterführenden Experiment sollte daher eine Detektion von Metaboliten, die sich als wenig beeinflusst von der Gewebefixierungszeit erwiesen hatten (CVs < 20 %, siehe Kapitel 3.1.3.) mittels einer unabhängigen analytischen Technologie erfolgen. Hierzu wurde das MALDI-FT-ICR-MS *imaging*-Verfahren in einer unabhängigen Kohorte von ccRCC TMAs (*n* = 64) und korrespondierendem Normalgewebe[96] eingesetzt.

Von den gesuchten Metaboliten konnten vier (LysoPE 18:0, PC O-34:3 sowie die Fettsäuren 16:0 und 18:0) in den MALDI-FT-ICR-MS *imaging*-Daten annotiert werden. Mit Ausnahme von PC O-34:3, waren diese im Tumor, im Vergleich zu normalem Gewebe, signifikant reduziert. Eine Reduzierung des relativen Gehalts an LysoPE 18:0 in ccRCC-Gewebe im Vergleich zu korrespondierendem Normalgewebe, wurde ebenfalls in den oben beschriebenen Ergebnissen der LC-QTOF-MS-basierten Experimente (siehe Kapitel 3.1.2 und Leuthold *et al*. 2017[8]) beobachtet. Folglich wurde

diese molekulare Veränderung des Lipidstoffwechsels nun in drei unabhängigen ccRCC-Kohorten durch unterschiedliche, analytische Messverfahren bestätigt.
Die erfolgreiche *in-situ*-Detektion „stabiler“ Moleküle in TMAs bietet eine erste Grundlage für die Etablierung eines Panels besonders geeigneter Metaboliten für die FFPE Gewebe-basierte Biomarkerforschung. In dieser Hinsicht könnten weitere Experimente zur Korrelation von MALDI *imaging*-Daten mit LC-MS-Experimenten zielführend sein.

3.1.5. **Fazit**

Die LC-MS-Metabolomics-Technologie stellt, aufgrund ihrer Robustheit und der Fähigkeit ein breites Spektrum strukturell unterschiedlicher Metaboliten zu erfassen, ein wichtiges Werkzeug zur metabolischen Charakterisierung von gefrorenen Gewebeproben dar.[8,97] Da FF Gewebe in Biobanken oft nur in limitierter Probenzahl vorhanden ist, sind entsprechende Metabolomics-Biomarker-Studien in ihrer Aussagekraft teilweise durch kleine Kohortengrößen limitiert. FFPE Proben hingegen werden weltweit in großer Anzahl in Pathologiearchiven gelagert und könnten daher, als alternatives Probenmaterial, zur Überwindung dieser Limitation beitragen. Zudem können sie bei Raumtemperatur gelagert werden, wodurch sich Platz- und Kostenvorteile ergeben.
Im vorliegenden Manuskript wird ein optimiertes Protokoll zur Probenaufarbeitung für LC-QTOF-MS-Metabolomics und -Lipidomics in klinisch archivierten FFPE Gewebeproben vorgestellt. Die Vorteile des etablierten Protokolls werden insbesondere in Bezug auf die verbesserte Analytik von Lipiden (z.B. TAG und GSL), die bekanntermaßen in der Krebsdiagnose und -therapie eine wichtige Rolle spielen,[98,99] deutlich. Das etablierte Protokoll zeichnet sich zudem durch seine hohe analytische und methodische Präzision sowie durch seine Wiederholbarkeit aus, was dessen Einsatz in groß angelegten Studien ermöglicht.
Die Eignung des optimierten Protokolls zur Unterscheidung von normalen und tumorösen FFPE Gewebeproben wurde in einer Machbarkeitsstudie demonstriert. Hierbei konnten metabolische Veränderungen beobachtet werden, die weitgehend mit den Ergebnissen von vorangegangenen Studien in FF Gewebe vergleichbar sind. Dennoch ist zu betonen, dass die Resultate bezüglich metabolischer Veränderungen in ccRCC-Gewebe nur als Hinweise interpretiert werden dürfen und es einer eingehenden Validierung in unabhängigen ccRCC Kohorten, unter Berücksichtigung

größerer Fallzahlen, bedarf. In dieser Hinsicht könnte eine Kreuzvalidierung biologischer Effekte via MALDI-*imaging* eine Rolle spielen, da die hier vorgestellten Ergebnisse eine erste Grundlage für eine synergistische Kombination von LC-MS und MALDI *imaging*[65] im Bereich Nierenkrebs-Metabolomics darstellen.
Darüber hinaus wurde das Protokoll zur Bewertung von präanalytischen Faktoren, die die Ergebnisse FFPE Gewebe basierter Studien beeinflussen könnten, eingesetzt. Hierdurch wird die Anwendbarkeit des neuen Protokolls auf eine Vielzahl zukünftiger Fragestellungen (z.B. Einfluss der ischämischen Zeit) unterstrichen.

3.2. **Publikation 2: Metabolic Drug Response Phenotyping in Colorectal Cancer Organoids by LC-QTOF-MS**

In der vorliegenden Veröffentlichung wird die Evaluierung von Extraktionsprotokollen zur metabolischen Phänotypisierung von in ECM kultivierten Organoiden des kolorektalen Karzinoms (*colorectal cancer*, CRC) mittels *non-targeted* LC-QTOF-MS beschrieben. Da, vor allem bei der Analyse sehr geringer Probenmengen, nicht informative Hintergrundsignale die Normalisierung und statistische Auswertung beeinträchtigen können,[100] wird ein Filterprozess zur Entfernung nicht zellabgeleiteter Daten eingeführt. Dieser basiert auf einem Signifikanztest (*p*-Wert Welch's Test) sowie auf *fold change* (FC)-Grenzwerten (Quotient biologisches Signal/Blanksignal) und zielt darauf ab auch kleine, aber potentiell relevante, biologische Signale im Datensatz zu behalten. Die Qualität der optimierten Methode wird durch die reproduzierbare Analyse der dosisabhängigen metabolischen Antwort von CRC Organoiden auf die Behandlung mit 5-FU, über drei unabhängige Experimente hinweg, gezeigt. In diesem Rahmen wird zudem die Wiederholbarkeit der gesamten Methodik demonstriert.

3.2.1. **Methodenentwicklung**

Um ein optimiertes Extraktionsprotokoll für die metabolische Phänotypisierung von in ECM kultivierten CRC-Organoiden via *non-targeted* LC-QTOF-MS zu ermitteln, wurden drei Methoden verglichen (siehe Abbildung 2). Die Protokolle wurden jeweils an fünf technischen Replikaten (fünffache Aufarbeitung von Organoidproben derselben Kultur und Passage) getestet. Für jedes Replikat wurden 1.000 Zellen ausgesät. Vor der Extraktion wurden die Zellen drei Tage kultiviert, was gemäß einer

in unabhängigen Experimenten ermittelten Verdopplungszeit von ~3,4 Tagen zu einer angenommenen Zahl von 2.000–3.000 Zellen führt (siehe Abbildung 2).

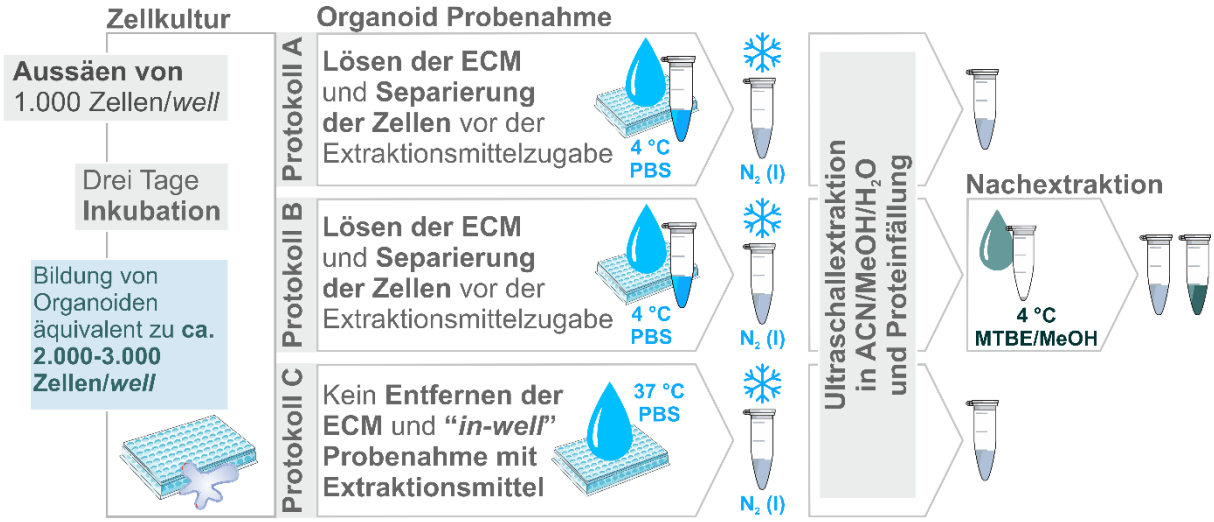

Abbildung 2 Schematische Darstellung von Kernelementen der evaluierten Extraktionsprotokolle. Die in die Extraktion eingehende Zellzahl von 2.000–3.000 Zellen wurde basierend auf der gesäten Zellzahl von 1.000 Zellen (ermittelt mit einer Zählkammer) und einer Verdopplungszeit von 3,4 Tagen (ermittelt in begleitenden Experimenten) abgeschätzt.

Aufgrund der physikochemischen Eigenschaften der genutzten ECM (Matrigel®) tritt bei niedrigen Temperaturen (< 8 °C)[101] eine Verflüssigung ein, da nicht genug Energie vorhanden ist, um die zur strukturellen Organisation notwendigen Bindungen aufrecht zu erhalten. Diese Eigenschaft wurde in den Protokollen A und B genutzt, um vor der Extraktion die Verflüssigung der ECM in kalter phosphatgepufferter Salzlösung (PBS, 4 °C) zu erzielen, was die Freisetzung der Organoide zur Folge hat. In einem weiteren Schritt wurden diese dann durch Zentrifugation abgetrennt. Im Gegensatz hierzu wurde im Protokoll C die Matrix mit warmer PBS (37 °C, Protokoll C) gewaschen, wodurch diese die Form eines intakten Hydrogels behielt. Es folgte bei Protokoll C eine „*in-well*"-Probenahme direkt mit der Extraktionslösung. In allen drei Protokollen wurde zur Extraktion eine Mischung aus Acetonitril, Methanol und Wasser (ACN/MeOH/H_2O, 2:2:1, *v*/*v*/*v*) genutzt. Dieses Extraktionsmittel wurde bereits zuvor in *targeted*[102] und *non-targeted*[42] Metabolomics-Methoden für humane Zellen sowie, in leicht modifizierter Zusammensetzung (ACN/MeOH/H_2O, 3:5:2, *v*/*v*/*v*), für Organoide[75] eingesetzt.

Aufgrund der eher polaren Natur des verwendeten Lösungsmittelgemisches könnte sich dessen Verwendung nachteilig auf die Extraktion von unpolaren Metaboliten (z.B. unpolare Lipide) auswirken. Daher wurde als Teil des Protokolls B untersucht, ob die

Detektion von Lipiden durch eine erneute Extraktion[8,103] des Zellpellets mittels Methyl-tert-butylether/Methanol (MTBE/MeOH, 3:1, *v*/*v*, einphasiges Gemisch) verbessert werden kann. Die Methodenqualität wurde auf Basis der Anzahl von detektierten, zellulären Metaboliten, sowie über die Methodenpräzision (median CVs der detektierten, zellulären Metaboliten) bewertet. Zur Auswahl der Metaboliten wurden folgende Kriterien angewandt: FC > 1 verglichen mit dem Median-Signal von ECM-Blindproben (ECM ohne enthaltene Zellen, die unter identischen Kulturbedingungen parallel zu den Organoid-Proben auf der Kulturplatte mitgeführt wurde) und *p*-Wert < 0,05 Welch's Test, *n* = 5 technische Wiederholungen.

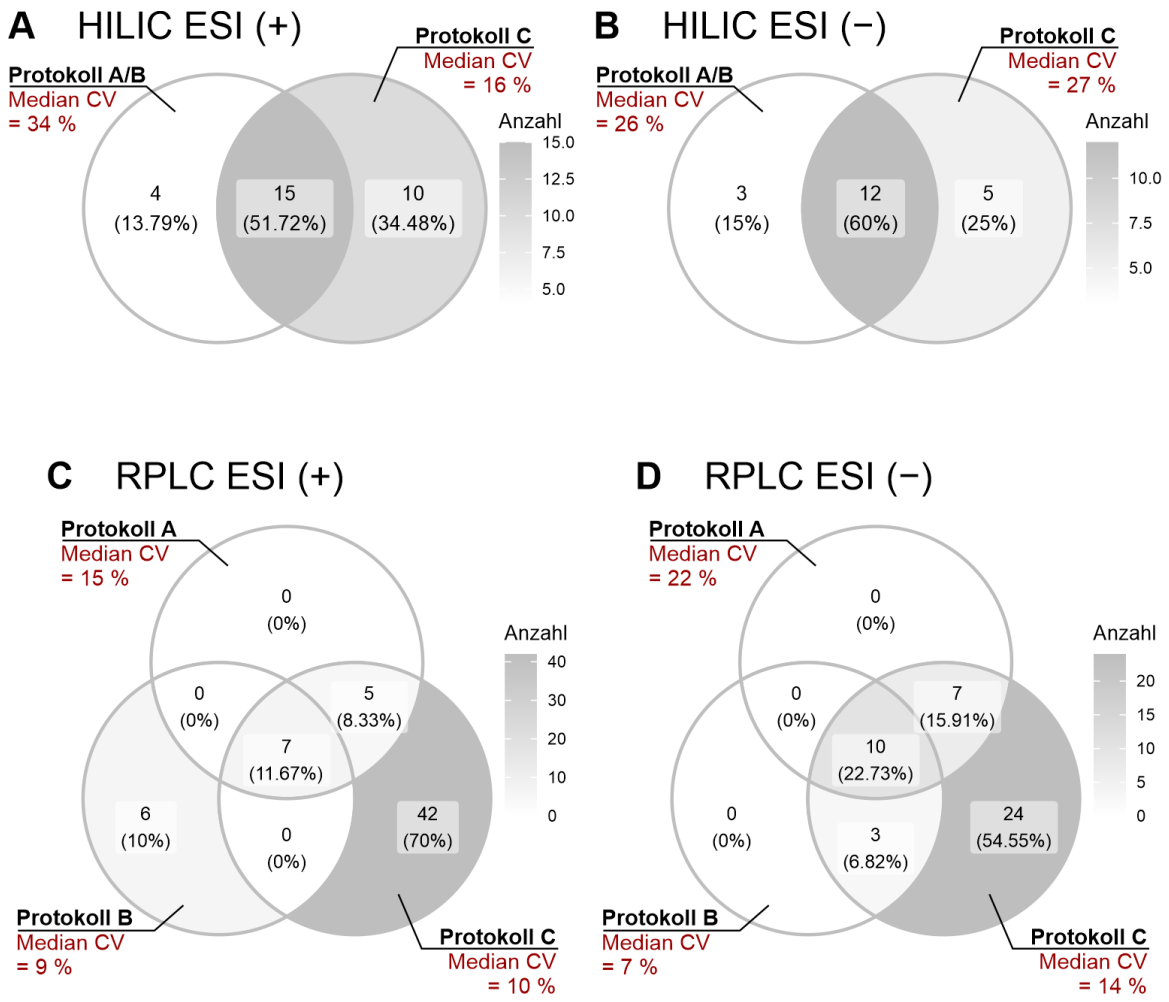

Abbildung 3 Überlappung der getesteten Extraktionsverfahren (siehe Abbildung 2) in Bezug auf Metaboliten, die in Organoid-Proben über dem ECM-Blank Signal detektiert wurden. A: HILIC ESI (+) Modus, B: HILIC ESI (−) Modus, C: RPLC ESI (+) Modus und D: RPLC ESI (−) Modus. In roter Schrift ist jeweils der für das Protokoll bestimmte Median-Variationskoeffizient (Median CV) der detektierten Metaboliten angegeben. Da die Protokolle A und B für die mittels HILIC analysierten Proben identisch sind, wurden diese gemeinsam ausgewertet (Diagramme A und B).

Hinsichtlich der Anzahl von detektierten zellulären Metaboliten, betrug die Überlappung zwischen den untersuchten Protokollen in Abhängigkeit des Analysenmodus 12–60 % (siehe Abbildung 3). Unter Verwendung des Protokolls C konnte, im Vergleich zu den Protokollen A und B, die höchste Anzahl an polaren Molekülen und Lipiden detektiert werden (siehe Abbildung 3). Insbesondere die Anzahl an Phospholipid-Spezies (z.B. PCs und PIs) und Sphingolipiden (z.B. Cers und Sphingomyeline [SMs]) wurde durch Anwendung des Protokolls C deutlich verbessert. Die geringere Anzahl an Lipidspezies, die mit den Protokollen A und B nachgewiesen wurden (siehe Abbildung 3 C und D), ist möglicherweise auf das direkte Waschen der Zellen mit PBS und den zusätzlichen Zentrifugationsschritt zurückzuführen. Hierbei könnten Zellen mechanisch beschädigt werden und/oder Lipide austreten. Beide Szenarien können ohne weitere Untersuchungen jedoch nicht belegt werden. Eine Verringerung der Signalintensitäten lipidähnlicher Spezies nach dem Waschen von CRC-Zelllinien mit PBS oder Wasser, wurde in der Literatur jedoch bereits beschrieben.[104]

An dieser Stelle ist hervorzuheben, dass die im Protokoll B eingeführte erneute Extraktion mit unpolarem Lösemittel (MTBE/MeOH, 3:1, *v*/*v*) die Detektion von Triglyceriden ermöglichte (z.B. TAG 52:2), welche in den auf einstufiger Extraktion mit ACN/MeOH/H_2O (2:2:1, *v*/*v*/*v*) beruhenden Protokollen (Protokoll A und C) nicht nachgewiesen werden konnten. Dies deutet darauf hin, dass die Polarität von ACN/MeOH/H_2O (2:2:1, *v*/*v*/*v*) zu hoch und dadurch die Extraktionskraft in Bezug auf unpolare Lipide zu gering ist, um die unpolaren TAGs aus den Organoid-Proben zu extrahieren.

Des Weiteren konnten mit Protokoll B zwar vergleichsweise wenig Lipide detektiert werden (jeweils 13 in RPLC ESI (+) und ESI (−), verglichen mit 44 und 54 in RPLC ESI (+) bzw. ESI (−) durch Protokoll C, siehe Abbildung 3), die Methodenpräzision des Protokolls war jedoch zufriedenstellend (medianer CV = 9%). Daher könnte Protokoll B für spezielle Fragestellungen, wie z.B. die Untersuchung TAG-haltiger Lipidtröpfchen, die als neue funktionelle Marker in CRC-Stammzellen vorgeschlagen wurden, geeignet sein.[105]

Zusammenfassend lässt sich feststellen, dass Protokoll C den besten Kompromiss zwischen präziser (median CVs von 10%–27%) Analytik und angemessener Abdeckung von detektierbaren Metaboliten und Lipiden (17–54 Metaboliten für alle Modi) darstellt. Dabei betrug die Überlappung zwischen den Chromatographie-Modi

(HILIC und RPLC) nur ca. 6 %, was demonstriert, dass die Kombination verschiedener chromatographischer Systeme zu Erhöhung der Metabolom-Erfassung führt. Protokoll C ermöglicht des Weiteren ein rasches Stoppen von Stoffwechselreaktionen (weniger als eine Minute pro Probe) und eine schnelle und einfache Probenaufarbeitung (~30 Proben in < 2 h) für die LC-QTOF-MS-Analyse. Die Beobachtung, dass eine zügige Extraktion mit wenigen Behandlungsschritten von Vorteil ist, steht im Einklang mit jüngsten Erkenntnissen. In einer kürzlich veröffentlichten Arbeit zur Entwicklung einer Extraktionsmethode für *targeted* Metabolomics-Analysen von Tumor-Sphäroiden, bestand das optimierte Protokoll aus einem schnellen Wasch-Schritt der Zellen auf der Zellkulturplatte mit anschließender methanolischer Extraktion.[106]

Neben der Schnelligkeit und Einfachheit der Probenaufarbeitung zeichnet sich das optimierte Protokoll durch seine Empfindlichkeit aus. Basierend auf der ermittelten Zellzahl von 2.000–3.000 Zellen/*well* (siehe Abbildung 2) und den sich aus dem Protokoll ergebenden Verdünnungsschritten kann eine injizierte Metabolitenmenge angenommen werden, die dem Metabolom von < 500 Zellen entspricht. Von den 273 Metaboliten, die in vorausgegangenen Experimenten[8] annotiert wurden und die zur Bewertung des Protokolls genutzt wurden, konnten in den Organoid-Extrakten 107 Metaboliten detektiert werden. Dies ist in Anbetracht der eingesetzten Zellzahl ein beachtliches Ergebnis.

3.2.2. Etablierung eines statistischen Ansatzes zur Ermittlung von *Features* mit signifikant und relevant erhöhtem Signal in Organoid-Proben im Vergleich zu ECM-Blindproben

Wie andere „omics“ basierte Messtechnologien unterliegen auch *non-targeted* Metabolomics-Experimente Schwankungen aufgrund von unerwünschtem experimentellem oder biologischem Rauschen. Für Organoide stellt besonders die ECM, als biologische Matrix, welche überwiegend aus Biomolekülen (z.B. Strukturproteinen) besteht, eine Quelle unerwünschter Signale dar. Diese können wiederum die anschließende Normalisierung und statistische Analyse beeinflussen (z.B. Verringerung der statistischen Aussagekraft aufgrund der hohen Anzahl von Tests). Daher sind statistische Ansätze zur Entfernung von nicht informativen Hintergrundsignalen aus dem zu interpretierenden Datensatz ein wichtiger Schritt, der im Bereich *non-targeted* Organoid-Metabolomics noch nicht eingehend betrachtet wurde.

Die Verwendung von FC-Grenzwerten (biologisches Signal/Blanksignal) zur Entfernung von Signalen mit unzureichender Abundanz in biologischen Proben ist eine gängige Filtermethode.[107,108]

Für unsere experimentellen Daten wurde ein zweistufiges Filterverfahren auf der Grundlage eines FC von 1,2 (median Signalfläche in Organoid-Proben/median Signalfläche in ECM-Blindproben) und einem nicht korrigierten Signifikanzniveau von 5 % (Welch‘s t-Test *p*-Wert < 0,05) als geeignet erachtet. Der ausgewählte FC-Grenzwert (Kriterium für ein relevant erhöhtes Signal) wurde auf der Grundlage ausgewählt, dass in *non-targeted* Metabolomics-Experimenten das Herausfiltern von Signalen mit geringer Reproduzierbarkeit über einen CV > 20 % (in QC-Replikaten) eine etablierte Methode ist.[107,109,110] Dieses Verfahren erkennt eine Variabilität von < 20 % als akzeptabel und daher als nicht relevant an. Auf dieser Basis wurde in unserem Verfahren ein Signalunterschied von ≥ 20 % (≙ FC Organoid Proben/ECM-Blindproben ≥ 1,2) als relevant erachtet und als Filterkriterium eingesetzt.

In den Daten der HILIC-Messungen erfüllten 19,5 % bzw. 26 % der *Features* und in den Daten der RPLC-Messungen 25,7 % bzw. 28,6 % der *Features* die strengen Filterkriterien, im positiven bzw. negativen Modus. Diese Signale wurden für die weitere statistische Datenanalyse genutzt, während die Mehrheit der Signale (> 70 %) herausgefiltert wurde. Die auf diese Art und Weise eliminierten *Features* werden als nicht informativer Hintergrund aus der Zellkulturumgebung oder als Verunreinigungen (z.B. aus dem Lösungsmittel)[44] betrachtet.

Die Eliminierung eines solchen Anteils an Daten ist nicht ungewöhnlich. Eine kürzlich veröffentlichte Studie etablierte ein ebenfalls auf Blindproben basiertes Filterverfahren und schloss 74 % bzw. 76 % der "*Features* mit geringer Qualität" aus öffentlich verfügbaren *non-targeted* Metabolomics-Datensätzen (Analysen von Urinproben sowie Zell-Extrakten) aus.[111] Bemerkenswert ist, dass durch unser zweistufiges Filterverfahren *Features* mit hoher Variabilität (max. CV = 214% vor und 76,1% nach der Filterung) entfernt wurden, was einen positiven Effekt unseres hier etablierten Ansatzes auf die Wiederholbarkeit der Analyse demonstriert.

Es wurde ferner beobachtet, dass einige Signale in ECM-Blindproben größer waren als in Organoid Proben (FC < 0,8, *p*-Wert < 0,05). Dies könnte auf Matrixeffekte[112] oder auf im Kulturmedium vorhandene Verbindungen, die in Abwesenheit von Zellen in der ECM angereichert werden,[113] zurückzuführen sein. Eine weitere Erklärung wären in der ECM vorkommende Moleküle,[112,114] die in Gegenwart von Zellen aufgenommen

und metabolisiert werden. Zur Untersuchung dieser Signale wurden über die CEU-*Mass mediator batch*-Suche[115,116] Metaboliten mit identischer exakten Masse (± 10 ppm) gesucht. Dieses Verfahren lieferte Hinweise, dass ein Teil der Verbindungen (9 *Features*) Di- und Tripeptide sein könnten. Da die genutzte ECM Matrigel in erster Linie aus Proteinen (unter anderem Laminin oder Kollagen) aufgebaut ist,[117] lässt sich die Detektion von Peptiden (Protein-Fragmenten) erklären. Zudem deuten einige exakte Massen (18 *Features*) auf Phospholipid-Spezies hin, die bereits zuvor als Bestandteile der eingesetzten ECM benannt wurden.[112] Darüber hinaus ergab die Datenbanksuche, dass kleine Moleküle wie organische Säuren (z.B. Cumarsäure) und freie Fettsäuren (z.B. C18:3) zu der komplexen ECM-Zusammensetzung beitragen können.

Eine vollständige Liste der exakten Massen und möglicher Metaboliten ist im ergänzenden Material der Publikation enthalten. Eine detaillierte proteomische und metabolomische Charakterisierung der verwendeten ECM sprengt jedoch den Rahmen unserer Studie und bedarf weiterer Untersuchungen.

3.2.3. **Machbarkeitsstudie: Frühe Metabolom-Antwort von CRC Organoiden auf Behandlung mit 5-Fluorouracil**

Um die Anwendbarkeit des optimierten Protokolls C in Kombination mit dem etablierten Filterverfahren nachzuweisen, wurde die frühzeitige Reaktion des Metaboloms von CRC-Organoiden auf die Behandlung mit 5-Fluorouracil (5-FU) untersucht.

Der Antimetabolit (Uracil-Analogon) 5-FU wird zur Behandlung des kolorektalen Karzinoms eingesetzt. Er wirkt durch die Hemmung der Thymidylat-Synthase[118,119] und den Einbau seiner Metaboliten in RNA und DNA.[119,120] Dabei wird die Enzym-Hemmung als Hauptmechanismus betrachtet[121], der durch Behinderung der DNA- und RNA-Synthese letztendlich zum Zelltod führt.

Um innerhalb einer 24-stündigen Behandlung spezifische Stoffwechselstörungen zu induzieren, wurden Konzentrationen angewandt, bei denen in Vorexperimenten keine Veränderungen der Zellviabilität und -morphologie nachweisbar waren (1, 10 und 100 µM). Zur Überprüfung der Wiederholbarkeit des gesamten Verfahrens wurden drei identische aber unabhängige Experimente durchgeführt. Die resultierenden Daten jedes Experiments wurden unabhängig voneinander ausgewertet und dann miteinander verglichen.

In Abhängigkeit des analytischen Modus konnten aus den LC-QTOF-MS Rohdaten 470–2.489 *Features* extrahiert werden. Diese wurden über das etablierte Verfahren (siehe Kapitel 3.2.2.) gefiltert und auf die Summe der Signale normalisiert (jedes *Feature* geteilt durch das Gesamtsignal der Probe). Die resultierenden Daten wurden auf *Features* untersucht, deren Intensität in Abhängigkeit der Arzneimitteldosis eine signifikante (Spearman-Korrelationskoeffizient r_S > |0.7|) und relevante (Benjamini-Hochberg korrigierter *p*-Wert < 0,05) Veränderung aufzeigten. Je nach Analysemodus wurden 3-29 *Features* identifiziert, die den angewandten Kriterien entsprachen. Von diesen korrelierten 12 *Features* in mindestens zwei von drei Experimenten signifikant und relevant mit der angewandten 5-FU-Konzentration (siehe Tabelle 3). Zehn dieser *Features* konnten zuvor beschriebenen Kriterien entsprechend (Zuordnungskriterien der *Metabolomics Standard Initiative* [MSI])[122] einzelnen Metaboliten zugeordnet werden, während zwei *Features* strukturell nicht näher charakterisiert werden konnten (siehe Tabelle 3). Die Übereinstimmung der Ergebnisse zwischen den drei Experimenten zeigt eine gute Wiederholbarkeit der etablierten *non-targeted* Metabolomics-Methode.

Tabelle 3: Signifikant und relevant regulierte Metaboliten nach 5-FU Behandlung in CRC Organoiden

Analytischer Modus	Anzahl der Experimente[1]	Median Masse	Retentions-zeit [min]	Regulation	Zuordnung	MSI Level[4]
HILIC ESI (+)	3	111.0436	3.21	↑	Cytosin[2]	2
		251.1026	2.42	↓	2'-Deoxyadenosin	1
		257.1022	3.21	↑	2'-O-Methylcytidin	1
	2	231.1468	5.95	↓	AC 4:0	2
		268.0828	4.89	↑	Inosin	2
		281.1115	7.90	↑	1-Methyladenosin	1
		633.4739	3.78	↓	LysoPC 26:1	2
HILIC ESI (−)	3	228.0731	2.12	↑	2'-Deoxyuridin	2
		264.0507	2.12	↑	na[3]	-
	2	536.1892	2.17	↑	na	-
RPLC ESI (+)	2	705.5341	6.75	↓	PC 30:0	2
		729.5347	6.48	↓	PC 32:2	2

[1] Experimente, in denen die Kriterien für eine signifikante und relevante Regulierung erfüllt wurden
[2] *In-source* Fragment von 2'-O-Methylcytidin
[3] Aufgrund des Fragments *m/z* 111.0211 im Spektrum von *m/z* 264.0507 wird eine Strukturverwandtschaft zu Uracil angenommen
[4] Zuordnung entsprechend den Kriterien der *Metabolomics Standard Initiative* (MSI) [122]
AC, Acylcarnitin; LysoPC, Lysophosphatidylcholin; PC, Phosphatidylcholin; na, nicht zugeordnet.

Bei gemeinsamer Analyse aller drei Experimente erfüllten 2'-Desoxyuridin, 2'-O-Methylcytidin, 1-Methyladenosin, 2'-Desoxyadenosin, AC 4:0 und PC 32:2 sowie das nicht zugeordnete *Feature m/z* 264 (Retentionszeit t_R = 2,1 min) immer noch die angewandten Kriterien (Spearman-Korrelationskoeffizient r_S > |0,7| und Benjamini-Hochberg angepasster *p*-Wert < 0,05) für eine signifikante und relevante dosisabhängige Regulation.

Die meisten Metaboliten, die durch die 5-FU-Behandlung reguliert wurden, sind direkt am Pyrimidin- und Purinmetabolismus beteiligt. Unsere Beobachtungen von erhöhten 2'-Desoxyuridin und gesenkten 2'-Desoxyadenosin Gehalten stimmen weitgehend mit den zellulären Mechanismen von 5-FU und früheren Befunden aus der Untersuchung von Zellkulturmodellen,[123–126] murinem Plasma[123] und klinischen Studien[127,128] überein. Der beobachtete dosisabhängige Anstieg des relativen Inosin-Gehalts könnte z.B. durch eine Hochregulierung der Inosin-Synthese erklärt werden, die durch einen erhöhten Verbrauch von Inosin aufgrund seiner Rolle als Ribose-1-phosphat-Spender im Aktivierungsweg von 5-FU ausgelöst wurde.[129] Die methylierten Nukleoside 2'-O-Methylcytidin und 1-Methyladenosin kommen in verschiedenen RNA-Spezies vor und sind nach der Behandlung von CRC Organoiden mit 5-FU in unseren Experimenten erhöht. Im Einklang mit den hier vorgestellten Ergebnissen beschreibt eine kürzlich erschienene Publikation einen beträchtlichen Anstieg des intrazellulären 1-Methyladenosin-Spiegels nach Behandlung von HCT116-Darmkrebszellen mit 5-FU.[130] Darüber hinaus wurden bereits tRNA-Modifikationen durch Einbau von 2'-O-Methylcytidin in 5-FU-behandelten *Escherichia coli* beschrieben.[131]

Des Weiteren weisen verringerte Konzentrationen von AC 4:0, PC 30:0 und PC 32:2 auf eine Beeinflussung des Lipidmetabolismus hin. Veränderungen der intrazellulären AC-Spiegel nach 5-FU Behandlung wurden bereits in einer früheren Untersuchung an verschiedenen CRC-Zelllinien[124] beschrieben. Die Ergebnisse waren jedoch zwischen den verschiedenen getesteten Zelllinien nicht konsistent und sind in gewissem Maße gegensätzlich zu unseren Beobachtungen. Darüber hinaus wurde in früheren Untersuchungen berichtet, dass erhöhte Mengen an Phospholipiden sowie eine veränderte Phospholipid-Zusammensetzung der Zellmembran charakteristisch für CRC sind.[132–134] Dementsprechend könnte die gezielte Behandlung von Tumorzellen zu einer Senkung der PC-Werte führen. Eine eingehende Interpretation der Störung des Lipidstoffwechsels in 5-FU-behandelten CRC Organoiden übersteigt jedoch den Rahmen dieser Machbarkeitsstudie. Es ist zu betonen, dass es sich bei den

beschriebenen Resultaten um vorläufige Ergebnisse handelt und weitere Untersuchungen in größeren Kohorten mit Organoiden von verschiedenen Spendern erforderlich sind, um diese zu bestätigen.

3.2.4. **Fazit**

Die Verwendung von Organoiden als innovatives *in vitro* Modellsystem zur Erforschung pathobiologischer Mechanismen und pharmakologischer Fragestellungen steigt stetig. Dennoch finden sich derzeit nur wenige Studien die eine Analyse des Metaboloms bzw. Lipidoms von Organoiden beschreiben. Über eine systematische Optimierung der genutzten Protokolle für *non-targeted* LC-MS-Metabolomics wird hierbei nicht berichtet.

In der vorliegenden Arbeit wurde über eine eingehende Methodenoptimierung ein neues Protokoll für *non-targeted* Metabolomics- und Lipidomics-Analysen von in ECM kultivierten CRC Organoiden via LC-QTOF-MS etabliert. Das neue Protokoll ermöglicht die präzise Detektion eines breiten metabolischen Spektrums aus dem Extrakt von weniger als 3.000 Zellen (< 500 Zellen pro Injektion).

Die Ergebnisse der durchgeführten Machbarkeitsstudie demonstrieren, dass das etablierte Protokoll die Erfassung frühzeitiger metabolischer Reaktionen von CRC Organoiden auf die Behandlung mit 5-FU ermöglicht. Dabei waren die Ergebnisse über drei unabhängige Experimente hinweg vergleichbar, was die hohe Wiederholpräzision der gesamten Methodik belegt.

Das vorgestellte Protokoll zeichnet sich durch seine Schnelligkeit und Einfachheit aus (benötigte Zeit für die Extraktion von ca. 30 Proben < 2 h). Diese besonderen Eigenschaften ebnen den Weg für weitere Untersuchungen von metabolischen Veränderungen in humanen CRC Organoiden sowie den Einsatz des Protokolls in größer angelegten Studien.

In zukünftigen Projekten könnte eine Anpassung des neuen Protokolls zur metabolischen ^{13}C-Stoffflussanalyse[135] in 3D-Organoid-Modellen angestrebt werden. Eine Verknüpfung komplexer Flussanalysen mit der innovativen Organoid-Technologie könnte einen wichtigen Beitrag leisten, um molekulare Mechanismen der Pathobiochemie sowie von Medikamentenwechselwirkungen besser zu verstehen.

3.3. Manuskript in Vorbereitung: Performance comparison of narrow-bore and capillary liquid-chromatography for non-targeted metabolomics profiling of small sample amounts by LC-QTOF-MS

Die Reduzierung des Säuleninnendurchmessers (i.D.) und der Flussrate in der Chromatographie führt zu einer geringeren Verdünnung der injizierten Probenbande. Dies wiederum kann zu einer Erhöhung der Konzentration in der Ionenquelle des MS und damit zu einer enormen Steigerung der Messempfindlichkeit führen.[14,15] Daher wurden in den letzten Jahrzenten vermehrt miniaturisierte Chromatographie-Systeme entwickelt, die ein wertvolles Werkzeug für Metabolomics-Untersuchungen im Spurenbereich[136] und zur Analyse kleinster Probenmengen[137] geworden sind.
Non-targeted Metabolomics-Analysen zur Entdeckung potentieller prognostischer und diagnostischer Biomarker könnten vom Einsatz chromatographischer Systeme mit reduzierten Flussraten (z.B. Kapillar-Flüssigkeitschromatographie, CapLC, siehe in Kapitel 1.1., Tabelle 1 eingeführte Nomenklatur für Flüssigkeitschromatographie-Systeme) profitieren, insbesondere wenn biologisches Probenmaterial nur in geringer Menge vorliegt (z.B. Metastasen oder Tumor-Organoide, siehe auch Publikation 2 in dieser Arbeit).

In dem hier behandelten Teilprojekt der Dissertation wurde ein neues CapLC-System in Betrieb genommen, das aus einem Zirconium™ CUBE Autosampler (Prolab, Reinach, Schweiz) und einer Zirconium™ Ultra Nano- und Micro-UHPLC Pumpe (Prolab) bestand. Die Pumpe wurde über eine speziell vom Hersteller (Prolab) angefertigte Mikro-ESI-Ionenquelle (Prolab) mit dem 6550 iFunnel QTOF-MS (Agilent Technologies, Waldbronn, Deutschland) verbunden.
Die Leistungsfähigkeit der neuen Anlage, zur *non-targeted* Metabolomics-Analyse kleiner Probenmengen, wurde mit der bereits in den vorangegangenen Arbeiten (Publikation 1 und 2 dieser Dissertation) genutzten analytischen Plattform für *non-targeted* Metabolomics mittels LC-QTOF-MS (nachfolgend *narrow-bore* LC genannt),[8] die auf analytischen Flussraten (0,4 mL/min, siehe Tabelle 1) basiert, verglichen.

Die Qualität der Analysen wurde hierbei auf der Basis einer gepoolten QC Probe aus FFPE Nierengewebeextrakten vom Schwein in Bezug auf folgende Parameter bewertet:

- die Anzahl detektierbarer *Features*
- das S/N-Verhältnis (als allgemein akzeptiertes Maß für die analytische Sensitivität[138])
- die Peakfläche und -höhe (als Maß für die Signalintensität[139])
- die Messpräzision

Zur Bewertung der letzten drei Punkte wurden die Signale (extrahierte Ionenchromatogramme, *extracted ion chromatograms*, EICs) von 16 annotierten Metaboliten, die zu den Klassen der LysoPEs, der Aminosäuren, der Purin-Derivate, der Nukleoside und der organischen Säuren gehören, genutzt.
Um die bestmögliche Vergleichbarkeit der verwendeten LC-Systeme zu erzielen, wurden beide Systeme mit Säulen identischer Länge (150 mm) und identischer stationärer Phase (BEH Amide HILIC-Material, Partikelgröße: 1,7 µm, hergestellt von Waters) betrieben. Zudem wurde die gleiche Menge (1 µL) an Probenextrakt injiziert und die chromatographischen Bedingungen (Gradient und Fließmittel) wurden, mit Ausnahme des Säulendurchmessers (2,1 mm vs. 0,3 mm) und der Flussraten (400 µL/min vs. 5 µL/min), so ähnlich wie möglich gestaltet. Selbiges gilt für die Quellenparameter des QTOF-MS-Systems (siehe Methodenteil des angehängten Manuskriptes in Bearbeitung).

Des Weiteren wurde in einem unabhängigen Experiment der Einfluss des chromatographischen Gradienten (Mischungsverhältnis der Fließmittel A und B) auf die CapLC-QTOF-MS-Analyse von Gallensäure-Referenzsubstanzen untersucht.

3.3.1. **Plattform-Vergleich**

Abbildung 4 A zeigt exemplarisch die Gesamtionenchromatogramme (*total ion chromatograms*, TICs, ESI (−) Modus) der Analyse von FFPE Schweinenierengewebeextrakten mittels *narrow-bore* oder CapLC-QTOF-MS. Es ist ersichtlich, dass die Gesamtsignalintensität im Fall der *narrow-bore* LC (blaue Linie) in einem höheren Wert (Basislinie ~ 1.3×10^7 counts) resultierte als bei Verwendung der CapLC (schwarze Linie, Basislinie ~ 0.3×10^7 counts). Diese Unterschiede in den TICs beider Methoden resultierten jedoch nicht in nennenswerten Unterschieden in der

Anzahl an detektierten *Features*. So konnten unter Verwendung der CapLC 140 und unter Verwendung der *narrow-bore* 141 *Features* detektiert werden.

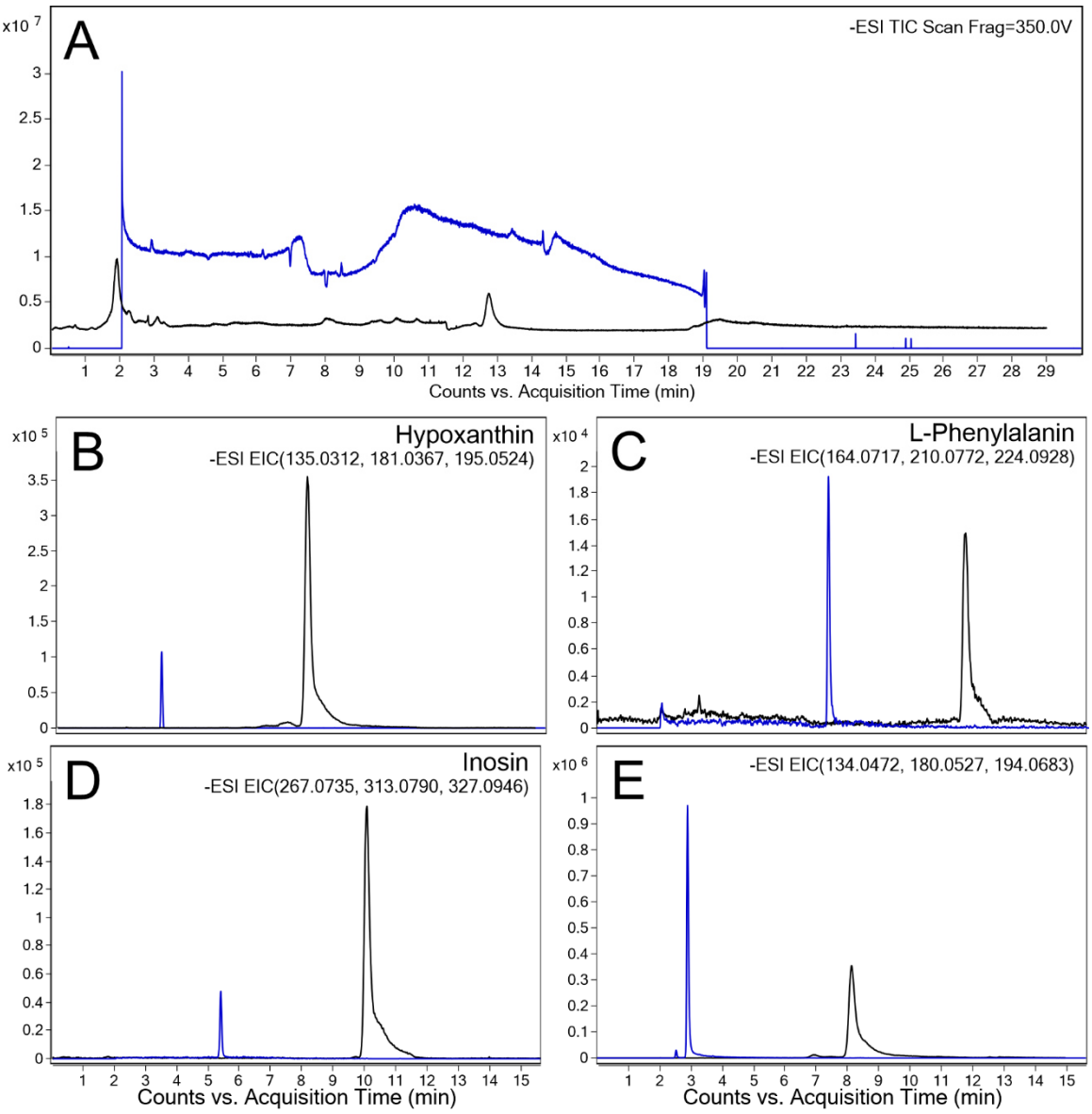

Abbildung 4 (A) Gesamtionenchromatogramme einer QC Probe von FFPE Gewebeextrakten der Schweineniere analysiert mittels *narrow-bore* LC-QTOF-MS (blau) und CapLC-QTOF-MS (schwarz) im ESI (−) Modus. Extrahierte Ionenchromatogramme der Metaboliten (B) Hypoxanthin, (C) L-Phenylalanin, (D) Inosin und (E) Adenin, analysiert in einer QC Probe von FFPE Nierengewebeextrakten des Schweins mittels *narrow-bore* LC-QTOF-MS (blau) und CapLC-QTOF-MS (schwarz) im ESI (−) Modus.

Hierbei sei erwähnt, dass für diesen Vergleich alle detektierbaren *Features* die zwischen der D-Pantothensäure (frühe Elution, siehe Tabelle 4) und L-Carnitin (späte Elution, siehe Tabelle 4) eluieren, herangezogen wurden. Dies ist dadurch zu

begründen, dass in den Messungen mittels *narrow-bore* LC (siehe Abbildung 4 A, blaue Linie) der Fluss während der ersten 2 min, sowie ab Minute 19, in den Lösemittelabfall geleitet wurde, was eine Methode zum Schutz der analytischen Säule und der Ionenquelle vor Verunreinigungen durch unerwünschte Matrixkomponenten ist und üblicherweise bei der LC-MS basierten Analyse komplexer Proben angewandt wird.[140,141] Mit dem verwendeten CapLC-System ist es technisch nicht möglich Teile des Lösemittelflusses in den Abfall zu führen.

In Bezug auf die Empfindlichkeit der Analyse konnte hinsichtlich des S/N-Verhältnisses für 50 % der zur Bewertung herangezogenen Metaboliten eine Verbesserung erreicht werden (siehe Tabelle 4). Der stärkste Effekt zeigte sich hierbei für die Nukleoside Adenosin, Guanosin, Uridin und Inosin (3 bis 5-fach erhöhtes S/N-Verhältnis) sowie für Succinat (4-fach erhöhtes S/N-Verhältnis). Für die zu den LysoPEs, Aminosäuren und organischen Säuren gehörenden Metaboliten konnte in der CapLC-Analyse keine, oder nur eine leichte Verbesserung der Empfindlichkeit (Quotient der S/N-Verhältnisse = 1–2, siehe Tabelle 4) erzielt werden. Lactat, dessen S/N-Verhältnis verringert war (Quotient der S/N-Verhältnisse = 0,4), bildet hierbei eine Ausnahme.

In Hinblick auf die Signalintensität waren die Peakflächen bei Verwendung der CapLC-Analyse für alle bewerteten Metaboliten im Vergleich zur *narrow-bore* LC erhöht (FC [Fläche $_{\text{CapLC}}$/Fläche $_{\text{narrow-bore LC}}$] > 1, siehe Tabelle 4). Im Gegensatz hierzu war die Signalhöhe für vier Metaboliten (Adenin, D-Pantothensäure, L-Leucin und L-Phenylalanin) reduziert (FC (Höhe $_{\text{CapLC}}$/Höhe $_{\text{narrow-bore LC}}$) < 1, siehe Tabelle 1 sowie Abbildung 4 C und E).
Die niedrigere Höhe der Peaks lässt sich teilweise auf die relativ schlechte Peakform (breite Peaks mit *Tailing*, siehe Abbildung 4 B–E, schwarze Linien) zurückführen. Die Höhe eines Peaks repräsentiert die maximale Signalintensität (maximale Ionenzahl, die in der Ionenquelle zu einem Zeitpunkt erreicht wurde), während die Fläche alle Intensitäten über die Zeit der Elution einer Verbindung aufsummiert. Da die Fläche aller Metaboliten, die zur Bewertung der Signalintensität herangezogen wurden, bei Verwendung der CapLC höher war, würde sich auch die Signalhöhe nach Optimierung der chromatographischen Bedingungen (z. B. Gradient oder Säulenmaterial zur Erzielung schmälerer Peaks) steigern.

Tabelle 4: Ermittelte Ergebnisse für Signalintensität (Flächenverhältnis und Höhenverhältnis), Empfindlichkeit (S/N-Verhältnis) und Messpräzision der annotierten Metaboliten

Metaboliten	***Narrow-bore* LC**			**CapLC**			**Verglichene Parameter**		
	RT [min]	CV[1] [%]	S/N	RT [min]	CV[1] [%]	S/N	FC der Fläche[2]	FC der Höhe[3]	FC der S/N[4]
Adenin	2.9	1.7	462	8.2	8.9	9	2	0.4	1
Adenosin	3.3	2.1	9	8.4	8.3	8	9	2	3
D-Pantothen-säure	3.1	2.4	30	5.4	11.5	12	3	0.6	1
Guanosin	7.3	4.3	12	11.8	9.4	9	9	2	3
Hypoxanthin	3.4	1.3	77	8.0	8.9	9	16	3	1
Inosin	5.4	1.8	24	10.1	11.8	12	18	4	5
Lactat	4.0	10.9	34	8.0	18.6	19	3	2	0.4
L-Carnitin	8.9	14.0	4	13.5	20.2	20	7	2	2
L-Isoleucin	7.7	8.2	10	12.2	27.1	27	5	3	1
L-Leucin	7.4	6.3	20	11.9	19.4	19	3	0.4	2
L-Phenylalanin	7.4	5.2	23	11.8	20.7	21	3	0.8	1
LysoPE 16:0	6.0	3.5	15	9.5	22.0	22	7	1	2
LysoPE 18:0	5.6	2.1	77	9.3	11.8	12	10	2	1
LysoPE 20:4	5.8	1.2	96	9.4	21.6	22	8	1	1
Succinat	3.4	7.6	6	4.9	11.0	11	8	2	4
Uridin	3.3	1.7	7	7.9	8.4	8	15	3	3

[1] Variationskoeffizienten der Flächen über wiederholte Injektionen (n = 4)
[2] (Mittlere Fläche CapLC/Mittlere Fläche *narrow-bore* LC), Mittelwert über jeweils vier Probeninjektionen ermittelt
[3] (Mittlere Höhe CapLC/Mittlere Höhe *narrow-bore* LC), Mittelwert über jeweils vier Probeninjektionen ermittelt
[4] (S/N-Verhältnis CapLC/S/N-Verhältnis *narrow-bore* LC), in jeweils einer repräsentativen Messung ermittelt
RT, Retentionszeit; S/N, Signal/Rausch-Verhältnis; CV, Variationskoeffizient; FC, *fold change* (Quotient)

Der Effekt einer Anpassung des Gradienten auf die Signalintensität wurde in unabhängigen Experimenten durch die Analyse von Gallensäure-Referenzlösungen untersucht. Bei Verwendung eines steileren Flussgradienten (Anstieg von 2 %–95 % Eluent B in 3–10 min statt von 5 %–95 % Eluent B in 3–18 min), wurde für Taurocholsäure (TCA) eine bis zu 79-fache Erhöhung der Signalintensität (bestimmt über das Flächenverhältnis, n = 1, siehe Abbildung 5 A) erreicht. Im Vergleich hierzu wurde mit dem flacheren Gradienten ein Quotient der Flächen (n = 1, siehe Abbildung 5 B) von 33 erzielt. Die Anpassung der chromatographischen Bedingungen führte zudem zu einer deutlichen Verbesserung der Peakform und einer Verringerung des beobachteten *Tailings* (vgl. Abbildung 5 A mit Abbildung 5 B). Auch wenn diese Steigerung der Intensität mit einer leichten Verringerung des S/N-Verhältnisses von 86 (*narrow-bore* LC) auf 79 (CapLC) einherging, zeigt dieses Ergebnis, dass unter optimaleren chromatographischen Bedingungen eine bemerkenswerte Steigerung der

Signalintensität bestimmter Metaboliten durch den Einsatz des hier getesteten CapLC-Systems möglich ist.

An dieser Stelle sei zudem anzumerken, dass der genutzte Prototyp der Mikro-ESI-Quelle aus technischen Gründen eine Nutzung des direkt angeschlossenen Säulenofens nicht zuließ. Die Temperatur ist ein wichtiger Parameter in der Optimierung von HILIC-Chromatographie-Methoden.[142] Daher sollte nach einer technischen Optimierung des ESI-Interface zudem der Einfluss der Temperatur auf die Peakform und damit auf die Signalintensität und das S/N-Verhältnis überprüft werden.

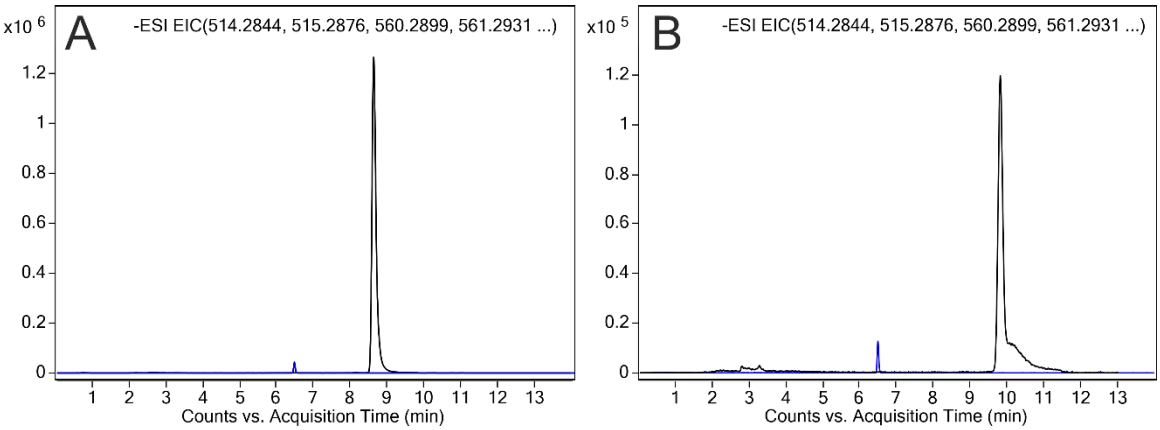

Abbildung 5 Extrahierte Ionenchromatogramme von Taurocholsäure (TCA), analysiert mit *narrow-bore* LC-QTOF-MS (blau) und CapLC-QTOF-MS (schwarz) im ESI (−) Modus: (A) Analyse einer Standardlösung mit 0,2 pmol TCA/µL unter den gleichen Bedingungen wie im Methodenteil des angehängten Manuskripts beschrieben mit einer angepassten Gradientenelution (0–3 min, 2% B; 3–10 min, 2–95% B; 10–30 min, 95% B) für die CapLC-Analyse; (B) Analyse einer Standardlösung mit 0,1 pmol TCA/µL unter den gleichen Bedingungen wie im Methodenteil des angehängten Manuskripts beschrieben ohne Anpassung des Gradienten für die CapLC-Analyse (0−3 min, 5% B; 3−18 min, 5−95% B; 18−30 min, 95% B).

Unsere Experimente zeigen, dass die Leistung der CapLC-Analyse in Bezug auf die Signalintensität und Empfindlichkeit (Bewertet über das S/N-Verhältnis) zwischen den verschiedenen Metabolitenklassen stark variiert. Mit Ausnahme von Adenin wurde für alle Metaboliten die zu den Purinen und Nukleosiden gehören (Adenosin, Guanosin, Hypoxanthin, Inosin und Uridin) bei Einsatz der CapLC eine deutliche Steigerung der Signalintensität beobachtet, auch wenn im Falle von Hypoxanthin das S/N-Verhältnis (siehe Abbildung 4 B, Tabelle 4) nicht verbessert wurde. In der Analyse von LysoPE-Spezies wurde hingegen eine eher moderate Verbesserung von Signalintensität und S/N-Verhältnis beobachtet (Tabelle 4), während hinsichtlich der Aminosäuren und

organischen Säuren eine nur geringfügige (z.B. Isoleucin, Tabelle 4) oder keine (z.B. Phenylalanin, Tabelle 4 und Abbildung 4 C) Verbesserung zu beobachten war. Insgesamt zeigte Inosin die stärkste Verbesserung des S/N-Verhältnisses und der Signalintensität (siehe Abbildung 4 D), während die Analyse von Adenin durch Nutzung der CapLC eher verschlechtert war (siehe Abbildung 4 E).

In Hinblick auf die Messpräzision (CV der Flächen, n = 4) konnten hingegen keine spezifischen Unterschiede zwischen verschiedenen Metabolitenklassen beobachtet werden. Hier war für jeden der 16 untersuchten Metaboliten eine durchweg schlechtere Präzision des CapLC-Systems (median CV = 11,8 %) im Vergleich zum *narrow-bore* LC-System (median CV = 2,9 %, siehe Tabelle 4) feststellbar. Im Falle von fünf Metaboliten (31 %) wurde ein CV > 20 % bestimmt, während bei Nutzung des *narrow-bore* LC-Systems alle CVs < 15 % lagen. Dennoch lagen die ermittelten CVs weitestgehend in einem für *non-targeted* Metabolomics-Analysen akzeptablen Bereich von CV < 20%. [107,110] An dieser Stelle ist zu erwähnen, dass die analytische Präzision im Bereich *non-targeted* Metabolomics typischerweise durch in regelmäßigen Abständen über die Messserie verteilte, wiederholte Injektionen einer gepoolten QC Probe bestimmt wird. Im Laufe der hier durchgeführten Vergleichsmessungen wurde jedoch festgestellt, dass es die aktuelle Softwareversion des CapLC-Systems nicht zulässt, im Verlauf einer Messserie, an eine zuvor vermessene Probe zurück zu springen.

In den begleitenden Experimenten mit reinen Gallensäure-Referenzlösungen konnte eine verbesserte Messpräzision (CV [%]: Glycocholsäure [GCA], 4,2; Glycolithocholsäure [GLCA], 6,2; TCA, 4,0; Taurolithocholsäure [TLCA], 7,1; Median, 5,2) erzielt werden. Ob diese hohe Messpräzision auch in Anwesenheit biologischer Matrix reproduziert werden kann, muss jedoch noch überprüft werden. Darüber hinaus sollte untersucht werden, ob die analytische Präzision durch Anpassung der Methode (z. B. *Modifier* in der mobilen Phase[143]) oder des verwendeten Systems (z. B. Ausstattung des genutzten ESI-Quellen-Prototypen mit ACN-angereichertem Stickstoffgas zur effizienteren Ionisierung und Stabilisierung des Elektrosprays[144]) für weitere Metaboliten-Klassen verbessert werden kann.

3.3.2. **Fazit**

Zusammenfassend lässt sich feststellen, dass durch Verwendung des hier evaluierten CapLC-Systems für einzelne Metaboliten (z.B. Nukleoside) eine deutliche Erhöhung der Signalintensität und eine Verbesserung des S/N-Verhältnisses erreicht werden konnte. Zudem ist die Analyse bestimmter Metaboliten (z.B. Adenosin und Uridin in FFPE Schweinenierengewebeextrakten sowie die Gallensäuren GCA, GLCA, TCA und TLCA in Referenzlösungen) mit zufriedenstellender Messpräzision möglich. Ein bedeutender Nachteil des getesteten CapLC-Systems ist jedoch die Tatsache, dass die aktuelle Software nicht die Möglichkeit bietet, über den Verlauf einer Messreihe hinweg wiederholt aus ein und demselben *Vial* zu injizieren. Da für *non-targeted* Metabolomics-Analysen die wiederholte Injektion von QC-Proben zur Überwachung der analytischen Präzision (und auch Korrektur von Signalschwankungen im Verlauf der Messreihe) ein Kernelement ist, kann das hier getestete System nur eingesetzt werden, wenn genügend Probe vorhanden ist, um für jede QC-Injektion ein eigenes *Vial* zu befüllen. Aus diesem Grund ist das getestete System in der aktuellen Softwarekonfiguration nur in limitierter Weise für *non-targeted* Metabolomics-Analysen geeignet.

Die Ergebnisse dieser Untersuchung deuten jedoch darauf hin, dass das verwendete CapLC-System für spezielle *targeted* Metabolomics-Ansätze geeignet sein könnte. Dabei wäre z.B. die gezielte und durch stabil-isotopenmarkierte interne Standards unterstützte Analyse von Metaboliten mit besonders niedrigen Konzentrationen, wie beispielsweise Oxylipinen in Plasma und Thrombozyten,[136] eine denkbare Anwendung. Des Weiteren könnte die gezielte Analyse spezifischer Metabolitenklassen (z.B. LysoPCs und SM), die zuvor als differentielle Metaboliten zwischen den Nierentumor-Subtypen des klarzelligen und chromophoben Nierenzellkarzinoms identifiziert wurden,[10] in Kombination mit bildgebender Massenspektrometrie und *laser capture microdissection* definierter Regionen aus FFPE Gewebeschnitten, ein nützlicher Ansatz zur Findung von Biomarkern zur klinischen Tumor-Subtyp-Klassifizierung sein.

Zur abschließenden Beurteilung einer möglichen Umsetzung dieser Anwendungsmöglichkeiten steht jedoch noch eine eingehende Bewertung des hier verwendeten CapLC-Systems, in Hinblick auf dessen Eignung für die gezielte quantitative Analyse von Metaboliten, aus.

Literaturverzeichnis

1. Cortes, M., García-Cañaveras, J. C., Pareja, E. & Lahoz, A. in *Biomarkers in Liver Disease,* edited by V. B. Patel & V. R. Preedy (Springer Netherlands, Dordrecht, 2017).
2. Buck, A. *et al.* High-resolution MALDI-FT-ICR MS imaging for the analysis of metabolites from formalin-fixed, paraffin-embedded clinical tissue samples. *The Journal of pathology* **237,** 123–132; 10.1002/path.4560 (2015).
3. Schmidt, C. W. Metabolomics. What's happening downstream of DNA. *Environmental health perspectives* **112,** A410-5; 10.1289/ehp.112-a410 (2004).
4. Bouatra, S. *et al.* The Human Urine Metabolome. *PloS one* **8,** e73076; 10.1371/journal.pone.0073076 (2013).
5. Psychogios, N. *et al.* The Human Serum Metabolome. *PloS one* **6,** e16957; 10.1371/journal.pone.0016957 (2011).
6. Corona, G., Rizzolio, F., Giordano, A. & Toffoli, G. Pharmaco-metabolomics. An emerging "omics" tool for the personalization of anticancer treatments and identification of new valuable therapeutic targets. *Journal of cellular physiology* **227,** 2827–2831; 10.1002/jcp.24003 (2012).
7. Wang, R., Li, B., Lam, S. M. & Shui, G. Integration of lipidomics and metabolomics for in-depth understanding of cellular mechanism and disease progression. *Journal of genetics and genomics = Yi chuan xue bao* **47,** 69–83; 10.1016/j.jgg.2019.11.009 (2020).
8. Leuthold, P. *et al.* Comprehensive Metabolomic and Lipidomic Profiling of Human Kidney Tissue. A Platform Comparison. *Journal of proteome research* **16,** 933–944; 10.1021/acs.jproteome.6b00875 (2017).
9. Beloribi-Djefaflia, S., Vasseur, S. & Guillaumond, F. Lipid metabolic reprogramming in cancer cells. *Oncogenesis* **5,** e189; 10.1038/oncsis.2015.49 (2016).
10. Schaeffeler, E. *et al.* Metabolic and Lipidomic Reprogramming in Renal Cell Carcinoma Subtypes Reflects Regions of Tumor Origin. *European urology focus*; 10.1016/j.euf.2018.01.016 (2018).
11. Armitage, E. G. & Southam, A. D. Monitoring cancer prognosis, diagnosis and treatment efficacy using metabolomics and lipidomics. *Metabolomics : Official journal of the Metabolomic Society* **12,** 146; 10.1007/s11306-016-1093-7 (2016).

12. Lu, W. *et al.* Metabolite Measurement. Pitfalls to Avoid and Practices to Follow. *Annual review of biochemistry* **86,** 277–304; 10.1146/annurev-biochem-061516-044952 (2017).
13. Sanders, K. L. & Edwards, J. L. Nano-liquid chromatography-mass spectrometry and recent applications in omics investigations. *Analytical methods : advancing methods and applications* **12,** 4404–4417; 10.1039/d0ay01194k (2020).
14. Asensio-Ramos, M., Fanali, C., D'Orazio, G. & Fanali, S. in *Liquid Chromatography* (Elsevier2017), pp. 637–695.
15. Smith, N. W., Legido-Quigley, C., Marlin, N. D., Melin, V. & Mutton, I. in *Reference Module in Chemistry, Molecular Sciences and Chemical Engineering* (Elsevier2013).
16. Abian, J. & Carrascal, M. in *Emerging technologies in protein and genomic material analysis* (Elsevier2003), pp. 39–73.
17. Rapp, E. & Tallarek, U. Liquid flow in capillary (electro)chromatography. Generation and control of micro- and nanoliter volumes. *J. Sep. Science* **26,** 453–470; 10.1002/jssc.200390062 (2003).
18. Baptista, R., Fazakerley, D. M., Beckmann, M., Baillie, L. & Mur, L. A. J. Untargeted metabolomics reveals a new mode of action of pretomanid (PA-824). *Scientific reports* **8,** 5084; 10.1038/s41598-018-23110-1 (2018).
19. Chen, Y. *et al.* Integrated proteomics and metabolomics reveals the comprehensive characterization of antitumor mechanism underlying Shikonin on colon cancer patient-derived xenograft model. *Scientific reports* **10,** 14092; 10.1038/s41598-020-71116-5 (2020).
20. Lehotay, D. C. *et al.* LC–MS/MS progress in newborn screening. *Clinical Biochemistry* **44,** 21–31; 10.1016/j.clinbiochem.2010.08.007 (2011).
21. Wilcken, B. *et al.* Expanded newborn screening. Outcome in screened and unscreened patients at age 6 years. *Pediatrics* **124,** e241-8; 10.1542/peds.2008-0586 (2009).
22. Chace, D. H., Sherwin, J. E., Hillman, S. L., Lorey, F. & Cunningham, G. C. Use of phenylalanine-to-tyrosine ratio determined by tandem mass spectrometry to improve newborn screening for phenylketonuria of early discharge specimens collected in the first 24 hours. *Clinical chemistry* **44,** 2405–2409; 10.1093/clinchem/44.12.2405 (1998).

23. WARBURG, O. On the origin of cancer cells. *Science (New York, N.Y.)* **123,** 309–314; 10.1126/science.123.3191.309 (1956).
24. Coller, H. A. Is cancer a metabolic disease? *The American journal of pathology* **184,** 4–17; 10.1016/j.ajpath.2013.07.035 (2014).
25. Sun, H., Chen, L., Cao, S., Liang, Y. & Xu, Y. Warburg Effects in Cancer and Normal Proliferating Cells. Two Tales of the Same Name. *Genomics, proteomics & bioinformatics* **17,** 273–286; 10.1016/j.gpb.2018.12.006 (2019).
26. Courtney, K. D. *et al.* Isotope Tracing of Human Clear Cell Renal Cell Carcinomas Demonstrates Suppressed Glucose Oxidation In Vivo. *Cell metabolism* **28,** 793-800.e2; 10.1016/j.cmet.2018.07.020 (2018).
27. Armitage, E. G. & Barbas, C. Metabolomics in cancer biomarker discovery. Current trends and future perspectives. *Journal of pharmaceutical and biomedical analysis* **87,** 1–11; 10.1016/j.jpba.2013.08.041 (2014).
28. Seyfried, T. N., Flores, R. E., Poff, A. M. & D'Agostino, D. P. Cancer as a metabolic disease. Implications for novel therapeutics. *Carcinogenesis* **35,** 515–527; 10.1093/carcin/bgt480 (2014).
29. Yoshizaki, H., Ogiso, H., Okazaki, T. & Kiyokawa, E. Comparative lipid analysis in the normal and cancerous organoids of MDCK cells. *Journal of biochemistry* **159,** 573–584; 10.1093/jb/mvw001 (2016).
30. Li, B., He, X., Jia, W. & Li, H. Novel Applications of Metabolomics in Personalized Medicine. A Mini-Review. *Molecules (Basel, Switzerland)* **22**; 10.3390/molecules22071173 (2017).
31. Everett, J. R. Pharmacometabonomics in humans. A new tool for personalized medicine. *Pharmacogenomics* **16,** 737–754; 10.2217/pgs.15.20 (2015).
32. Relling, M. V. & Evans, W. E. Pharmacogenomics in the clinic. *Nature* **526,** 343–350; 10.1038/nature15817. (2015).
33. Haag, M. *et al.* Quantitative bile acid profiling by liquid chromatography quadrupole time-of-flight mass spectrometry. Monitoring hepatitis B therapy by a novel Na(+)-taurocholate cotransporting polypeptide inhibitor. *Analytical and bioanalytical chemistry* **407,** 6815–6825; 10.1007/s00216-015-8853-5 (2015).
34. Blank, A. *et al.* First-in-human application of the novel hepatitis B and hepatitis D virus entry inhibitor myrcludex B. *Journal of hepatology* **65,** 483–489; 10.1016/j.jhep.2016.04.013 (2016).

35. Blank, A. *et al.* The NTCP-inhibitor Myrcludex B. Effects on Bile Acid Disposition and Tenofovir Pharmacokinetics. *Clinical pharmacology and therapeutics* **103,** 341–348; 10.1002/cpt.744 (2018).
36. Bogomolov, P. *et al.* Treatment of chronic hepatitis D with the entry inhibitor myrcludex B. First results of a phase Ib/IIa study. *Journal of hepatology* **65,** 490–498; 10.1016/j.jhep.2016.04.016 (2016).
37. Masson, P., Alves, A. C., Ebbels, T. M. D., Nicholson, J. K. & Want, E. J. Optimization and evaluation of metabolite extraction protocols for untargeted metabolic profiling of liver samples by UPLC-MS. *Analytical chemistry* **82,** 7779–7786; 10.1021/ac101722e (2010).
38. Sheikh, K. D., Khanna, S., Byers, S. W., Fornace, A. & Cheema, A. K. Small molecule metabolite extraction strategy for improving LC/MS detection of cancer cell metabolome. *Journal of biomolecular techniques : JBT* **22,** 1–4 (2011).
39. Vorkas, P. A. *et al.* Untargeted UPLC-MS profiling pipeline to expand tissue metabolome coverage. Application to cardiovascular disease. *Analytical chemistry* **87,** 4184–4193; 10.1021/ac503775m (2015).
40. Cacciatore, S. *et al.* Metabolic Profiling in Formalin-Fixed and Paraffin-Embedded Prostate Cancer Tissues. *Molecular cancer research : MCR* **15,** 439–447; 10.1158/1541-7786.MCR-16-0262 (2017).
41. Montrose, D. C. *et al.* Metabolic profiling, a noninvasive approach for the detection of experimental colorectal neoplasia. *Cancer prevention research (Philadelphia, Pa.)* **5,** 1358–1367; 10.1158/1940-6207.CAPR-12-0160 (2012).
42. Ivanisevic, J. *et al.* Toward 'omic scale metabolite profiling. A dual separation-mass spectrometry approach for coverage of lipid and central carbon metabolism. *Analytical chemistry* **85,** 6876–6884; 10.1021/ac401140h (2013).
43. Naz, S., Vallejo, M., García, A. & Barbas, C. Method validation strategies involved in non-targeted metabolomics. *Journal of chromatography. A* **1353,** 99–105; 10.1016/j.chroma.2014.04.071 (2014).
44. Ivanisevic, J. & Want, E. J. From Samples to Insights into Metabolism. Uncovering Biologically Relevant Information in LC-HRMS Metabolomics Data. *Metabolites* **9**; 10.3390/metabo9120308 (2019).
45. Kromidas, S. ed. *Handbuch Validierung in der Analytik* (Wiley-VCH, Weinheim, 2011).

46. Leuthold, P. *et al.* Simultaneous Extraction of RNA and Metabolites from Single Kidney Tissue Specimens for Combined Transcriptomic and Metabolomic Profiling. *Journal of proteome research* **17,** 3039–3049 (2018).
47. Pezzatti, J. *et al.* Choosing an Optimal Sample Preparation in Caulobacter crescentus for Untargeted Metabolomics Approaches. *Metabolites* **9**; 10.3390/metabo9100193 (2019).
48. Want, E. J. *et al.* Global metabolic profiling of animal and human tissues via UPLC-MS. *Nature protocols* **8,** 17–32; 10.1038/nprot.2012.135 (2013).
49. Lang, G. *Histotechnik. Praxislehrbuch für die Biomedizinische Analytik.* 2nd ed. (Springer, Vienna, 2013).
50. Fox, C. H., Johnson, F. B., Whiting, J. & Roller, P. P. Formaldehyde fixation. *The journal of histochemistry and cytochemistry : official journal of the Histochemistry Society* **33,** 845–853; 10.1177/33.8.3894502 (1985).
51. Thavarajah, R., Mudimbaimannar, V., Rao, U., Ranganathan, K. & Elizabeth, J. Chemical and physical basics of routine formaldehyde fixation. *J Oral Maxillofac Pathol* **16,** 400; 10.4103/0973-029X.102496 (2012).
52. FRAENKEL-CONRAT, H. & OLCOTT, H. S. The reaction of formaldehyde with proteins; cross-linking between amino and primary amide or guanidyl groups. *J. Am. Chem. Soc.* **70,** 2673–2684; 10.1021/ja01188a018 (1948).
53. Wolff, A. C. *et al.* Recommendations for human epidermal growth factor receptor 2 testing in breast cancer. American Society of Clinical Oncology/College of American Pathologists clinical practice guideline update. *Journal of clinical oncology : official journal of the American Society of Clinical Oncology* **31,** 3997–4013; 10.1200/JCO.2013.50.9984 (2013).
54. Gustafsson, O. J. R., Arentz, G. & Hoffmann, P. Proteomic developments in the analysis of formalin-fixed tissue. *Biochimica et biophysica acta* **1854,** 559–580; 10.1016/j.bbapap.2014.10.003 (2015).
55. Donczo, B. & Guttman, A. Biomedical analysis of formalin-fixed, paraffin-embedded tissue samples. The Holy Grail for molecular diagnostics. *Journal of pharmaceutical and biomedical analysis* **155,** 125–134; 10.1016/j.jpba.2018.03.065 (2018).
56. Kokkat, T. J., Patel, M. S., McGarvey, D., LiVolsi, V. A. & Baloch, Z. W. Archived formalin-fixed paraffin-embedded (FFPE) blocks. A valuable underexploited

resource for extraction of DNA, RNA, and protein. *Biopreservation and biobanking* **11,** 101–106; 10.1089/bio.2012.0052 (2013).

57. Kelly, A. D. *et al.* Metabolomic profiling from formalin-fixed, paraffin-embedded tumor tissue using targeted LC/MS/MS. Application in sarcoma. *PloS one* **6,** e25357; 10.1371/journal.pone.0025357 (2011).
58. Yuan, M., Breitkopf, S. B., Yang, X. & Asara, J. M. A positive/negative ion-switching, targeted mass spectrometry-based metabolomics platform for bodily fluids, cells, and fresh and fixed tissue. *Nature protocols* **7,** 872–881; 10.1038/nprot.2012.024 (2012).
59. Feng, D. *et al.* UPLC-MS/MS-based metabolomic characterization and comparison of pancreatic adenocarcinoma tissues using formalin-fixed, paraffin-embedded and optimal cutting temperature-embedded materials. *International journal of oncology* **55,** 1249–1260; 10.3892/ijo.2019.4898 (2019).
60. Arima, K. *et al.* Metabolic Profiling of Formalin-Fixed Paraffin-Embedded Tissues Discriminates Normal Colon from Colorectal Cancer. *Molecular cancer research : MCR* **18,** 883–890; 10.1158/1541-7786.MCR-19-1091 (2020).
61. Wojakowska, A. *et al.* An Optimized Method of Metabolite Extraction from Formalin-Fixed Paraffin-Embedded Tissue for GC/MS Analysis. *PloS one* **10,** e0136902; 10.1371/journal.pone.0136902 (2015).
62. Wojakowska, A. *et al.* Detection of metabolites discriminating subtypes of thyroid cancer. Molecular profiling of FFPE samples using the GC/MS approach. *Molecular and cellular endocrinology* **417,** 149–157; 10.1016/j.mce.2015.09.021 (2015).
63. Buszewska-Forajta, M. *et al.* Paraffin-Embedded Tissue as a Novel Matrix in Metabolomics Study. Optimization of Metabolite Extraction Method. *Chromatographia* **82,** 1501–1513; 10.1007/s10337-019-03769-y (2019).
64. Ly, A. *et al.* High-mass-resolution MALDI mass spectrometry imaging of metabolites from formalin-fixed paraffin-embedded tissue. *Nature protocols* **11,** 1428–1443; 10.1038/nprot.2016.081 (2016).
65. Longuespée, R. *et al.* MALDI mass spectrometry imaging. A cutting-edge tool for fundamental and clinical histopathology. *Proteomics. Clinical applications* **10,** 701–719; 10.1002/prca.201500140 (2016).

66. Lancaster, M. A. & Knoblich, J. A. Organogenesis in a dish. Modeling development and disease using organoid technologies. *Science (New York, N.Y.)* **345,** 1247125; 10.1126/science.1247125 (2014).
67. Rossi, G., Manfrin, A. & Lutolf, M. P. Progress and potential in organoid research. *Nature reviews. Genetics* **19,** 671–687; 10.1038/s41576-018-0051-9 (2018).
68. Sato, T. *et al.* Single Lgr5 stem cells build crypt-villus structures in vitro without a mesenchymal niche. *Nature* **459,** 262–265; 10.1038/nature07935 (2009).
69. Eiraku, M. *et al.* Self-organizing optic-cup morphogenesis in three-dimensional culture. *Nature* **472,** 51–56; 10.1038/nature09941 (2011).
70. Takahashi, K. *et al.* Induction of pluripotent stem cells from adult human fibroblasts by defined factors. *Cell* **131,** 861–872; 10.1016/j.cell.2007.11.019 (2007).
71. Dekkers, J. F. *et al.* Characterizing responses to CFTR-modulating drugs using rectal organoids derived from subjects with cystic fibrosis. *Science translational medicine* **8,** 344ra84; 10.1126/scitranslmed.aad8278 (2016).
72. Lancaster, M. A. *et al.* Cerebral organoids model human brain development and microcephaly. *Nature* **501,** 373–379; 10.1038/nature12517 (2013).
73. Bartfeld, S. *et al.* In Vitro Expansion of Human Gastric Epithelial Stem Cells and Their Responses to Bacterial Infection. *Gastroenterology* **148,** 126-136.e6; 10.1053/j.gastro.2014.09.042 (2015).
74. Finkbeiner, S. R. *et al.* Stem Cell-Derived Human Intestinal Organoids as an Infection Model for Rotaviruses. *mBio* **3,** 807; 10.1128/mBio.00159-12 (2012).
75. Maddocks, O. D. K. *et al.* Modulating the therapeutic response of tumours to dietary serine and glycine starvation. *Nature* **544,** 372–376; 10.1038/nature22056 (2017).
76. Clevers, H. Modeling Development and Disease with Organoids. *Cell* **165,** 1586–1597; 10.1016/j.cell.2016.05.082 (2016).
77. Hayton, S., Maker, G. L., Mullaney, I. & Trengove, R. D. Experimental design and reporting standards for metabolomics studies of mammalian cell lines. *Cellular and molecular life sciences : CMLS* **74,** 4421–4441; 10.1007/s00018-017-2582-1 (2017).
78. Lindeboom, R. G. *et al.* Integrative multi-omics analysis of intestinal organoid differentiation. *Molecular systems biology* **14,** e8227; 10.15252/msb.20188227 (2018).

79. Feldman, A. *et al.* Blimp1+ cells generate functional mouse sebaceous gland organoids in vitro. *Nature communications* **10,** 2348; 10.1038/s41467-019-10261-6 (2019).
80. Sato, T. *et al.* Long-term expansion of epithelial organoids from human colon, adenoma, adenocarcinoma, and Barrett's epithelium. *Gastroenterology* **141,** 1762–1772; 10.1053/j.gastro.2011.07.050 (2011).
81. Benton, G., Kleinman, H. K., George, J. & Arnaoutova, I. Multiple uses of basement membrane-like matrix (BME/Matrigel) in vitro and in vivo with cancer cells. *International journal of cancer* **128,** 1751–1757; 10.1002/ijc.25781 (2011).
82. Gaudin, M. *et al.* Ultra performance liquid chromatography - mass spectrometry studies of formalin-induced alterations of human brain lipidome. *Journal of mass spectrometry : JMS* **49,** 1035–1042; 10.1002/jms.3424 (2014).
83. Al-Jahdari, W. S. *et al.* Prediction of total propofol clearance based on enzyme activities in microsomes from human kidney and liver. *European journal of clinical pharmacology* **62,** 527–533; 10.1007/s00228-006-0130-2 (2006).
84. Dinis-Oliveira, R. J. Metabolic Profiles of Propofol and Fospropofol. Clinical and Forensic Interpretative Aspects. *BioMed research international* **2018,** 6852857; 10.1155/2018/6852857 (2018).
85. Hiraoka, H. *et al.* Kidneys contribute to the extrahepatic clearance of propofol in humans, but not lungs and brain. *British journal of clinical pharmacology* **60,** 176–182; 10.1111/j.1365-2125.2005.02393.x (2005).
86. Takizawa, D., Hiraoka, H., Goto, F., Yamamoto, K. & Horiuchi, R. Human kidneys play an important role in the elimination of propofol. *Anesthesiology* **102,** 327–330 (2005).
87. Raoof, A. A., van Obbergh, L. J., Ville Goyet, J. de & Verbeeck, R. K. Extrahepatic glucuronidation of propofol in man. Possible contribution of gut wall and kidney. *European journal of clinical pharmacology* **50,** 91–96 (1996).
88. Heslinga, F. J. M. & Deierkauf, F. A. The action of formaldehyde solutions on human brain lipids. *The journal of histochemistry and cytochemistry : official journal of the Histochemistry Society* **10,** 704–709; 10.1177/10.6.704 (1962).
89. French, D. & Edsall, J. T. (Elsevier1945), pp. 277–335.
90. Jones, D. & Gresham, G. A. Reaction of formaldehyde with unsaturated fatty acids during histological fixation. *Nature* **210,** 1386–1388; 10.1038/2101386b0 (1966).

91. Hackett, M. J. *et al.* Chemical alterations to murine brain tissue induced by formalin fixation. Implications for biospectroscopic imaging and mapping studies of disease pathogenesis. *The Analyst* **136,** 2941–2952; 10.1039/c0an00269k (2011).
92. Barberà, A. *et al.* The Immunohistochemical Expression of Programmed Death Ligand 1 (PD-L1) Is Affected by Sample Overfixation. *Applied immunohistochemistry & molecular morphology : AIMM*; 10.1097/PAI.0000000000000847 (2020).
93. Pathologists' Guideline Recommendations for Immunohistochemical Testing of Estrogen and Progesterone Receptors in Breast Cancer. *Breast care (Basel, Switzerland)* **5,** 185–187; 10.1159/000315039 (2010).
94. Engel, K. B. & Moore, H. M. Effects of preanalytical variables on the detection of proteins by immunohistochemistry in formalin-fixed, paraffin-embedded tissue. *Archives of pathology & laboratory medicine* **135,** 537–543; 10.1043/2010-0702-RAIR.1 (2011).
95. Bass, B. P., Engel, K. B., Greytak, S. R. & Moore, H. M. A review of preanalytical factors affecting molecular, protein, and morphological analysis of formalin-fixed, paraffin-embedded (FFPE) tissue. How well do you know your FFPE specimen? *Archives of pathology & laboratory medicine* **138,** 1520–1530; 10.5858/arpa.2013-0691-RA (2014).
96. Reustle, A. *et al.* Characterization of the breast cancer resistance protein (BCRP/ABCG2) in clear cell renal cell carcinoma. *International journal of cancer* **143,** 3181–3193; 10.1002/ijc.31741 (2018).
97. Patel, S. & Ahmed, S. Emerging field of metabolomics. Big promise for cancer biomarker identification and drug discovery. *Journal of pharmaceutical and biomedical analysis* **107,** 63–74; 10.1016/j.jpba.2014.12.020 (2015).
98. Ackerman, D. *et al.* Triglycerides Promote Lipid Homeostasis during Hypoxic Stress by Balancing Fatty Acid Saturation. *Cell reports* **24,** 2596-2605.e5; 10.1016/j.celrep.2018.08.015 (2018).
99. Zhuo, D., Li, X. & Guan, F. Biological Roles of Aberrantly Expressed Glycosphingolipids and Related Enzymes in Human Cancer Development and Progression. *Frontiers in physiology* **9,** 466; 10.3389/fphys.2018.00466 (2018).

100. Silva, L. P. *et al.* Measurement of DNA concentration as a normalization strategy for metabolomic data from adherent cell lines. *Analytical chemistry* **85,** 9536–9542; 10.1021/ac401559v (2013).
101. Kane, K. I. W. *et al.* Determination of the rheological properties of Matrigel for optimum seeding conditions in microfluidic cell cultures. *AIP Advances* **8,** 125332; 10.1063/1.5067382 (2018).
102. Villaret-Cazadamont, J. *et al.* An Optimized Dual Extraction Method for the Simultaneous and Accurate Analysis of Polar Metabolites and Lipids Carried out on Single Biological Samples. *Metabolites* **10**; 10.3390/metabo10090338 (2020).
103. Haag, M., Schmidt, A., Sachsenheimer, T. & Brügger, B. Quantification of Signaling Lipids by Nano-Electrospray Ionization Tandem Mass Spectrometry (Nano-ESI MS/MS). *Metabolites* **2,** 57–76; 10.3390/metabo2010057 (2012).
104. Ser, Z., Liu, X., Tang, N. N. & Locasale, J. W. Extraction parameters for metabolomics from cultured cells. *Analytical biochemistry* **475,** 22–28; 10.1016/j.ab.2015.01.003 (2015).
105. Tirinato, L. *et al.* ROS and Lipid Droplet accumulation induced by high glucose exposure in healthy colon and Colorectal Cancer Stem Cells. *Genes & Diseases*; 10.1016/j.gendis.2019.09.010 (2019).
106. Rusz, M., Rampler, E., Keppler, B. K., Jakupec, M. A. & Koellensperger, G. Single Spheroid Metabolomics. Optimizing Sample Preparation of Three-Dimensional Multicellular Tumor Spheroids. *Metabolites* **9**; 10.3390/metabo9120304 (2019).
107. Broadhurst, D. *et al.* Guidelines and considerations for the use of system suitability and quality control samples in mass spectrometry assays applied in untargeted clinical metabolomic studies. *Metabolomics : Official journal of the Metabolomic Society* **14,** 72; 10.1007/s11306-018-1367-3 (2018).
108. Verkh, Y., Rozman, M. & Petrovic, M. Extraction and cleansing of data for a non-targeted analysis of high-resolution mass spectrometry data of wastewater. *MethodsX* **5,** 395–402; 10.1016/j.mex.2018.04.008 (2018).
109. Sangster, T., Major, H., Plumb, R., Wilson, A. J. & Wilson, I. D. A pragmatic and readily implemented quality control strategy for HPLC-MS and GC-MS-based metabonomic analysis. *The Analyst* **131,** 1075–1078; 10.1039/b604498k (2006).

110. Dunn, W. B. *et al.* Procedures for large-scale metabolic profiling of serum and plasma using gas chromatography and liquid chromatography coupled to mass spectrometry. *Nature protocols* **6,** 1060–1083; 10.1038/nprot.2011.335 (2011).
111. Schiffman, C. *et al.* Filtering procedures for untargeted LC-MS metabolomics data. *BMC bioinformatics* **20,** 334; 10.1186/s12859-019-2871-9 (2019).
112. Abe, Y. *et al.* Improved phosphoproteomic analysis for phosphosignaling and active-kinome profiling in Matrigel-embedded spheroids and patient-derived organoids. *Sci Rep* **8,** 29; 10.1038/s41598-018-29837-1 (2018).
113. Zhang, Y., Lukacova, V., Reindl, K. & Balaz, S. Quantitative characterization of binding of small molecules to extracellular matrix. *Journal of Biochemical and Biophysical Methods* **67,** 107–122; 10.1016/j.jbbm.2006.01.007 (2006).
114. Giobbe, G. G. *et al.* Extracellular matrix hydrogel derived from decellularized tissues enables endodermal organoid culture. *Nat Commun* **10,** 246; 10.1038/s41467-019-13605-4 (2019).
115. Gil de la Fuente, Alberto *et al.* Knowledge-based metabolite annotation tool. CEU Mass Mediator. *Journal of pharmaceutical and biomedical analysis* **154,** 138–149; 10.1016/j.jpba.2018.02.046 (2018).
116. Gil-de-la-Fuente, A. *et al.* CEU Mass Mediator 3.0. A Metabolite Annotation Tool. *Journal of proteome research* **18,** 797–802; 10.1021/acs.jproteome.8b00720 (2019).
117. Hughes, C. S., Postovit, L. M. & Lajoie, G. A. Matrigel. A complex protein mixture required for optimal growth of cell culture. *Proteomics* **10,** 1886–1890; 10.1002/pmic.200900758 (2010).
118. CHAUDHURI, N. K., MONTAG, B. J. & HEIDELBERGER, C. Studies on fluorinated pyrimidines. III. The metabolism of 5-fluorouracil-2-C14 and 5-fluoroorotic-2-C14 acid in vivo. *Cancer research* **18,** 318–328 (1958).
119. Longley, D. B., Harkin, D. P. & Johnston, P. G. 5-fluorouracil. Mechanisms of action and clinical strategies. *Nature reviews. Cancer* **3,** 330–338; 10.1038/nrc1074 (2003).
120. HEIDELBERGER, C. *et al.* Fluorinated pyrimidines, a new class of tumour-inhibitory compounds. *Nature* **179,** 663–666; 10.1038/179663a0 (1957).
121. Zhang, N., Yin, Y., Xu, S.-J. & Chen, W.-S. 5-Fluorouracil. Mechanisms of resistance and reversal strategies. *Molecules (Basel, Switzerland)* **13,** 1551–1569; 10.3390/molecules13081551 (2008).

122. Sumner, L. W. *et al.* Proposed minimum reporting standards for chemical analysis Chemical Analysis Working Group (CAWG) Metabolomics Standards Initiative (MSI). *Metabolomics : Official journal of the Metabolomic Society* **3,** 211–221; 10.1007/s11306-007-0082-2 (2007).

123. Grem, J. L. 5-Fluorouracil. Forty-plus and still ticking. A review of its preclinical and clinical development. *Investigational new drugs* **18,** 299–313; 10.1023/a:1006416410198 (2000).

124. Ser, Z. *et al.* Targeting One Carbon Metabolism with an Antimetabolite Disrupts Pyrimidine Homeostasis and Induces Nucleotide Overflow. *Cell reports* **15,** 2367–2376; 10.1016/j.celrep.2016.05.035 (2016).

125. Chong, L. & Tattersall, M.H.N. 5,10-Dideazatetrahydrofolic acid reduces toxicity and deoxyadenosine triphosphate pool expansion in cultured L1210 cells treated with inhibitors of thymidylate synthase. *Biochemical Pharmacology* **49,** 819–827; 10.1016/0006-2952(94)00458-X (1995).

126. Houghton, J. A., Tillman, D. M. & Harwood, F. G. Ratio of 2'-deoxyadenosine-5'-triphosphate/thymidine-5'-triphosphate influences the commitment of human colon carcinoma cells to thymineless death. *Clinical cancer research : an official journal of the American Association for Cancer Research* **1,** 723–730 (1995).

127. O'Dwyer, P. J. *et al.* Phase I trial of the thymidylate synthase inhibitor AG331 as a 5-day continuous infusion. *Clinical cancer research : an official journal of the American Association for Cancer Research* **2,** 1685–1692 (1996).

128. Rafi, I. *et al.* Preclinical and phase I clinical studies with the nonclassical antifolate thymidylate synthase inhibitor nolatrexed dihydrochloride given by prolonged administration in patients with solid tumors. *Journal of clinical oncology : official journal of the American Society of Clinical Oncology* **16,** 1131–1141; 10.1200/JCO.1998.16.3.1131 (1998).

129. Peters, G. J., Laurensse, E., Leyva, A. & Pinedo, H. M. Purine nucleosides as cell-specific modulators of 5-fluorouracil metabolism and cytotoxicity. *European journal of cancer & clinical oncology* **23,** 1869–1881; 10.1016/0277-5379(87)90053-8 (1987).

130. Tanigawara, Y., Nishimuta, A., Otani, Y. & Matsuo, M. *METHOD FOR DETERMINING SENSITIVITY TO FLUOROURACIL IN A SUBJECT HAVING COLORECTAL CANCER* (Sept. 19).

131. Hills, D. C., Cotten, M. L. & Horowitz, J. Isolation and characterization of two 5-fluorouracil-substituted Escherichia coli initiator methionine transfer ribonucleic acids. *Biochemistry* **22,** 1113–1122; 10.1021/bi00274a019 (1983).

132. Dobrzyńska, I., Szachowicz-Petelska, B., Sulkowski, S. & Figaszewski, Z. Changes in electric charge and phospholipids composition in human colorectal cancer cells. *Molecular and cellular biochemistry* **276,** 113–119; 10.1007/s11010-005-3557-3 (2005).

133. Dueck, D. A. *et al.* The modulation of choline phosphoglyceride metabolism in human colon cancer. *Molecular and cellular biochemistry* **162,** 97–103; 10.1007/bf00227535 (1996).

134. Kurabe, N. *et al.* Accumulated phosphatidylcholine (16:0/16:1) in human colorectal cancer; possible involvement of LPCAT4. *Cancer science* **104,** 1295–1302; 10.1111/cas.12221 (2013).

135. Weindl, D., Wegner, A., Jäger, C. & Hiller, K. Isotopologue ratio normalization for non-targeted metabolomics. *Journal of chromatography. A* **1389,** 112–119; 10.1016/j.chroma.2015.02.025 (2015).

136. Cebo, M., Fu, X., Gawaz, M., Chatterjee, M. & Lämmerhofer, M. Micro-UHPLC-MS/MS method for analysis of oxylipins in plasma and platelets. *Journal of pharmaceutical and biomedical analysis* **189,** 113426; 10.1016/j.jpba.2020.113426 (2020).

137. Luo, X. & Li, L. Metabolomics of Small Numbers of Cells. Metabolomic Profiling of 100, 1000, and 10000 Human Breast Cancer Cells. *Analytical chemistry* **89,** 11664–11671; 10.1021/acs.analchem.7b03100 (2017).

138. Li, M., Alnouti, Y., Leverence, R., Bi, H. & Gusev, A. I. Increase of the LC-MS/MS sensitivity and detection limits using on-line sample preparation with large volume plasma injection. *Journal of chromatography. B, Analytical technologies in the biomedical and life sciences* **825,** 152–160; 10.1016/j.jchromb.2005.03.047 (2005).

139. Galani, J. H. Y., Houbraken, M., van Hulle, M. & Spanoghe, P. Comparison of electrospray and UniSpray, a novel atmospheric pressure ionization interface, for LC-MS/MS analysis of 81 pesticide residues in food and water matrices. *Analytical and bioanalytical chemistry* **411,** 5099–5113; 10.1007/s00216-019-01886-z (2019).

140. Berset, J.-D., Brenneisen, R. & Mathieu, C. Analysis of llicit and illicit drugs in waste, surface and lake water samples using large volume direct injection high performance liquid chromatography--electrospray tandem mass spectrometry (HPLC-MS/MS). *Chemosphere* **81,** 859–866; 10.1016/j.chemosphere.2010.08.011 (2010).

141. Gao, L. *et al.* Simultaneous quantification of malonyl-CoA and several other short-chain acyl-CoAs in animal tissues by ion-pairing reversed-phase HPLC/MS. *Journal of chromatography. B, Analytical technologies in the biomedical and life sciences* **853,** 303–313; 10.1016/j.jchromb.2007.03.029 (2007).

142. Kumar, A., Heaton, J. C. & McCalley, D. V. Practical investigation of the factors that affect the selectivity in hydrophilic interaction chromatography. *Journal of chromatography. A* **1276,** 33–46; 10.1016/j.chroma.2012.12.037 (2013).

143. van Midwoud, P. M., Rieux, L., Bischoff, R., Verpoorte, E. & Niederländer, H. A. G. Improvement of recovery and repeatability in liquid chromatography-mass spectrometry analysis of peptides. *Journal of proteome research* **6,** 781–791; 10.1021/pr0604099 (2007).

144. Kammeijer, G. S. M. *et al.* Dopant Enriched Nitrogen Gas Combined with Sheathless Capillary Electrophoresis-Electrospray Ionization-Mass Spectrometry for Improved Sensitivity and Repeatability in Glycopeptide Analysis. *Analytical chemistry* **88,** 5849–5856; 10.1021/acs.analchem.6b00479 (2016).

4. Danksagung

An erster Stelle möchte ich Herrn Prof. Dr. Matthias Schwab für die Möglichkeit danken, meine Dissertation als Stipendiatin am Dr. Margarete Fischer-Bosch-Institut für Klinische Pharmakologie in Stuttgart anzufertigen und auch weiter an diesem innovativen Institut forschen zu dürfen. Zudem danke ich für die Bereitschaft, meine Dissertation als Betreuer seitens der Eberhard Karls Universität Tübingen zu übernehmen und die dafür investierte Zeit und Mühe.

Herrn Prof. Dr. Lämmerhofer danke ich für die Übernahme des zweiten Gutachtens seitens der Eberhard Karls Universität Tübingen und das Interesse an meiner Arbeit.

Ein ganz besonderer Dank gilt Dr. Mathias Haag für die intensive Betreuung in den vergangenen drei Jahren. Dafür, dass er immer ein offenes Ohr für Fragen hatte, mir mit Rat und Tat zur Seite stand und stets ein guter Diskussionspartner war. Danke für die Geduld und alles was ich lernen durfte.

Zudem danke ich der gesamten Arbeitsgruppe Analytik für die gute Arbeitsatmosphäre, insbesondere Dr. Thomas Mürdter, Dr. Ute Hofmann und Markus König, die mir in technischen und analytischen Fragestellungen immer beiseite standen.

Dr. Thomas Mürdter gilt zudem mein Dank für die gute Zusammenarbeit während der Erstellung der zweiten Publikation.

Besonders danken möchte ich meinem Freund Dirk, der mich immer und in jeder Lebenslage unterstützt und natürlich Frau Dr. Nicole Janssen „*for outstanding social competence and communication abilities*“…du bist eine gute Freundin geworden!

5. Lebenslauf

Persönliche Daten	Sylvia Karin Neef
	Geboren am 11.01.1987 in Esslingen am Neckar
Promotion	
Seit November 2017	Dissertation zum Thema „Entwicklung und Anwendung von Methoden zur metabolischen Phänotypisierung von Formalin-fixiertem, Paraffin-eingebettetem Gewebe und Tumor-Organoiden“ am Dr. Margarete Fischer-Bosch-Institut für Klinische Pharmakologie in Stuttgart
Studium und Ausbildung	
05/2016 – 05/2017	Praktikum der Lebensmittelchemie (2. Staatsexamen) am Landesuntersuchungsamt Rheinlandpfalz Lebensmittelchemische Institute Speyer und Koblenz
10/2011 – 03/2016	Studium der Lebensmittelchemie Diplom/1. Staatsexamen an der Technischen Universität Kaiserslautern Diplomarbeit: „Gaschromatographische Bestimmung flüchtiger Schwefelverbindungen in Wein mittels Stabilisotopenverdünnungsassay ohne massenselektive Detektion“, verfasst am Dienstleistungszentrum Ländlicher Raum Rheinpfalz (DLR) in Neustadt a. d. Weinstraße
09/2006 – 07/2008	Kerschensteinerschule Stuttgart-Feuerbach Berufskolleg zur Chemisch-technischen Assistentin
09/1997 – 05/2006	Freie Waldorfschule Engelberg Abschluss: Fachhochschulreife
Berufstätigkeit	
06/2017 – 11/2017	Prüfleiterin Rückstandsanalytik Eurofins Agroscience Services EcoChem GmbH, Niefern-Öschelbronn
11/2012 – 01/2016	Wissenschaftliche Hilfskraft am Lehrstuhl für Thermodynamik, Technische Universität Kaiserslautern

03/2012 – 04/2012	Werkstudentin im Labor für Mykotoxinanalytik, Abteilung RK, Chemisches und Veterinäruntersuchungsamt Stuttgart
08/2008 – 09/2011	Technische Assistentin im Labor für Mykotoxinanalytik, Abteilung RK, Chemisches und Veterinäruntersuchungsamt Stuttgart

Auszeichnungen

2017	Steinhofer-Preis 2016 für ein herausragendes Diplom in Lebensmittelchemie
10/2014 – 03/2016	Förderung als Deutschlandstipendiatin durch die BASF SE

6. Anhang

6.1. Akzeptierte Publikationen

6.1.1. Akzeptierte Publikation 1:

Optimized protocol for metabolomic and lipidomic profiling in formalin-fixed paraffin-embedded kidney tissue by LC-MS

Sylvia K. Neef [a], Stefan Winter [a], Ute Hofmann [a], Thomas E. Muerdter [a], Elke Schaeffeler [a,g], Heike Horn [a], Achim Buck [d], Axel Walch [d], Jörg Hennenlotter [e], German Ott [a,b], Falko Fend [e,f], Jens Bedke [e], Matthias Schwab[a,c,g] and Mathias Haag[a,*]

[a] *Dr. Margarete Fischer-Bosch-Institute of Clinical Pharmacology, Stuttgart, Germany and University of Tübingen, Tübingen, Germany*
[b] *Department of Clinical Pathology, Robert-Bosch Hospital, Stuttgart, Germany*
[c] *Departments of Clinical Pharmacology, Pharmacy and Biochemistry University Tübingen, Tübingen, Germany*
[d] *Research Unit Analytical Pathology, Helmholtz Zentrum München, Neuherberg, Germany*
[e] *Department of Urology, University Hospital Tübingen, Tübingen, Germany*
[f] *Institute of Pathology and Neuropathology, University Hospital Tübingen, Tübingen, Germany*
[g] *iFIT Cluster of Excellence (EXC2180) "Image Guided and Functionally Instructed Tumor Therapies", University of Tübingen, Tübingen, Germany*

Analytica Chimica Acta **2020**,1134, 125–135; doi: 10.1016/j.aca.2020.08.005

Analytica Chimica Acta 1134 (2020) 125–135

Contents lists available at ScienceDirect

Analytica Chimica Acta

journal homepage: www.elsevier.com/locate/aca

Optimized protocol for metabolomic and lipidomic profiling in formalin-fixed paraffin-embedded kidney tissue by LC-MS

Sylvia K. Neef [a], Stefan Winter [a], Ute Hofmann [a], Thomas E. Mürdter [a], Elke Schaeffeler [a, g], Heike Horn [a], Achim Buck [d], Axel Walch [d], Jorg Hennenlotter [e], German Ott [a, b], Falko Fend [f], Jens Bedke [e], Matthias Schwab [a, c, g], Mathias Haag [a, *]

[a] Dr. Margarete Fischer-Bosch-Institute of Clinical Pharmacology, Stuttgart, Germany and University of Tübingen, Tübingen, Germany
[b] Department of Clinical Pathology, Robert-Bosch Hospital, Stuttgart, Germany
[c] Department of Clinical Pharmacology, Pharmacy and Biochemistry, University Tübingen, Tübingen, Germany
[d] Research Unit Analytical Pathology, Helmholtz Zentrum München, Neuherberg, Germany
[e] Department of Urology, University Hospital Tübingen, Tübingen, Germany
[f] Institute of Pathology and Neuropathology, University Hospital Tübingen, Tübingen, Germany
[g] Cluster of Excellence iFIT (EXC 2180) "Image-Guided and Functionally Instructed Tumor Therapies", University of Tübingen, Tübingen, Germany

HIGHLIGHTS

- New protocol for metabolomic and improved lipidomic profiling in FFPE kidney tissue.
- Repeatable sample preparation and high inter-day precision is achieved.
- Proof of concept experiment on tumorous and non-tumorous FFPE kidney tissue.
- Formalin fixation time affects FFPE tissue metabolomic and lipidomic profiles.
- MALDI imaging of lipids that were found to be unaffected by tissue fixation time.

GRAPHICAL ABSTRACT

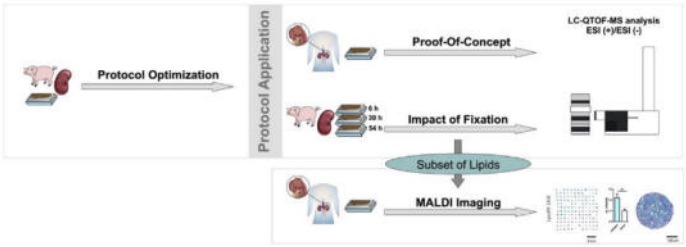

ARTICLE INFO

Article history:
Received 12 May 2020
Received in revised form
31 July 2020
Accepted 2 August 2020
Available online 13 August 2020

Keywords:
Formalin-fixed paraffin-embedded kidney tissue
Metabolite extraction
Metabolomics
Lipidomics
Non-targeted metabolomics
Mass spectrometry

ABSTRACT

Formalin-fixed and paraffin-embedded (FFPE) tissue represents a valuable resource to examine cancer metabolic alterations and to identify potential markers of disease. Protocols commonly used for liquid-chromatography mass spectrometry (LC-MS)-based FFPE metabolomics have not been optimized for lipidomic analysis and pre-analytical factors, that potentially affect metabolite levels, were scarcely investigated. We here demonstrate the assessment and optimization of sample preparation procedures for comprehensive metabolomic and lipidomic profiling in FFPE kidney tissue by LC-QTOF-MS. The optimized protocol allows improved monitoring of lipids including ceramides (Cer), glycosphingolipids (GSL) and triglycerides (TAGs) while the profiling capability for small polar molecules is maintained. Further, repeatable sample preparation (CVs < 20%) along with high analytical (CVs < 10%) and inter-day precision (CVs < 20%) is achieved. As proof of concept, we analyzed a set of clear cell renal cell carcinoma (ccRCC) and corresponding non-tumorous FFPE tissue samples, achieving phenotypic distinction. Investigation of the impact of tissue fixation time (6 h, 30 h and 54 h) on FFPE tissue metabolic profiles revealed metabolite class-dependent differences on their detection abundance. Whereas specific lipids (e.g. phosphatidylinositoles, GSLs, saturated fatty acids and saturated lyso-phosphatidytlethanolamines

* Corresponding author. Dr. Margarete Fischer-Bosch-Institute of Clinical Pharmacology, Auerbachstr. 112, 70376, Stuttgart, Germany.
E-mail address: mathias.haag@ikp-stuttgart.de (M. Haag).

https://doi.org/10.1016/j.aca.2020.08.005

[LPE]) remained largely unaffected (CVs < 20% between groups of fixation time), neutral lipids (e.g. Cer and TAGs) exhibited high variability (CVs > 80%). Strikingly, out of the lipid classes assigned as unaffected, fatty acids 18:0, 16:0 and LPE 18:0 were detectable by high-resolution MALDI-FT-ICR MS imaging in an independent cohort of ccRCC tissues (n = 64) and exhibited significant differences between tumor and non-tumor regions.

1. Introduction

Increasing evidence suggests that cancer should be considered as a metabolic disease [1,2]. In this context, liquid-chromatography mass spectrometry (LC-MS)-based metabolomics of tissue samples can provide unique information on physiological and pathological mechanisms. Kidney cancer metabolomics in fresh-frozen (FF) tissue has been successfully used to investigate the metabolite and lipid composition of tumor subtypes derived from different cells of origin [3,4]. Moreover, non-targeted approaches [5] allow for the comprehensive metabolomic and lipidomic profiling of tissue samples [6–8] and are continuously refined to maximize information yield from single pieces of tissue [9,10] or to enable in-depth profiling with accurate metabolite quantification [11]. Although FF tissue reflects the matrix of choice for metabolite profiling of localized tumors, well annotated specimens are a limited resource and technically demanding regarding storage and handling. In contrast, formalin-fixed paraffin-embedded (FFPE) tissue, as part of routine diagnostic applications in pathology [12,13], represents a promising alternative already used in genomic, transcriptomic and proteomic biomarker research [14–16]. With respect to LC-MS the limited number of available protocols for FFPE metabolomics rather focus on the profiling of small, polar molecules [17] while lipids have been scarcely considered [18]. In addition, employing high-resolution matrix-assisted laser desorption-/ionization Fourier-transform ion cyclotron resonance mass spectrometric imaging (MALDI-FT-ICR MSI) has allowed for the *in situ* detection and spatial analysis of small molecules with minimum requirements on FFPE tissue sample amounts [19,20]. However, the inability of monitoring isobaric species and the decreased detection of lipids [20] are limitations of imaging technologies that hamper the assessment of pre-analytical factors in a comprehensive fashion. In this regard, the capability of LC-MS to enable broad metabolite profiling, including lipids, allows for a more complete estimation of FFPE tissue metabolite content potentially affected by pre-analytical factors such as fixation time.

We here present a novel sample preparation protocol for comprehensive metabolomic and lipidomic profiling of FFPE tissue by LC-MS. Assessment of different extraction strategies, extraction solvents and conditions enabled us to determine methods with improved lipid detection from FFPE tissue. All procedures were evaluated regarding repeatability of sample preparation, analytical precision and day-to-day variation. To verify protocol applicability, a proof of concept experiment was carried out by analyzing FFPE tissue samples of clear cell renal cell carcinoma (ccRCC) and corresponding non-tumorous material. To assess pre-analytical factors, the impact of tissue fixation time on metabolite and lipid profiles was investigated, followed by MALDI-FT-ICR MS detection of compounds found to be unaffected by fixation time in an independent cohort of ccRCC tissue microarrays (TMAs). Ultimately, protocol optimization and assessment of pre-analytical factors by LC-MS with subsequent detection of selected lipid species by an independent *in situ* imaging approach demonstrates the complementary use of both techniques.

2. Experimental

2.1. Chemicals and reagents

Ultra LC-MS grade acetonitrile (ACN) and methanol (MeOH) were purchased from Carl Roth GmbH & Co KG (Karlsruhe, Germany) and LC-MS grade methyl tert-butyl ether (MTBE), isopropanol (IPA), formic acid (FA) and ammonium acetate (AmAc) was obtained from Sigma-Aldrich (Taufkirchen, Germany). Pure water was provided by a Milli-Q system (Millipore, Billerica, MA, USA) and used for the preparation of aqueous solvents.

2.2. FFPE kidney tissue samples

Porcine kidney was obtained as fresh food product and used to prepare formalin fixed paraffin-embedded (FFPE) samples. Kidney collection was carried out according to standard techniques in meat processing. In brief, after slaughtering the kidney was washed with water and removed from the carcass by scission followed by immediate cooling to 4 C and storage for 4 h in the cold. For tissue sampling, replicate pieces (approx. 1 cm 1 cm x 0.5 cm in size) were collected across the kidney cortex and fixed in 4% buffered formalin solution for 6 h. For the assessment of longer fixation times (i.e. 30 h and 54 h) the remaining kidney was completely fixed with 4% buffered formalin solution followed by collection of replicate samples (approx. 1 cm 1 cm x 0.5 cm in size) from the cortex. Time points were chosen as commonly applied (e.g. 6–72 h as recommended for resection specimens in breast cancer testing [21,22]) and selected tissue sizes were in accordance with different types of biopsies typically submerged in formalin reflecting excisional biopsies (0.5 cm^3 pieces) and nephrectomies (remaining kidney). Since small tissue specimens don't require overnight fixation (expected penetration rate of 1 mm/h [23]) the minimum, recommended fixation time of 6 h was chosen for the excisional biopsies. In contrast, as complete organs (e.g. nephrectomies of renal tumors) are submerged in fixation solution for overnight [24] or longer (e.g. over a weekend) incubation times of 30 h and 54 h were considered. Hence the chosen sample set mirrors typical differences in tissue size and fixation time observed in routine clinical pathology. Following fixation, tissue samples were embedded in paraffin according to the standard procedure of the Department of Clinical Pathology (Robert-Bosch-Hospital, Stuttgart, Germany) and the histopathological evaluation of tissue sections was performed. The proof of concept experiment was achieved by using four human ccRCC FFPE samples as part of the Robert-Bosch-Hospital biobank (#448/2009BO2). After nephrectomy, fixation of all human kidney tissue samples was done at the Pathology Department within 30 min. Tissue fixation time was 24 h. All samples were anonymized for LC-MS analysis.

For MALDI-FT-ICR MS imaging an independent cohort consisting of ccRCC (n = 64) and corresponding non-tumor samples was used as previously described [25]. Patients were treated at the Department of Urology, University Hospital Tübingen, Germany, and underwent partial or radical nephrectomy. FFPE tumor and

matching surrounding non-tumor tissue was established at the Pathology Department. Tissue fixation was achieved within 30–45 min and the fixation time was between 12 h and 24 h. After routine pathological evaluation of FFPE tissue slices, tissue microarrays (TMA) of the respective areas were established. Informed written consent was provided by each patient before surgical resection (#150/2012BO2). The sample specimens were anonymized for MALDI-FT-ICR MS imaging.

2.3. Metabolite extraction from FFPE tissue and LC-MS analysis

Prior to metabolite extraction 10 μm slices were cut from FFPE blocks and discarded to remove possible surface contaminants. For each biological replicate of porcine or human FFPE kidney tissue samples three technical replicate punches (1 mm 3 mm) were obtained with a 1.0 mm Manual Tissue Arrayer Punch (Beecher Instruments Inc., Wisconsin USA). The punches were placed in preweighed polypropylene tubes (Eppendorf, Germany) and the gross weight was determined (range: 4.1–9 mg). Within this range repeatable samples analysis was achieved as indicated by median CVs <20% (repeatability of technical replicates in Fig. 1B, Fig. 2 and Fig. 4). For each batch a paraffin blank (three pure paraffin cores) was prepared in parallel. For the optimized extraction protocol B1 (Fig. 1A), 500 μl of 50% MeOH was added to the cores independent of sample weight followed by incubation at 70 C for 45 min at 1000 rpm. After centrifugation (15.000 rpm, 5 min at 4 C) the supernatant was transferred to a new vial and centrifuged again to remove residual debris. The clean supernatant was dried in a new vial by SpeedVac and dissolved in 95% ACN to achieve a solvent/tissue ratio of 25 μl/mg for pre-acquisition normalization of aqueous extracts. Re-extraction of the remaining pellet was achieved with 100% IPA at a solvent/tissue ratio of 24 μl/mg by manual shaking (vortexing for 5 s) and incubation at 70 C for 15 min at 1000 rpm. After incubation in heated IPA, methanol was added to adjust an IPA:MeOH proportion of 3:1 and a solvent/tissue ratio of 32 μl/mg (normalization of organic extracts) followed by manual shaking and two centrifugation steps as described for the aqueous extracts. For LC-QTOF-MS analysis metabolite extracts were transferred into 2 mL vials containing 250 μL glass inserts with polymer feet and covered with pre-slit PTFE/silicone screw caps. Aqueous extracts were analyzed by hydrophilic interaction liquid chromatography (HILIC) and organic extracts were analyzed by reversed

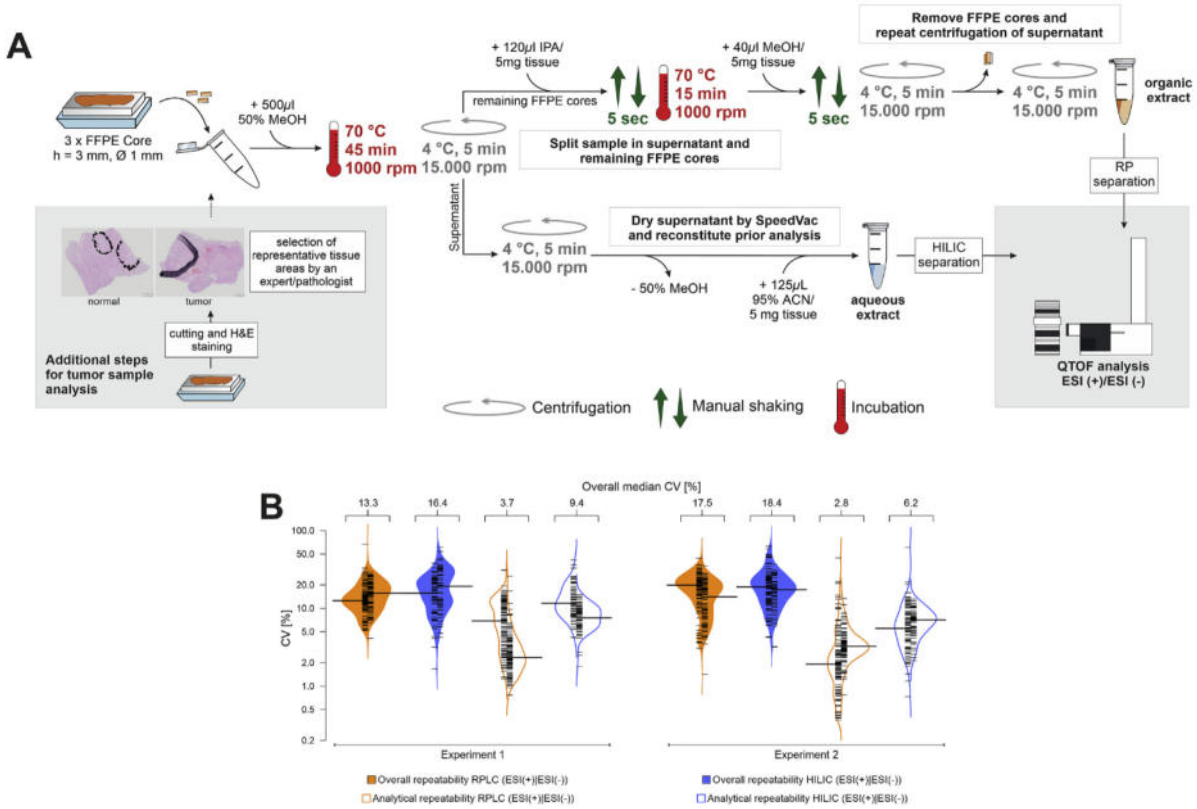

Fig. 1. Workflow summary and day-to-day repeatability of optimized sample preparation protocol. A: Overview of sample preparation steps of protocol B1 (see Fig. S1) for non-targeted metabolomic and lipidomic profiling of FFPE tissue by LC-QTOF-MS. The use of incubation in heated solvent is indicated by a red temperature sign. Manual shaking (vortexing) and centrifugation is displayed by green and grey arrows, respectively. Small orange pieces indicate FFPE tissue core samples. Grey inserts (left side) indicate additional steps carried out for human kidney cancer sample analysis in the proof of concept experiment (Figs. 2 and 3). B: Day-to-day repeatability of protocol B1 as assessed by two independent experiments (each n = 5, technical replicates). Overall repeatability comprises the variability of the sample preparation and the analytical variation. Bean plots representing the mean coefficient of variation (CVs) of 268 metabolite species (black thin lines) previously annotated in fresh frozen kidney tissue [6] analyzed in organic (orange) and aqueous (blue) extracts. Median CVs of each single mode are indicated by large horizontal black lines. Overall median CVs, representing combined data from positive (left beans) and negative (right beans) ionization mode, are listed above the beanplots. The average mass accuracy (mean ppm ± SD) of sum formula matched features was 3.2 ± 1.7 (Experiment 1). (For interpretation of the references to color in this figure legend, the reader is referred to the Web version of this article.)

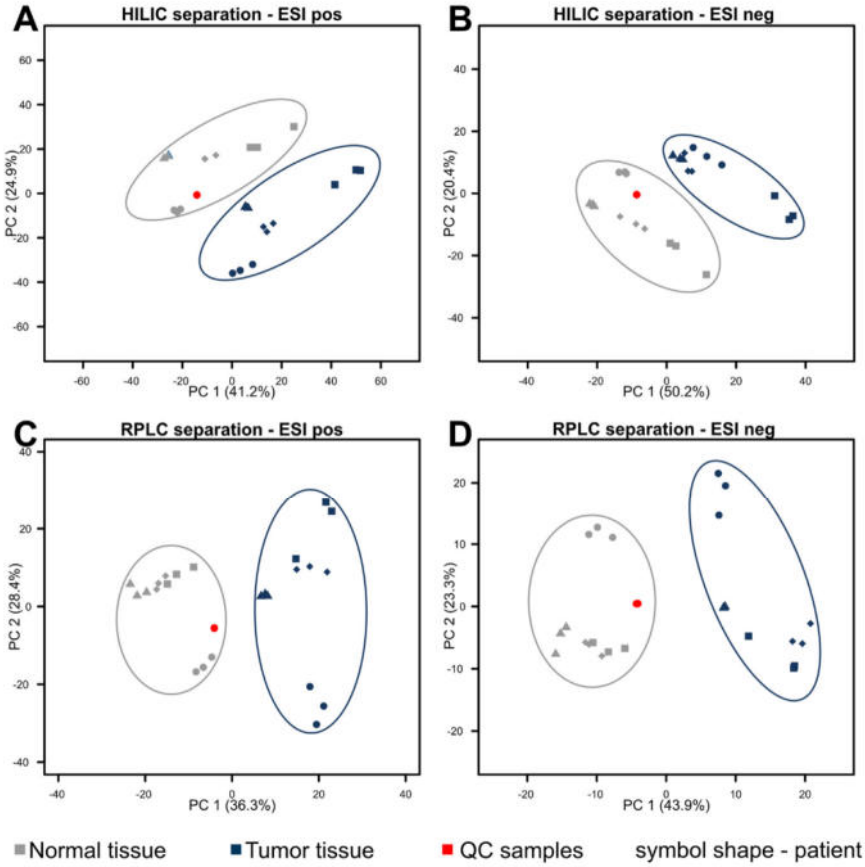

Fig. 2. Proof of concept experiment: differentiation of ccRCC and nontumor FFPE tissue by the optimized protocol B1: Principle component analysis of ccRCC (blue) and adjacent nontumor FFPE tissue samples (grey) of 4 male donors (indicated by symbol shape) analyzed by HILIC in aqueous (A, 606 features and B, 251 features) and by RPLC in organic (C, 776 features and D, 439 features) extracts by the indicated ionization mode (ESI pos and ESI neg). Three replicate FFPE tissue sample were prepared for each donor to assess tissue heterogeneity. The overall median CV (all features, all modes) over the replicate samples was 13.02%. Six QC samples were analyzed per mode (i.e. HILIC-ESI(+), HILIC-ESI( ), RPLC-ESI(+) and RPLC-ESI( )). The average mass accuracy (mean ppm ± SD) of all detected features was 1.2 ± 1.2. Note: RPLC ESI pos data (C) was evaluated under exclusion of variable features (retention time 14 min) [6]. (For interpretation of the references to color in this figure legend, the reader is referred to the Web version of this article.)

phase liquid chromatography (RPLC) coupled to a quadrupole time-of-flight mass spectrometer (QTOF-MS) as previously described [6]. Method details about LC-QTOF-MS analysis and other sample preparation protocols are provided in the supplementary data.

2.4. Data preprocessing

Preprocessing of LC-MS data was carried out with Mass Hunter Profinder Software (version B.08.00, Agilent Technologies). For optimization of sample preparation, repeatability assessment and determination of metabolites differentially affected by formalin fixation time (Tables S4–S7), targeted feature extraction of metabolites previously annotated in fresh frozen kidney tissue [6] was applied. Formula matching tolerances were set to ±15 ppm for masses and ±0.5 min for retention times (RT). Intensity threshold was set to 1000 with an extracted ion chromatogram (EIC) range of ±35 ppm. TOF-MS spectra above 30% of saturation were excluded. For the proof of concept experiment (Figs. 2 and 3) and assessment of fixation time on metabolomic profiles (Fig. 4) batch recursive feature extraction was applied with an intensity threshold 1000. Unless stated otherwise, protonated (H^+) and Na^+/NH_4^+ adducts were considered for positive ion data and deprotonated (H) and CH_3COO^-/$HCOO^-$ adducts for negative mode data. Binning and alignment parameters within the recursive workflow, which control grouping of features (e.g. different adducts) to individual compounds, were set to ± (0.1% + 0.3 min) for the RT tolerance and to ± (15 ppm + 2 mDa) [26] for the mass tolerance. For example, for a mass of 1000 Da with an expected RT of 2 min the window would be 1.698–2.302 min and the mass tolerance 999.993–1000.007 Da for a feature being considered as part of the same compound. The EIC range was set to ±35 ppm. For peak integration, Agile 2 algorithm was selected. TOF-MS spectra were excluded if above 30% of saturation. For targeted and recursive feature extraction, EICs were visually inspected and peak integrations manually adjusted to ensure RT and peak alignment throughout the batch. Average mass accuracies of the visually inspected features were all <5 ppm for targeted (Fig. 1) and recursive (Figs. 2 and 4) feature extraction batches. Values were exported as peak area in a comma separated value (csv) file and used for statistical analysis.

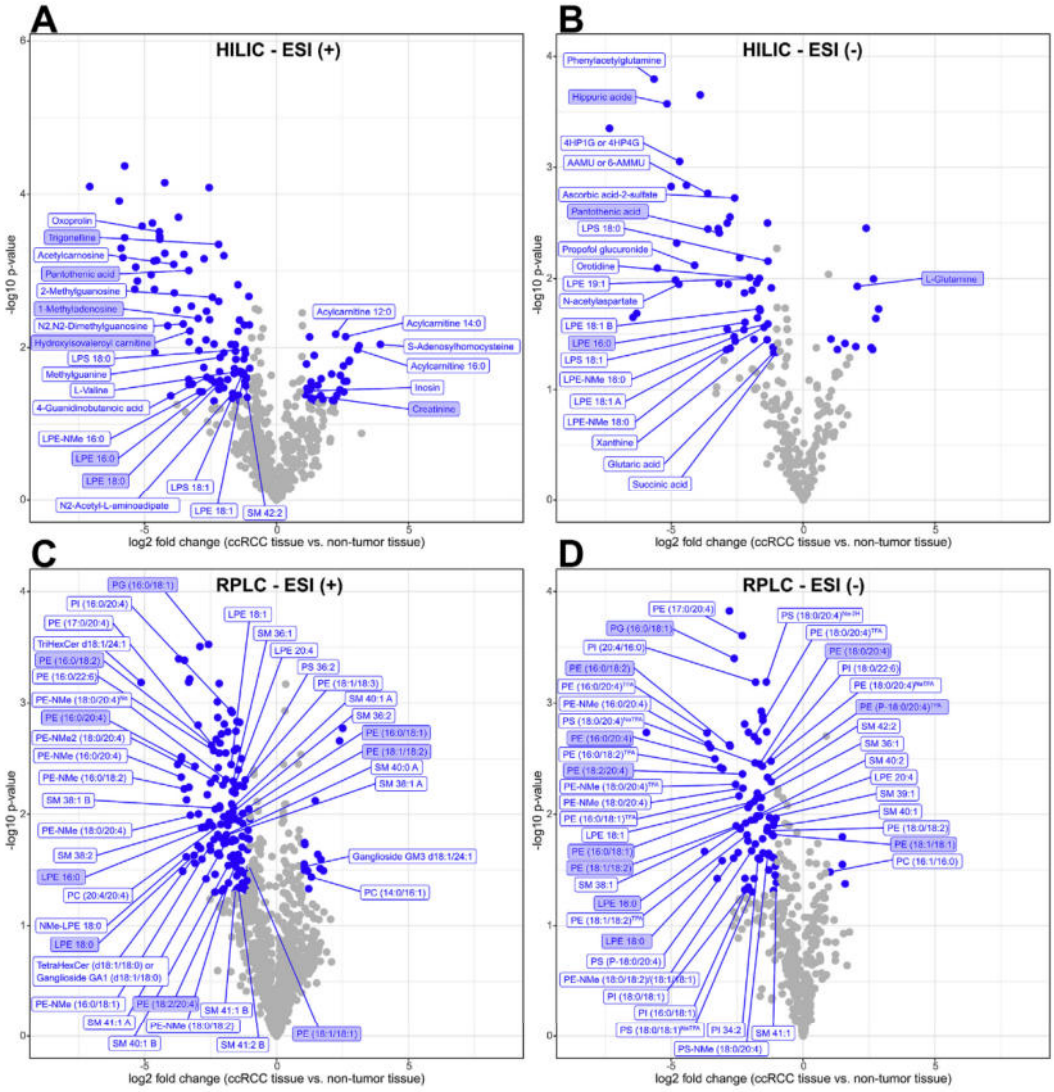

Fig. 3. Proof of concept experiment: significantly altered metabolites between ccRCC and nontumor FFPE tissue. Results of the non-targeted metabolomics analysis of differentially regulated features between ccRCC and adjacent nontumor tissue samples derived from four male donors. The volcano plots display log2 fold changes (ccRCC/nontumor tissue) versus log10 transformed p-values. Features that exhibited an absolute log2 fold change >1 and p-value <0.05 are colored in blue, whereas the remaining are marked in grey. Structurally annotated metabolites are labeled with the corresponding name. Labels of metabolites that could previously be assigned in studies based on fresh frozen ccRCC tissue [6] are filed with light blue. (A) and (B) represents data from aqueous extracts analyzed in positive and negative mode, respectively. (C) and (D) represents data from organic extracts analyzed in positive and negative mode, respectively. TFA indicates trifluoroacetic acid (CF_3COO^-) adducts. (For interpretation of the references to color in this figure legend, the reader is referred to the Web version of this article.)

2.5. Statistical analysis

Statistical data analyses were performed with R-3.3.2 and R studio (http://www.r-project.org) [27], including additional packages beanplot [28], gplots [29], ggplot2 [30], ggrepel [31], pheatmap [32] and beeswarm [33]. Method quality rating of protocol assessment was carried out without data normalization (Fig. 1B, Fig. S2, Fig. S3 and Fig. S4). For all other experiments features with a coefficient of variation (CV) 20% in QC samples were excluded. Non-targeted data for formalin fixation time assessment (Fig. 4) was sum normalized (peak area of each feature divided by the sum of peak areas of all features in one sample). All other experiments (Figs. 2 and 3) were normalized by locally weighted scatterplot smoothing (LOESS) correction over QC samples. All normalized data was log2-transformed. Principal component analysis (PCA) was performed with R function prcomp using default settings. Ward's minimum variance method was used for hierarchical clustering of feature-wise centered data. Paired t-tests were applied to identify features regulated differently between ccRCC and corresponding non-tumorous tissues. All statistical tests were two sided and statistical significance was defined as p-value <0.05.

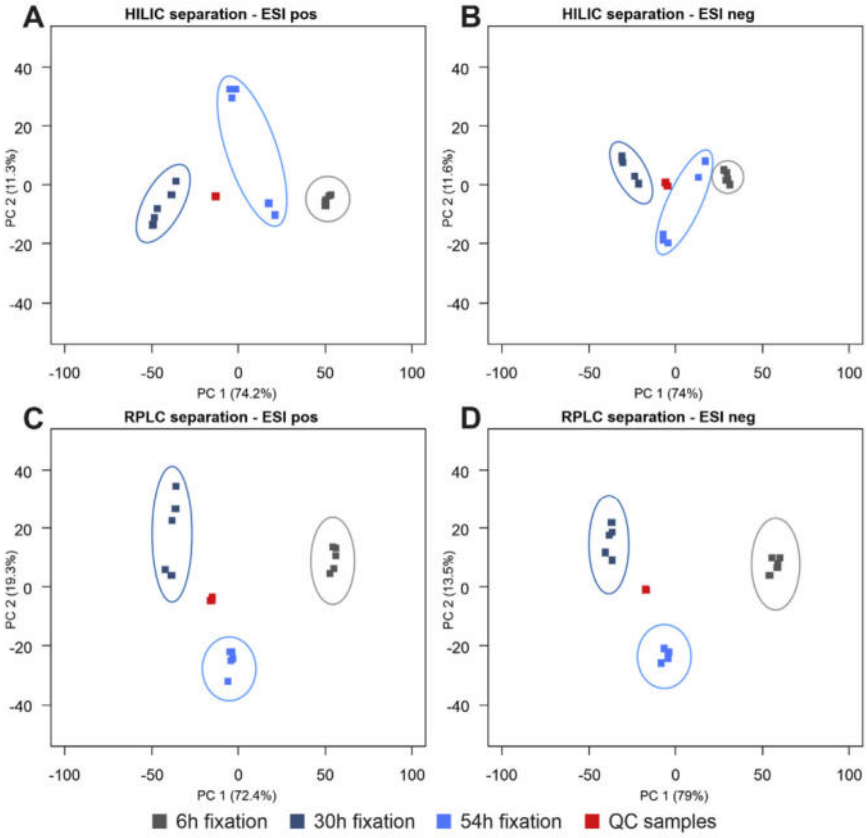

Fig. 4. Assessment of formalin fixation time on FFPE tissue metabolomic and lipidomic profiles. Principle component analysis of FFPE tissue extracts prepared from fresh frozen tissue fixed for 6 h (grey), 30 h (dark blue) and 54 h (light blue). Samples were analyzed by HILIC in aqueous extracts (A, 1881 features and B, 1266 features) and by RPLC in organic extracts (C, 1848 features and D, 1844 features) in the indicated ionization mode. FFPE kidney tissue was prepared from fresh frozen porcine kidney (n = 5, technical replicates per incubation group). The overall median CV (all features, all modes) over replicate samples was 14.02%. Four QC samples were analyzed per mode (i.e. HILIC-ESI(+), HILIC-ESI( ), RPLC-ESI(+) and RPLC-ESI( )). The average mass accuracy (mean ppm ± SD) of all detected features was 2.0 ± 2.8. (For interpretation of the references to color in this figure legend, the reader is referred to the Web version of this article.)

2.6. Matrix-assisted laser desorption/ionization mass spectrometry imaging

A tissue microarray (TMA) was constructed using matching tumor and surrounding non-tumor FFPE tissue from 64 ccRCC patients as previously described [25,34]. Tissue preparation for MALDI imaging analysis was performed as previously described [19,20]. Details about the method are provided in the supplementary data.

3. Results and discussion

3.1. Optimization of sample preparation for metabolomic and lipidomic profiling in FFPE tissue

Metabolomics analysis from FFPE specimens requires paraffin removal in order to make tissue accessible for subsequent metabolite extraction. Incubation in xylene for deparaffinization has been applied for metabolomics analysis of small polar molecules [35,36]. However, due to the non-polar nature of the solvent, lipid losses are expected hence making lipidomics analysis unreliable. Alternatively, incubation in 80% heated methanol for a combined deparaffinization and analyte extraction has been successfully applied for FFPE metabolite profiling [17,18,37]. We evaluated and optimized methanol-based deparaffinization and metabolite extraction protocols to improve lipid analysis in FFPE kidney tissue while maintaining the profiling capability for small polar molecules. Ten different protocols, covering one- and two-step extraction methods either in combination with bead beating and/or solvent incubation, were tested (Supplementary Fig. S1). Method quality rating was carried out regarding signal intensity (metabolite peak areas), repeatability and signal-to-noise (S/N) assessment.

With respect to signal intensities, the one-step extraction procedure A2 (80% methanol, bead beating and heating) and the two-step protocols B1 (50% methanol followed by 100% IPA, heating only) and B3 (50% methanol followed by 100% IPA, bead beating only) resulted in highest signals for polar molecules (Fig. S2 A and B, blue bars) and lipids (Fig. S2 A and B, orange bars). The high detection sensitivity of these protocols is further reflected by their excellent repeatability (Fig. S3) as indicated by low median coefficients of variation (CVs) of 19.5% (protocol A2), 14.1% (protocol B1) and 16% (protocol B3). Notably, regarding lipid profiling, organic extraction with MTBE:MeOH (protocols C1–C3) did not improve, neither signal intensities nor repeatabilities compared to IPA-based protocols (B1 and B3) as demonstrated by low mean areas (Fig. S2 A, ~2.5 10^8 counts, protocols C1–C3) and CVs 25% (Fig. S3). Thus, as previously demonstrated for plasma lipids [38],

IPA-based extraction enabled repeatable lipid profiling also in FFPE tissue extracts. In this regard it remains to be investigated whether the extraction solvent (IPA vs. MTBE:MeOH) or a potential, beneficial effect of the dilute-and-shoot sample analysis approach (see legend to Fig. S1) used for protocols B1–B3 compared to analysis after resuspension of dried extracts (protocols C1–C3) affect signal intensities of the lipid measurements. Further, bead beating didn't improve neither sensitivity nor repeatability of lipid profiling in two-step extraction protocols indicating that mechanical disruption of FFPE tissue does not add beneficial effects to the sample preparation procedure.

Next, the detection performance of individual metabolite and lipid species in protocols A2, B1 and B3 was assessed by signal to noise ratios (S/N, Supplementary Tables S1 and S2). In accordance with previous findings from *in situ* MALDI imaging experiments [19] a high number of metabolites (>80% of those found in FF tissue [6]) could be detected (S/N > 3) in FFPE tissue, however with noticeable differences between protocols. Whereas a broad range of polar molecules (i.e. hexose, several acylcarnitine species and amino acids like arginine, asparagine and serine) remained undetected (S/N < 3) by all three protocols (Table S1), individual lipid classes (ceramides, hexylceramides and triglycerides) exhibited improved signals (S/N > 10) by employing two-step extraction (protocols B1 and B3, Table S2).

Considering the beneficial effects on lipid detection together with findings from signal intensity and repeatability assessment, we concluded that the preferred method for comprehensive and repeatable profiling of polar molecules and lipids from FFPE tissue is combined deparaffinization and extraction in 50% heated methanol followed by organic extraction with 100% IPA (protocol B1, see Fig. 1 A for workflow summary). In addition to an improved detection of lipids potentially relevant for cancer (e.g. glycosphingolipids in kidney cancer [39]) and metabolic disorders (e.g. TAGs in fatty liver disease [40]), the protocol demonstrates a high inter-day precision both for sample preparation (CVs < 20%, all modes) and the analytical method (CVs < 10%, all modes) (Fig. 1 B). This is an important prerequisite for the analysis of larger FFPE tissue cohorts (n > 100) which require sample preparation and measurement on multiple days. Moreover, albeit signal intensity was reduced, repeatability of IPA extraction was not compromised by a higher share of methanol (80% vs. 50%) during the initial, aqueous extraction step, as determined by comparison of protocol D1 with protocol B1 in an independent experiment (Fig. S4). Thus, IPA-based lipid extraction is compatible with commonly applied single-step incubation procedures using 80% methanol [17,18,37] allowing for a rapid adaption of the optimized protocol B1 into already existing workflows for FFPE tissue metabolomics.

3.2. Proof of concept: differentiation of ccRCC and nontumor tissue based on metabolic profiling

In order to proof the protocol's applicability (Fig. 1 A) to discriminate between tumorous and corresponding non-tumorous FFPE tissue material, samples from four ccRCC and matched non-tumor tissue were investigated (biological replicates). As depicted in the PCA (Fig. 2) a clear differentiation of ccRCC and adjacent normal tissue was evident in all analytical modes. Statistical analysis revealed metabolites that were significantly reduced or elevated (p-value < 0.05 and absolute log2 fold change > 1) in ccRCC tissue compared to non-tumorous tissue (Fig. 3, blue filled dots). Strikingly, as observed previously in extracts from fresh frozen (FF) ccRCC tissue [6], phosphoethanolamine lipids (e.g. PE 16:0/18:2) were also found decreased in ccRCC FFPE tissue hence demonstrating metabolite conservation between FF and FFPE tissue [19]. Conservation of metabolic alterations in FFPE tissue was further substantiated by significant changes observed for small, polar molecules such as reduced levels of 1-methyladenosine, trigonelline, hydroxyisovaleroyl carnitine and hippurate in ccRCC accompanied by higher amounts of L-glutamine that all were comparable to alterations detected in FF tissue [6]. Strikingly, with respect to lipids, N-methylated derivatives of the amine-containing lipids phosphatidylethanolamine (PE) and phosphatidylserine (PS) such as PE-NMe 16:0/18:2 and PS-NMe 18:0/20:4 could be exclusively detected in FFPE tissue extracts (Fig. 3 and Supplementary Table S3) but not in FF tissue (data not shown) and exhibited similar alterations as their unmodified reactants (PE 16:0/18:2 and PS 18:0/20:4). This is a novel finding and demonstrates that, albeit formalin fixation alters the chemical composition of amine-containing lipid headgroups, biological changes remain sustained in FFPE tissue. A further notable observation was the detection of altered levels of xenobiotics such as reduced amounts of the anesthetic metabolites propofol glucuronide and 4-hydroxy-3,5-bis(1-methylethyl)phenyl glucuronide/4-hydroxy-2,6-bis(1-methylethyl)phenyl glucuronide (4HP1G/4HPUG) as well as the caffeine metabolite 5-acetylamino-6-amino-3-methyluracil/6-amino-5[N-methylformylamino]-1-methyluracil (AAMU/6-AMMU) in ccRCC compared to normal tissue (Fig. 3 B). Reduced levels of these compounds in tumorous kidney tissue likely reflects loss of renal function and further demonstrates the ability to perform combined analysis of xenobiotics and endogenous molecules in FFPE tissue by our non-targeted metabolomics protocol. The feasibility of using FFPE kidney tissue specimens to assess extrahepatic contribution to propofol elimination [41–45] or to examine renal drug-drug interactions, which may affect tubular secretion of xenobiotics, remains to be investigated.

3.3. Assessment of the impact of formalin fixation time on FFPE tissue metabolomic and lipidomic profiles

We next compared metabolomic and lipidomic profiles acquired in FFPE samples derived from porcine kidney tissue exposed to different times of formalin incubation (6 h, 30 h and 54 h). As shown in Fig. 4, tissue fixation time had a strong impact on the profiles of lipids (Fig. 4C and D) and small molecules (Fig. 4A and B) demonstrated by pronounced separation of treatment groups (>70% of variability explained by PC1). In order to determine metabolic features that drive differences in FFPE molecular composition, variabilities (CV) between groups of fixation time were used to categorize metabolites. Of the 381 annotated features, 78 remained unaffected (Supplementary Tables S4–S7; CV < 20%, resulting in maximum log2 fold-changes of 0.06–0.75, highlighted in green) and 48 were strongly affected by fixation time (Supplementary Tables S4–S7; CV > 80%, resulting in maximum log2 fold-changes of 1.9–5.4, highlighted in red). Whereas individual species of membrane phospholipids (i.e. phosphatidylcholines (PC), PS and PE) exhibited high variability (CV range: 20–80%) the majority of phosphatidylinositol (PI) species remained unaffected (highest CV = 24.6% for PI 16:0/18:2, Table S7 and Fig. S9). In addition, glycosphingolipids (GSL, di- and tri-hexylceramides) demonstrated low CVs (highest CV = 31.15 for HexCer d18:1/24:1, Table S7 and Fig. S9) indicating that these compounds together with PIs are largely protected from formalin due to the absence of reactive groups. In accordance unaltered amounts of inositol-containing lipids (phosphoinositides) and cerebrosides (glycosphingolipids) in brain tissue exposed to formalin has been observed previously [46] thus supporting our findings. In contrast, the high variability of ethanolamine-containing lipids (i.e. PE and PS species CV range: 20–80%, Tables S6 and S7 and Figs. S8 and S9) reflects their reactivity with formaldehyde due to the amine-containing headgroup [47]. In fact, the relative distribution of

individual PE derivatives (i.e. monomethylated, dimethylated and formylated species) strongly varied with fixation time (Supplementary Fig. S5) hence providing an explanation for the observed variability. Likewise, formalin altered the level of amino acids such as glutamic acid, glutamine and tryptophan (Figs. S6 and S7 and Tables S4 and S5, CVs >30%) possibly reflecting their structural diversity and the multiplicity of reactions with formaldehyde [48]. In addition, lipid species like TAGs and Cer (Fig. S8) or N-acetylated amino acids (Fig. S7) formed distinct sub-clusters dependent on their structural similarity. In contrast, other amino acids such as isoleucine, phenylalanine, tyrosine, leucine, intermediates of the metabolism (taurine and creatinine), several acylcarnitine (AC) species (AC 12:0, AC 16:1, AC 12:0, AC 6:0, AC 14:1, AC 18:0, AC 18:1) and molecules comprising a saturated fatty acid (i.e. Lyso PE 16:0 and 18:0 and fatty acids 16:0 and 18:0) were affected only in a limited fashion (Figs. S6 and S7 and Tables S4 and S5, CVs <20%). Regarding the latter observation, acyl chain saturation seems to be protective towards formalin reactivity as unsaturated fatty acids are well known to react with formaldehyde [49].

So far, alterations in the abundance of some metabolite classes can't be explained unambiguously. At that time we cannot exclude whether the different sizes of kidney tissue samples submerged in formalin (e.g. small pieces vs. complete organ) have an influence on the metabolic profiles which requires further investigation. Nevertheless, given that large differences were observed between the 30 h and 54 h incubation (complete organ submerged in formalin) argues against this assumption. In particular for the 54 h time point, and even much longer fixation times (e.g. >72 h), a more detailed investigation of the impact of sample overfixation [50] on FFPE metabolic profiles will be desired. Albeit beyond the scope of our study, other pre-analytical factors than tissue fixation time may have an influence. These include metabolite leaching during fixation [51], chemical hydrolysis and formaldehyde-induced changes on lipid biosynthesis [52]. Moreover, albeit often quite standardized (e.g. < 1 h as in our cohorts) the time between tissue removal from the patient and fixation is a further parameter that may induce stress due to hypoxia with possible consequences on metabolic profiles. In addition, treatment steps that take place after fixation (i.e. dehydration) could induce metabolite depletion from FFPE tissue and warrants further investigation. In this regard, employing FFPE-embedded adherent 2D culture [18] or mouse-derived kidney tissue [35] may provide appropriate experimental systems. Although these approaches do not reflect heterogeneity of tissue samples typically observed in pathology labs they may allow for a more systematic investigation of formalin-induced changes on FFPE metabolic profiles. In addition, as tissue size (i.e. thickness of paraffin slices) has been demonstrated to impact on FFPE tissue metabolite level [36] a more rigorous investigation of different tissue core sizes (i.e. diameter) subjected to sample preparation is desired.

3.4. Proof of concept: in situ imaging of lipid species found to be unaffected by tissue fixation time

Next we aimed at MALDI-FT-ICR MS imaging analysis within an independent cohort of tissue microarrays (TMA) consisting of ccRCC (n = 64) and corresponding non-tumor tissue [25] focusing on the detection of metabolites found to be unaffected by tissue fixation time (Tables S4–S7, highlighted in green). These compounds were suitable candidates for a proof of concept study since clinical TMAs are compiled as multi-patient arrays which comprise tissue cores derived from different FFPE blocks. The respective tissue specimens likely have faced different fixation times, if collection was done over a period of several years in routine pathology, which may contribute to metabolic alterations as we have observed for porcine kidney (see section 3.3). As these pre-analytical factors cannot be accounted for during TMA preparation in clinical routine, the successful detection of metabolites unaffected by fixation time is highly desirable and may provide a starting point for the discovery of novel prognostic and diagnostic biomarker signatures down to the single-cell level [53].

Out of the metabolites found as unaffected, four species (Lyso PE 18:0, Fatty acids 16:0 and 18:0 as well as PC O-34:3) could be identified in tissues of the TMA that all, except for PC O-34:3, were significantly reduced in tumorous compared to non-tumor (benign) tissue (Fig. 5). Reduced levels of LPE 18:0 in ccRCC were also evident in our proof of concept experiment (Fig. 3 A and C) thus confirming molecular alterations observed in an independent RCC cohort by a different, analytical technology. The successful *in situ* detection of these molecules in TMAs provides a first basis to establish a "stable" panel of molecular features that warrants further investigation with respect to their potential use in high-throughput biomarker discovery and validation by MALDI imaging and LC-MS-based metabolic profiling. In this regard, a broader detection of lipid classes unaffected by fixation time (i.e. glycosphingolipids) is desired and may be achieved by employing ultra-high mass resolving power instruments (i.e. 21-Tesla FT-ICR MS [54]) or by the use of matrix mixtures [55] or new preparations such as 2,6-dihydroxyacetophenone [DHA]/ammonium sulfate/hepta-fluorobutyric acid [HFBA]), as previously demonstrated for sialylated brain glycosphingolipids [56].

4. Conclusion

Because of its broad metabolite profiling capability and robustness, LC-MS-based analytical chemistry provides an important tool to investigate metabolites and lipids in frozen tissue specimens [6,57]. Nevertheless, biomarker discovery in frozen tissue samples is often limited by small cohort sizes as repositories with high numbers of well-annotated samples are limited. These limitations could be overcome by using FFPE tissue samples from which large cohorts are available in pathology archives worldwide. In the present manuscript, we provide a novel sample preparation protocol that allows profiling of metabolites and improved analysis of lipids in clinically archived FFPE tissue specimens. The protocol extends the spectrum of methods to characterize the metabolomic and lipidomic content of histologically defined FFPE tissue cores in a semi-quantitative fashion and may thus complement the examination of histopathological tissue in clinical pathology. This is substantiated by the improved detection of lipid classes (i.e. triglycerides and glycosphingolipids) known to be involved in cancer diagnosis and therapy [39,58]. The repeatability assessment further demonstrated robust and repeatable sample preparation and analysis between different batches (inter-day precision) which may minimize the need for inter-batch corrections in large scale studies. The feasibility of the optimized protocol to discriminate normal and tumorous FFPE tissue samples was shown in a proof of concept experiment and revealed metabolite conservation and metabolic changes that are largely comparable to fresh frozen tissue. In this regard, we note that results of the proof of concept experiment are preliminary and interpretations are limited by the small number of biological replicates. Hence, further investigations in larger sample cohorts are required to confirm these findings. In addition, besides using non-targeted metabolomic profiling methods that are semi-quantitative in nature (as it is impossible to use internal standards comprehensively for hundreds or thousands of metabolites [59]), the use of independent analytical methods is required to reproduce the observed biological effects. Here FFPE tissue sample analysis by quantitative, targeted LC-MS assays [60,61], that rely on

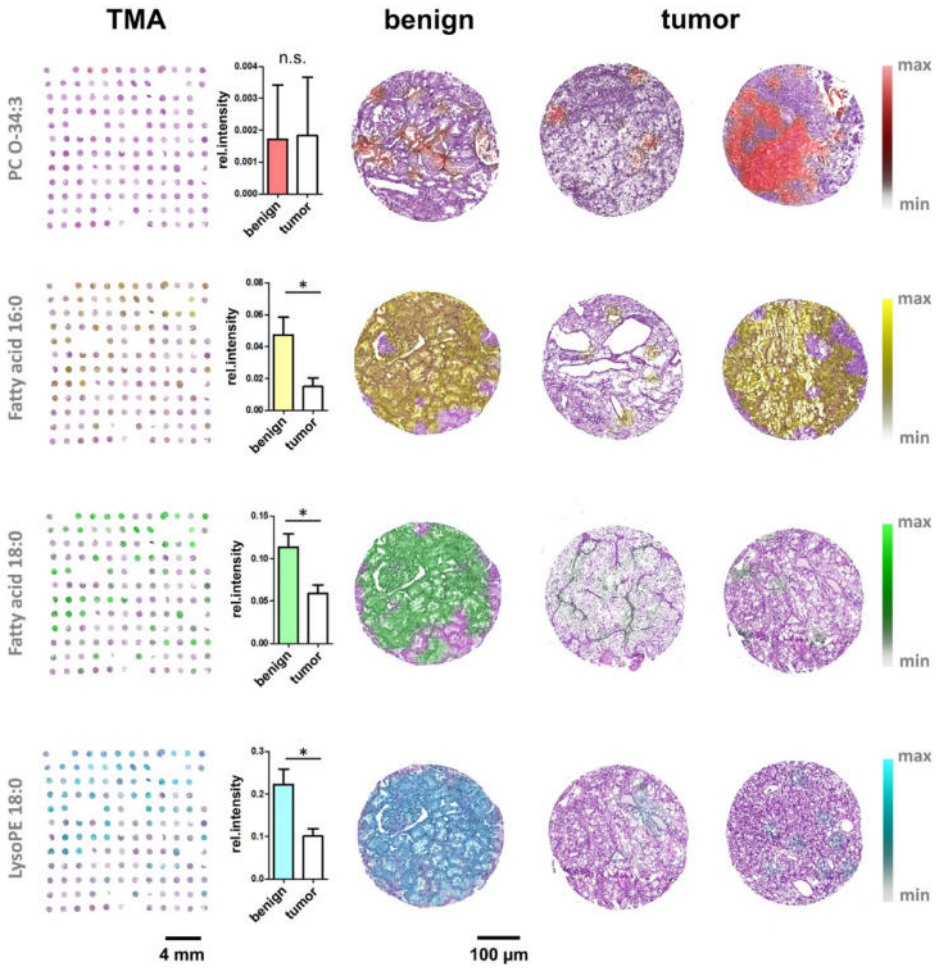

Fig. 5. *In situ* imaging of lipid species in an RCC FFPE tissue microarray. MALDI-FT-ICR MS detection of 4 lipid species on an RCC tissue microarray (TMA) comprising non-tumor and tumor tissue (n = 64, left panel). Higher magnification images of representative patient samples of either non-tumor (benign) or tumor tissue from the TMA are indicated in the right panel. Bar plots in the middle represent the distribution of the relative signal intensities (mean ± SEM) in benign and tumorous TMAs. Lyso PE, Lyso-phosphatidylethanolamine 18:0; PC O-34:3, alkyl ether-linked phosphatidylcholine 34:3. *p < 0.001 (Mann-Whitney *U*-test); n.s., not significant.

isotopically-labeled internal standards and metabolite specific calibration curves, is warranted.

Moreover, we have shown that knowledge gained from LC-MS experiments (i.e. metabolite classes that remain unaffected by fixation time) can guide down-stream analysis by *in situ* imaging as demonstrated by cross validation of biological effects in an independent kidney cancer cohort. Overall, the optimized sample preparation protocol could be applied to an in-depth assessment of pre-analytical factors like ischemic time and length of FFPE tissue storage [62] that likely impact on the result obtained by both LC-MS and imaging-based biomarker research. We emphasize that the LC-MS method used here, operating at analytical flow rates (400–450 µl/min) with narrow-bore columns, did not run at its highest sensitivity. Hence, the use of micro- and nano-flow systems for metabolic profiling of small numbers of cells [63] with improved metabolome coverage [64] will be an important prerequisite to acquire metabolomic or lipidomic [65] profiles of spatially defined areas in the future. In this regard, the high analytical specificity of LC-MS may be further improved by employing ion mobility spectrometry [66–69] and hence support annotation of features that are often unresolved by MALDI imaging approaches. The results presented here provide a first basis for a synergistic combination of LC-MS and MALDI imaging technology in kidney cancer research, which likely will facilitate biomarker discovery and validation in the future.

CRediT authorship contribution statement

Sylvia K. Neef: Methodology, Formal analysis, Investigation, Visualization, Writing - original draft. **Stefan Winter:** Conceptualization, Supervision, Funding acquisition, Writing - review & editing. **Ute Hofmann:** Conceptualization, Supervision, Writing - review & editing. **Thomas E. Mürdter:** Conceptualization, Supervision, Writing - review & editing. **Elke Schaeffeler:** Conceptualization, Supervision, Funding acquisition, Writing - review & editing. **Heike Horn:** Resources, Writing - review & editing. **Achim Buck:** Methodology, Resources, Investigation, Visualization. **Axel Walch:** Methodology, Resources, Funding acquisition, Writing -

review & editing. **Jorg Hennenlotter:** Resources, Writing - review & editing. **German Ott:** Resources, Writing - review & editing. **Falko Fend:** Resources, Writing - review & editing. **Jens Bedke:** Resources, Writing - review & editing. **Matthias Schwab:** Conceptualization, Project administration, Supervision, Funding acquisition, Writing - review & editing. **Mathias Haag:** Conceptualization, Supervision, Writing - original draft, Writing - review & editing, Project administration, Funding acquisition.

Declaration of competing interest

The authors declare that they have no known competing financial interests or personal relationships that could have appeared to influence the work reported in this paper.

Acknowledgements

We gratefully acknowledge Ursula Waldherr and Petra Hitschke for excellent technical assistance. This work was supported by the Robert Bosch Stiftung (Stuttgart, Germany), the Deutsche Forschungsgemeinschaft (DFG, German Research Foundation) under Germany's Excellence Strategy – EXC 2180–390900677, and the ICEPHA Graduate Program, University of Tübingen (Tübingen, Germany). Funding was provided by the Ministry of Education and Research of the Federal Republic of Germany (BMBF; Grant Nos. 01ZX1610B and 01KT1615), the Deutsche Forschungsgemeinschaft (Grant Nos. SFB 824 TP C04, CRC/TRR 205 S01) and the Deutsche Krebshilfe (No. 70112617) to A. Walch.

Appendix A. Supplementary data

Supplementary data to this article can be found online at https://doi.org/10.1016/j.aca.2020.08.005.

References

[1] H.A. Coller, Is cancer a metabolic disease? Am. J. Pathol. 184 (1) (2014) 4–17, https://doi.org/10.1016/j.ajpath.2013.07.035.
[2] T.N. Seyfried, R.E. Flores, A.M. Poff, D.P. D'Agostino, Cancer as a metabolic disease: implications for novel therapeutics, Carcinogenesis 35 (3) (2014) 515–527, https://doi.org/10.1093/carcin/bgt480.
[3] E. Schaeffeler, F. Büttner, A. Reustle, V. Klumpp, S. Winter, S. Rausch, P. Fisel, J. Hennenlotter, S. Kruck, A. Stenzl, J. Wahrheit, D. Sonntag, M. Scharpf, F. Fend, A. Agaimy, A. Hartmann, J. Bedke, M. Schwab, Metabolic and lipidomic reprogramming in renal cell carcinoma subtypes reflects regions of tumor origin, Eur. Urol. Focus 5 (4) (2018) 608–618, https://doi.org/10.1016/j.euf.2018.01.016.
[4] L. Jing, J.-M. Guigonis, D. Borchiellini, M. Durand, T. Pourcher, D. Ambrosetti, LC-MS based metabolomic profiling for renal cell carcinoma histologic subtypes, Sci. Rep. 9 (1) (2019) 15635, https://doi.org/10.1038/s41598-019-52059-y.
[5] J. Pezzatti, J. Boccard, S. Codesido, Y. Gagnebin, A. Joshi, D. Picard, V. Gonzalez-Ruiz, S. Rudaz, Implementation of liquid chromatography-high resolution mass spectrometry methods for untargeted metabolomic analyses of biological samples: a tutorial, Anal. Chim. Acta 1105 (2020) 28–44, https://doi.org/10.1016/j.aca.2019.12.062.
[6] P. Leuthold, E. Schaeffeler, S. Winter, F. Buttner, U. Hofmann, T.E. Murdter, S. Rausch, D. Sonntag, J. Wahrheit, F. Fend, J. Hennenlotter, J. Bedke, M. Schwab, M. Haag, Comprehensive metabolomic and lipidomic profiling of human kidney tissue: a platform comparison, J. Proteome Res. 16 (2) (2017) 933–944, https://doi.org/10.1021/acs.jproteome.6b00875.
[7] P.A. Vorkas, G. Isaac, M.A. Anwar, A.H. Davies, E.J. Want, J.K. Nicholson, E. Holmes, Untargeted UPLC-MS profiling pipeline to expand tissue metabolome coverage: application to cardiovascular disease, Anal. Chem. 87 (8) (2015) 4184–4193, https://doi.org/10.1021/ac503775m.
[8] C. Rombouts, M. de Spiegeleer, L. van Meulebroek, W.H. de Vos, L. Vanhaecke, Validated comprehensive metabolomics and lipidomics analysis of colon tissue and cell lines, Anal. Chim. Acta 1066 (2019) 79–92, https://doi.org/10.1016/j.aca.2019.03.020.
[9] P. Leuthold, M. Schwab, U. Hofmann, S. Winter, S. Rausch, M.N. Pollak, J. Hennenlotter, J. Bedke, E. Schaeffeler, M. Haag, Simultaneous extraction of RNA and metabolites from single kidney tissue specimens for combined transcriptomic and metabolomic profiling, J. Proteome Res. 17 (9) (2018) 3039–3049, https://doi.org/10.1021/acs.jproteome.8b00199.
[10] S. Chen, M. Hoene, J. Li, Y. Li, X. Zhao, H.-U. Haring, E.D. Schleicher, C. Weigert, G. Xu, R. Lehmann, Simultaneous extraction of metabolome and lipidome with methyl tert-butyl ether from a single small tissue sample for ultra-high performance liquid chromatography/mass spectrometry, J. Chromatogr. A 1298 (2013) 9–16, https://doi.org/10.1016/j.chroma.2013.05.019.
[11] X. Wang, W. Han, J. Yang, D. Westaway, L. Li, Development of chemical isotope labeling LC-MS for tissue metabolomics and its application for brain and liver metabolome profiling in Alzheimer's disease mouse model, Anal. Chim. Acta 1050 (2019) 95–104, https://doi.org/10.1016/j.aca.2018.10.060.
[12] H. Horn, J. Bausinger, A.M. Staiger, M. Sohn, C. Schmelter, K. Gruber, C. Kalla, M.M. Ott, A. Rosenwald, G. Ott, Numerical and structural genomic aberrations are reliably detectable in tissue microarrays of formalin-fixed paraffin-embedded tumor samples by fluorescence in-situ hybridization, PLoS One 9 (4) (2014), e95047, https://doi.org/10.1371/journal.pone.0095047.
[13] H. Horn, C. Pott, J. Kalla, M. Dreyling, A. Rosenwald, G. Ott, M. Schwab, E. Schaeffeler, A multiplex MALDI-TOF MS approach facilitates genotyping of DNA from formalin-fixed paraffin-embedded tumour specimens, Pharmacogenetics Genom. 20 (10) (2010) 598–604, https://doi.org/10.1097/FPC.0b013e32833deb16.
[14] O.J.R. Gustafsson, G. Arentz, P. Hoffmann, Proteomic developments in the analysis of formalin-fixed tissue, Biochim. Biophys. Acta 1854 (6) (2015) 559–580, https://doi.org/10.1016/j.bbapap.2014.10.003.
[15] B. Donczo, A. Guttman, Biomedical analysis of formalin-fixed, paraffin-embedded tissue samples: the Holy Grail for molecular diagnostics, J. Pharmaceut. Biomed. Anal. 155 (2018) 125–134, https://doi.org/10.1016/j.jpba.2018.03.065.
[16] T.J. Kokkat, M.S. Patel, D. McGarvey, V.A. LiVolsi, Z.W. Baloch, Archived formalin-fixed paraffin-embedded (FFPE) blocks: a valuable underexploited resource for extraction of DNA, RNA, and protein, Biopreserv. Biobanking 11 (2) (2013) 101–106, https://doi.org/10.1089/bio.2012.0052.
[17] A.D. Kelly, S.B. Breitkopf, M. Yuan, J. Goldsmith, D. Spentzos, J.M. Asara, Metabolomic profiling from formalin-fixed, paraffin-embedded tumor tissue using targeted LC/MS/MS: application in sarcoma, PLoS One 6 (10) (2011), e25357, https://doi.org/10.1371/journal.pone.0025357.
[18] S. Cacciatore, G. Zadra, C. Bango, K.L. Penney, S. Tyekucheva, O. Yanes, M. Loda, Metabolic profiling in formalin-fixed and paraffin-embedded prostate cancer tissues, Mol. Canc. Res. 15 (4) (2017) 439–447, https://doi.org/10.1158/1541-7786.MCR-16-0262.
[19] A. Buck, A. Ly, B. Balluff, N. Sun, K. Gorzolka, A. Feuchtinger, K.-P. Janssen, P.J.K. Kuppen, C.J.H. van de Velde, G. Weirich, F. Erlmeier, R. Langer, M. Aubele, H. Zitzelsberger, M. Aichler, A. Walch, High-resolution MALDI-FT-ICR MS imaging for the analysis of metabolites from formalin-fixed, paraffin-embedded clinical tissue samples, J. Pathol. 237 (1) (2015) 123–132, https://doi.org/10.1002/path.4560.
[20] A. Ly, A. Buck, B. Balluff, N. Sun, K. Gorzolka, A. Feuchtinger, K.-P. Janssen, P.J.K. Kuppen, C.J.H. van de Velde, G. Weirich, F. Erlmeier, R. Langer, M. Aubele, H. Zitzelsberger, L. McDonnell, M. Aichler, A. Walch, High-mass-resolution MALDI mass spectrometry imaging of metabolites from formalin-fixed paraffin-embedded tissue, Nat. Protoc. 11 (8) (2016) 1428–1443, https://doi.org/10.1038/nprot.2016.081.
[21] A.C. Wolff, M.E.H. Hammond, D.G. Hicks, M. Dowsett, L.M. McShane, K.H. Allison, D.C. Allred, J.M.S. Bartlett, M. Bilous, P. Fitzgibbons, W. Hanna, R.B. Jenkins, P.B. Mangu, S. Paik, E.A. Perez, M.F. Press, P.A. Spears, G.H. Vance, G. Viale, D.F. Hayes, Recommendations for human epidermal growth factor receptor 2 testing in breast cancer: American Society of Clinical Oncology/College of American Pathologists clinical practice guideline update, J. Clin. Oncol. 31 (31) (2013) 3997–4013, https://doi.org/10.1200/JCO.2013.50.9984.
[22] Pathologists' guideline recommendations for immunohistochemical testing of estrogen and progesterone receptors in breast cancer, Breast Care (Basel) 5 (3) (2010) 185–187, https://doi.org/10.1159/000315039.
[23] W.J. Howat, B.A. Wilson, Tissue fixation and the effect of molecular fixatives on downstream staining procedures, Methods 70 (1) (2014) 12–19, https://doi.org/10.1016/j.ymeth.2014.01.022.
[24] F. Algaba, I. Trias, M. Scarpelli, L. Boccon-Gibod, Z. Kirkali, H. van Poppel, Handling and pathology reporting of renal tumor specimens, Eur. Urol. 45 (4) (2004) 437–443, https://doi.org/10.1016/j.eururo.2003.11.026.
[25] A. Reustle, P. Fisel, O. Renner, F. Büttner, S. Winter, S. Rausch, S. Kruck, A.T. Nies, J. Hennenlotter, M. Scharpf, F. Fend, A. Stenzl, J. Bedke, M. Schwab, E. Schaeffeler, Characterization of the breast cancer resistance protein (BCRP/ABCG2) in clear cell renal cell carcinoma, Int. J. Canc. 143 (12) (2018) 3181–3193, https://doi.org/10.1002/ijc.31741.
[26] A. Di Minno, B. Porro, L. Turnu, C.M. Manega, S. Eligini, S. Barbieri, M. Chiesa, P. Poggio, I. Squellerio, A. Anesi, S. Fiorelli, D. Caruso, F. Veglia, V. Cavalca, E. Tremoli, Untargeted metabolomics to go beyond the canonical effect of acetylsalicylic acid, J. Clin. Med. 9 (1) (2019), https://doi.org/10.3390/jcm9010051.
[27] R Development Core Team, R: A Language and Environment for Statistical Computing, R Foundation for Statistical Computing, Vienna, Austria, 2017. http://www.R-project.org/.
[28] P. Kampstra, Beanplot: a boxplot alternative for visual comparison of distributions, J. Stat. Softw. Code (28) (2008) 1–9, https://doi.org/10.18637/jss.v028.c01.
[29] G.R. Warnes, B. Bolker, L. Bonebakker, R. Gentleman, W.H.A. Liaw, T. Lumley, M. Maechler, A. Magnusson, S. Moeller, M. Schwartz, B. Venables, Gplots: various R programming tools for plotting data: R package version 3.0.1.

https://CRAN.R-project.org/package=gplots, 2016.
[30] H. Wickham, ggplot2: Elegant Graphics for Data Analysis, Springer-Verlag, New York, 2016.
[31] K. Slowikowski, Ggrepel: automatically position non-overlapping text labels with 'ggplot2': R package version 0.8.0. https://CRAN.R-project.org/package=ggrepel, 2018.
[32] R. Kolde, pheatmap: pretty Heatmaps: R package version 1.0.12. https://CRAN.R-project.org/package=pheatmap, 2019.
[33] A. Eklund, Beeswarm: the bee swarm plot, an alternative to stripchart.: R package version 0.2.3. https://CRAN.R-project.org/package=beeswarm, 2016.
[34] P. Fisel, S. Kruck, S. Winter, J. Bedke, J. Hennenlotter, A.T. Nies, M. Scharpf, F. Fend, A. Stenzl, M. Schwab, E. Schaeffeler, DNA methylation of the SLC16A3 promoter regulates expression of the human lactate transporter MCT4 in renal cancer with consequences for clinical outcome,, Clin. Canc. Res. 19 (18) (2013) 5170–5181, https://doi.org/10.1158/1078-0432.CCR-13-1180.
[35] A. Wojakowska, Ł. Marczak, K. Jelonek, K. Polanski, P. Widlak, M. Pietrowska, An optimized method of metabolite extraction from formalin-fixed paraffin-embedded tissue for GC/MS analysis, PLoS One 10 (9) (2015), e0136902, https://doi.org/10.1371/journal.pone.0136902.
[36] M. Buszewska-Forajta, M. Patejko, S. Macioszek, D. Sigorski, E. Iżycka-Swieszewska, M.J. Markuszewski, Paraffin-embedded tissue as a novel matrix in metabolomics study: optimization of metabolite extraction method, Chromatographia 82 (10) (2019) 1501–1513, https://doi.org/10.1007/s10337-019-03769-y.
[37] M. Yuan. S.B. Breitkopf. X. Yang. J.M. Asara. A positive/negative ion-switching. targeted mass spectrometry-based metabolomics platform for bodily fluids, cells, and fresh and fixed tissue, Nat. Protoc. 7 (5) (2012) 872–881, https://doi.org/10.1038/nprot.2012.024.
[38] M.H. Sarafian, M. Gaudin, M.R. Lewis, F.-P. Martin, E. Holmes, J.K. Nicholson, M.-E. Dumas, Objective set of criteria for optimization of sample preparation procedures for ultra-high throughput untargeted blood plasma lipid profiling by ultra performance liquid chromatography-mass spectrometry, Anal. Chem. 86 (12) (2014) 5766–5774, https://doi.org/10.1021/ac500317c.
[39] D. Zhuo, X. Li, F. Guan, Biological roles of aberrantly expressed glycosphingolipids and related enzymes in human cancer development and progression, Front. Physiol. 9 (2018) 466, https://doi.org/10.3389/fphys.2018.00466.
[40] P. Puri, R.A. Baillie, M.M. Wiest, F. Mirshahi, J. Choudhury, O. Cheung, C. Sargeant, M.J. Contos, A.J. Sanyal, A lipidomic analysis of nonalcoholic fatty liver disease, Hepatology 46 (4) (2007) 1081–1090, https://doi.org/10.1002/hep.21763.
[41] W.S. Al-Jahdari, K. Yamamoto, H. Hiraoka, K. Nakamura, F. Goto, R. Horiuchi, Prediction of total propofol clearance based on enzyme activities in microsomes from human kidney and liver, Eur. J. Clin. Pharmacol. 62 (7) (2006) 527–533, https://doi.org/10.1007/s00228-006-0130-2.
[42] R.J. Dinis-Oliveira, Metabolic profiles of propofol and fospropofol: clinical and forensic interpretative aspects, BioMed Res. Int. 2018 (2018) 6852857, https://doi.org/10.1155/2018/6852857.
[43] H. Hiraoka, K. Yamamoto, S. Miyoshi, T. Morita, K. Nakamura, Y. Kadoi, F. Kunimoto, R. Horiuchi, Kidneys contribute to the extrahepatic clearance of propofol in humans, but not lungs and brain, Br. J. Clin. Pharmacol. 60 (2) (2005) 176–182, https://doi.org/10.1111/j.1365-2125.2005.02393.x.
[44] D. Takizawa, H. Hiraoka, F. Goto, K. Yamamoto, R. Horiuchi, Human kidneys play an important role in the elimination of propofol, Anesthesiology 102 (2) (2005) 327–330, https://doi.org/10.1097/00000542-200502000-00014.
[45] A.A. Raoof, L.J. van Obbergh, J. de Ville Goyet, R.K. Verbeeck, Extrahepatic glucuronidation of propofol in man: possible contribution of gut wall and kidney, Eur. J. Clin. Pharmacol. 50 (1–2) (1996) 91–96, https://doi.org/10.1007/s002280050074.
[46] F.J.M. Heslinga, F.A. Deierkauf, The action of formaldehyde solutions on human brain lipids, J. Histochem. Cytochem. 10 (6) (1962) 704–709, https://doi.org/10.1177/10.6.704.
[47] M. Gaudin, M. Panchal, S. Ayciriex, E. Werner, A. Brunelle, D. Touboul, C. Boursier-Neyret, N. Auzeil, B. Walther, C. Duyckaerts, O. Laprevote, Ultra performance liquid chromatography - mass spectrometry studies of formalin-induced alterations of human brain lipidome, J. Mass Spectrom. 49 (10) (2014) 1035–1042, https://doi.org/10.1002/jms.3424.
[48] D. French, J.T. Edsall, The reactions of formaldehyde with amino acids and proteins, Elsevier (1945) 277–335.
[49] D. Jones, G.A. Gresham, Reaction of formaldehyde with unsaturated fatty acids during histological fixation, Nature 210 (5043) (1966) 1386–1388, https://doi.org/10.1038/2101386b0.
[50] A. Barbera, R. Marginet Flinch, M. Martin, J.L. Mate, A. Oriol, F. Martínez-Soler, T. Santalucia, P.L. Fernandez, The immunohistochemical expression of programmed death ligand 1 (PD-L1) is affected by sample overfixation, Appl. Immunohistochem. Mol. Morphol. (2020), https://doi.org/10.1097/PAI.0000000000000847 [published online ahead of print].
[51] M.J. Hackett, J.A. McQuillan, F. El-Assaad, J.B. Aitken, A. Levina, D.D. Cohen, R. Siegele, E.A. Carter, G.E. Grau, N.H. Hunt, P.A. Lay, Chemical alterations to murine brain tissue induced by formalin fixation: implications for biospectroscopic imaging and mapping studies of disease pathogenesis, Analyst 136 (14) (2011) 2941–2952, https://doi.org/10.1039/c0an00269k.
[52] J. Bai, P. Wang, Y. Liu, Y. Zhang, Y. Li, Z. He, L. Hou, R. Liang, Formaldehyde alters triglyceride synthesis and very low-density lipoprotein secretion in a time-dependent manner, Environ. Toxicol. Pharmacol. 56 (2017) 15–20, https://doi.org/10.1016/j.etap.2017.08.023.
[53] M. Allam, S. Cai, A.F. Coskun, Multiplex bioimaging of single-cell spatial profiles for precision cancer diagnostics and therapeutics, NPJ Precis. Oncol. 4 (2020) 11, https://doi.org/10.1038/s41698-020-0114-1.
[54] A.P. Bowman, G.T. Blakney, C.L. Hendrickson, S.R. Ellis, R.M.A. Heeren, D.F. Smith, Ultra-high mass resolving power, mass accuracy, and dynamic range MALDI mass spectrometry imaging by 21-tesla FT-ICR MS, Anal. Chem. (2020), https://doi.org/10.1021/acs.analchem.9b04768.
[55] J. Wang, C. Wang, X. Han, Enhanced coverage of lipid analysis and imaging by matrix-assisted laser desorption/ionization mass spectrometry via a strategy with an optimized mixture of matrices, Anal. Chim. Acta 1000 (2018) 155–162, https://doi.org/10.1016/j.aca.2017.09.046.
[56] B. Colsch, A.S. Woods, Localization and imaging of sialylated glycosphingolipids in brain tissue sections by MALDI mass spectrometry, Glycobiology 20 (6) (2010) 661–667, https://doi.org/10.1093/glycob/cwq031.
[57] J. Diab, T. Hansen, R. Goll, H. Stenlund, M. Ahnlund, E. Jensen, T. Moritz, J. Florholmen, G. Forsdahl, Lipidomics in ulcerative colitis reveal alteration in mucosal lipid composition associated with the disease state, Inflamm. Bowel Dis. 25 (11) (2019) 1780–1787. https://doi.org/10.1093/ibd/izz098.
[58] D. Ackerman, S. Tumanov, B. Qiu, E. Michalopoulou, M. Spata, A. Azzam, H. Xie, M.C. Simon, J.J. Kamphorst, Triglycerides promote lipid homeostasis during hypoxic stress by balancing fatty acid saturation, e5, Cell Rep. 24 (10) (2018) 2596–2605, https://doi.org/10.1016/j.celrep.2018.08.015.
[59] D. Broadhurst, R. Goodacre, S.N. Reinke, J. Kuligowski, I.D. Wilson, M.R. Lewis, W.B. Dunn, Guidelines and considerations for the use of system suitability and quality control samples in mass spectrometry assays applied in untargeted clinical metabolomic studies, Metabolomics 14 (6) (2018) 72, https://doi.org/10.1007/s11306-018-1367-3.
[60] A.T. Godoy, M.N. Eberlin, A.V.C. Simionato, Targeted metabolomics: liquid chromatography coupled to mass spectrometry method development and validation for the identification and quantitation of modified nucleosides as putative cancer biomarkers, Talanta 210 (2020) 120640, https://doi.org/10.1016/j.talanta.2019.120640.
[61] J.M. Buescher, S. Moco, U. Sauer, N. Zamboni, Ultrahigh performance liquid chromatography-tandem mass spectrometry method for fast and robust quantification of anionic and aromatic metabolites, Anal. Chem. 82 (11) (2010) 4403–4412, https://doi.org/10.1021/ac100101d.
[62] S.M. Thompson, R.A. Craven, N.J. Nirmalan, P. Harnden, P.J. Selby, R.E. Banks, Impact of pre-analytical factors on the proteomic analysis of formalin-fixed paraffin-embedded tissue, Proteom. Clin. Appl. 7 (3–4) (2013) 241–251, https://doi.org/10.1002/prca.201200086.
[63] X. Luo, L. Li, Metabolomics of small numbers of cells: metabolomic profiling of 100, 1000, and 10000 human breast cancer cells, Anal. Chem. 89 (21) (2017) 11664–11671, https://doi.org/10.1021/acs.analchem.7b03100.
[64] A.J. Chetwynd, A. David, A review of nanoscale LC-ESI for metabolomics and its potential to enhance the metabolome coverage, Talanta 182 (2018) 380–390, https://doi.org/10.1016/j.talanta.2018.01.084.
[65] O. Knittelfelder, S. Traikov, O. Vvedenskaya, A. Schuhmann, S. Segeletz, A. Shevchenko, A. Shevchenko, Shotgun lipidomics combined with laser capture microdissection: a tool to analyze histological zones in cryosections of tissues, Anal. Chem. 90 (16) (2018) 9868–9878, https://doi.org/10.1021/acs.analchem.8b02004.
[66] C. Hinz, S. Liggi, G. Mocciaro, S. Jung, I. Induruwa, M. Pereira, C.E. Bryant, S.W. Meckelmann, V.B. O'Donnell, R.W. Farndale, J. Fjeldsted, J.L. Griffin, A comprehensive UHPLC ion mobility quadrupole time-of-flight method for profiling and quantification of eicosanoids, other oxylipins, and fatty acids, Anal. Chem. 91 (13) (2019) 8025–8035, https://doi.org/10.1021/acs.analchem.8b04615.
[67] J.D. Quell, W. Romisch-Margl, M. Haid, J. Krumsiek, T. Skurk, A. Halama, N. Stephan, J. Adamski, H. Hauner, D. Mook-Kanamori, R.P. Mohney, H. Daniel, K. Suhre, G. Kastenmüller, Characterization of bulk phosphatidylcholine compositions in human plasma using side-chain resolving lipidomics, Metabolites 9 (6) (2019), https://doi.org/10.3390/metabo9060109.
[68] X. Zheng, F.B. Smith, N.A. Aly, J. Cai, R.D. Smith, A.D. Patterson, E.S. Baker, Evaluating the structural complexity of isomeric bile acids with ion mobility spectrometry, Anal. Bioanal. Chem. 411 (19) (2019) 4673–4682, https://doi.org/10.1007/s00216-019-01869-0.
[69] P.D. Rainville, I.D. Wilson, J.K. Nicholson, G. Isaac, L. Mullin, J.I. Langridge, R.S. Plumb, Ion mobility spectrometry combined with ultra performance liquid chromatography/mass spectrometry for metabolic phenotyping of urine: effects of column length, gradient duration and ion mobility spectrometry on metabolite detection, Anal. Chim. Acta 982 (2017) 1–8, https://doi.org/10.1016/j.aca.2017.06.020.

Supplementary Figures

Optimized Protocol for Metabolomic and Lipidomic Profiling in Formalin-Fixed Paraffin-Embedded Kidney Tissue by LC-MS

Sylvia K. Neef [a], Stefan Winter [a], Ute Hofmann [a], Thomas E. Muerdter [a], Elke Schaeffeler [a,g], Heike Horn [a], Achim Buck [d], Axel Walch [d], Jörg Hennenlotter [e], German Ott [a,b], Falko Fend [e,f], Jens Bedke [e], Matthias Schwab[a,c,g] and Mathias Haag[a,*]

[a] Dr. Margarete Fischer-Bosch-Institute of Clinical Pharmacology, Stuttgart, Germany and University of Tübingen, Tübingen, Germany

[b] Department of Clinical Pathology, Robert-Bosch Hospital, Stuttgart, Germany

[c] Departments of Clinical Pharmacology, Pharmacy and Biochemistry University Tübingen, Tübingen, Germany

[d] Research Unit Analytical Pathology, Helmholtz Zentrum München, Neuherberg, Germany

[e] Department of Urology, University Hospital Tübingen, Tübingen, Germany

[f] Institute of Pathology and Neuropathology, University Hospital Tübingen, Tübingen, Germany

[g] iFIT Cluster of Excellence (EXC2180) "Image Guided and Functionally Instructed Tumor Therapies", University of Tübingen, Tübingen, Germany

***Corresponding Author**

Mathias Haag, PhD
Dr. Margarete Fischer-Bosch-Institute of Clinical Pharmacology
Auerbachstr. 112, 70376 Stuttgart, Germany
Phone: +49(0)711/8101-5429. Fax: +49(0)711/85 91 95
E-mail: mathias.haag@ikp-stuttgart.de

Fig. S1

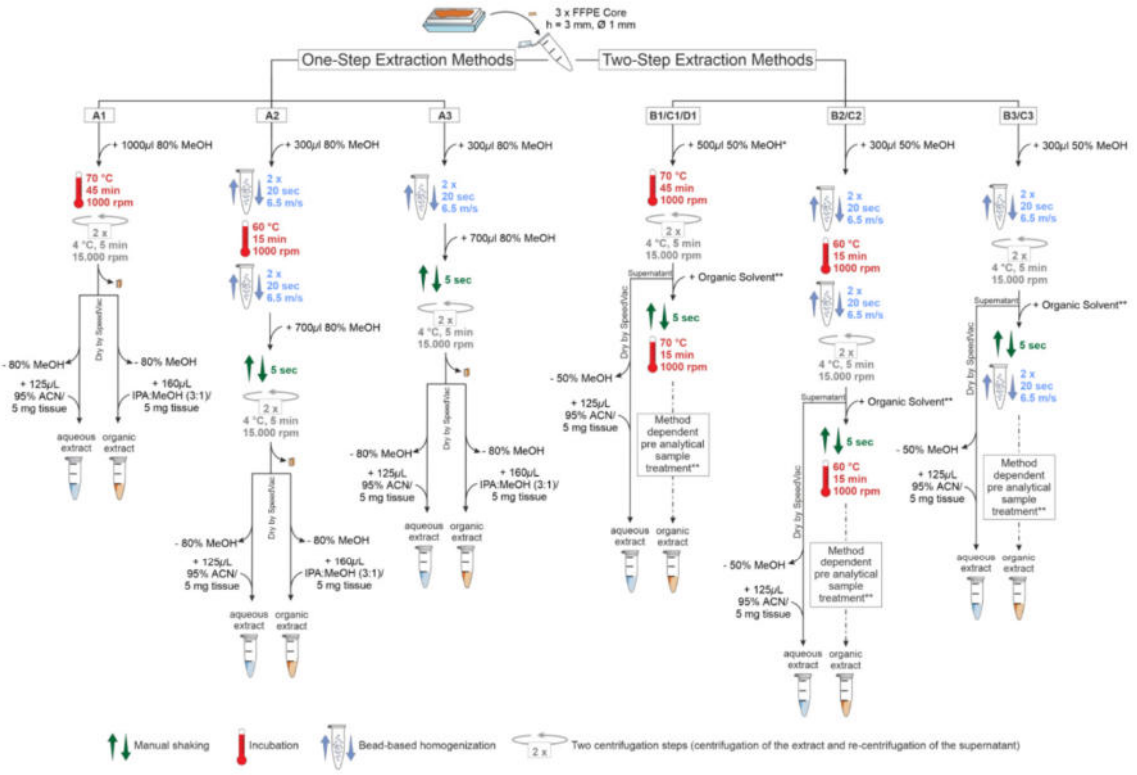

Sample preparation protocols tested for metabolomic and lipidomic profiling in FFPE tissue by LC-MS. Ten different methods, covering one-step (A1–A3) and two-step (B1–B3, C1-C3 and D1) sample preparation protocols were assessed. FFPE kidney tissue was prepared from fresh frozen porcine kidney. Three technical replicates (FFPE cores) were prepared per biological replicate, and each protocol was assessed by five biological replicates. The use of incubation in heated solvent and/or bead beating is indicated by a red temperature sign and reaction vessel filled with beads. Manual shaking (vortexing) and centrifugation is displayed by green and grey arrows, respectively. Small orange pieces indicate FFPE tissue core samples. Note: protocol A1 represents an adaption from protocols that have been used for FFPE metabolite profiling previously [1–3]. Protocol C3 represents an adaption from a protocol used for fresh frozen tissue homogenization [4]. *80% methanol was used for protocol D1 to assess a potential contribution of the methanol proportion (50% vs. 80%) as part of the aqueous extraction step on subsequent detection sensitivity and repeatability of lipids (see Fig. S4). **Organic extraction in methods B and D was done with 120µl isopropanol (IPA)/5 mg of FFPE tissue weight followed by dilution with 40µl MeOH/5mg and LC-MS analysis after centrifugation without drying. Organic extraction in methods C was done with 300µl MTBE:MeOH (3:1, v/v) followed by drying and re-suspending in 125 μL ACN:H_2O (95:5)/5 mg FFPE. Aqueous and organic extracts were analyzed by HILIC-QTOF-MS and RPLC-QTOF-MS, respectively [4].

Fig. S2

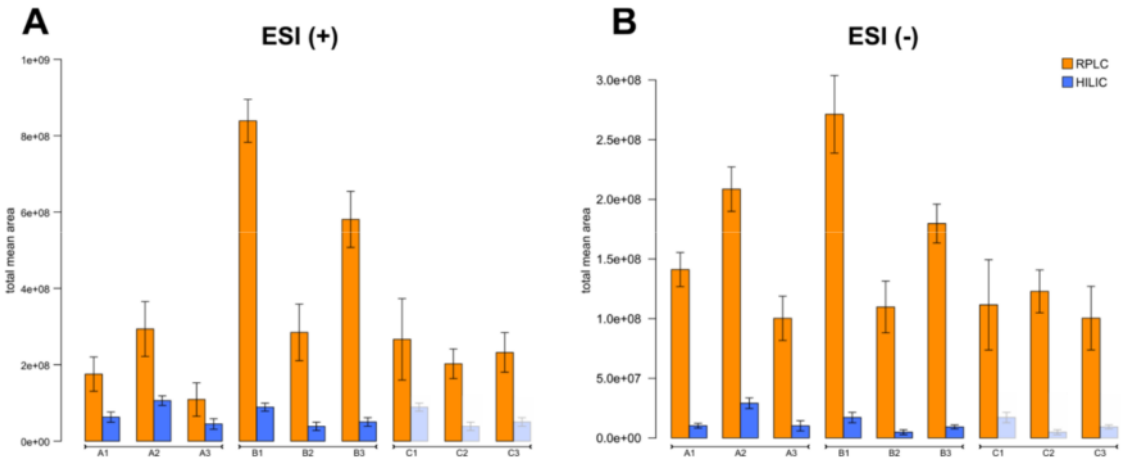

Assessment of detection sensitivity for metabolomic and lipidomic profiling in FFPE tissue by LC-MS. Bar plots displaying total mean areas ± standard deviation (n = 5, biological replicates) of signal intensities achieved by different FFPE tissue sample preparation protocols (see Fig. S1). Total mean area represents the non-normalized sum of extracted ion chromatograms of 268 metabolite species [4] preprocessed by targeted feature extraction. LC-MS analysis of polar molecules in aqueous (HILIC, blue bars) and lipids in organic extracts (RPLC, orange bars) in ESI positive (A) and negative (B) ionization mode is indicated. Information on signal intensities achieved with protocol D1 is displayed in Fig. S4. Note: barplot data for protocols C1–C3 (HILIC mode) is identical to data from protocols B1–B3 and therefore displayed in light blue.

Fig. S3

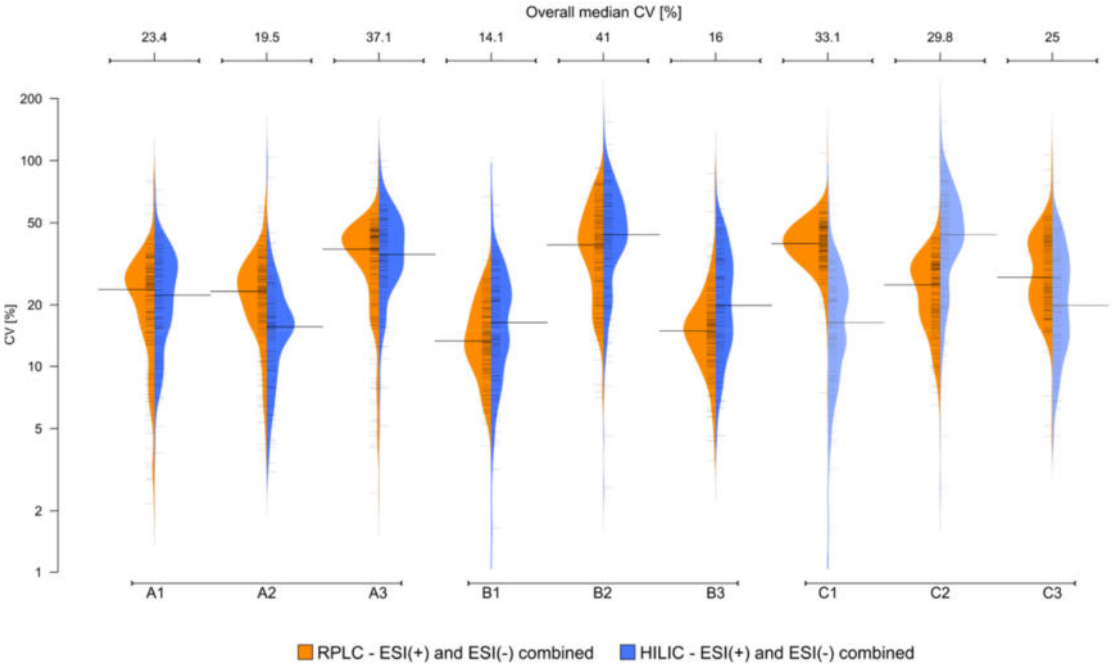

Repeatability assessment of metabolomic and lipidomic profiling in FFPE tissue by LC-MS. Bean plots representing the mean coefficient of variation (CVs) of 268 metabolite species [4] (black thin lines) preprocessed by targeted feature extraction. Data acquired in organic (orange) and aqueous (blue) extracts after sample preparation by different protocols (see Fig. S1) is presented. Non-normalized peak areas were used for CV calculation and corresponding results for positive and negative ionization mode were combined. Median CVs are indicated by the larger horizontal black lines. Overall method CVs are listed above the beanplots. Note: beanplot data for protocols C1–C3 (HILIC mode) is identical to data from protocols B1–B3 and therefore displayed in light blue.

Fig. S4

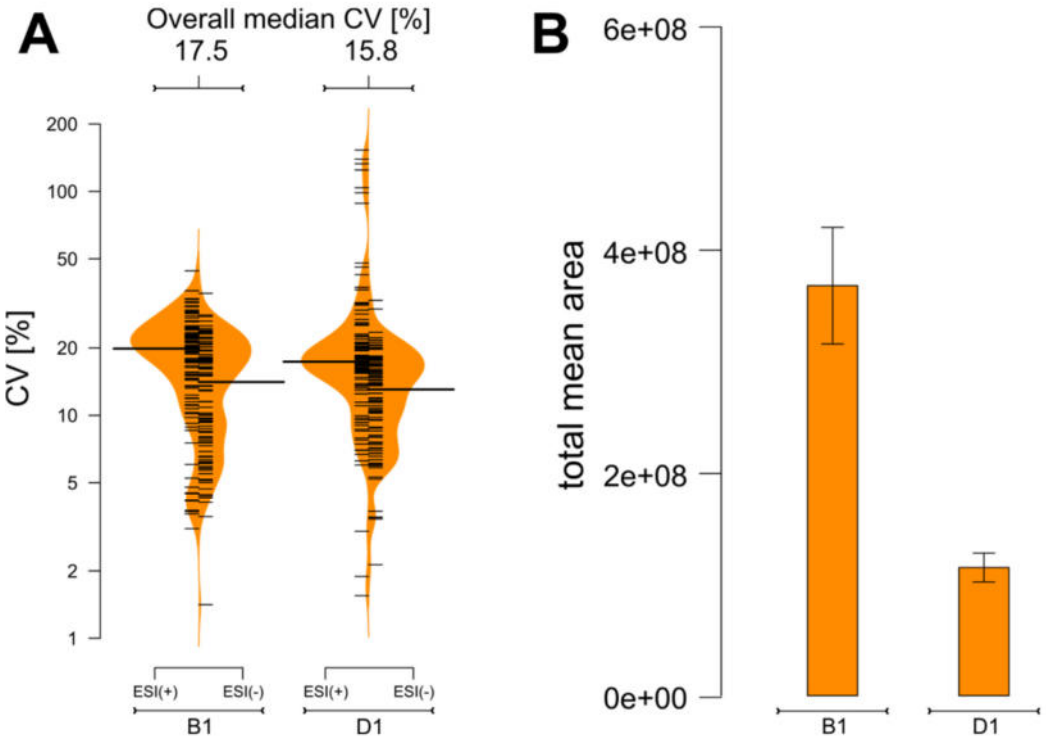

Assessment of methanol proportion used in aqueous extraction on the detection sensitivity and repeatability of lipid analysis. Bean plots (A) and bar plots (B) displaying the coefficients of variation (CVs) and mean signal intensities (total mean area) ± standard deviation of 268 metabolite species previously annotated in fresh frozen kidney tissue [4]. Data from organic extraction with IPA is presented preceding aqueous pre-extraction with 50% (B1) or 80% (D1) methanol. The left side of the beanplots show results analysed in positive ionization mode while negative ionization mode data is displayed on the right side. Median CVs of each single mode are indicated by the larger horizontal black lines. Black thin lines are representing the CV of each metabolite analyzed. Combined median CVs (ESI pos and ESI neg) are listed above the beanplots.

Fig. S5

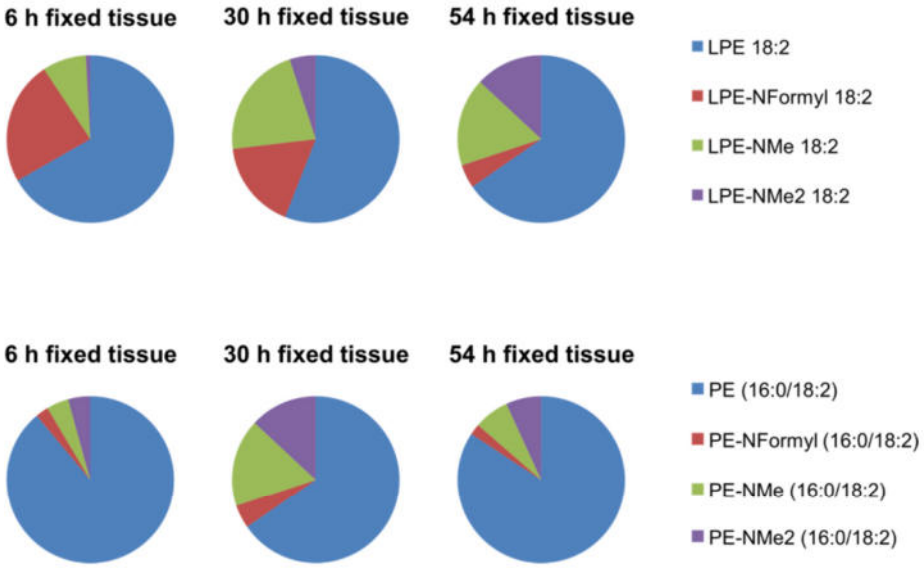

Relative proportion of endogenous and formalin-induced derivatives of phosphatidylethanolamine dependent on tissue fixation time. The proportion of lyso-phosphatidylethanolamine (LPE) 18:2 and phosphatidylethanolamine (PE) 16:0/18:2 and corresponding monomethylated (NMe), dimethylated (NMe2) and formylated (NFormyl) derivatives is displayed for 6 h, 30 h and 54 h tissue fixation. See Table S3 for characteristic fragment ions used to annotate methylated PE species [5]. Pie charts represent mean data from five technical replicates acquired in HILIC ESI (-) mode (LPE species) and RPLC ESI (-) mode (PE species).

Fig. S6

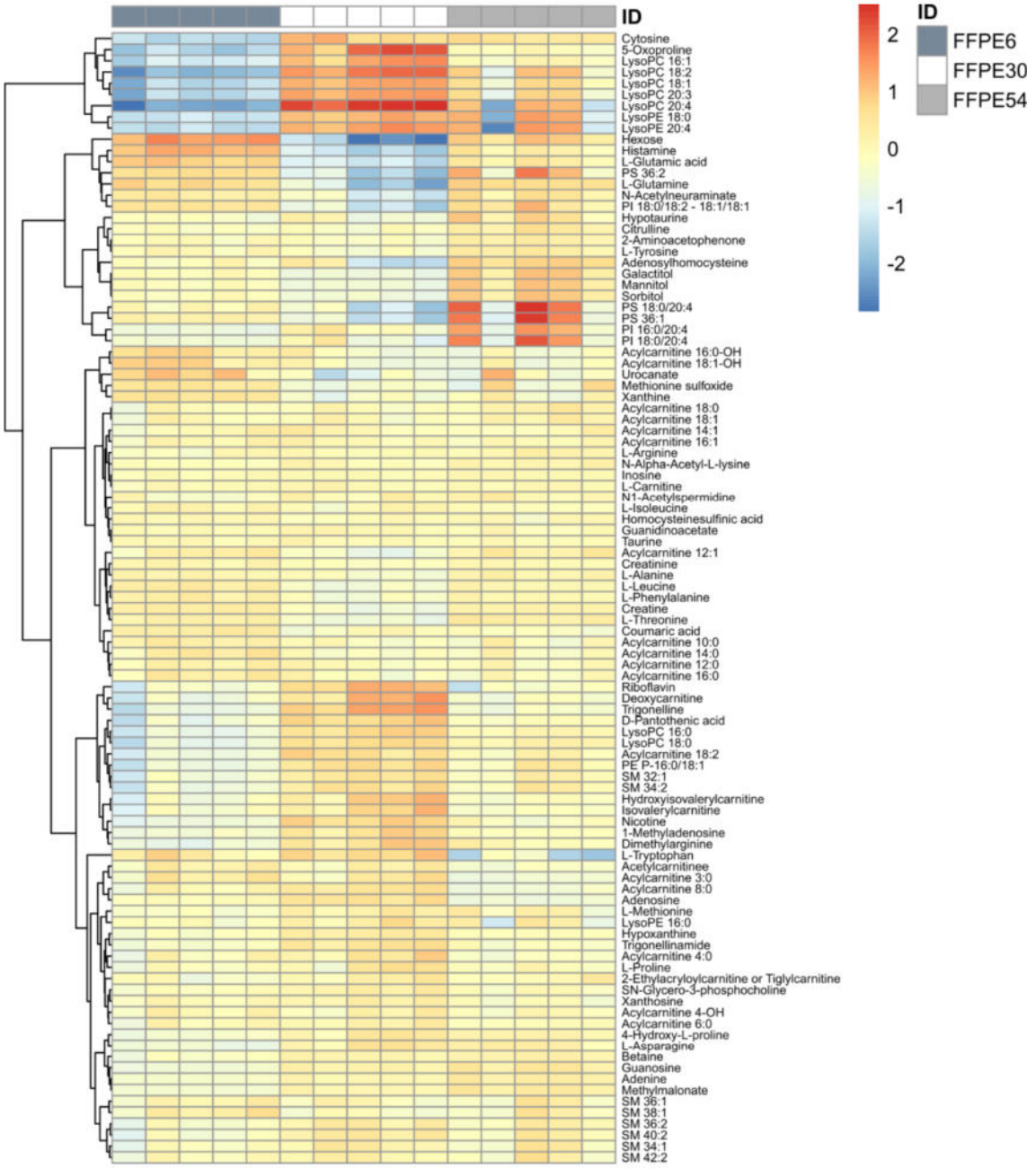

Hierarchical clustering of metabolites in FFPE kidney tissue dependent on formalin fixation time – HILIC-ESI (+) mode. List of assigned metabolites in fresh frozen kidney tissue extracts [4] was used for data preprocessing by targeted feature extraction. FFPE kidney tissue was prepared from fresh frozen porcine kidney (n = 5, technical replicates per incubation group) fixed for 6 h, 30 h and 54 h.

Fig. S7

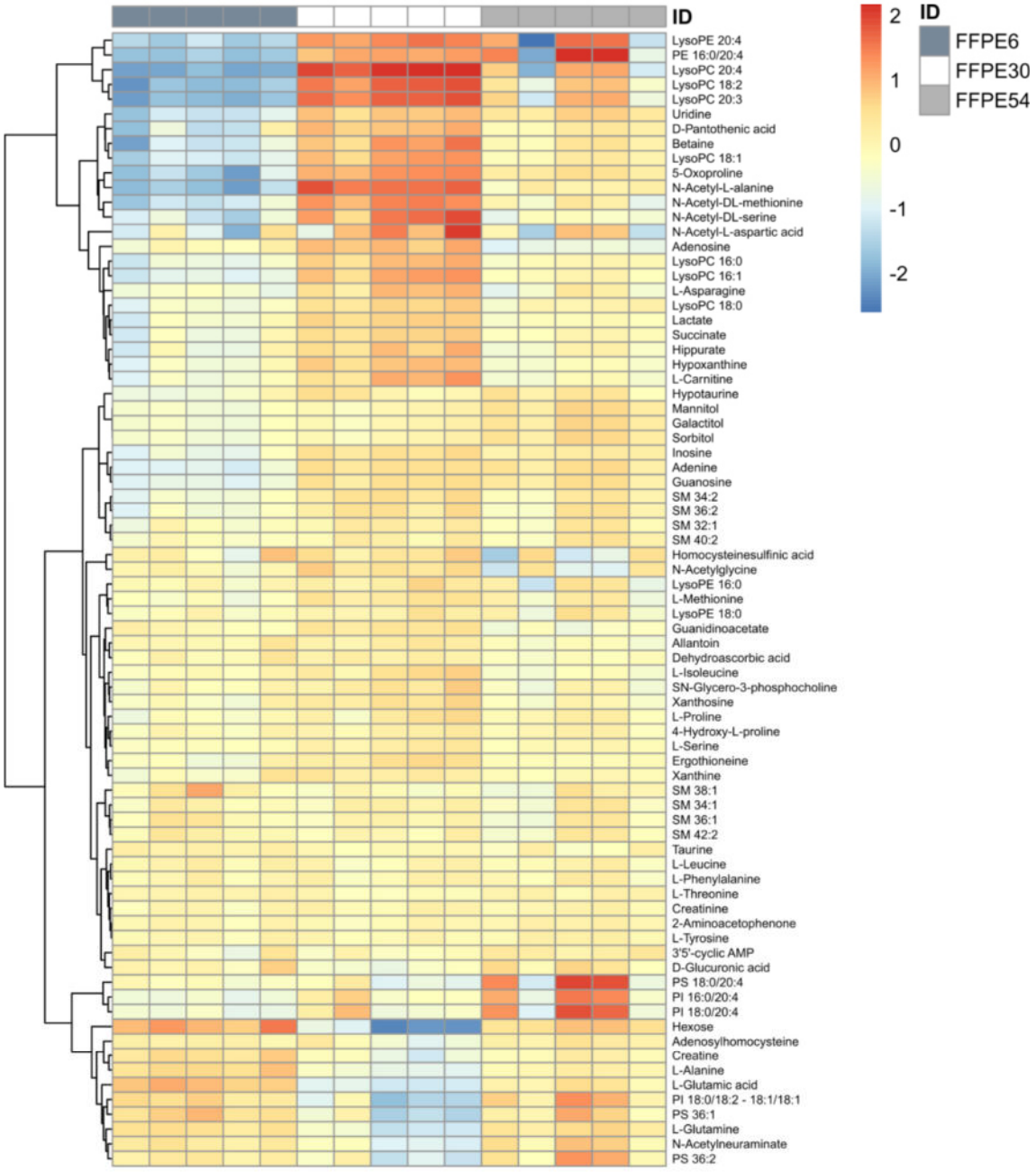

Hierarchical clustering of metabolites in FFPE kidney tissue dependent on formalin fixation time – HILIC-ESI (-) mode. List of assigned metabolites in fresh frozen kidney tissue extracts [4] was used for data preprocessing by targeted feature extraction. FFPE kidney tissue was prepared from fresh frozen porcine kidney (n = 5, technical replicates per incubation group) fixed for 6 h, 30 h and 54 h.

Fig. S8

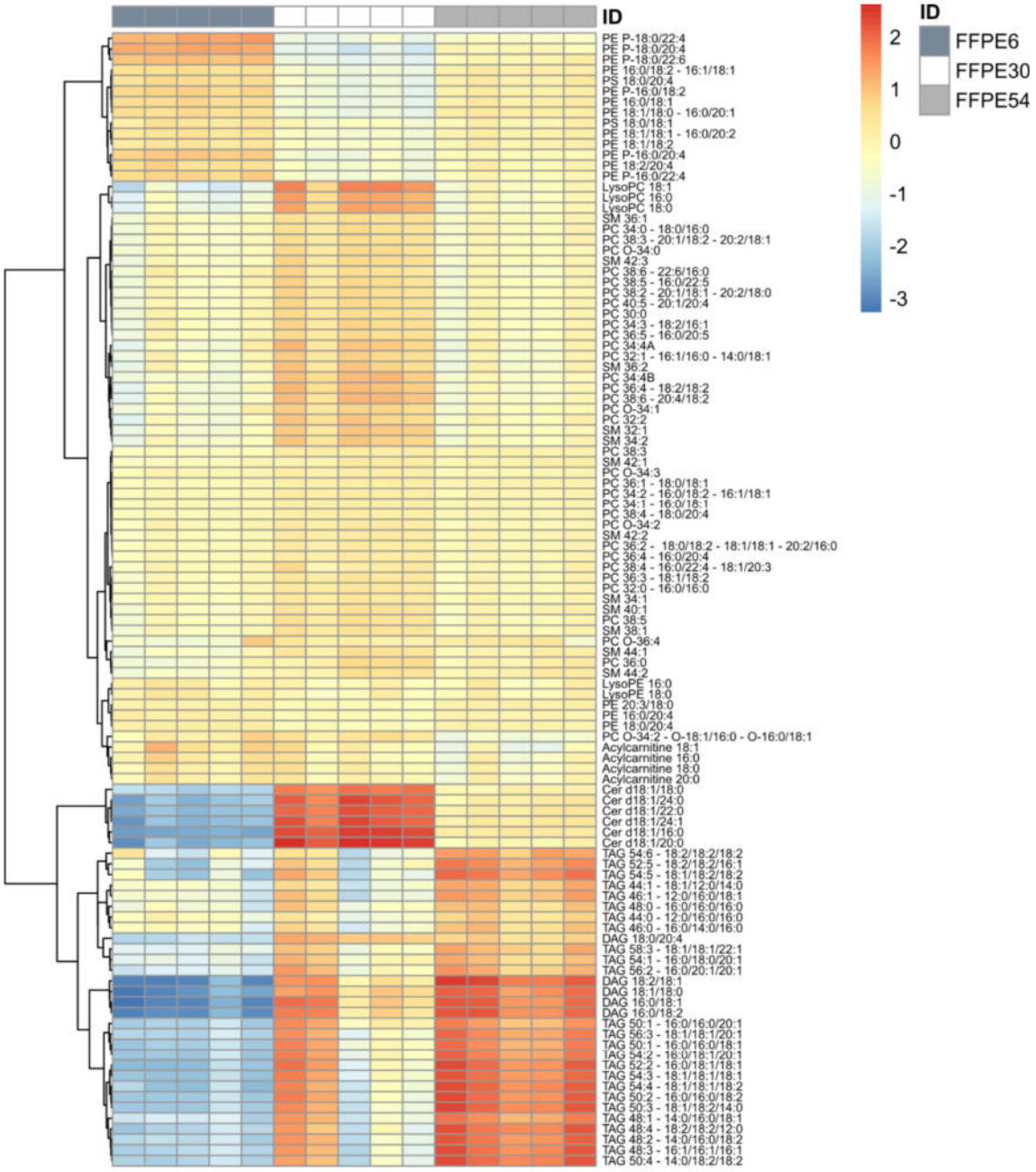

Hierarchical clustering of metabolites in FFPE kidney tissue dependent on formalin fixation time – RPLC-ESI (+) mode. List of assigned metabolites in fresh frozen kidney tissue extracts [4] was used for data preprocessing by targeted feature extraction. FFPE kidney tissue was prepared from fresh frozen porcine kidney (n = 5, technical replicates per incubation group) fixed for 6 h, 30 h and 54 h.

Fig. S9

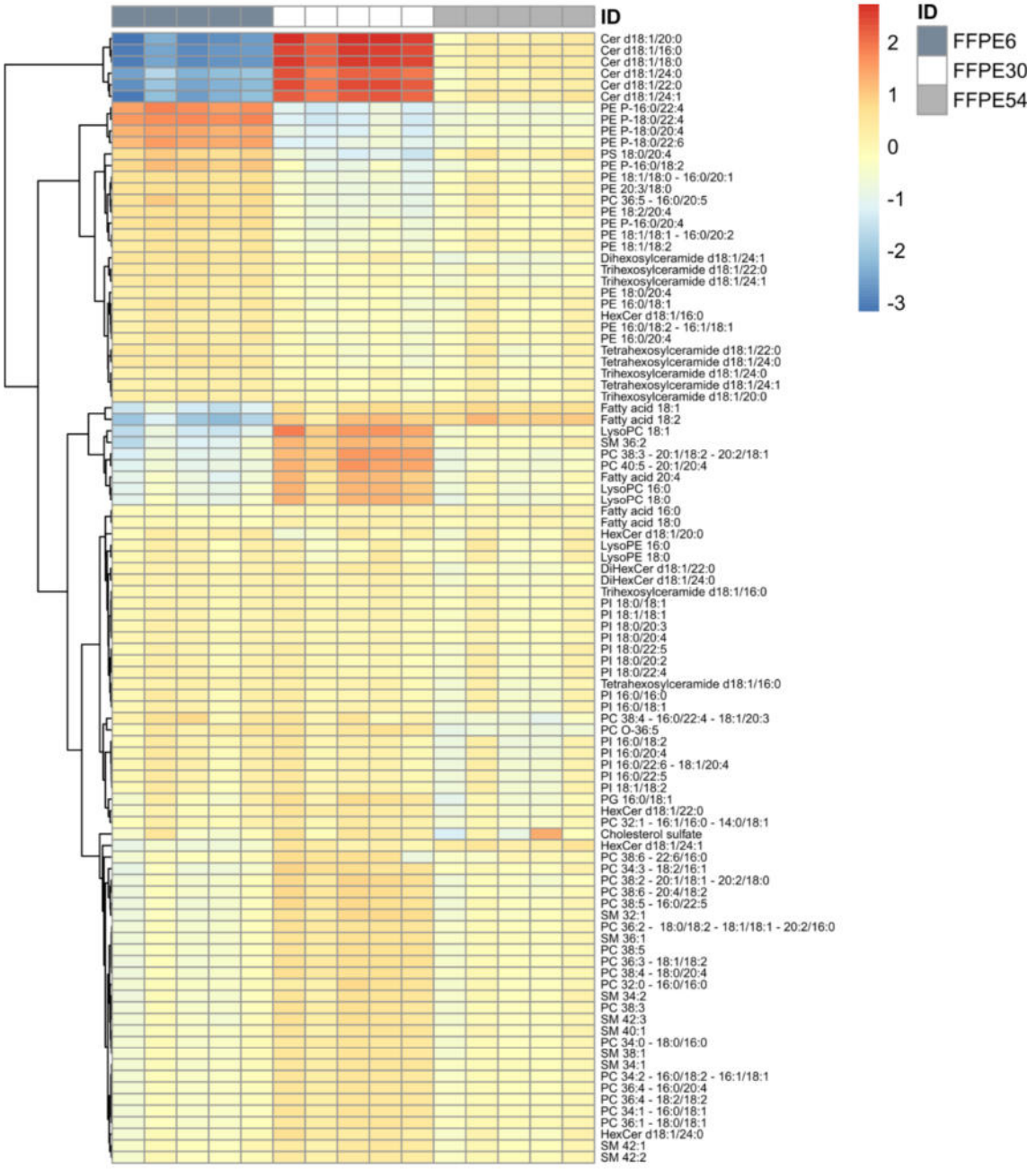

Hierarchical clustering of metabolites in FFPE kidney tissue dependent on formalin fixation time – RPLC-ESI (-) mode. List of assigned metabolites in fresh frozen kidney tissue extracts [4] was used for data preprocessing by targeted feature extraction. FFPE kidney tissue was prepared from fresh frozen porcine kidney (n = 5, technical replicates per incubation group) fixed for 6 h, 30 h and 54 h.

References

[1] M. Yuan, S.B. Breitkopf, X. Yang, J.M. Asara, A positive/negative ion-switching, targeted mass spectrometry-based metabolomics platform for bodily fluids, cells, and fresh and fixed tissue, Nat. Protoc. 7 (5) (2012) 872–881. https://doi.org/10.1038/nprot.2012.024.

[2] A.D. Kelly, S.B. Breitkopf, M. Yuan, J. Goldsmith, D. Spentzos, J.M. Asara, Metabolomic profiling from formalin-fixed, paraffin-embedded tumor tissue using targeted LC/MS/MS: Application in sarcoma, PLoS ONE 6 (10) (2011) e25357. https://doi.org/10.1371/journal.pone.0025357.

[3] S. Cacciatore, G. Zadra, C. Bango, K.L. Penney, S. Tyekucheva, O. Yanes, M. Loda, Metabolic Profiling in Formalin-Fixed and Paraffin-Embedded Prostate Cancer Tissues, Mol. Cancer Res. 15 (4) (2017) 439–447. https://doi.org/10.1158/1541-7786.MCR-16-0262.

[4] P. Leuthold, E. Schaeffeler, S. Winter, F. Buttner, U. Hofmann, T.E. Murdter, S. Rausch, D. Sonntag, J. Wahrheit, F. Fend, J. Hennenlotter, J. Bedke, M. Schwab, M. Haag, Comprehensive Metabolomic and Lipidomic Profiling of Human Kidney Tissue: A Platform Comparison, J. Proteome Res. 16 (2) (2017) 933–944. https://doi.org/10.1021/acs.jproteome.6b00875.

[5] M. Gaudin, M. Panchal, S. Ayciriex, E. Werner, A. Brunelle, D. Touboul, C. Boursier-Neyret, N. Auzeil, B. Walther, C. Duyckaerts, O. Laprévote, Ultra performance liquid chromatography - mass spectrometry studies of formalin-induced alterations of human brain lipidome, J. Mass Spectrom. 49 (10) (2014) 1035–1042. https://doi.org/10.1002/jms.3424.

Supplementary Methods

Optimized Protocol for Metabolomic and Lipidomic Profiling in Formalin-Fixed Paraffin-Embedded Kidney Tissue by LC-MS

Sylvia K. Neef [a], Stefan Winter [a], Ute Hofmann [a], Thomas E. Muerdter [a], Elke Schaeffeler [a,g], Heike Horn [a], Achim Buck [d], Axel Walch [d], Jörg Hennenlotter [e], German Ott [a,b], Falko Fend [e,f], Jens Bedke [e], Matthias Schwab[a,c,g] and Mathias Haag[a,*]

[a] Dr. Margarete Fischer-Bosch-Institute of Clinical Pharmacology, Stuttgart, Germany and University of Tübingen, Tübingen, Germany

[b] Department of Clinical Pathology, Robert-Bosch Hospital, Stuttgart, Germany

[c] Departments of Clinical Pharmacology, Pharmacy and Biochemistry University Tübingen, Tübingen, Germany

[d] Research Unit Analytical Pathology, Helmholtz Zentrum München, Neuherberg, Germany

[e] Department of Urology, University Hospital Tübingen, Tübingen, Germany

[f] Institute of Pathology and Neuropathology, University Hospital Tübingen, Tübingen, Germany

[g] iFIT Cluster of Excellence (EXC2180) "Image Guided and Functionally Instructed Tumor Therapies", University of Tübingen, Tübingen, Germany

***Corresponding Author**

Mathias Haag, PhD
Dr. Margarete Fischer-Bosch-Institute of Clinical Pharmacology
Auerbachstr. 112, 70376 Stuttgart, Germany
Phone: +49(0)711/8101-5429. Fax: +49(0)711/85 91 95
E-mail: mathias.haag@ikp-stuttgart.de

1. LC-QTOF-MS analysis

Aqueous extracts were analyzed by HILIC (Acquity UPLC BEH Amide Column, 1.7 µm, 2.1 mm × 150 mm; Waters, Eschborn, Germany) and organic extracts were analyzed by RPLC (Acquity UPLC BEH C8, 1.7 µm, 2.1 mm × 100 mm; Waters, Eschborn, Germany) coupled to the 6550 iFunnel quadrupole time-of-flight mass spectrometer (QTOF-MS) from Agilent Technologies as previously described [1]. Gradient elution at analytical flow rates (µl/min) for HILIC and RPLC analysis each with a total run time of 30 min per sample was applied as follows:

Column	Flow-rate (mL/min)	Mobile phase A	Mobile phase B	Injection volume (μL)	Needle wash	Gradient	
						Time (min)	% B
HILIC	0.40	10 mM AmAc and 0.125% FA in water:ACN 1:1, v/v	10 mM AmAc and 0.125% FA in water:ACN 5:95, v/v	5	95 % ACN	0.00	92
						3.00	92
						18.00	0
						18.01	92
						30	92
RPLC	0.45	5 mM AmAc in water:MeOH 8:2, v/v	5 mM AmAc in MeOH:ACN:IPA 7.5:2:0.5, v/v/v	3	100 % IPA	0.00	65
						1.00	65
						4.00	80
						20.00	100
						25.00	100
						26.50	65
						30	65

For both separation systems the autosampler was operated at 6 °C and the column oven at 60 °C. Analytical batches were analyzed by mass spectrometry in positive and negative ion mode in a subsequent manner with the same solvent mixture to ensure retention time comparability between ionization modes. After finishing the analysis for a particular stationary phase (HILIC or RPLC), the solvent system and the analytical column was manually changed, followed by sample analysis on the remaining stationary phase. For each batch, quality control (QC) samples were prepared by pooling equal volumes of reconstituted sample extracts. For each mode (i.e. HILIC ESI(+), HILIC ESI(-), RPLC ESI(+) and RPLC ESI(-)), an individual QC sample was prepared (i.e. one organic and one aqueous QC sample

from FFPE tissue extracts). Paraffin blank extracts were not included in the preparation of QC samples. FFPE samples were analyzed without additional dilution. For column conditioning five to ten QC sample injections were carried out at the beginning of each batch. In addition, after five to six samples a QC sample injections was performed. Data acquisition was performed with the Mass Hunter Acquisition Software (version B.05.01) and auto MS/MS analysis (pooled QC sample) and reference mass correction were applied as described [2]. Electrospray parameters were as follows for the analytical modes (HILIC/RPLC): gas and sheath gas temperature, 175/ 225 and 200/250 °C; drying gas and sheath gas flow, 16 L/min and 12 L/min; nebulizer pressure, 45 psig; capillary and nozzle voltage, 3500/3800 and 100/300 V; fragmentor and octopole radio frequency peak voltage, 350 and 750 V. The QTOF was operated in the extended dynamic range mode (~2 GHz) and low mass range (up to 1700 m/z) resulting in mass resolutions between 20.000 and 25.000 (m/z-range: 600−630) for positive and negative ion mode. The slicer was set to high resolution. The mass analyzer was calibrated on a daily basis immediately before starting an analytical run. TOF-MS spectra acquisition was carried out in centroid mode (intensity threshold 10 counts/ 0.001%) at an acquisition rate of 4 spectra/s from m/z 50 to 1650. Fragment spectra acquisition by auto MS/MS analysis (data-dependent mode) was done at a rate of 3 spectra/s for MS1 and MS/MS acquisitions. MS/MS spectra were triggered from precursors that exceeded an absolute threshold of 200 counts and by selecting maximal 3 precursors per cycle. Collision energy (V) was adjusted as a function of m/z ($3.5 \times m/z \times 100^{-1} + 7$) and the quadrupole band-pass for precursor isolation was set to medium (~4 m/z). Metabolite structural assignment with auto MS/MS fragment spectra information was done as described [1] and by searching metabolites in the CEU Mass Mediator tool [3,4].

2. MALDI imaging

For MALDI imaging, tissue sectioning of the FFPE TMA was performed with a thickness of 4 µm and mounted onto 1:1 (v/v) poly-L-lysine: 0.1% Nonidet P-40 pretreated (Sigma-Aldrich) indium tin-oxide glass slides (Bruker Daltonics, Bremen, Germany). Subsequently, the FFPE section was incubated for 1 h at 70°C, deparaffinized in xylene (2 × 8 min), and allowed to air-dry. 10 mg/ml 9-aminoacridine hydrochloride monohydrate matrix (Sigma-Aldrich) in 70% methanol was deposited in eight passes (ascending flow rates 10 µl/min, 20 µl/min, 30 µl/min for layers 1–3, and layers 4–8 with 40 µl/min, line distance: 2 mm, spray velocity: 900 mm/min) onto the section using the SunCollect™ sprayer (Sunchrom, Friedrichsdorf, Germany). MALDI-FT-ICR MS imaging was performed on a Bruker Solarix 7 T FT-ICR MS (Bruker Daltonics), controlled by solariXcontrol (v.1.5.0, Bruker Daltonics) and flexImaging (v.4.0, Bruker Daltonics). Data were acquired in negative ion mode over a mass range of *m/z* 50–1000 with a 1 M data point transient (0.367 s duration) and an estimated resolution of 49,000 at m/z 400. The laser operated at a frequency of 1,000 Hz utilizing 100 laser shots and 60 µm lateral resolution. L-Arginine was used for external calibration in the ESI mode. Following measurement, 9-aminoacridine matrix was removed from the TMA with 70% ethanol, tissues were stained with hematoxylin and eosin (H&E), coverslipped and scanned with a Mirax Desk scanner (Zeiss, Göttingen, Germany) using an objective with 20× magnification. The digitized image was coregistered to respective MSI data using flexImaging 4.0.

References

[1] P. Leuthold, E. Schaeffeler, S. Winter, F. Buttner, U. Hofmann, T.E. Murdter, S. Rausch, D. Sonntag, J. Wahrheit, F. Fend, J. Hennenlotter, J. Bedke, M. Schwab, M. Haag, Comprehensive Metabolomic and Lipidomic Profiling of Human Kidney Tissue: A Platform Comparison, J. Proteome Res. 16 (2) (2017) 933–944. https://doi.org/10.1021/acs.jproteome.6b00875.

[2] P. Leuthold, M. Schwab, U. Hofmann, S. Winter, S. Rausch, M.N. Pollak, J. Hennenlotter, J. Bedke, E. Schaeffeler, M. Haag, Simultaneous Extraction of RNA and Metabolites from Single Kidney Tissue Specimens for Combined Transcriptomic and Metabolomic Profiling, J. Proteome Res. 17 (9) (2018) 3039–3049. https://doi.org/10.1021/acs.jproteome.8b00199.

[3] Gil de la Fuente, Alberto, J. Godzien, M. Fernández López, F.J. Rupérez, C. Barbas, A. Otero, Knowledge-based metabolite annotation tool: CEU Mass Mediator, J. Pharm. Biomed. Anal. 154 (2018) 138–149. https://doi.org/10.1016/j.jpba.2018.02.046.

[4] A. Gil-de-la-Fuente, J. Godzien, S. Saugar, R. Garcia-Carmona, H. Badran, D.S. Wishart, C. Barbas, A. Otero, CEU Mass Mediator 3.0: A Metabolite Annotation Tool, J. Proteome Res. 18 (2) (2019) 797–802. https://doi.org/10.1021/acs.jproteome.8b00720.

6.1.2. **Akzeptierte Publikation 2:**

Metabolic Drug Response Phenotyping in Colorectal Cancer Organoids by LC-QTOF-MS

Sylvia K. Neef [1,#], Nicole Janssen [1,#], Stefan Winter [1], Svenja K. Wallisch [1], Ute Hofmann [1], Marc H. Dahlke [1,2], Matthias Schwab [1,3,4], Thomas E. Mürdter [1,#] and Mathias Haag [1,#]

[1] *Dr. Margarete Fischer-Bosch-Institute of Clinical Pharmacology, Stuttgart, Germany and University of Tuebingen, Tuebingen, Germany*
[2] *Department of Surgery, Robert-Bosch Hospital, Stuttgart, Germany*
[3] *Departments of Clinical Pharmacology, and of Pharmacy and Biochemistry, University of Tuebingen, Tuebingen, Germany*
[4] *Cluster of Excellence iFIT (EXC 2180) „Image-Guided and Functionally Instructed Tumor Therapies“, University of Tuebingen, Germany*
[#] *contributed equally*

Metabolites **2020**, 10, 494; doi: 10.3390/metabo10120494

metabolites

MDPI

Article

Metabolic Drug Response Phenotyping in Colorectal Cancer Organoids by LC-QTOF-MS

Sylvia K. Neef [1,†], Nicole Janssen [1,†], Stefan Winter [1], Svenja K. Wallisch [1], Ute Hofmann [1], Marc H. Dahlke [1,2], Matthias Schwab [1,3,4], Thomas E. M rdter [1,†] and Mathias Haag [1,*,†]

1 Dr. Margarete Fischer-Bosch-Institute of Clinical Pharmacology, Stuttgart, Germany and University of Tuebingen, 70376 Tuebingen, Germany; Sylvia.Neef@ikp-stuttgart.de (S.K.N.); Nicole.Janssen@ikp-stuttgart.de (N.J.); Stefan.Winter@ikp-stuttgart.de (S.W.); Svenja.Wallisch@ikp-stuttgart.de (S.K.W.); Ute.Hofmann@ikp-stuttgart.de (U.H.); Marc.Dahlke@rbk.de (M.H.D.); Matthias.Schwab@ikp-stuttgart.de (M.S.); Thomas.Muerdter@ikp-stuttgart.de (T.E.M.)

2 Department of Surgery, Robert-Bosch Hospital, 70376 Stuttgart, Germany

3 Departments of Clinical Pharmacology, and of Pharmacy and Biochemistry, University of Tuebingen, 72074 Tuebingen, Germany

4 Cluster of Excellence iFIT (EXC 2180), Image-Guided and Functionally Instructed Tumor Therapies, University of Tuebingen, 72074 Tuebingen, Germany

* Correspondence: mathias.haag@ikp-stuttgart.de; Tel.: +49-711-8101-5429

† These authors have contributed equally to this work.

Received: 25 September 2020; Accepted: 27 November 2020; Published: 1 December 2020

Abstract: As metabolic rewiring is crucial for cancer cell proliferation, metabolic phenotyping of patient-derived organoids is desirable to identify drug-induced changes and trace metabolic vulnerabilities of tumor subtypes. We established a novel protocol for metabolomic and lipidomic proling of colorectal cancer organoids by liquid chromatography quadrupole time-of-ight mass spectrometry (LC-QTOF-MS) facing the challenge of capturing metabolic information from a minimal sample amount (<500 cells/injection) in the presence of an extracellular matrix (ECM). The best procedure of the tested protocols included ultrasonic metabolite extraction with acetonitrile/methanol/water (2:2:1, *v/v/v*) without ECM removal. To eliminate ECM-derived background signals, we implemented a data ltering procedure based on the *p*-value and fold change cut-offs, which retained features with signal intensities >120% compared to matrix-derived signals present in blank samples. As a proof-of-concept, the method was applied to examine the early metabolic response of colorectal cancer organoids to 5-uorouracil treatment. Statistical analysis revealed dose-dependent changes in the metabolic proles of treated organoids including elevated levels of 2′-deoxyuridine, 2′-*O*-methylcytidine, inosine and 1-methyladenosine and depletion of 2′-deoxyadenosine and specic phospholipids. In accordance with the mechanism of action of 5-uorouracil, changed metabolites are mainly involved in purine and pyrimidine metabolism. The novel protocol provides a rst basis for the assessment of metabolic drug response phenotypes in 3D organoid models.

Keywords: metabolomics; lipidomics; metabolic proling; organoids; colorectal cancer; QTOF; LC-MS

1. Introduction

Around one decade ago the groups of Hans Clevers [1] and Yoshiki Sasai [2] revolutionized cell culture with their pioneering work in the eld of organoids. Organoids are stem cell-derived 3D structures that mimic the in vivo situation more precisely in terms of architecture, cell-type composition and self-renewal properties compared to current 2D cell culture models [1 5]. Thus, organoid cultures

have emerged as a promising model in the elds of drug discovery, personalized medicine and cancer research [6,7]. In particular, in the context of cancer, organoids gained great importance as they can be generated from patient biopsies allowing the analysis of tumor evolution, heterogeneity and even patient-specic treatment responses [8]. With colorectal cancer (CRC) being the third most common cancer in both sexes [9] and an overall response rate of 1736% to standard chemotherapy [10], it is highly relevant to identify biomarkers that accurately predict the patient response.

Like other cancer entities [11,12] CRC undergoes specic metabolic reprogramming during carcinogenesis [13] including dysregulation of energy [13] and lipid metabolism [14,15]. Therefore, metabolism has been suggested as a targetable vulnerability in CRC [16]. Further, a comprehensive analysis of metabolic changes upon treatment might help to identify a composite set of metabolites serving as a biomarker for the patient response. Consequently, the combination of well-established culture strategies for primary CRC organoids [1,4] and non-targeted metabolomic and lipidomic proling [17,18] is a promising approach in drug research and biomarker discovery. The combination of these techniques enables a high-throughput drug screening using a patient derived model that mimics the in vivo situation more closely and may support new approaches towards personalized therapies.

In contrast to other omics-technologies including genomics [8], transcriptomics [19] and proteomics [20] metabolomics is rarely used for characterization of organoid models. Whereas protocols for cell culture metabolomics are well established [21], only a few studies captured the metabolome from organoids by using NMR [22] and targeted [23] or non-targeted [24 26] LC-MS based proling. In terms of non-targeted metabolomic proling, there is an acute lack of optimization studies addressing problems such as the required sample amount and sampling conditions. Moreover, the inuence of background signals derived from the protein based hydrogel, which is often indispensable for organoid culturing as a basal membrane matrix, on metabolomics data preprocessing has not been addressed comprehensively.

In this work, we describe the evaluation of an optimized extraction protocol enabling untargeted metabolomic and lipidomic proling of CRC organoids grown in the extracellular matrix (ECM) via hydrophilic interaction liquid chromatography (HILIC)- and reversed phase liquid chromatography (RPLC)-QTOF-MS [17].

2. Results and Discussion

2.1. Assessment of Sample Preparation for Metabolomic and Lipidomic Proling in CRC Organoids

To maintain their 3D-structure, organoids need to be cultured surrounded by an ECM. The ECM used in our experiments is a gelatinous protein mixture that is liquid at low temperatures but polymerizes upon incubation at 37 °C. In order to establish a sample preparation protocol for non-targeted metabolomic and lipidomic proling of CRC organoids cultured in ECM, we tested different organoid sampling procedures (see Figure 1). Washing with phosphate-buffered saline (PBS) was carried out at two different temperatures. First, washing with 4 °C PBS (protocols A and B) was chosen, as cold washing is a commonly used procedure for metabolism quenching and to remove extracellular medium components for untargeted metabolomics of cultured cells [27]. As ECM becomes depolymerized (i.e., liqueed) in the cold, washing at physiological temperature (37 °C) was tested as alternative (protocol C). The higher temperature keeps matrix proteins in the polymerized state and in consequence retains organoid cells embedded in their matrix.

For all three protocols, metabolite recovery from organoids was achieved by extraction with the solvent mixture acetonitrile/methanol/water (ACN/MeOH/H_2O, 2:2:1, *v/v/v*), which has previously been applied to targeted [28] and untargeted [18] metabolic proling of human cells and organoids [24] in a slightly modied composition (3:5:2, *v/v/v*). However, the rather polar nature of the solvent may compromise the recovery of non-polar lipids. As two-step extraction protocols are frequently applied to increase metabolite coverage [17,29], a potential benet of organic re-extraction with monophasic methyl tert-butyl ether/methanol (MTBE/MeOH, 3:1, *v/v*), as part of the protocol B, was investigated.

Method quality rating was achieved based on the number of metabolites that could be detected (p-value <0.05, Welchs test, fold change [FC] > 1, n = 5 technical replicates) above ECM blank samples. Further method repeatability was assessed by the median coefficients of variation (CVs) of those metabolites.

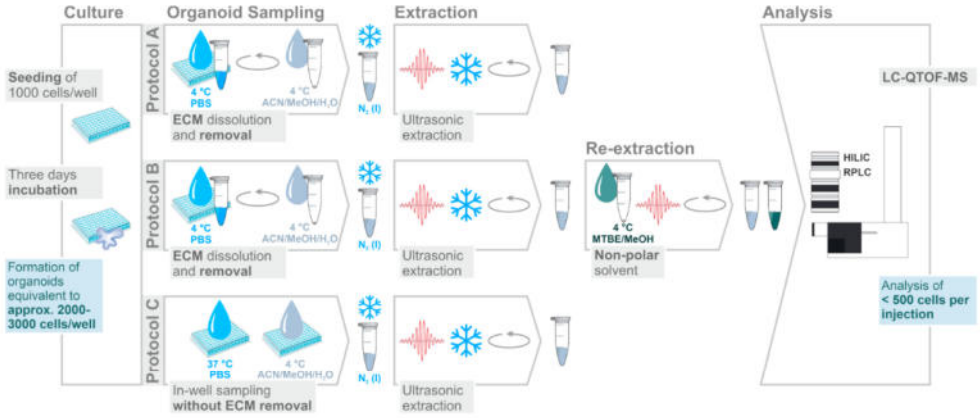

Figure 1. Extraction protocols evaluated for metabolomic and lipidomic proling of colorectal cancer (CRC) organoids using LC-QTOF-MS after dual LC separation by HILIC and RPLC. The number of seeded cells/well was determined using an hemocytometer. Cell numbers after incubation were approximated based on the doubling time (3.4 days) as determined in concomitant experiments. Cell numbers for LC-MS analysis were calculated based on the solvent volumes used for sample preparation (optimized protocol C, see Supplementary Figure S7). Resulting extracts were dried and reconstituted in appropriate solvent prior to LC-QTOF-MS analysis.

In total, 107 unique metabolites could be detected (above ECM blank, Supplementary Figures S1S4) with an overlap between protocols ranging from 12% to 60% depending on the LC-MS mode (Supplementary Figure S5). As becomes evident from the diagrams the sample preparation protocol C resulted in the highest number of polar molecules (Table 1 and Supplementary Figures S1B, S2B, S5A and S5B) and lipids (Table 1 and Supplementary Figures S3C, S4C, S5C and S5D) compared to protocols A and B. Notably, the overlap between RPLC and HILIC was only 6% for protocol C (Supplementary Figure S6) indicating an increase in metabolome coverage by employing multiple LC-MS methods used together with this sample preparation protocol. In particular, the quantity of phospholipid species (e.g., belonging to phosphatidylcholines (PCs) and phosphatidylinositols (PIs)) and sphingolipids (e.g., ceramides (Cers) and sphingomyelins (SMs)) was markedly improved by in-well sampling without ECM removal (protocol C) compared to the ECM dissolution and removal procedure (protocols A and B). An explanation for the lower number of lipid species detected with protocols A and B may be due to the additional centrifugation step, which likely retains residual lipids in the supernatant. An alternative scenario may be metabolite leakage during ECM dissolution and removal, as indicated by reduced signal intensity of lipid-like species in colon carcinoma cells after cell washing with PBS or water [27]. Both scenarios however warrant further investigation. Notably, albeit protocol C resulted in a general improvement of the detection of phospholipids, only two-step extraction (protocol B) allowed for the analysis of non-polar triacylglycerols (e.g., TAG 52:2, Supplementary Figure S3B). Hence, as the formation of TAG-containing lipid droplets (LD) has been associated with tumorigenicity [30] in intestinal stem cells, sequential extraction may be an appropriate procedure to examine neutral lipid metabolism in CRC organoids. While protocol B enabled most repeatable measurements of lipids (median CV < 9%, Table 1), protocol C represented the best compromise between metabolite coverage (1754 metabolites for all modes) and repeatability as indicated by median CVs 1027% (Table 1). Thus, protocol C (37 °C PBS washing and in well sampling) offers a fast and simple procedure for repeatable metabolic phenotyping of colon cancer organoids with reasonable coverage of metabolites and lipids. In particular, the protocol enables

rapid quenching of metabolic reactions in less than 1 min and metabolite extracts from 30 samples are ready for LC-MS analysis within less than 2 h. Such advantages of fast extraction with minimal cell manipulation are in accordance with recent ndings from protocol optimization experiments for tumor spheroid metabolomics, where the optimized protocol consisted of rapid on plate washing followed by cold methanol extraction [31].

Table 1. Number of metabolites with signicantly and relevantly higher abundance in organoid samples compared to respective controls (ECM only) following different sample preparation protocols and LC QTOF-MS methods in the indicated electrospray ionization (ESI) mode.

Protocol	Analytical Mode	No. of Signicant and Relevant Metabolites (Organoids vs. ECM Controls)	Median CV of Signicant and Relevant Metabolites (%)
A	RPLC ESI (−)	17	21.7
	RPLC ESI (+)	12	14.7
B	RPLC ESI (−)	13	7.0
	RPLC ESI (+)	13	8.9
A/B [1]	HILIC ESI (−)	15	25.7
	HILIC ESI (+)	19	33.5
C	RPLC ESI (−)	44	13.6
	RPLC ESI (+)	54	10.4
	HILIC ESI (−)	17	26.8
	HILIC ESI (+)	25	16.2

[1] Data of protocols A and B was combined for statistical evaluation, as sample preparation for both protocols is identical in the HILIC mode, see Figure 1.

2.2. *Filtering of ECM-Derived Background Features by Fold Change and p-Value*

Like other high throughput assays, non-targeted metabolomic proling experiments are subject to variations due to unwanted experimental or biological noise. Especially for 3D organoids, the basement membrane matrix, which is inherently composed of biomolecules (e.g., structural proteins), represents a rich source of signals that can affect downstream normalization and statistical analysis (i.e., reduced statistical power due to high number of tests). Thus, ltering of background features is an important step that has not yet received sufficient attention in the untargeted metabolomics analysis of cultured organoids.

The use of fold change (FC) cutoffs (biological signal/blank signal) to remove features with insufficient abundance in biological samples is a common ltering method [32,33]. The two-step ltering procedure that we had chosen, which was based on a fold change (FC) of 1.2 (mean abundance of ECM blank samples + 20%) and an uncorrected signicance level of 5% (i.e., Welchs *t*-test *p*-value < 0.05, comparing biological samples vs. ECM blank samples), retained 19.5% and 26% of features in HILIC and 25.7% and 28.6% in RPLC in the positive and negative mode, respectively (Figure 2, green dots). The majority of features was ltered out (>70%, Figure 2, grey and purple dots) and was considered to be uninformative background derived from cell culture environment and other contaminants (e.g., vials or solvents) [34].

Such a proportion of eliminated features are typically achieved by other procedures that also make use of blank samples [35] where 74% and 76% of low quality features were excluded from publicly available urine and cell line test datasets, respectively. Notably, our two-step ltering procedure further removed features with high variability (max CV = 214% before and 76.1% after ltering, Supplementary Figure S8) hence demonstrating a benecial e ffect of background noise elimination on the repeatability of organoid sample analysis.

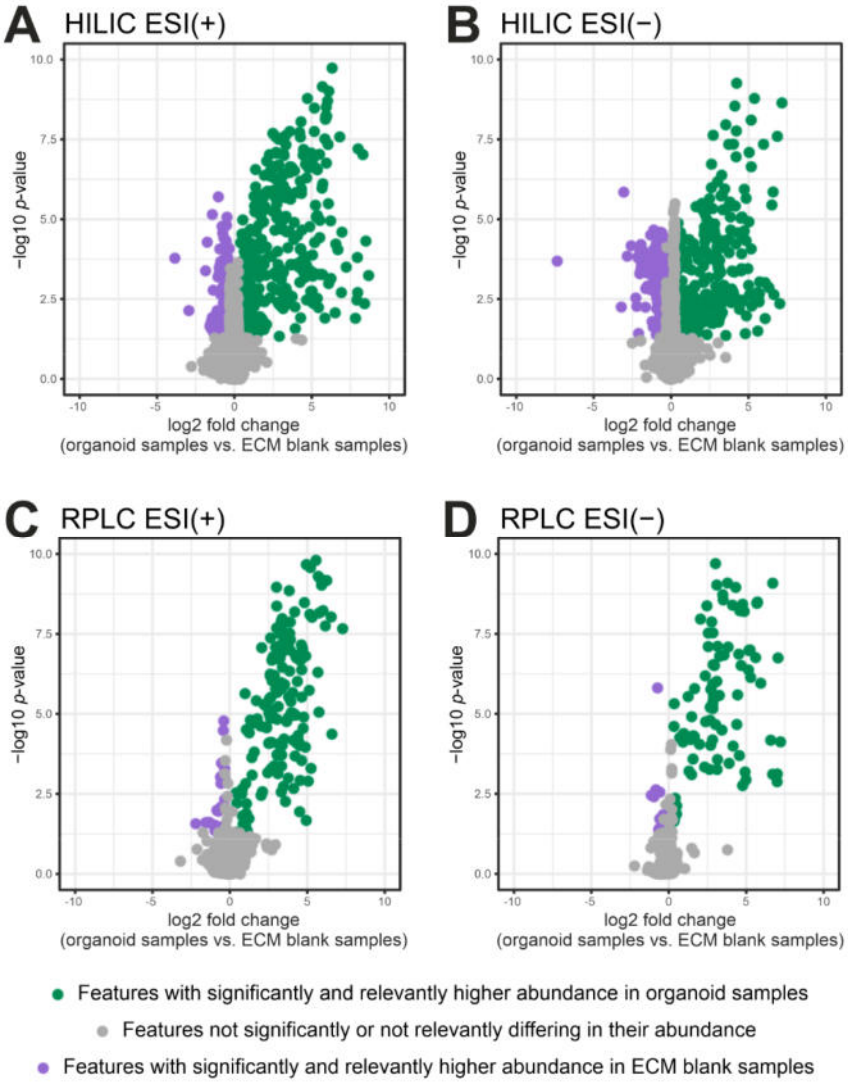

Figure 2. Volcano plots comparing the abundance of features detected in organoid samples (n = 5) and ECM-blank samples (n = 3): (**A**) HILIC ESI (+) mode; (**B**) HILIC ESI (−) mode; (**C**) RPLC ESI (+) mode; (**D**) RPLC ESI (−) mode. Features with signicantly and relevantly higher abundance in organoid samples (fold change (FC) > 1.2, $p < 0.05$, HILIC ESI (+)/(−): 311/299 features and RPLC ESI (+)/(−): 149/92 features) are colored in green and are considered to be cell derived. Features with signicantly and relevantly higher abundance in ECM-blank samples (FC < 0.8, $p < 0.05$, HILIC ESI (+)/(−): 113/117 features and RPLC ESI (+)/(−): 25/13 features) are colored in purple. Grey dots represent features not signicantly or not relevantly di ffering in their abundance (HILIC ESI (+)/(−): 1170/735 features and RPLC ESI (+)/(−): 406/217 features). Purple and grey features were considered to represent uninformative background signals and were removed prior to subsequent statistical analysis.

We further observed that 268 features exhibited higher abundance in ECM blank samples compared to organoid containing samples (FC < 0.8, p-value < 0.05, purple dots in Figure 2). This observation could be attributed to matrix effects [36], to components present in culture medium and enriched in the ECM in the absence of cells [37] or to ECM derived components [36,38] that are taken up and metabolized in the presence of cells. CEU mass mediator batch search [39,40] based on their exact mass revealed that some of these compounds could be di- and tripeptides (nine features, see Supplementary Tables S6S9) thus pointing to subproducts of proteins (i.e., laminin or collagen) as major Matrigel components [41]. In addition, phospholipid species (19 features), which were previously reported to be ECM derived contaminants [36], were reported by exact mass search.

Further, the search indicated that small molecules like organic acids and free fatty acids may contribute to the complex ECM composition. A full list of exact masses and potential annotation is provided in the supplementary material (see Supplementary Tables S6S9). However, a detailed proteomic and metabolomic characterization of the used ECM is beyond the scope of our study and warrants further investigation. In this regard, the use of mass spectrometry-peptidomics will be pivotal to bridge the gap between proteomics and metabolomics [42] and to characterize the molecular composition of ECMs in much more detail.

Taken together, we introduced a simple two-step lter strategy based on FC and p-value cut-offs to assess the distributional properties of features in ECM blank and biological samples. The approach makes use of blank samples not incorporated in conventional ltering pipelines, which rely on generic cut-offs (e.g., remove the lowest 40% based on mean/median abundance [43]) and presumably eliminate features of biological relevance. The retention of fewer, but biological relevant features will improve the results of subsequent statistical analysis and facilitate the interpretation of biomarker discovery and drug response phenotyping experiments.

2.3. *Proof-of-Concept: Early Metabolic Response of CRC Organoids to 5-Fluorouracil Treatment*

To proof the feasibility of the optimized protocol C (Supplementary Figure S7) together with the established ltering procedure we investigated the early metabolic response of CRC organoids to 5-uorouracil (5-FU) treatment. The antimetabolite 5-FU, commonly used in the treatment of colorectal cancer, exerts its anticancer activity through inhibition of thymidylate synthase [44,45] and misincorporation of its metabolites into RNA and DNA [45,46]. Concentrations of 1, 10 and 100 µM (that did not affect cell viability and morphology, Supplementary Figure S9), were used in three independent experiments to induce specic metabolic perturbations within 24 h of treatment. To monitor the repeatability of the whole procedure, the resulting data of each experiment were evaluated independently and then compared.

As a result, non-targeted feature extraction yielded 4702489 compounds per analytical mode. Further analysis of ltered and sum normalized data revealed, depending on the analytical mode, 329 features signicantly and relevantly altered upon drug exposure (see Supplementary Table S10). In total, 12 features were signicantly and relevantly correlated with 5-FU concentrations in at least two of three experiments (see Table 2). Finally, 10 of those features could be assigned according to levels of assignment proposed by the metabolomics standard initiative (MSI) [47] while two features remained unknown (see Table 2). The consistency of results between the three experiments demonstrates good repeatability of the non-targeted workow.

Table 2. Features signicantly and relevantly altered upon 5-FU treatment of CRC organoids.

Analytical Mode	No. of Experiments [1]	Mean Mass	Retention Time	Regulation	Annotation	MSI Level [4]
HILIC ESI (+)	3	111.0436	3.21	↑	Cytosine [2]	2
		251.1026	2.42	↓	2′-Deoxyadenosine	1
		257.1022	3.21	↑	2′-O-Methylcytidine	1
	2	231.1468	5.95	↓	AC 4:0	2
		268.0828	4.89	↑	Inosine	2
		281.1115	7.90	↑	1-Methyladenosine	1
		633.4739	3.78	↓	LysoPC 26:1	2
HILIC ESI (−)	3	228.0731	2.12	↑	2′-Deoxyuridine	2
		264.0507	2.12	↑	na [3]	-
	2	536.1892	2.17	↑	na	-
RPLC ESI (+)	2	705.5341	6.75	↓	PC 30:0	2
		729.5347	6.48	↓	PC 32:2	2

[1] No. of experiments where the applied criteria for signicant and relevant response to 5-FU treatment are met. [2] In-source fragment of 2′-*O*-methylcytidine. [3] Supposed to be related to uracil due to detection of m/z 111.0211 in the fragment spectra of 264.0507. [4] Assignment level according to the metabolomics standard initiative (MSI) [47]. AC, acylcarnitine; LysoPC, lysophosphatidylcholine; PC, phosphatidylcholine; na, not assigned.

In a joint analysis of all three experiments, 2′-deoxyuridine, 2′-O-methylcytidine, 1-methyladenosine, 2′-deoxyadenosine, acylcarnitine (AC) 4:0 and phosphatidylcholine (PC) 32:2, and the unassigned feature *m/z* 264.0507 eluting at 2.1 min, still met the applied criteria (Spearman correlation coefficient $r_S > |0.7|$ and BenjaminiHochberg adjusted p value < 0.05) for the signicant and relevant dose-dependent regulation (see Figure 3).

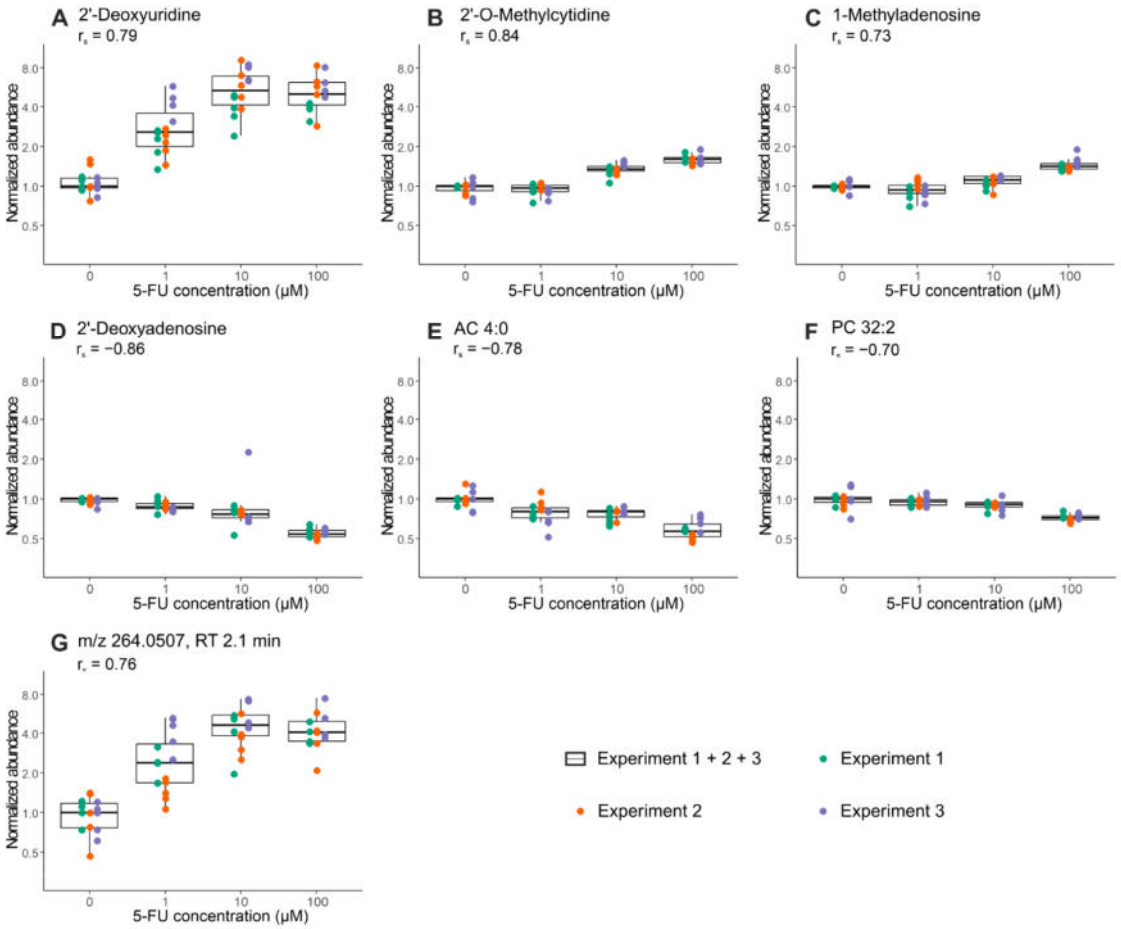

Figure 3. Tukeys boxplots of dose-dependent changes in metabolite abundance after 24 h of treatment with 5-FU at increasing concentrations assessed in three independent experiments: (**A**) 2′-Deoxyuridine; (**B**) 2′-*O*-Methylcytidine; (**C**) 1-Methyladenosine; (**D**) 2′-Deoxyadenosine; (**E**) AC 4:0; (**F**) PC 32:2; (**G**) feature *m/z* 264.0507 eluting at 2.1 min. Overlaid scatter plots represent individual data points (n = 5 technical replicates, except for 100 µM experiment 1 (n = 4)) from all three experiments (experiment 1 (green), experiment 2 (orange) and experiment 3 (purple)). Peak areas of individual features were excluded prior to statistical analysis if the measured value was <1% of the group median within the corresponding treatment group (max one value per treatment group). Displayed are all features signicantly and relevantly correlated with 5-FU concentration in the joint analysis of all three experiments (Spearman correlation coefficient $r_S > |0.7|$ and BenjaminiHochberg adjusted p-value < 0.05). The preprocessed data was normalized to the mean of the corresponding control group.

Most metabolites found to be regulated upon 5-FU treatment are directly involved in pyrimidine and purine metabolism. Our observation of elevated 2′-deoxyuridine and depletion of 2′-deoxyadenosine are largely in accordance with the cellular mechanisms of 5-FU and previous ndings in cell culture models [48 51], rodent derived plasma [48] and clinical trials [52,53]. The observed dose depended increase of inosine levels might be explained by an upregulation of inosine synthesis triggered by increased inosine consumption due to its role as Rib-1-P donor in the activation pathway of 5-FU [54]. The methylated nucleosides 2′-*O*-methylcytidine and 1-methyladenosine occur in different

RNA species and are found to be elevated in our experiments. In line with the results presented here, a recent publication describes a considerable increase in the intracellular 1-methyladenosine level after treatment of HCT116 colon cancer cells with 5-FU [55]. In addition tRNA modication by incorporation of 2′-*O*-methylcytidine were previously described in 5-FU-treated *Escherichia coli* [56].

Furthermore, we found an impact on lipid metabolism with decreased levels of AC 4:0, PC 30:0 and PC 32:2. Previous studies in ve di fferent CRC cell lines [49] already described an effect of 5-FU treatment on AC metabolism. However, results were not consistent between the different cell lines tested and to some extent in contrast to our ndings. In addition, previous studies have reported that increased amounts of phospholipids and altered phospholipid composition of the cell membrane are characteristics of CRC [57 59]. Corresponding to this, targeting cancer cells by anticancer treatment could result in decreased PC levels. However, an in-depth biological interpretation of the perturbation of lipid metabolism in 5-FU treated CRC organoids is beyond the scope of this study. We note that results from the proof-of-concept experiment are preliminary and more investigations, carried out in larger cohorts with organoids from different donors, are needed to conrm these ndings.

3. Materials and Methods

3.1. Chemicals and Reagents

Ultra LC-MS grade acetonitrile (ACN) and methanol (MeOH) were purchased from Carl Roth GmbH and Co KG (Karlsruhe, Germany). LC-MS grade methyl tert-butyl ether (MTBE), 2-propanol (IPA), formic acid (FA), ammonium acetate (AmAc) and 5-uorouracil (5-FU) were purchased from Sigma-Aldrich (Taufkirchen, Germany). Pure water was in-house produced by a Milli-Q system (Millipore, Billerica, MA, USA) and used for the preparation of aqueous solvents. For further details see Supplementary Table S11.

3.2. Patient Samples

Colorectal cancer samples were obtained from patients who underwent surgery at the Robert-Bosch-Krankenhaus, Stuttgart. The study was approved by the Ethical Committee at the Eberhard Karls University T bingen and written informed consent was obtained (project-numbers: 264/2013BO2 and 696/2016BO2). Residual tissue samples not used for pathological routine examination were transferred to the laboratory for cell isolation within a maximum of 8 h after surgery.

3.3. Organoid Culture and Viability Assay

Organoid cultures were established and maintained as described previously [4]. Human tumor organoids were cultured in the complete medium (advanced DMEM/F12 (Fisher Scientic /gibco, Grand Island, NY, USA) supplemented with 10 mM Hepes (Carl Roth GmbH and Co KG, Karlsruhe, Germany), 1× Glutamax (Fisher Scientic /gibco, Grand Island, NY, USA), 1× penicillin/streptomycin (Fisher Scientic /gibco, Grand Island, NY, USA), 1× B-27 supplement (Fisher Scientic /gibco, Grand Island, NY, USA), 1× N-2 supplement (Fisher Scientic /gibco, Grand Island, NY, USA), 1 mM N-acetylcysteine (Sigma, St. Louis, MO, USA), 50 ng/mL human EGF (Peprotech, London, UK), 10 µM Y-27632 (Absource Diagnostics, M nchen, Germany) and 1.25 µg/mL amphotericin (MERCK, Darmstadt, Germany)).

For cell metabolomics and viability analysis, organoids were dissociated to single cells using the TrypLE Express enzyme (Fisher Scientic /gibco, Paisley, UK). Disaggregation was stopped with advanced DMEM/F12 and cells were counted. Cells were suspended in growth factor-reduced Matrigel™ (Corning, Bedford, MA, USA) and the complete culture medium (3:1, *v/v*). For the protocol evaluation experiments cells were cultured for 3 days in 300 µL of the complete medium prior to analysis. For the proof-of-concept experiments and the viability analysis, a 5-FU stock solution (10 mM 5-FU in water) was diluted with complete medium to nal concentrations of 1, 10 and 100 µM 5-FU. After preculturing of the cells for 3 days in 300 µL of complete medium, the medium was replaced by 300 µL of the corresponding 5-FU solution or by the complete culture medium for control

(0 µM 5-FU). The organoids were treated for 24 h and then subjected to the metabolomics analysis. The proof-of-concept experiments were performed in 3 independent biological replicates (passage number 39-72).

The CellTiter Glo 3D cell viability assay (Promega, Madison, WI, USA) was used to analyze cell viability according to the manufacturers instructions. In brief, an equal volume of reagent was added to the culture medium, mixed thoroughly, incubated for 30 min at room temperature, and transferred into opaque-walled 96-well plates. The intensity of luminescence was measured using the EnSpire plate reader (PerkinElmer, Hamburg, Germany). In addition, cell death was analyzed using the NucRed™ Dead 647 ReadyProbes™ Reagent (ThermoFisher Scientic, Eugene, OR, USA). The reagent was added to the culture medium, incubated for 15 min, and brighteld and uorescence images (excitation: 642 nm, emission: 661 nm, Cy5 lter cube) were acquired from each well of the 48-well plate using a Cytation 1 Cell Imaging Multi-Mode Reader (BioTek, Winooski, VT, USA). For details about the used reagents and supplements, see Supplementary Table S11.

3.4. Sampling and Extraction Procedures

Three protocol variants were compared to nd an optimized procedure. The extraction was mainly based on a 2D-cell metabolomics protocol reported by Ivanisevic et al. [18] modied as described below. Each protocol was performed on ve organoid sample replicates and three ECM blanks (extracellular matrix without organoids). The samples were collected at room temperature to avoid premature ECM liquefaction. Sample extraction and analysis was performed in a randomized manner.

Protocol A: After removal of the culture medium, 1000 µL of cold PBS (4 °C) was added to each well. Liqueed ECM and organoids were carefully resuspended and transferred into a BSA-coated polypropylene tube (ThermoFisher Scientic, Rockford, IL, USA) sitting on ice. For transfer BSA-coated pipette tips were used. Samples were centrifuged (30 s, 2370× *g*, 4 °C) and the supernatant (PBS-ECM-suspension) was removed. The organoid pellet was resuspended in 100 µL of MeOH/ACN/H_2O (2:2:1, *v/v/v*) by vortex mixing for approximately 5 s followed by snap-freezing in liquid nitrogen. Samples were stored in liquid nitrogen until further processing.

The samples were thawed at 4 °C and cells were extracted by ultrasonication (ultrasonic wave output power: 320 W, ultrasonic on/off cycles: 0.5 min, total disruption time: 4 min and T = 4 °C; Bioruptor UCD-200, Diagenode s.a., Li ge, Belgium). In order to precipitate proteins, the samples were incubated for at least 30 min at −20 °C, followed by 5 min centrifugation at 21,130× *g* and 4 °C. The resulting supernatant was removed and transferred to a fresh tube. The pellet was resuspended in 100 µL MeOH/ACN/H_2O (2:2:1, *v/v/v*) on a vortex mixer (approximately 5 s) and centrifugation was repeated. The supernatants were combined and divided in equal aliquots used for HILIC and RPLC analysis.

Protocol B: The samples were extracted as described in protocol A. The remaining organoid pellet was resuspended in 100 µL of MTBE/MeOH (3:1, *v/v*) on a vortex mixer (approximately 5 s) and re-extracted by ultrasonication using the same parameters as before. After centrifugation at 21,130× *g* and 4 °C the supernatant was combined with the aliquot intended for RPLC analysis.

Protocol C: After removal of the culture medium, the surface of the ECM and of the well were washed with 500 µL of warm PBS (37 °C), which was immediately removed and discarded. Cells and ECM were resuspended in 500 µL of ice-cold MeOH/ACN/H_2O (2:2:1, *v/v/v*), transferred to a polypropylene tube (Eppendorf, Hamburg, Germany) and immediately snap-frozen in liquid nitrogen. Further sample extraction was performed as described for protocol A.

3.5. Sample Storage and Preparation

All extract aliquots were evaporated to dryness in a rotational vacuum concentrator (RVC 2-25 CDplus, Christ, Germany) at ambient temperature and stored at −20 °C until analysis. Prior to analysis the dry extracts were reconstituted in 70 µL of solvent (HILIC analysis: ACN:H_2O (95:5, *v/v*), RPLC analysis: IPA:MeOH (3:1, *v/v*)) by vortex mixing (10 min) and ultrasonication (2 min)

followed by centrifugation (5 min, 21,130× *g*, 4 °C). Fifty microliters of the supernatants were transferred into 250 µL glass inserts with polymer feet in 2 mL sample vials (Agilent Technologies, Waldbronn, Germany) covered with preslit polytetrauoroethylene (PTFE) /silicone screw caps (Agilent Technologies, Waldbronn, Germany). The remaining extracts of all samples (approximately 20 µL each) including ECM blanks were pooled to prepare quality control (QC) samples. Optionally, a 50 µL aliquot was taken for the acquisition of fragmentation spectra while the remaining solution was diluted with the corresponding solvent to achieve an appropriate QC sample volume for monitoring and correction of experimental drifts.

3.6. LC-QTOF-MS Analysis

LC/MS analysis was carried out similar as described [17,60]. In brief, aqueous extracts were analyzed by HILIC (Acquity UPLC BEH Amide Column, 1.7 µm, 2.1 mm × 150 mm; Waters, Eschborn, Germany) and organic extracts were analyzed by RPLC (Acquity UPLC BEH C8, 1.7 µm, 2.1 mm × 100 mm; Waters, Eschborn, Germany). Gradient elution at analytical ow rates for HILIC (0.4 mL/min) and RPLC (0.45 mL/min) analysis, each with a total run time of 30 min per sample, was applied (HILIC mobile phase A: 5 mM AmAc and 0.06% FA in water:ACN 1:1, *v/v*, mobile phase B: 5 mM AmAc and 0.06% FA in water:ACN 5:95, *v/v*; RPLC mobile phase A: 5 mM AmAc in water:MeOH 8:2, *v/v*, mobile phase B: 5 mM AmAc in MeOH:ACN:IPA 7.5:2:0.5, *v/v/v*). For both separation systems the autosampler was operated at 6 °C and the column oven at 60 °C. Sample sequence and injection volumes were adjusted as described in Supplementary Table S1. Data acquisition was done using the Mass Hunter Data Acquisition Software (version B.08.00, Agilent Technologies). Fragment spectra were acquired using auto MS/MS analysis in pooled QC samples. Electrospray parameters for MS1 and MS/MS acquisitions were applied as described [17,60]. To obtain the mass accuracy during the batch QTOF reference mass correction (recalibration) was applied according to Leuthold et al. [61].

The calculated amount of <500 cells/injection (see Figure 1) was estimated for the optimized protocol C (Supplementary Figure S7) based on the number of seeded cells (1000 cells/well as determined using a hemocytometer) and a doubling time of 3.4 days. The resulting 20003000 cells /well after three days of incubation were subjected to metabolite extraction followed by dividing the extract in equal volumes (one extract for HILIC and one extract for RPLC analysis, see Supplementary Figure S7) resulting in 10001500 cells per extract. The dried extracts were reconstituted in 70 µL of solvent from which 20 µL were injected into the LC-MS system thus ending up with an estimated amount of 286429 cells on column.

3.7. Data Preprocessing and Statistical Analysis

Preprocessing of data derived from the non-targeted approach was carried out by using the Mass Hunter Pronder Software (version B.08.00, Agilent Technologies).

3.7.1. Feature Extraction

For protocol assessment, Batch Targeted Feature Extraction on the basis of structurally assigned metabolites [17] was used. Values were matched based on sum formula searching results to mass and retention time with a retention time window match tolerance set to ± 0.7 min and a mass match tolerance set to ± 15 ppm. H^+, Na^+ and $NH4^+$ adducts were considered for spectra acquired in the positive mode while for negative mode data acquisition the deprotonated molecular ions and $CH3COO^-$ and $HCOO^-$ adducts were expected. An intensity threshold was not set and an extracted ion chromatogram (EIC) range of ±35 ppm was applied. TOF-MS spectra above 30% of saturation were excluded.

For subsequent experiments non-targeted feature extraction by batch recursive feature extraction (RFE) was applied. The intensity threshold was set to 500750 counts. Unless specically stated otherwise, H^+, Na^+ and $NH4^+$ adducts were selected for positive mode data while the deprotonated molecular ions and CH_3COO^- and $HCOO^-$ adducts were expected for negative mode data.

The retention time window was set to ±0.2 min, the mass window was set to ± (20 ppm + 2 mDa) and the extracted ion chromatogram (EIC) range to ±35 ppm. For peak integration, Agile2 algorithm was selected. TOF-MS spectra were excluded if their intensity was above 30% saturation. The list of extracted features was inspected visually in order to ensure correct retention time alignment and peak integration throughout the batch. More precisely, extracted ion chromatograms (EICs) of individual features and their chromatographic alignment throughout the analytical batch were reviewed using a graphical interface. Curations were made by manual reintegration of EICs that were falsely integrated by the software algorithm (e.g., correct peak integrations of closely coeluting isomer compounds in two different samples). Such a kind of data curation turned out to be important as poor peak integration and false positive peak detection remains a prevalent problem in untargeted metabolomics data generated using LC-MS [62].

3.7.2. Data Filtration, Normalization and Analysis

Extracted feature data were exported as comma separated value les to perform further data preprocessing and statistical analysis with R-4.0.0 and R studio (http://www.r-project.org) [63], including additional packages (ggplot2 [64], ggrepel [65], ggpubr [66], tidyverse [67], matrixStats [68], matrixTests [69], HybridMTest [70] and ggVennDiagram [71]).

For protocol optimization experiments metabolites with signicant and relevant abundance, compared to the metabolite background of the corresponding ECM blank samples, were identied by Welchs *t*-test on log2 transformed data ($p < 0.05$) and median fold change > 1. In analogy to the commonly applied thresholds used in gene expression analysis [72] the signicance level is denoted as 5% throughout the manuscript. The threshold for relevant signal intensities is specied by the indicated fold-change thresholds of the different experiments.

In the proof-of-concept experiments, signal drifts were corrected using locally weighted scatterplot smoothing (LOESS) correction over QC samples. Features with a coefficient of variation (CV) ≥20% in QC samples analyzed throughout the batch were removed from the data after LOESS. Furthermore, data was ltered for features with signicant and relevant abundance compared to the mean of the corresponding ECM blank samples. Therefore, Welchs *t*-test was applied to log2 transformed data of the control and ECM blank samples. Signicant and relevant features with a fold-change of >1.2 were included in further data analysis. A signal intensity variability of <20% is well established to remove features of low reproducibility in non-targeted metabolomics [32,73,74]. Based on this assumption, that a variability of <20% is acceptable and therefore non-relevant, we conversely concluded that a difference of >20% (e.g., a > 1.2-fold abundance of a feature in organoids compared to ECM blanks) is of relevance.

Filtered data was normalized (peak area of each feature divided by the sum of peak areas of all features in one sample). Signicantly and relevantly dose-dependent regulated features were identied by Spearman correlation analysis, considering $r_s > |0.7|$ and Benjamini-Hochberg adjusted [75] *p*-value < 0.05. All statistical tests were two sided.

3.8. Metabolite Identication and Annotation

Metabolite identication and annotation was performed based on accurate mass and RT-matching for reported compounds from targeted feature extraction whereas two of the following criteria had to be met: mass tolerance: ± 15 ppm, retention time tolerance: ± 0.2 min and a targeted matching score >70% with the following weightings for score calculation: mass score: 100%; isotope abundance score: 60%; isotope spacing score: 50% and retention time score: 20%.

In the proof-of-concept experiments metabolite identication and annotation was performed by comparison of spectral information (accurate mass, fragment ions and/or retention time) acquired in QC samples to available spectral information from databases or from pure standard compounds. MS/MS spectra were accessed by the Mass Hunter Qualitative Analysis Software (Version B.07.00, Agilent Technologies) and spectral matching was assessed based on scores reported by the indicated

search engine (Supplementary Tables S2S5): MassBank of North America (MS /MS Similarity Search, https://mona.ehnlab.ucdavis.edu /), CEU Mass Mediator (MS/MS Search) [39,40] and Lipid Annotator (Version 1.0, Agilent Technologies). Score values for spectra matching to selected reference compounds or those provided in the METLIN Metabolite PCDL (Version B.07.00, Agilent Technologies) were obtained by spectral comparison within the MassHunter PCDL Manager Software (Version B.07.00, Agilent Technologies). Assignment levels proposed by the Metabolomics Standard Initiative (MSI) [47] are provided in the Supplementary Tables S2S5.

4. Conclusions

To the best of our knowledge this is the rst study on method optimization for non-targeted metabolic and lipidomic proling of ECM-based organoid cultures. We could show that reliable and repeatable data acquisition of a broad metabolic range is possible from the extract of less than 500 cells per injection via untargeted LC-QTOF-MS. This rapid and sensitive procedure enables the determination of the early metabolic response of CRC organoids to 5-FU treatment and paves the way for high throughput investigations of metabolic changes in patient derived CRC organoids.

In future projects, an adaption of the new protocol for metabolic ux proling in 3D-organoid models by non-targeted stable isotope labeling analysis [76] may improve the understanding of pathobiochemical mechanisms and drug response effects. In this regard, the implementation of non-targeted isotope dilution normalization [77] may facilitate the quantication of unidentied features in a retrospective fashion.

Supplementary Materials: The following are available online at http://www.mdpi.com/2218-1989/10/12/494/s1. Supplementary Figures: Figure S1: Metabolites found to be of signicant and relevant abundance in organoid samples compared to corresponding ECM blank samples (protocols A/B and C in HILIC ESI (+) mode). Figure S2: Metabolites found to be of signicant and relevant abundance in organoid samples compared to corresponding ECM blank samples (protocols A/B and C in HILIC ESI (−) mode). Figure S3: Metabolites found to be of signicant and relevant abundance in organoid samples compared to corresponding ECM blank samples (protocols A, B and C in RPLC ESI (+)). Figure S4: Metabolites found to be of signicant and relevant abundance in organoid samples compared to corresponding ECM blank samples (protocols A, B and C in the RPLC ESI (−) mode). Figure S5: Venn diagrams displaying the overlap of the tested extraction procedures with respect to metabolites present in organoid samples with signicant and relevant abundance. Figure S6: Venn diagrams displaying the extent of overlap between the different analytical modes for signicantly and relevantly detected metabolites in protocol C. Figure S7: Optimized protocol for comprehensive and reproducible metabolomic and lipidomic proling of CRC organoids using LC-QTOF-MS after dual LC separation. Figure S8: Inuence of the established data ltering procedure on data quality with regard to the variability of retained features in the HILIC ESI (+) mode, HILIC ESI (−) mode, RPLC ESI (+) mode and RPLC ESI (−) mode. Figure S9: Exemplary pictures from preliminary experiments to ensure cell viability at the time of sampling. Supplementary Table S1: Analytical batch structure. Table S2: Putatively annotated/identied compounds in the HILIC ESI (+) mode. Table S3: Putatively annotated/identied compounds in the HILIC ESI (−) mode. Table S4: Putatively annotated/identied compounds in the RPLC ESI (+) mode. Table S5: Putatively annotated/identied compounds in the RPLC ESI (−) mode. Table S6: Search result from the accurate mass batch search (CEU mass mediator) of compounds found with higher abundance in ECM blank samplesHILIC ESI (+) mode. Table S7: Search result from the accurate mass batch search (CEU mass mediator) of compounds found with higher abundance in ECM blank samplesHILIC ESI (−) mode. Table S8: Search result from the accurate mass batch search (CEU mass mediator) of compounds found with higher abundance in ECM blank samplesRPLC ESI (+) mode. Table S9: Search result from the accurate mass batch search (CEU mass mediator) of compounds found with higher abundance in ECM blank samplesRPLC ESI (−) mode. Table S10: Signicantly and relevantly regulated features detected upon 5-urouracil treatmentall modes. Table S11: Used chemicals and reagents. Metabolomics data have been deposited to the EMBL-EBI MetaboLights database [78] with the identier MTBLS2130.

Author Contributions: Conceptualization, S.K.N., N.J., S.W., U.H., T.E.M. and M.H.; Formal analysis, S.K.N.; Funding acquisition, S.W., U.H., M.H.D., M.S., T.E.M. and M.H.; Investigation, S.K.N., N.J. and S.K.W.; Methodology, S.K.N.; Project administration, M.S., T.E.M. and M.H.; Resources, M.H.D.; Supervision, S.W., M.S., T.E.M. and M.H.; Validation, S.K.N.; Visualization, S.K.N.; Writingoriginal draft, S.K.N., N.J., T.E.M. and M.H.; Writingreview and editing, S.K.N., N.J., S.W., S.K.W., U.H., M.H.D., M.S., T.E.M. and M.H. All authors have read and agreed to the published version of the manuscript.

Funding: This work was supported by the Robert Bosch Stiftung (Stuttgart, Germany), the Deutsche Krebshilfe (No. 70112583), the Deutsche Forschungsgemeinschaft (DFG) im Rahmen der Exzellenzstrategie des Bundes und der L nderEXC 2180390900677, the ICEPHA Graduate Program, University of T bingen (T bingen, Germany) and in part by the Deutsche Forschungsgemeinschaft (grant DA572/11-4).

Acknowledgments: We gratefully acknowledge Kathleen Siegel for excellent technical assistance.

Conicts of Interest: The authors declare no conict of interest. The funders had no role in the design of the study; in the collection, analyses, or interpretation of data; in the writing of the manuscript, or in the decision to publish the results.

References

1. Sato, T.; Vries, R.G.; Snippert, H.J.; van de Wetering, M.; Barker, N.; Stange, D.E.; van Es, J.H.; Abo, A.; Kujala, P.; Peters, P.J.; et al. Single Lgr5 stem cells build crypt-villus structures in vitro without a mesenchymal niche. *Nature* **2009**, *459*, 262265. [CrossRef[ ]PubMed]
2. Eiraku, M.; Takata, N.; Ishibashi, H.; Kawada, M.; Sakakura, E.; Okuda, S.; Sekiguchi, K.; Adachi, T.; Sasai, Y. Self-organizing optic-cup morphogenesis in three-dimensional culture. *Nature* **2011**, *472*, 5156. [CrossRef] [PubMed]
3. Barker, N.; Huch, M.; Kujala, P.; van de Wetering, M.; Snippert, H.J.; van Es, J.H.; Sato, T.; Stange, D.E.; Begthel, H.; van den Born, M.; et al. Lgr5(+ve) stem cells drive self-renewal in the stomach and build long-lived gastric units in vitro. *Cell Stem Cell* **2010**, *6*, 2536. [CrossRef[ ]PubMed]
4. Sato, T.; Stange, D.E.; Ferrante, M.; Vries, R.G.J.; van Es, J.H.; van den Brink, S.; van Houdt, W.J.; Pronk, A.; van Gorp, J.; Siersema, P.D.; et al. Long-term expansion of epithelial organoids from human colon, adenoma, adenocarcinoma, and Barretts epithelium. *Gastroenterology* **2011**, *141*, 17621772. [CrossRef[ ]PubMed]
5. Sasai, Y. Cytosystems dynamics in self-organization of tissue architecture. *Nature* **2013**, *493*, 318326. [CrossRef[ ]PubMed]
6. Rossi, G.; Manfrin, A.; Lutolf, M.P. Progress and potential in organoid research. *Nat. Rev. Genet.* **2018**, *19*, 671687. [CrossRef[ ]PubMed]
7. Clevers, H. Modeling Development and Disease with Organoids. *Cell* **2016**, *165*, 15861597. [CrossRef]
8. Artegiani, B.; Clevers, H. Use and application of 3D-organoid technology. *Hum. Mol. Genet.* **2018**, *27*, R99R107. [CrossRef]
9. Wild, C.P.; Weiderpass, E.; Stewart, B.W. *World Cancer Report 2020*; International Agency for Research on Cancer/World Health Organization: Lyon, France, 2020.
10. Moreau, L.-C.; Rajan, R.; Thirlwell, M.P.; Alcindor, T. Response to chemotherapy in metastatic colorectal cancer after exposure to oxaliplatin in the adjuvant setting. *Anticancer Res.* **2013**, *33*, 17651768.
11. Schaeffeler, E.; B ttner, F.; Reustle, A.; Klumpp, V.; Winter, S.; Rausch, S.; Fisel, P.; Hennenlotter, J.; Kruck, S.; Stenzl, A.; et al. Metabolic and Lipidomic Reprogramming in Renal Cell Carcinoma Subtypes Reects Regions of Tumor Origin. *Eur. Urol. Focus* **2018**, *5*, 608618. [CrossRef]
12. Njoku, K.; Sutton, C.J.; Whetton, A.D.; Crosbie, E.J. Metabolomic Biomarkers for Detection, Prognosis and Identifying Recurrence in Endometrial Cancer. *Metabolites* **2020**, *10*, 314. [CrossRef[ ]PubMed]
13. Brown, R.E.; Short, S.P.; Williams, C.S. Colorectal Cancer and Metabolism. *Curr. Colorectal Cancer Rep.* **2018**, *14*, 226241. [CrossRef[ ]PubMed]
14. Pakiet, A.; Kobiela, J.; Stepnowski, P.; Sledzinski, T.; Mika, A. Changes in lipids composition and metabolism in colorectal cancer: A review. *Lipids Health Dis.* **2019**, *18*, 29. [CrossRef[ ]PubMed]
15. Perttula, K.; Edmands, W.M.B.; Grigoryan, H.; Cai, X.; Iavarone, A.T.; Gunter, M.J.; Naccarati, A.; Polidoro, S.; Hubbard, A.; Vineis, P.; et al. Evaluating Ultra-long-Chain Fatty Acids as Biomarkers of Colorectal Cancer Risk. *Cancer Epidemiol. Biomarkers Prev.* **2016**, *25*, 12161223. [CrossRef[ ]PubMed]
16. La Vecchia, S.; Sebasti n, C. Metabolic pathways regulating colorectal cancer initiation and progression. *Semin. Cell Dev. Biol.* **2020**, *98*, 6370. [CrossRef[ ]PubMed]
17. Leuthold, P.; Schaeffeler, E.; Winter, S.; Buttner, F.; Hofmann, U.; Murdter, T.E.; Rausch, S.; Sonntag, D.; Wahrheit, J.; Fend, F.; et al. Comprehensive Metabolomic and Lipidomic Proling of Human Kidney Tissue: A Platform Comparison. *J. Proteome Res.* **2017**, *16*, 933944. [CrossRef]
18. Ivanisevic, J.; Zhu, Z.-J.; Plate, L.; Tautenhahn, R.; Chen, S.; OBrien, P.J.; Johnson, C.H.; Marletta, M.A.; Patti, G.J.; Siuzdak, G. Toward omic scale metabolite proling: A dual separation-mass spectrometry approach for coverage of lipid and central carbon metabolism. *Anal. Chem.* **2013**, *85*, 68766884. [CrossRef]
19. Nelson, S.R.; Zhang, C.; Roche, S.; ONeill, F.; Swan, N.; Luo, Y.; Larkin, A.; Crown, J.; Walsh, N. Modelling of pancreatic cancer biology: Transcriptomic signature for 3D PDX-derived organoids and primary cell line organoid development. *Sci. Rep.* **2020**, *10*, 3529. [CrossRef]

20. Gonneaud, A.; Asselin, C.; Boudreau, F.; Boisvert, F.-M. Phenotypic Analysis of Organoids by Proteomics. *Proteomics* **2017**, *17*, 1700023. [CrossRef]
21. Artati, A.; Prehn, C.; Adamski, J. LC-MS/MS-Based Metabolomics for Cell Cultures. *Methods Mol. Biol.* **2019**, *1994*, 119130.
22. Weygand, J.; Carter, S.E.; Salzillo, T.C.; Moussalli, M.; Dai, B.; Dutta, P.; Zuo, X.; Fleming, J.B.; Shureiqi, I.; Bhattacharya, P. Can an Organoid Recapitulate the Metabolome of its Parent Tissue?: A Pilot NMR Spectroscopy Study. *JCPCR* **2017**, *8*, 307.
23. Yoshizaki, H.; Ogiso, H.; Okazaki, T.; Kiyokawa, E. Comparative lipid analysis in the normal and cancerous organoids of MDCK cells. *J. Biochem.* **2016**, *159*, 573584. [CrossRef[ ]PubMed]
24. Maddocks, O.D.K.; Athineos, D.; Cheung, E.C.; Lee, P.; Zhang, T.; van den Broek, N.J.F.; Mackay, G.M.; Labuschagne, C.F.; Gay, D.; Kruiswijk, F.; et al. Modulating the therapeutic response of tumours to dietary serine and glycine starvation. *Nature* **2017**, *544*, 372376. [CrossRef[ ]PubMed]
25. Lindeboom, R.G.; van Voorthuijsen, L.; Oost, K.C.; Rodr guez-Colman, M.J.; Luna-Velez, M.V.; Furlan, C.; Baraille, F.; Jansen, P.W.; Ribeiro, A.; Burgering, B.M.; et al. Integrative multi-omics analysis of intestinal organoid differentiation. *Mol. Syst. Biol.* **2018**, *14*, e8227. [CrossRef[ ]PubMed]
26. Feldman, A.; Mukha, D.; Maor, I.I.; Sedov, E.; Koren, E.; Yosefzon, Y.; Shlomi, T.; Fuchs, Y. Blimp1+ cells generate functional mouse sebaceous gland organoids in vitro. *Nat. Commun.* **2019**, *10*, 2348. [CrossRef]
27. Ser, Z.; Liu, X.; Tang, N.N.; Locasale, J.W. Extraction parameters for metabolomics from cultured cells. *Anal. Biochem.* **2015**, *475*, 2228. [CrossRef]
28. Villaret-Cazadamont, J.; Poupin, N.; Tournadre, A.; Batut, A.; Gales, L.; Zalko, D.; Cabaton, N.J.; Bellvert, F. Bertrand-Michel, J. An Optimized Dual Extraction Method for the Simultaneous and Accurate Analysis of Polar Metabolites and Lipids Carried out on Single Biological Samples. *Metabolites* **2020**, *10*, 338. [CrossRef]
29. Haag, M.; Schmidt, A.; Sachsenheimer, T.; Br gger, B. Quantication of Signaling Lipids by Nano-Electrospray Ionization Tandem Mass Spectrometry (Nano-ESI MS/MS). *Metabolites* **2012**, *2*, 5776. [CrossRef]
30. Tirinato, L.; Pagliari, F.; Di Franco, S.; Sogne, E.; Maraoti, M.G.; Jansen, J.; Falqui, A.; Todaro, M.; Candeloro, P.; Liberale, C.; et al. ROS and Lipid Droplet accumulation induced by high glucose exposure in healthy colon and Colorectal Cancer Stem Cells. *Genes Dis.* **2019**[.CrossRef]
31. Rusz, M.; Rampler, E.; Keppler, B.K.; Jakupec, M.A.; Koellensperger, G. Single Spheroid Metabolomics: Optimizing Sample Preparation of Three-Dimensional Multicellular Tumor Spheroids. *Metabolites* **2019**, *9*, 304. [CrossRef]
32. Broadhurst, D.; Goodacre, R.; Reinke, S.N.; Kuligowski, J.; Wilson, I.D.; Lewis, M.R.; Dunn, W.B. Guidelines and considerations for the use of system suitability and quality control samples in mass spectrometry assays applied in untargeted clinical metabolomic studies. *Metabolomics* **2018**, *14*, 72. [CrossRef[ ]PubMed]
33. Verkh, Y.; Rozman, M.; Petrovic, M. Extraction and cleansing of data for a non-targeted analysis of high-resolution mass spectrometry data of wastewater. *MethodsX* **2018**, *5*, 395402. [CrossRef[ ]PubMed]
34. Ivanisevic, J.; Want, E.J. From Samples to Insights into Metabolism: Uncovering Biologically Relevant Information in LC-HRMS Metabolomics Data. *Metabolites* **2019**, *9*, 308. [CrossRef[ ]PubMed]
35. Schiffman, C.; Petrick, L.; Perttula, K.; Yano, Y.; Carlsson, H.; Whitehead, T.; Metayer, C.; Hayes, J.; Rappaport, S.; Dudoit, S. Filtering procedures for untargeted LC-MS metabolomics data. *BMC Bioinform.* **2019**, *20*, 334. [CrossRef]
36. Abe, Y.; Tada, A.; Isoyama, J.; Nagayama, S.; Yao, R.; Adachi, J.; Tomonaga, T. Improved phosphoproteomic analysis for phosphosignaling and active-kinome proling in Matrigel-embedded spheroids and patient-derived organoids. *Sci. Rep.* **2018**, *8*, 29. [CrossRef]
37. Zhang, Y.; Lukacova, V.; Reindl, K.; Balaz, S. Quantitative characterization of binding of small molecules to extracellular matrix. *J. Biochem. Biophys. Methods* **2006**, *67*, 107122. [CrossRef]
38. Giobbe, G.G.; Crowley, C.; Luni, C.; Campinoti, S.; Khedr, M.; Kretzschmar, K.; de Santis, M.M.; Zambaiti, E.; Michielin, F.; Meran, L.; et al. Extracellular matrix hydrogel derived from decellularized tissues enables endodermal organoid culture. *Nat. Commun.* **2019**, *10*, 246. [CrossRef]
39. de la Fuente, A.G.; Godzien, J.; L pez, M.F.; Rup rez, F.J.; Barbas, C.; Otero, A. Knowledge-based metabolite annotation tool: CEU Mass Mediator. *J. Pharm. Biomed. Anal.* **2018**, *154*, 138149. [CrossRef]
40. Gil-de-la-Fuente, A.; Godzien, J.; Saugar, S.; Garcia-Carmona, R.; Badran, H.; Wishart, D.S.; Barbas, C.; Otero, A. CEU Mass Mediator 3.0: A Metabolite Annotation Tool. *J. Proteome Res.* **2019**, *18*, 797802. [CrossRef]

41. Hughes, C.S.; Postovit, L.M.; Lajoie, G.A. Matrigel: A complex protein mixture required for optimal growth of cell culture. *Proteomics* **2010**, *10*, 18861890. [CrossRef]
42. Li, L.; Andr n, P.E.; Sweedler, J.V. Editorial and Review: 29th ASMS Sanibel Conference on Mass SpectrometryPeptidomics: Bridging the Gap between Proteomics and Metabolomics by MS. *J. Am. Soc. Mass Spectrom.* **2018**, *29*, 801806. [CrossRef[ ]PubMed]
43. Chong, J.; Soufan, O.; Li, C.; Caraus, I.; Li, S.; Bourque, G.; Wishart, D.S.; Xia, J. MetaboAnalyst 4.0: Towards more transparent and integrative metabolomics analysis. *Nucleic Acids Res.* **2018**, *46*, W486W494. [CrossRef] [PubMed]
44. Chaudhuri, N.K.; Montag, B.J.; Heidelberger, C. Studies on uorinated pyrimidines. III. The metabolism of 5-uorouracil-2-C14 and 5-uoroorotic-2-C14 acid in vivo. *Cancer Res.* **1958**, *18*, 318328. [PubMed]
45. Longley, D.B.; Harkin, D.P.; Johnston, P.G. 5-uorouracil: Mechanisms of action and clinical strategies. *Nat. Rev. Cancer* **2003**, *3*, 330338. [CrossRef]
46. Heidelberger, C.; Chaudhuri, N.K.; Danneberg, P.; Mooren, D.; Griesbach, L.; Duschinsky, R.; Schnitzer, R.J.; Pleven, E.; Scheiner, J. Fluorinated pyrimidines, a new class of tumour-inhibitory compounds. *Nature* **1957**, *179*, 663666. [CrossRef]
47. Sumner, L.W.; Amberg, A.; Barrett, D.; Beale, M.H.; Beger, R.; Daykin, C.A.; Fan, T.W.-M.; Fiehn, O.; Goodacre, R.; Griffin, J.L.; et al. Proposed minimum reporting standards for chemical analysis Chemical Analysis Working Group (CAWG) Metabolomics Standards Initiative (MSI). *Metabolomics* **2007**, *3*, 211221. [CrossRef]
48. Grem, J.L. 5-Fluorouracil: Forty-plus and still ticking. A review of its preclinical and clinical development. *Invest. New Drugs* **2000**, *18*, 299313. [CrossRef]
49. Ser, Z.; Gao, X.; Johnson, C.; Mehrmohamadi, M.; Liu, X.; Li, S.; Locasale, J.W. Targeting One Carbon Metabolism with an Antimetabolite Disrupts Pyrimidine Homeostasis and Induces Nucleotide Overow. *Cell Rep.* **2016**, *15*, 23672376. [CrossRef]
50. Chong, L.; Tattersall, M.H.N. 5,10-Dideazatetrahydrofolic acid reduces toxicity and deoxyadenosine triphosphate pool expansion in cultured L1210 cells treated with inhibitors of thymidylate synthase. *Biochem. Pharmacol.* **1995**, *49*, 819827. [CrossRef]
51. Houghton, J.A.; Tillman, D.M.; Harwood, F.G. Ratio of 2-deoxyadenosine-5-triphosphate /thymidine-5-triphosphate inuences the commitment of human colon carcinoma cells to thymineless death. *Clin. Cancer Res.* **1995**, *1*, 723730.
52. ODwyer, P.J.; Laub, P.B.; DeMaria, D.; Qian, M.; Reilly, D.; Giantonio, B.; Johnston, A.L.; Wu, E.Y.; Bauman, L.; Clendeninn, N.J.; et al. Phase I trial of the thymidylate synthase inhibitor AG331 as a 5-day continuous infusion. *Clin. Cancer Res.* **1996**, *2*, 16851692. [PubMed]
53. Ra, I.; Boddy, A.V.; Calvete, J.A.; Taylor, G.A.; Newell, D.R.; Bailey, N.P.; Lind, M.J.; Green, M.; Hines, J.; Johnstone, A.; et al. Preclinical and phase I clinical studies with the nonclassical antifolate thymidylate synthase inhibitor nolatrexed dihydrochloride given by prolonged administration in patients with solid tumors. *J. Clin. Oncol.* **1998**, *16*, 11311141. [CrossRef[ ]PubMed]
54. Peters, G.J.; Laurensse, E.; Leyva, A.; Pinedo, H.M. Purine nucleosides as cell-specic modulators of 5-uorouracil metabolism and cytotoxicity. *Eur. J. Cancer Clin. Oncol.* **1987**, *23*, 18691881. [CrossRef]
55. Tanigawara, Y.; Nishimuta, A.; Otani, Y.; Matsuo, M. Method for Determining Sensitivity to Fluorouracil in a Subject Having Colorectal Cancer. US 10,309,957 B2, 19 September 2019.
56. Hills, D.C.; Cotten, M.L.; Horowitz, J. Isolation and characterization of two 5-uorouracil-substituted Escherichia coli initiator methionine transfer ribonucleic acids. *Biochemistry* **1983**, *22*, 11131122. [CrossRef] [PubMed]
57. Dobrzynska, I.; Szachowicz-Petelska, B.; Sulkowski, S.; Figaszewski, Z. Changes in electric charge and phospholipids composition in human colorectal cancer cells. *Mol. Cell. Biochem.* **2005**, *276*, 113119. [CrossRef]
58. Dueck, D.A.; Chan, M.; Tran, K.; Wong, J.T.; Jay, F.T.; Littman, C.; Stimpson, R.; Choy, P.C. The modulation of choline phosphoglyceride metabolism in human colon cancer. *Mol. Cell. Biochem.* **1996**, *162*, 97103. [CrossRef]

59. Kurabe, N.; Hayasaka, T.; Ogawa, M.; Masaki, N.; Ide, Y.; Waki, M.; Nakamura, T.; Kurachi, K.; Kahyo, T.; Shinmura, K.; et al. Accumulated phosphatidylcholine (16:0/16:1) in human colorectal cancer; possible involvement of LPCAT4. *Cancer Sci.* **2013**, *104*, 12951302. [CrossRef]
60. Neef, S.K.; Winter, S.; Hofmann, U.; M rdter, T.E.; Schae ffeler, E.; Horn, H.; Buck, A.; Walch, A.; Hennenlotter, J.; Ott, G.; et al. Optimized protocol for metabolomic and lipidomic proling in formalin-xed paraffin-embedded kidney tissue by LC-MS. *Anal. Chim. Acta* **2020**, *1134*, 125135. [CrossRef]
61. Leuthold, P.; Schwab, M.; Hofmann, U.; Winter, S.; Rausch, S.; Pollak, M.N.; Hennenlotter, J.; Bedke, J.; Schaeffeler, E.; Haag, M. Simultaneous Extraction of RNA and Metabolites from Single Kidney Tissue Specimens for Combined Transcriptomic and Metabolomic Proling. *J. Proteome Res.* **2018**, *17*, 30393049. [CrossRef]
62. Chetnik, K.; Petrick, L.; Pandey, G. MetaClean: A machine learning-based classier for reduced false positive peak detection in untargeted LC-MS metabolomics data. *Metabolomics* **2020**, *16*, 117. [CrossRef]
63. R Development Core Team. *R: A Language and Environment for Statistical Computing*; R Foundation for Statistical Computing: Vienna, Austria, 2017.
64. Wickham, H. *ggplot2: Elegant Graphics for Data Analysis*; Springer: New York, NY, USA, 2016.
65. Slowikowski, K. ggrepel: Automatically Position Non-Overlapping Text Labels with ggplot2: R Package Version 0.8.0. 2018. Available online: https://CRAN.R-project.org/package=ggrepel (accessed on 11 September 2020).
66. Kassambara, A. ggpubr: ggplot2 Based Publication Ready Plots.: R Package Version 0.3.0. Available online: https://CRAN.R-project.org/package=ggpubr (accessed on 11 September 2020).
67. Wickham, H.; Averick, M.; Bryan, J.; Chang, W.; McGowan, L.; Fran ois, R.; Grolemund, G.; Hayes, A.; Henry, L.; Hester, J.; et al. Welcome to the Tidyverse. *JOSS* **2019**, *4*, 1686. [CrossRef]
68. Bengtsson, H. matrixStats: Functions that Apply to Rows and Columns of Matrices (and to Vectors): R Package Version 0.56.0. 2020. Available online: https://CRAN.R-project.org/package=matrixStats (accessed on 11 September 2020).
69. Koncevicius, K. matrixTests: Fast Statistical Hypothesis Tests on Rows and Columns of Matrices: R Package Version 0.1.9. 2020. Available online: https://CRAN.R-project.org/package=matrixTests (accessed on 11 September 2020).
70. Pounds, S.; Fofana, D. HybridMTest: Hybrid Multiple Testing: R Package Version 1.32.0. 2020. Available online: https://www.bioconductor.org/packages/release/bioc/html/HybridMTest.html (accessed on 11 September 2020).
71. Gao, C.-H. ggVennDiagram: A ggplot2 Implement of Venn Diagram.: R Package Version 0.3. 2019. Available online: https://CRAN.R-project.org/package=ggVennDiagram (accessed on 3 November 2020).
72. Gant, T.W.; Sauer, U.G.; Zhang, S.-D.; Chorley, B.N.; Hackerm ller, J.; Perdichizzi, S.; Tollefsen, K.E.; van Ravenzwaay, B.; Yauk, C.; Tong, W.; et al. A generic Transcriptomics Reporting Framework (TRF) for omics data processing and analysis. *Regul. Toxicol. Pharmacol.* **2017**, *91*, S36S45. [CrossRef[ ]PubMed]
73. Sangster, T.; Major, H.; Plumb, R.; Wilson, A.J.; Wilson, I.D. A pragmatic and readily implemented quality control strategy for HPLC-MS and GC-MS-based metabonomic analysis. *Analyst* **2006**, *131*, 10751078. [CrossRef[ ]PubMed]
74. Dunn, W.B.; Broadhurst, D.; Begley, P.; Zelena, E.; Francis-McIntyre, S.; Anderson, N.; Brown, M.; Knowles, J.D.; Halsall, A.; Haselden, J.N.; et al. Procedures for large-scale metabolic proling of serum and plasma using gas chromatography and liquid chromatography coupled to mass spectrometry. *Nat. Protoc.* **2011**, *6*, 10601083. [CrossRef[ ]PubMed]
75. Benjamini, Y.; Hochberg, Y. Controlling the False Discovery Rate: A Practical and Powerful Approach to Multiple Testing. *J. R. Stat. Soc. Ser. B (Methodol.)* **1995**, *57*, 289300. [CrossRef]
76. Weindl, D.; Wegner, A.; Hiller, K. Metabolome-Wide Analysis of Stable Isotope Labeling-Is It Worth the Effort? *Front. Physiol.* **2015**, *6*, 344. [CrossRef]
77. Weindl, D.; Wegner, A.; J ger, C.; Hiller, K. Isotopologue ratio normalization for non-targeted metabolomics. *J. Chromatogr. A* **2015**, *1389*, 112119. [CrossRef]

78. Haug, K.; Cochrane, K.; Nainala, V.C.; Williams, M.; Chang, J.; Jayaseelan, K.V. ODonovan, C. MetaboLights: A resource evolving in response to the needs of its scientic community. *Nucleic Acids Res.* **2020**, *48*, D440D444.

Supplementary Figures

Metabolic Drug Response Phenotyping in Colorectal Cancer Organoids by LC-QTOF-MS

Sylvia K. Neef [1,‡], Nicole Janssen [1,‡], Stefan Winter [1], Svenja K. Wallisch [1], Ute Hofmann [1], Marc H. Dahlke [1,2], Matthias Schwab [1,3,4], Thomas E. Mürdter [1,‡] and Mathias Haag [1,‡,*]

1 Dr. Margarete Fischer-Bosch-Institute of Clinical Pharmacology, Stuttgart, Germany and University of Tuebingen, Tuebingen, Germany
2 Department of Surgery, Robert-Bosch Hospital, Stuttgart, Germany
3 Departments of Clinical Pharmacology, and of Pharmacy and Biochemistry, University of Tuebingen, Tuebingen, Germany
4 Cluster of Excellence iFIT (EXC 2180) „Image-Guided and Functionally Instructed Tumor Therapies", University of Tuebingen, Germany
* Correspondence: mathias.haag@ikp-stuttgart.de; Phone +49 (0)711 / 8101-5429
‡ contributed equally

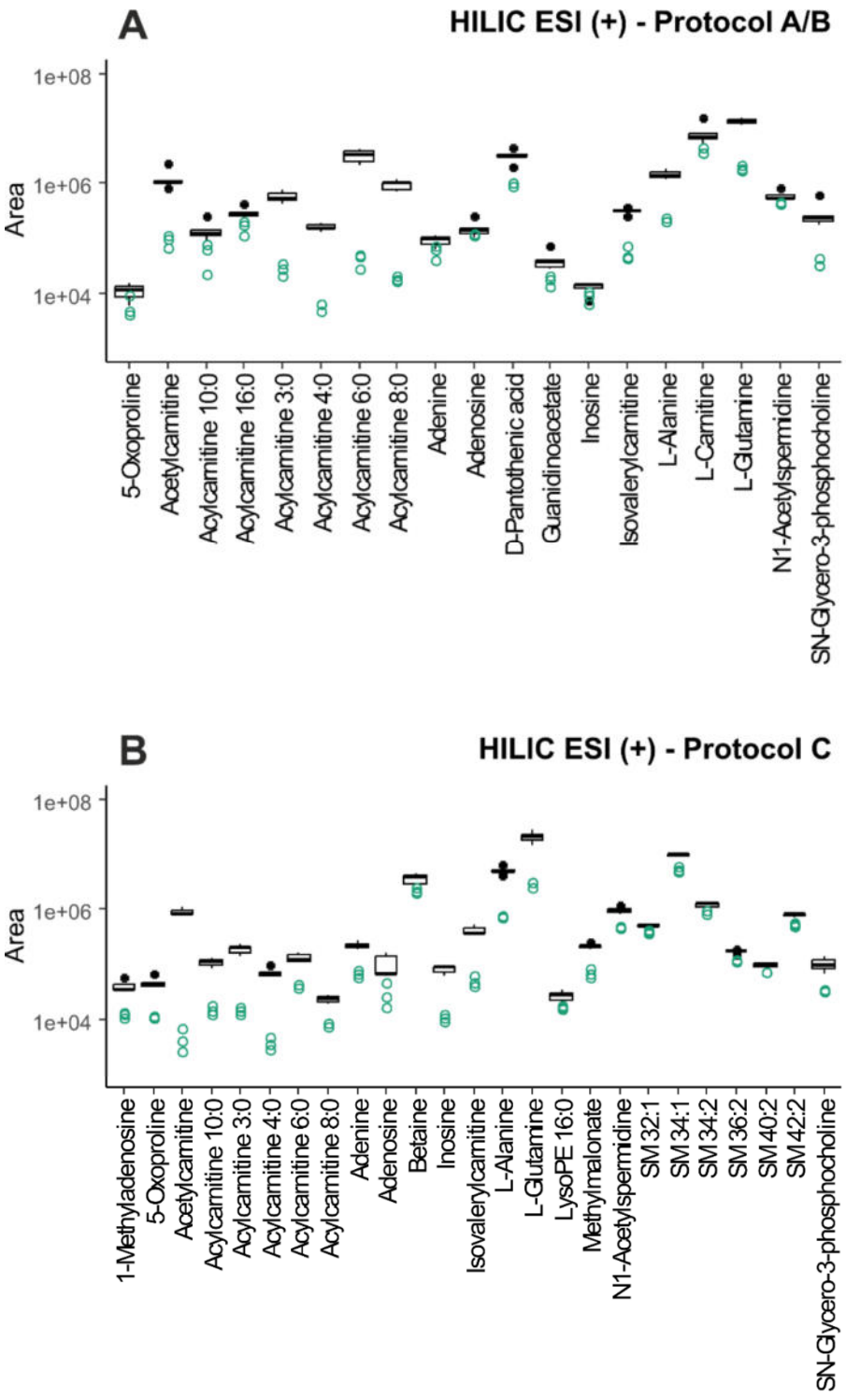

Figure S1. Metabolites found to be of significant and relevant abundance in organoid samples (black boxplots, $n = 10$ technical replicates, protocols A/B; $n = 5$ technical replicates, protocol C) compared to corresponding ECM blank samples (green circles, $n = 3$ technical replicates): **A** HILIC ESI (+) results of protocol A/B (data of these protocols was combined for statistical evaluation since sample preparation is identical for both protocols, see figure 1); **B** HILIC ESI (+) results of protocol C;

LysoPE, lysophosphatidylethanolamine; SM, sphingomyelin.

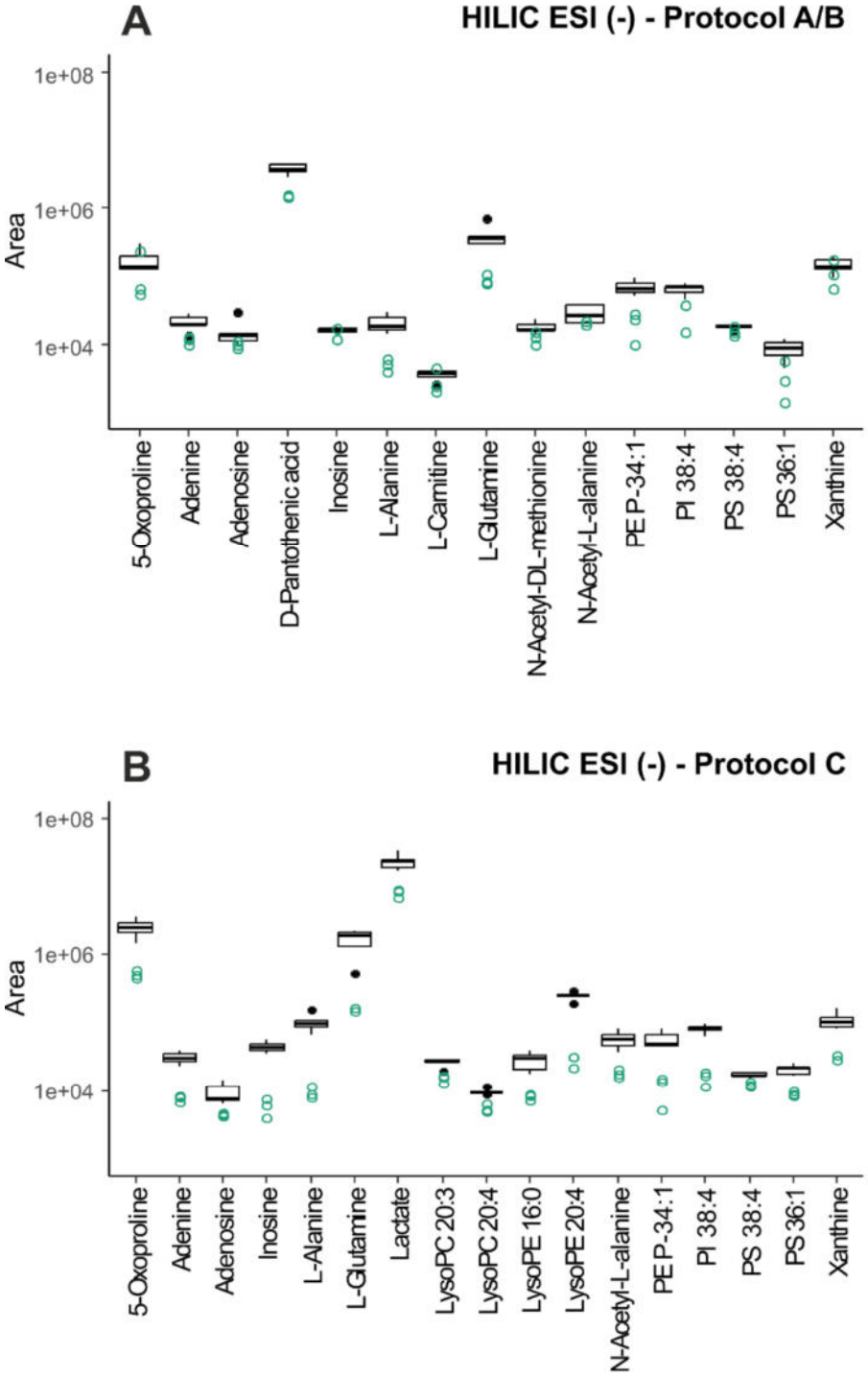

Figure S2. Metabolites found to be of significant and relevant abundance in organoid samples (black boxplots, $n = 10$ technical replicates, protocols A/B; $n = 5$ technical replicates, protocol C) compared to corresponding ECM blank samples (green circles, $n = 3$ technical replicates): **A** HILIC ESI (-) results of protocol A/B (data of these protocols was combined for statistical evaluation since sample preparation is identical for both protocols, see figure 1); **B** HILIC ESI (-) results of protocol C;

LysoPC, lysophosphatidylcholine; LysoPE, lysophosphatidylethanolamine; PE, phosphatidylethanolamine; PI, phosphatidylinositol; PS, phosphatidylserine.

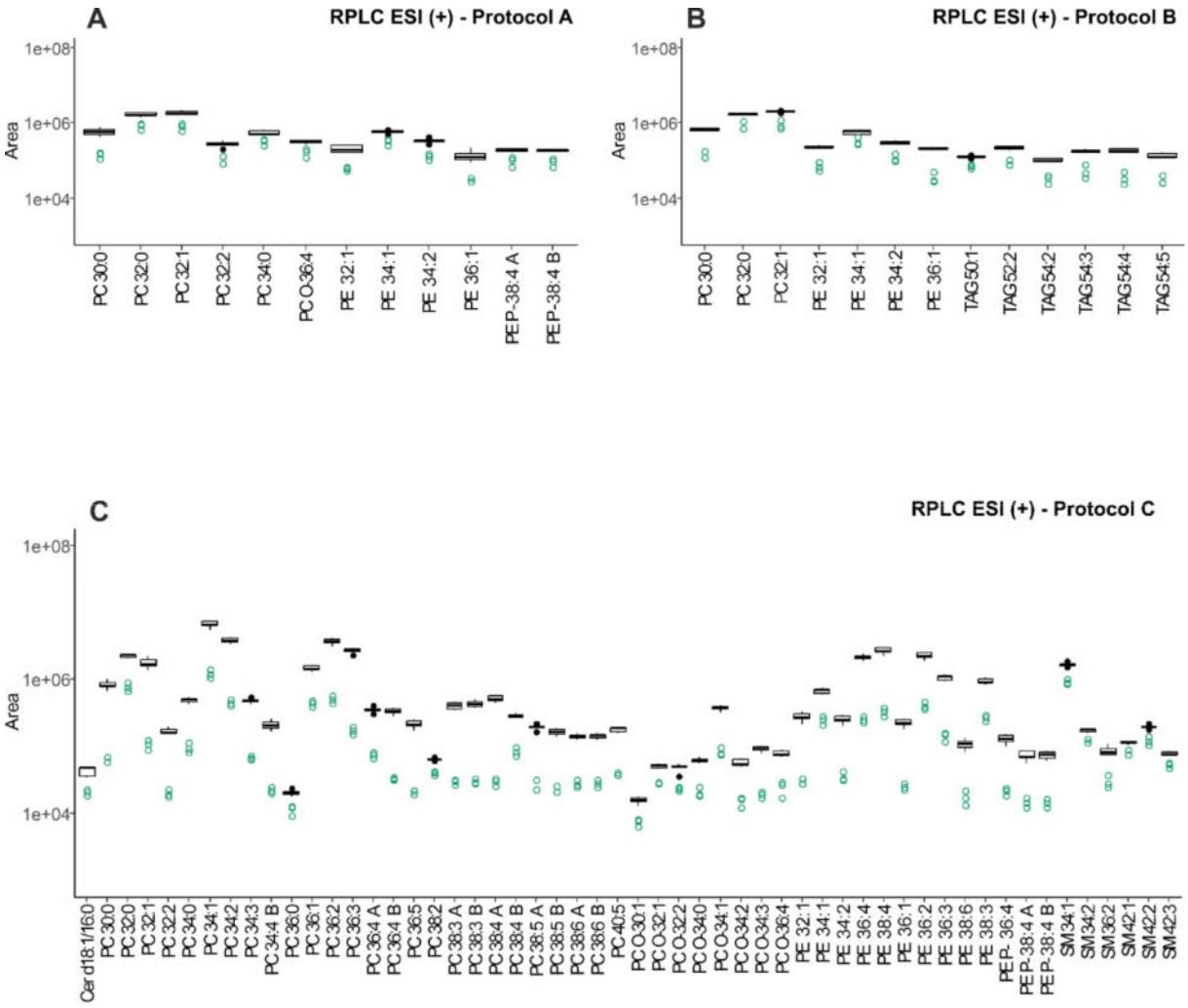

Figure S3. Metabolites found to be of significant and relevant abundance in organoid samples (black boxplots, $n = 5$ technical replicates) compared to corresponding ECM blank samples (green circles, $n = 3$ technical replicates): **A** RPLC ESI (+) results of protocol A; **B** RPLC ESI (+) results of protocol B; **C** RPLC ESI (+) results of protocol C.
Cer, ceramide; PC, phosphatidylcholine; PE, phosphatidylethanolamine; SM, sphingomyelin; TAG, triacylglycerol.

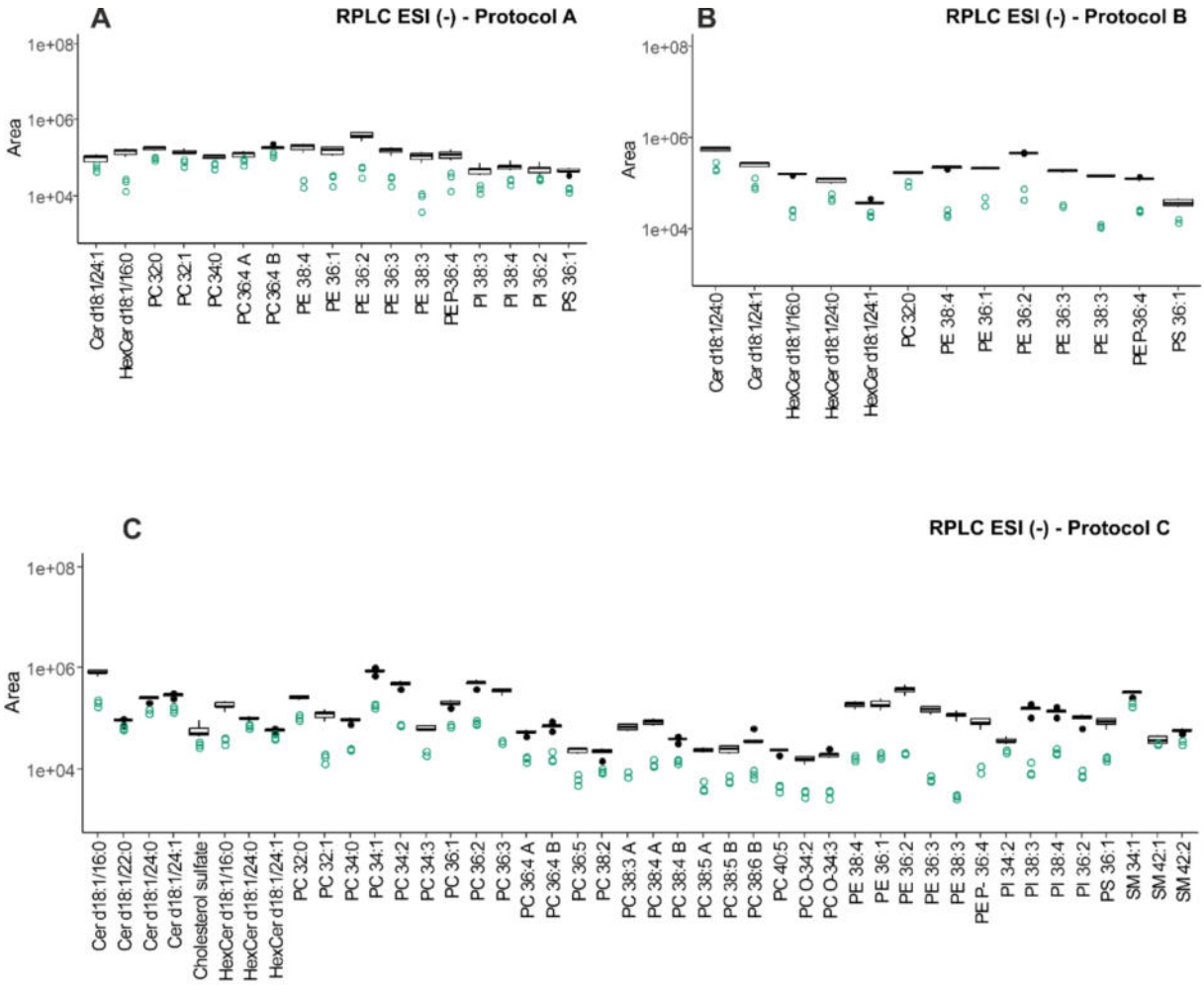

Figure S4. Metabolites found to be of significant and relevant abundance in organoid samples (black boxplots, $n = 5$ technical replicates) compared to corresponding ECM blank samples (green circles, $n = 3$ technical replicates): **A** RPLC ESI (-) results of protocol A; **B** RPLC ESI (-) results of protocol B; **C** RPLC ESI (-) results of protocol C.
Cer, ceramide; HexCer, hexosylceramide; PC, phosphatidylcholine; PE, phosphatidylethanolamine; SM, sphingomyelin; PI, phosphatidylinositol; PS, phosphatidylserine.

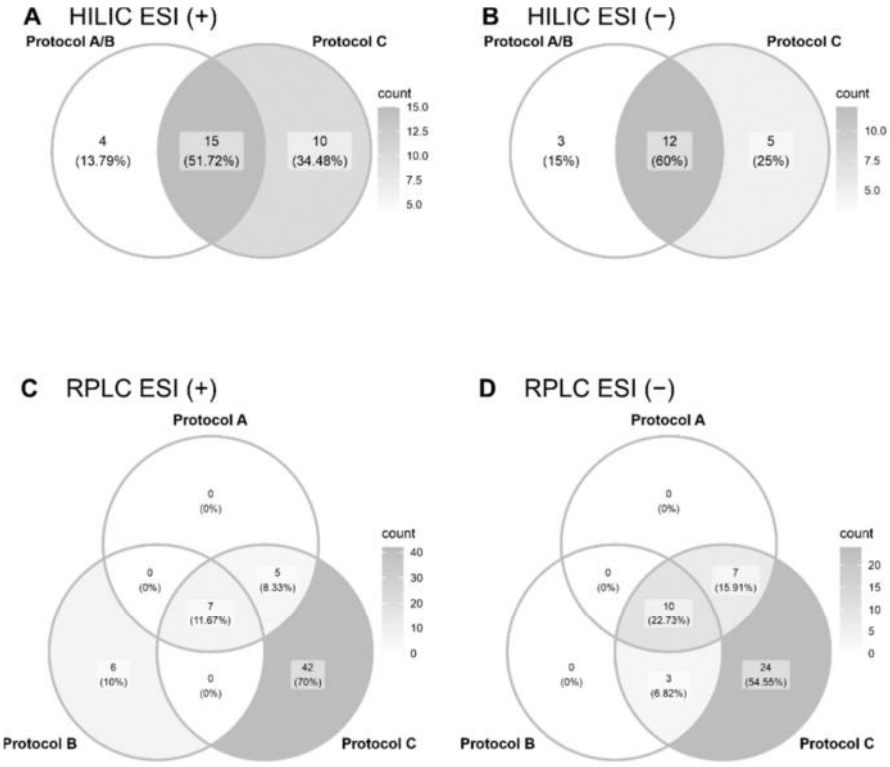

Figure S5. Venn diagrams displaying the overlap of the tested extraction procedures (see Figure 1) with respect to metabolites present in organoid samples with significant and relevant abundance. **A:** HILIC ESI (+) mode, **B:** HILIC ESI (-) mode, **C:** RPLC ESI (+) mode and **D:** RPLC ESI (-) mode. Since protocols A and B are identical for samples analyzed via HILIC, they were evaluated together (diagrams A and B).

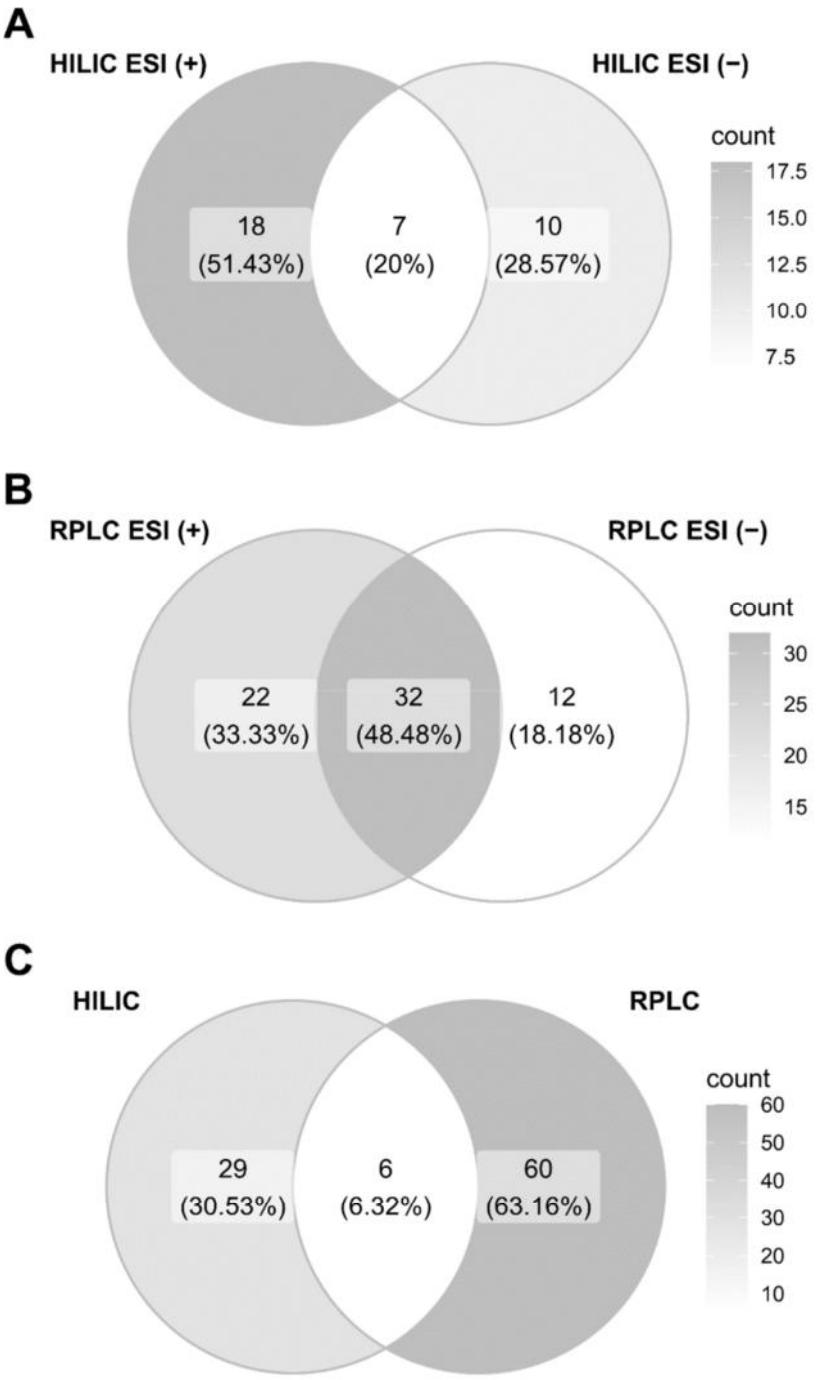

Figure S6. Venn diagrams displaying the extent of overlap between the different analytical modes for significantly and relevantly detected metabolites in protocol C (see Supplementary Figures S1-S4): **A** HILIC ESI(+) and HILIC ESI(-), **B** RPLC ESI(+) and RPLC ESI(-), and **C** HILIC and RPLC.

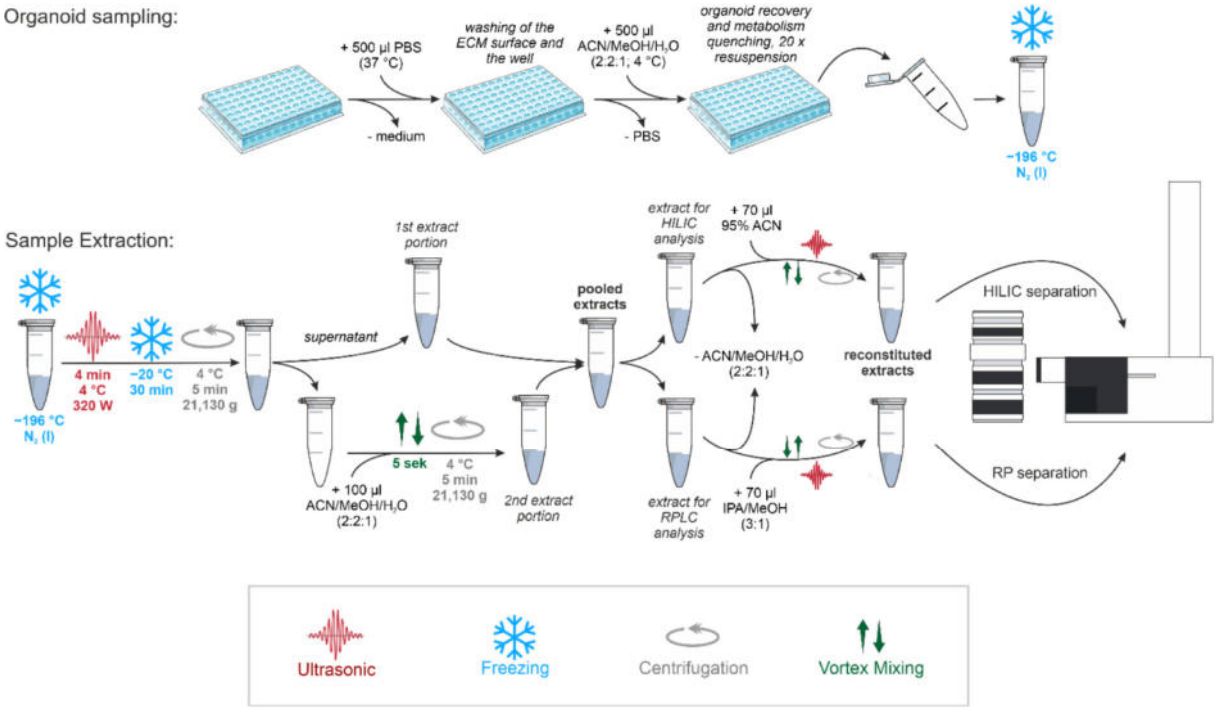

Figure S7. Optimized protocol for comprehensive and reproducible metabolomic and lipidomic profiling of CRC organoids using LC-QTOF-MS after dual LC separation by HILIC and RPLC. The red wave icon indicate ultrasonic cell extraction with on/off cycles of 0.5 min and total disruption time of 4 min. Blue snow flake icons represent sample freezing. Grey and green arrows display centrifugation and vortex mixing, respectively.
PBS, phosphate-buffered saline; ACN, acetonitrile; MeOH, methanol; IPA, isopropanol.

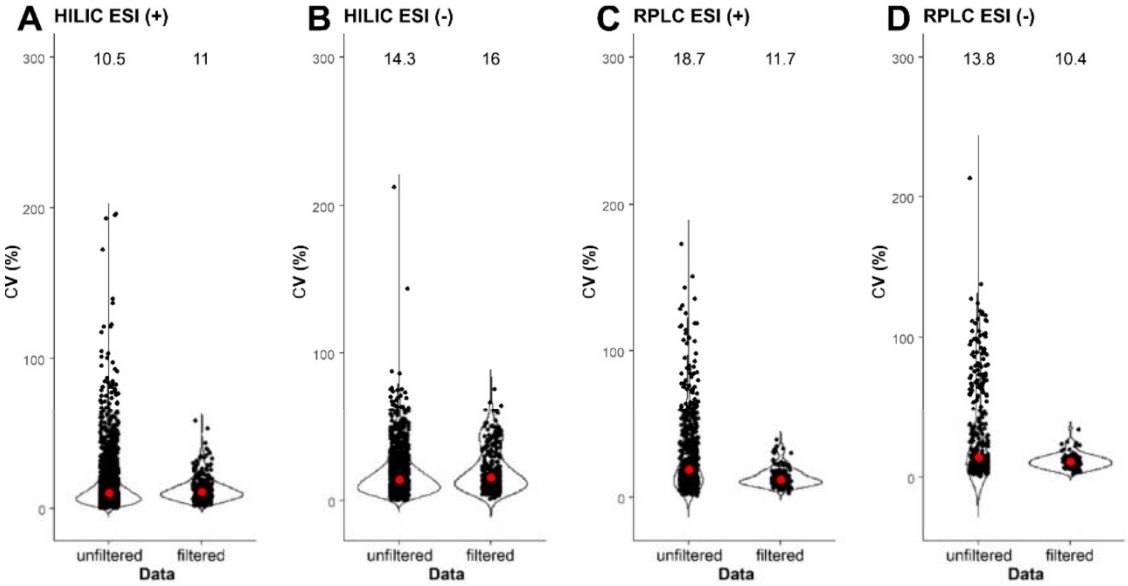

Figure S8. Influence of the established data filtering procedure on data quality with regard to the variability of retained features. **A:** HILIC ESI (+) mode, **B:** HILIC ESI (-) mode, **C:** RPLC ESI (+) mode and **D:** RPLC ESI (-) mode. A fold change (FC) of 1.2 (untreated organoid samples/ECM blank samples) and a significance level of 5% (uncorrected p-value < 0.05) were applied as filter cut-offs. Bean plots representing the coefficients of variation (CVs, $n = 5$ technical replicates) of features (black dots) detected in untreated organoid samples before and after data filtering workflow. Median CVs of each single mode are indicated by red dots and listed above the beanplots.

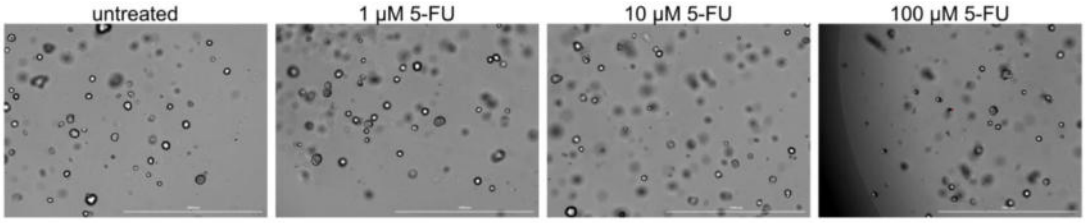

Figure S9. Exemplary pictures from preliminary experiments to ensure cell viability at the time of sampling. The nuclei of dead cells were stained with NucRed™ Dead 647 ReadyProbes™ Reagent (far-red).

Tables Overview	
Table S1	Analytical batch structure
Table S2	Putatively annotated/identified compounds in the HILIC ESI (+) mode
Table S3	Putatively annotated/identified compounds in the HILIC ESI (-) mode
Table S4	Putatively annotated/identified compounds in the RPLC ESI (+) mode
Table S5	Putatively annotated/identified compounds in the RPLC ESI (-) mode
Table S6	Search result from the accurate mass batch search (CEU mass mediator) of compounds found with higher abundance in ECM blank samples - HILIC ESI (+) mode
Table S7	Search result from the accurate mass batch search (CEU mass mediator) of compounds found with higher abundance in ECM blank samples - HILIC ESI (-) mode
Table S8	Search result from the accurate mass batch search (CEU mass mediator) of compounds found with higher abundance in ECM blank samples - RPLC ESI (+) mode
Table S9	Search result from the accurate mass batch search (CEU mass mediator) of compounds found with higher abundance in ECM blank samples - RPLC ESI (-) mode
Table S10	Significantly and relevantly regulated features detected upon 5-flurouracil treatment - all modes
Table S11	Used chemicals and reagents

Supplementary Table S1: Analytical batch structure

Sample Type		Injection Volume [µl]
column conditioning	Solvent Blank	20
	(diluted) QC sample	3
	(diluted) QC sample	
	(diluted) QC sample	
	(diluted) QC sample	
	(diluted) QC sample	
MS/MS data aquisition	QC sample	20
sample analysis and monitoring of analytical reproducibility	(diluted) QC sample	
	5 - 6 samples	
	(diluted) QC sample	
	5 - 6 samples	
	(diluted) QC sample	
	5 - 6 samples	
	(diluted) QC sample	
	[...]	
MS/MS data aquisition	(diluted) QC sample	
carry over monitoring	Solvent Blank	

Supplementary Table S2: Putatively annotated/identified compounds in the HILIC ESI (+) mode

Annotation	Formula	SMILES	InChI	Monoisotopic molecular weight	Observed mass	Δppm	Observed retention time [min]	Retention time difference [min] [3]	MSI assignment level [4]	Search engine score (MS/MS)	Profinder score (max)
Cytosine, in-source fragment of 2'-deoxycytidine [1]	-	-	-	111.0433	111.0431	1.4	4.41	-	2	-	-
Cytosine, in-source fragment of 2'-O-methylcytidine [1]	-	-	-	111.0433	111.0436	2.8	3.21	-	2	-	-
7-Methylguanine [1]	C6H7N5O	Cn1cnc2nc(N)[nH]c(=O)c12	InChI=1S/C6H7N5O/c1-11-2-8-4-3(11)5(12)10-6(7)9-4/h2H,1H3,(H3,7,9,10,12)	165.0651	165.0648	1.6	3.65	-	2	976 [5]	-
Acetylcarnitine [1]	C9H17NO4	CC(=O)OC(CC([O-])=O)C[N+](C)(C)C	InChI=1S/C9H17NO4/c1-7(11)14-8(5-9(12)13)6-10(2,3)4/h8H,5-6H2,1-4H3	203.1161	203.1161	0.0	7.61	-	2	982 [5]	-
Acylcarnitine 3:0 [1]	C10H19NO4	CCC(=O)O[C@H](CC([O-])=O)C[N+](C)(C)C	InChI=1S/C10H19NO4/c1-5-10(14)15-8(6-9(12)13)7-11(2,3)4/h8H,5-7H2,1-4H3/t8-/m1/s1	217.1314	217.1318	1.8	6.79	-	2	948 [5]	-
Deoxycytidine [1]	C9H13N3O4	Nc1ccn([C@H]2C[C@H](O)[C@@H](CO)O2)c(=O)n1	InChI=1S/C9H13N3O4/c10-7-1-2-12(9(15)11-7)8-3-5(14)6(4-13)16-8/h1-2,5-6,8,13-14H,3-4H2,(H2,10,11,15)/t5-,6+,8+/m0/s1	227.0906	227.0898	3.5	4.41	-	2	76.2 [6]	-
Acylcarnitine 4:0 [1]	C11H21NO4	CCCC(=O)O[C@H](CC([O-])=O)C[N+](C)(C)C	InChI=1S/C11H21NO4/c1-5-6-11(15)16-9(7-10(13)14)8-12(2,3)4/h9H,5-8H2,1-4H3/t9-/m1/s1	231.1471	231.1468	1.1	5.95	-	2	84.2 [7]	-
2'-Deoxyadenosine [1]	C10H13N5O3	Nc1ncnc2n(cnc12)[C@H]1C[C@H](O)[C@@H](CO)O1	InChI=1S/C10H13N5O3/c11-9-8-10(13-3-12-9)15(4-14-8)7-1-5(17)6(2-16)18-7/h3-7,16-17H,1-2H2,(H2,11,12,13)/t5-,6+,7+/m0/s1	251.1018	251.1026	3.2	2.42	0.06	1	91.7 [6]	-
2'-O-Metylcytidine [1]	C10H15N3O5	CO[C@@H]1[C@H](O)[C@@H](CO)O[C@H]1n1ccc(N)nc1=O	InChI=1S/C10H15N3O5/c1-17-8-7(15)5(4-14)18-9(8)13-3-2-6(11)12-10(13)16/h2-3,5,7,9,14-15H,4H2,1H3,(H2,11,12,16)/t5-,7-,8-,9-/m1/s1	257.1012	257.1022	4.0	3.21	-0.02	1	74.9 [6]	-
Inosine [1]	C10H12N4O5	OC[C@H]1O[C@H]([C@H](O)[C@@H]1O)n1cnc2c(O)ncnc12	InChI=1S/C10H12N4O5/c15-1-4-6(16)7(17)10(19-4)14-3-13-5-8(14)11-2-12-9(5)18/h2-4,6-7,10,15-17H,1H2,(H,11,12,18)/t4-,6-,7-,10-/m1/s1	268.0808	268.0828	7.6	4.89	-	2	91.1 [6]	-
1-Methyladenosine [1]	C11H15N5O4	Cn1cnc2n(cnc2c1=N)[C@@H]1O[C@H](CO)[C@@H](O)[C@H]1O	InChI=1S/C11H15N5O4/c1-15-3-14-10-6(9(15)12)13-4-16(10)11-8(19)7(18)5(2-17)20-11/h3-5,7-8,11-12,17-19H,2H2,1H3/t5-,7-,8-,11-/m1/s1	281.1124	281.1115	3.4	7.90	0.03	1	55.6 [6]	-
Acylcarnitine 8:0 [1]	C15H29NO4	CCCCCCCC(=O)OC(CC([O-])=O)C[N+](C)(C)C	InChI=1S/C15H29NO4/c1-5-6-7-8-9-10-15(19)20-13(11-14(17)18)12-16(2,3)4/h13H,5-12H2,1-4H3	287.2097	287.2098	0.5	3.90	-	2	83.2 [7]	-
Acylcarnitine 10:0 [1]	C17H33NO4	O([C@@H](C[N+](C)(C)C)CC([O-])=O)C(CCCCCCCCC)=O	InChI=1S/C17H33NO4/c1-5-6-7-8-9-10-11-12-17(21)22-15(13-16(19)20)14-18(2,3)4/h15H,5-14H2,1-4H3/t15-/m1/s1	315.2410	315.2420	3.3	3.35	-	2	72.9 [7]	-
Acylcarnitine 16:0 [1]	C23H45NO4	CCCCCCCCCCCCCCCC(=O)O[C@H](CC([O-])=O)C[N+](C)(C)C	InChI=1S/C23H45NO4/c1-5-6-7-8-9-10-11-12-13-14-15-16-17-18-23(27)28-21(19-22(25)26)20-24(2,3)4/h21H,5-20H2,1-4H3/t21-/m1/s1	399.3349	399.3355	1.6	2.61	-	2	80.6 [6]	-
LysoPC 26:1 [1]	C34H68NO7P	C[N+](C)(C)CCOP([O-])(=O)OC[C@@H](CO[*])O[*]	-	633.4733	633.4739	0.8	3.78	-	2	82.8 [7]	-
PC 28:0 [1]	C36H72NO8P	[H][C@@](COC([*])=O)(COP([O-])(=O)OCC[N+](C)(C)C)OC([*])=O	-	677.4996	677.4972	3.5	2.14	-	2	96.4 [7]	-

Annotation	Formula	SMILES	InChI	Monoisotopic molecular weight	Observed mass	Δppm	Observed retention time [min]	Retention time difference [min] [3]	MSI assignment level [4]	Search engine score (MS/MS)	Profinder score (max)
PC 29:2 [1]	C37H70NO8P	C(C[N+](C)(C)C)OP(=O)([O-])OC[C@H](OC(*)=O)COC(=O)*	-	687.4839	687.4865	3.8	2.37	-	2	82.4 [7]	-
PE 32:1 [1]	C37H72NO8P	[H][C@@](COC([*])=O)(COP([O-])(=O)OCC[NH3+])OC([*])=O	-	689.4996	689.4963	4.7	2.35	-	2	73.3 [7]	-
PE 34:3 [1]	C39H72NO8P	[H][C@@](COC([*])=O)(COP([O-])(=O)OCC[NH3+])OC([*])=O	-	713.4996	713.5029	4.7	2.33	-	2	68.8 [7]	-
PE 34:1 [1]	C39H76NO8P	O(P(=O)(OCCN)O)CC(OC(*)=O)COC(*)=O	-	717.5309	717.5288	2.9	2.29	-	2	92.1 [7]	-
1-Methyladenosine [2]	C11H15N5O4	Cn1cnc2n(cnc2c1=N)[C@@H]1O[C@H](CO)[C@@H](O)[C@H]1O	InChI=1S/C11H15N5O4/c1-15-3-14-10-6(9(15)12)13-4-16(10)11-8(19)7(18)5(2-17)20-11/h3-5,7-8,11-12,17-19H,2H2,1H3/t5-,7-,8-,11-/m1/s1	281.1124	281.1126	0.7	8.03	0.07	3	-	98.8
5-Oxoproline [2]	C5H7NO3	OC(=O)C1CCC(=O)N1	InChI=1S/C5H7NO3/c7-4-2-1-3(6-4)5(8)9/h3H,1-2H2,(H,6,7)(H,8,9)	129.0426	129.0428	1.5	8.26	0.02	3	-	99.4
Acetylcarnitine [2]	C9H17NO4	CC(=O)OC(CC([O-])=O)C[N+](C)(C)C	InChI=1S/C9H17NO4/c1-7(11)14-8(5-9(12)13)6-10(2,3)4/h8H,5-6H2,1-4H3	203.1158	203.1161	1.5	7.78	0.22	3	-	99.6
Acylcarnitine 10:0 [2]	C17H33NO4	O([C@@H](C[N+](C)(C)C)CC([O-])=O)C(CCCCCCCCC)=O	InChI=1S/C17H33NO4/c1-5-6-7-8-9-10-11-12-17(21)22-15(13-16(19)20)14-18(2,3)4/h15H,5-14H2,1-4H3/t15-/m1/s1	315.241	315.2424	4.4	3.62	0.72	3	-	98.5
Acylcarnitine 16:0 [2]	C23H45NO4	CCCCCCCCCCCCCCCC(=O)O[C@H](CC([O-])=O)C[N+](C)(C)C	InChI=1S/C23H45NO4/c1-5-6-7-8-9-10-11-12-13-14-15-16-17-18-23(27)28-21(19-22(25)26)20-24(2,3)4/h21H,5-20H2,1-4H3/t21-/m1/s1	399.3349	399.3350	0.3	2.80	0.54	3	-	99.4
Acylcarnitine 3:0 [2]	C10H19NO4	CCC(=O)O[C@H](CC([O-])=O)C[N+](C)(C)C	InChI=1S/C10H19NO4/c1-5-10(14)15-8(6-9(12)13)7-11(2,3)4/h8H,5-7H2,1-4H3/t8-/m1/s1	217.1314	217.1307	3.2	6.96	0.34	3	-	99.8
Acylcarnitine 4:0 [2]	C11H21NO4	CCCC(=O)O[C@H](CC([O-])=O)C[N+](C)(C)C	InChI=1S/C11H21NO4/c1-5-6-11(15)16-9(7-10(13)14)8-12(2,3)4/h9H,5-8H2,1-4H3/t9-/m1/s1	231.1471	231.1470	0.4	6.15	0.31	3	-	100.0
Acylcarnitine 6:0 [2]	C13H25NO4	C(OC(CCCCC)=O)(C[N+](C)(C)C)CC(=O)[O-]	InChI=1S/C13H25NO4/c1-5-6-7-8-13(17)18-11(9-12(15)16)10-14(2,3)4/h11H,5-10H2,1-4H3	259.1784	259.1785	0.4	5.21	0.88	3	-	99.7
Acylcarnitine 8:0 [2]	C15H29NO4	CCCCCCCC(=O)OC(CC([O-])=O)C[N+](C)(C)C	InChI=1S/C15H29NO4/c1-5-6-7-8-9-10-15(19)20-13(11-14(17)18)12-16(2,3)4/h13H,5-12H2,1-4H3	287.2097	287.2094	1.0	4.20	0.81	3	-	99.7
Adenine [2]	C5H5N5	Nc1ncnc2[nH]cnc12	InChI=1S/C5H5N5/c6-4-3-5(9-1-7-3)10-2-8-4/h1-2H,(H3,6,7,8,9,10)	135.0545	135.0543	1.5	2.82	0.06	3	-	99.3
Adenosine [2]	C10H13N5O4	Nc1ncnc2n(cnc12)[C@@H]1O[C@H](CO)[C@@H](O)[C@H]1O	InChI=1S/C10H13N5O4/c11-8-5-9(13-2-12-8)15(3-14-5)10-7(18)6(17)4(1-16)19-10/h2-4,6-7,10,16-18H,1H2,(H2,11,12,13)/t4-,6-,7-,10-/m1/s1	267.0968	267.0957	4.1	3.18	-0.03	3	-	99.0
Betaine [2]	C5H11NO2	C[N+](C)(C)CC([O-])=O	InChI=1S/C5H11NO2/c1-6(2,3)4-5(7)8/h4H2,1-3H3	117.079	117.0788	1.7	7.10	-0.05	3	-	99.8
D-Pantothenic acid [2]	C9H17NO5	CC(C)(CO)[C@@H](O)C(=O)NCCC(O)=O	InChI=1S/C9H17NO5/c1-9(2,5-11)7(14)8(15)10-4-3-6(12)13/h7,11,14H,3-5H2,1-2H3,(H,10,15)(H,12,13)/t7-/m0/s1	219.1107	219.1105	0.9	2.98	-0.09	3	-	96.8
Guanidinoacetate [2]	C3H7N3O2	C(CNC(=N)N)(O)=O	InChI=1S/C3H7N3O2/c4-3(5)6-1-2(7)8/h1H2,(H,7,8)(H4,4,5,6)	117.0538	117.0536	1.7	9.85	-0.01	3	-	87.9
Inosine [2]	C10H12N4O5	OC[C@H]1O[C@H]([C@H](O)[C@@H]1O)n1cnc2c(O)ncnc12	InChI=1S/C10H12N4O5/c15-1-4-6(16)7(17)10(19-4)14-3-13-5-8(14)11-2-12-9(5)18/h2-4,6-7,10,15-17H,1H2,(H,11,12,18)/t4-,6-,7-,10-/m1/s1	268.0808	268.0850	15.7	5.15	-0.36	3	-	99.0

Annotation	Formula	SMILES	InChI	Monoisotopic molecular weight	Observed mass	Δppm	Observed retention time [min]	Retention time difference [min] [3]	MSI assignment level [4]	Search engine score (MS/MS)	Profinder score (max)
Isovalerylcarnitine [2]	C12H23NO4	CC(C)CC(=O)OC(CC([O-])=O)C[N+](C)(C)C	InChI=1S/C12H23NO4/c1-9(2)6-12(16)17-10(7-11(14)15)8-13(3,4)5/h9-10H,6-8H2,1-5H3	245.1627	245.1631	1.6	5.81	0.71	3	-	99.4
L-Alanine [2]	C3H7NO2	C[C@H](N)C(O)=O	InChI=1S/C3H7NO2/c1-2(4)3(5)6/h2H,4H2,1H3,(H,5,6)/t2-/m0/s1	89.0477	89.0475	2.2	9.45	-0.11	3	-	100.0
L-Carnitine [2]	C7H15NO3	C[N+](C)(C)C[C@H](O)CC([O-])=O	InChI=1S/C7H15NO3/c1-8(2,3)5-6(9)4-7(10)11/h6,9H,4-5H2,1-3H3/t6-/m1/s1	161.1052	161.1051	0.6	8.91	0.02	3	-	99.6
L-Glutamine [2]	C5H10N2O3	N[C@@H](CCC(N)=O)C(O)=O	InChI=1S/C5H10N2O3/c6-3(5(9)10)1-2-4(7)8/h3H,1-2,6H2,(H2,7,8)(H,9,10)/t3-/m0/s1	146.0691	146.0688	2.1	10.41	-0.03	3	-	99.4
LysoPE 16:0 [2]	C21H44NO7P	[C@](CO*)(O*)([H])COP(OCCN)(=O)O	-	453.2855	453.2860	1.1	5.75	0.02	3	-	83.0
Methylmalonate [2]	C4H6O4	CC(C(O)=O)C(O)=O	InChI=1S/C4H6O4/c1-2(3(5)6)4(7)8/h2H,1H3,(H,5,6)(H,7,8)	118.0266	118.0276	8.5	2.82	0.08	3	-	96.0
N1-Acetylspermidine [2]	C9H21N3O	CC(=O)NCCCNCCCCN	InChI=1S/C9H21N3O/c1-9(13)12-8-4-7-11-6-3-2-5-10/h11H,2-8,10H2,1H3,(H,12,13)	187.1685	187.1696	5.9	11.26	0.31	3	-	100.0
SM 32:1 [2]	C37H75N2O6P	[H][C@](C)(O)[C@]([H])(COP([O-])(=O)OCC[N+](C)(C)C)NC(=O	-	674.5363	674.5361	0.3	4.02	0.60	3	-	91.0
SM 34:1 [2]	C39H79N2O6P	C[N+](C)(C)CCOP([O-])(=O)OC[C@H](NC([*])=O)[C@H](O)[*]	-	702.5676	702.5672	0.6	3.86	0.58	3	-	91.2
SM 34:2 [2]	C39H77N2O6P	[H][C@@](O)([*])[C@]([H])(COP([O-])(=O)OCC[N+](C)(C)C)NC([*])=O	-	700.5519	700.5527	1.1	3.91	0.61	3	-	84.6
SM 36:2 [2]	C41H81N2O6P	C[N+](C)(C)CCOP([O-])(=O)OC[C@H](NC([*])=O)[C@H](O)[*]	-	728.5832	728.5841	1.2	3.74	0.59	3	-	73.1
SM 40:2 [2]	C45H89N2O6P	C[N+](C)(C)CCOP([O-])(=O)OC[C@H](NC([*])=O)[C@H](O)[*]	-	784.6458	784.6509	6.5	3.46	0.49	3	-	95.1
SM 42:2 [2]	C47H93N2O6P	C[N+](C)(C)CCOP([O-])(=O)OC[C@H](NC([*])=O)[C@H](O)[*]	-	812.6771	812.6780	1.1	3.37	0.47	3	-	89.0
SN-Glycero-3-phosphocholine [2]	C8H20NO6P	C[N+](C)(C)CCOP([O-])(=O)OC[C@H](O)CO	InChI=1S/C8H20NO6P/c1-9(2,3)4-5-14-16(12,13)15-7-8(11)6-10/h8,10-11H,4-7H2,1-3H3/t8-/m1/s1	257.1028	257.1031	1.2	10.45	-0.04	3	-	99.9

[1] assigned in the proof of concept experiment

[2] assigned via Batch Targeted Feature Extraction in the protocol assessment experiment

[3] compared to reference standard or to previously assigned metabolites (Leuthold et al. Comprehensive Metabolomic and Lipidomic Profiling of Human Kidney Tissue: A Platform Comparison. J. Proteome Res. 2017, 16, 933–944

[4] Sumner et al. Proposed minimum reporting standards for chemical analysis Chemical Analysis Working Group (CAWG) Metabolomics Standards Initiative (MSI). Metabolomics 2007, 3, 211–221

[5] MassBank of North America

[6] PCDL Manager (Agilent)

[7] Lipid Annotator (Agilent)

[8] CEU Mass Mediator

PC - phosphatidylcholine, PE - phosphatidylethanolamine, SM - sphingomyelin

Supplementary Table S3: Putatively annotated/identified compounds in the HILIC ESI (-) mode

Annotation	Formula	SMILES	InChI	Monoisotopic molecular weight	Observed mass	Δppm	Observed retention time [min]	Retention time difference [min] [3]	MSI assignment level [4]	Search engine score (MS/MS)	Profinder score (max)
2'-Deoxyuridine [1]	C9H12N2O5	OC[C@H]1O[C@H](C[C@@H]1O)n1ccc(=O)[nH]c1=O	InChI=1S/C9H12N2O5/c12-4-6-5(13)3-8(16-6)11-2-1-7(14)10-9(11)15/h1-2,5-6,8,12-13H,3-4H2,(H,10,14,15)/t5-,6+,8+/m0/s1	228.0746	228.0731	6.5	2.12	0.08	2	-	-
1-Methyladenosine [1]	C11H15N5O4	Cn1cnc2n(cnc2c1=N)[C@@H]1O[C@H](CO)[C@@H](O)[C@H]1O	InChI=1S/C11H15N5O4/c1-15-3-14-10-6(9(15)12)13-4-16(10)11-8(19)7(18)5(2-17)20-11/h3-5,7-8,11-12,17-19H,2H2,1H3/t5-,7-,8-,11-/m1/s1	281.1124	281.1127	1.1	7.85	-0.01	2	-	-
5-Oxoproline [2]	C5H7NO3	OC(=O)C1CCC(=O)N1	InChI=1S/C5H7NO3/c7-4-2-1-3(6-4)5(8)9/h3H,1-2H2,(H,6,7)(H,8,9)	129.0426	129.0435	7.0	8.20	-0.05	3	-	99.7
Adenine [2]	C5H5N5	Nc1ncnc2[nH]cnc12	InChI=1S/C5H5N5/c6-4-3-5(9-1-7-3)10-2-8-4/h1-2H,(H3,6,7,8,9,10)	135.0545	135.0548	2.2	2.77	0.01	3	-	47.6
Adenosine [2]	C10H13N5O4	Nc1ncnc2n(cnc12)[C@@H]1O[C@H](CO)[C@@H](O)[C@H]1O	InChI=1S/C10H13N5O4/c11-8-5-9(13-2-12-8)15(3-14-5)10-7(18)6(17)4(1-16)19-10/h2-4,6-7,10,16-18H,1H2,(H2,11,12,13)/t4-,6-,7-,10-/m1/s1	267.0968	267.0998	11.2	3.13	-0.08	3	-	82.9
Allantoin [2]	C4H6N4O3	NC(=O)NC1NC(=O)NC1=O	InChI=1S/C4H6N4O3/c5-3(10)6-1-2(9)8-4(11)7-1/h1H,(H3,5,6,10)(H2,7,8,9,11)	158.0440	158.0446	3.8	4.23	-0.31	3	-	95.5
D-Pantothenic acid [2]	C9H17NO5	CC(C)(CO)[C@@H](O)C(=O)NCCC(O)=O	InChI=1S/C9H17NO5/c1-9(2,5-11)7(14)8(15)10-4-3-6(12)13/h7,11,14H,3-5H2,1-2H3,(H,10,15)(H,12,13)/t7-/m0/s1	219.1107	219.1103	1.8	2.94	-0.13	3	-	99.7
Inosine [2]	C10H12N4O5	OC[C@H]1O[C@H]([C@H](O)[C@@H]1O)n1cnc2c(O)ncnc12	InChI=1S/C10H12N4O5/c15-1-4-6(16)7(17)10(19-4)14-3-13-5-8(14)11-2-12-9(5)18/h2-4,6-7,10,15-17H,1H2,(H,11,12,18)/t4-,6-,7-,10-/m1/s1	268.0808	268.0759	18.3	5.09	-0.42	3	-	84.9
Lactate [2]	C3H6O3	CC(O)C(O)=O	InChI=1S/C3H6O3/c1-2(4)3(5)6/h2,4H,1H3,(H,5,6)	90.0317	90.0321	4.4	3.72	-0.30	3	-	100.0
L-Alanine [2]	C3H7NO2	C[C@H](N)C(O)=O	InChI=1S/C3H7NO2/c1-2(4)3(5)6/h2H,4H2,1H3,(H,5,6)/t2-/m0/s1	89.0477	89.0482	5.6	9.40	-0.15	3	-	99.7
L-Carnitine [2]	C7H15NO3	C[N+](C)(C)C[C@H](O)CC([O-])=O	InChI=1S/C7H15NO3/c1-8(2,3)5-6(9)4-7(10)11/h6,9H,4-5H2,1-3H3/t6-/m1/s1	161.1052	161.1058	3.7	8.87	-0.02	3	-	97.9
L-Glutamine [2]	C5H10N2O3	N[C@@H](CCC(N)=O)C(O)=O	InChI=1S/C5H10N2O3/c6-3(5(9)10)1-2-4(7)8/h3H,1-2,6H2,(H2,7,8)(H,9,10)/t3-/m0/s1	146.0691	146.0698	4.8	10.38	-0.06	3	-	99.5
LysoPC 20:3 [2]	C28H52NO7P	[H][C@@](COC(C)=O)(COP([O-])(=O)OCC[N+](C)(C)C)OC(C)=O	-	545.3481	545.3476	0.9	4.84	0.55	3	-	76.9
LysoPC 20:4 [2]	C28H50NO7P	[H][C@@](CO[*])(COP([O-])(=O)OCC[N+](C)(C)C)O[*]	-	543.3325	543.3389	11.8	4.27	0.49	3	-	89.3
LysoPE 16:0 [2]	C21H44NO7P	[C@](CO*)(O*)([H])COP(OCCN)(=O)O	-	453.2855	453.2872	3.8	5.60	-0.13	3	-	99.0
LysoPE 20:4 [2]	C25H44NO7P	[C@](CO*)(O*)([H])COP(OCCN)(=O)O	-	501.2855	501.2879	4.8	5.46	0.29	3	-	97.3
N-Acetyl-DL-methionine [2]	C7H12NO3S-	CC(NC(C([O-])=O)CCSC)=O	InChI=1S/C7H13NO3S/c1-5(9)8-6(7(10)11)3-4-12-2/h6H,3-4H2,1-2H3,(H,8,9)(H,10,11)/p-1	191.0616	191.0621	2.6	3.28	-0.09	3	-	99.6
N-Acetyl-L-alanine [2]	C5H9NO3	C[C@H](NC(C)=O)C(O)=O	InChI=1S/C5H9NO3/c1-3(5(8)9)6-4(2)7/h3H,1-2H3,(H,6,7)(H,8,9)/t3-/m0/s1	131.0582	131.0593	8.4	4.73	-0.27	3	-	89.5
PE P-34:1 [2]	C39H76NO7P	C(OC[C@H](COP(OCCN)(=O)O)OC(*)=O)=C*	-	701.5359	701.5361	8.3	2.26	0.06	3	-	96.1
PI 38:4 [2]	C47H83O13P	[C@@H]1([C@@H]([C@@H]([C@@H]([C@H]([C@@H]1O)O)O)O)OP(OC[C@@H](COC(*)=O)OC(=O)*)(=O)O)O	-	886.5571	886.5595	2.7	5.98	-0.09	3	-	87.3

Annotation	Formula	SMILES	InChI	Monoisotopic molecular weight	Observed mass	Δppm	Observed retention time [min]	Retention time difference [min] [3]	MSI assignment level [4]	Search engine score (MS/MS)	Profinder score (max)
PS 38:4 [2]	C44H78NO10P	[C@@H](COC(=O)*)(COP(OC[C@@H](C(=O)O)N)(=O)O)OC(=O)*	-	811.5363	811.5331	3.9	6.38	0.29	3	-	98.4
PS 36:1 [2]	C42H80NO10P	[C@@H](COC(=O)*)(COP(OC[C@@H](C(=O)O)N)(=O)O)OC(=O)*	-	789.552	789.5480	5.1	6.33	0.15	3	-	72.0
Xanthine [2]	C5H4N4O2	O=c1[nH]c2[nH]cnc2c(=O)[nH]1	InChI=1S/C5H4N4O2/c10-4-2-3(7-1-6-2)8-5(11)9-4/h1H,(H3,6,7,8,9,10,11)	152.0334	152.0345	7.2	4.12	-0.18	3	-	98.2

[1] assigned in the proof of concept experiment

[2] assigned via Batch Targeted Feature Extraction in the protocol assessment experiment

[3] compared to reference standard or to previously assigned metabolites (Leuthold et al. Comprehensive Metabolomic and Lipidomic Profiling of Human Kidney Tissue: A Platform Comparison. J. Proteome Res. 2017, 16, 933–944

[4] Sumner et al. Proposed minimum reporting standards for chemical analysis Chemical Analysis Working Group (CAWG) Metabolomics Standards Initiative (MSI). Metabolomics 2007, 3, 211–221

[5] MassBank of North America

[6] PCDL Manager (Agilent)

[7] Lipid Annotator (Agilent)

[8] CEU Mass Mediator

PC - phosphatidylcholine, PE - phosphatidylethanolamine, PI - phosphatidylinositol, PS - phosphatidylserine

Supplementary Table S4: Putatively annotated/identified compounds in the RPLC ESI (+) mode

Annotation	Formula	SMILES	InChI	Monoisotopic molecular weight	Observed mass	Δppm	Observed retention time [min]	Retention time difference [min] [3]	MSI assignment level [4]	Search engine score (MS/MS)	Profinder score (max)
PC 28:0 [1]	C36H72NO8P	[H][C@@](COC([*])=O)(COP([O-])(=O)OCC[N+](C)(C)C)OC([*])=O	-	677.4996	677.5040	6.6	6.0	-	2	93.5 [7]	-
PC 30:0 [1]	C38H76NO8P	[H][C@@](COC([*])=O)(COP([O-])(=O)OCC[N+](C)(C)C)OC([*])=O	-	705.5309	705.5341	4.5	6.7	-	2	913 [5]	-
PC 32:0 [1]	C40H80NO8P	[H][C@@](COC([*])=O)(COP([O-])(=O)OCC[N+](C)(C)C)OC([*])=O	-	733.5622	733.5596	3.5	7.6	-	2	913 [5]	-
PC 32:2 [1]	C40H76NO8P	[H][C@@](COC([*])=O)(COP([O-])(=O)OCC[N+](C)(C)C)OC([*])=O	-	729.5309	729.5347	5.3	6.5	-	2	912 [5]	-
PC 30:1 [1]	C38H74NO8P	[H][C@@](COC([*])=O)(COP([O-])(=O)OCC[N+](C)(C)C)OC([*])=O	-	703.5152	703.5198	6.5	6.3	-	2	90.4 [7]	-
PC 30:1 [1]	C38H74NO8P	[H][C@@](COC([*])=O)(COP([O-])(=O)OCC[N+](C)(C)C)OC([*])=O	-	703.5152	703.5203	7.2	6.2	-	2	90.4 [7]	-
PC 36:2 [1]	C44H84NO8P	[H][C@@](COC(C)=O)(COP([O-])(=O)OCC[N+](C)(C)C)OC(C)=O	-	785.5935	785.5901	4.3	8.1	-	2	913 [5]	-
PC 36:3 [1]	C44H82NO8P	[H][C@@](COC([*])=O)(COP([O-])(=O)OCC[N+](C)(C)C)OC([*])=O	-	783.5778	783.5790	1.5	7.7	-	2	909 [5]	-
PC 38:4 [1]	C46H84NO8P	[H][C@@](COC([*])=O)(COP([O-])(=O)OCC[N+](C)(C)C)OC([*])=O	-	809.5935	809.6006	8.8	7.9	-	2	913 [5]	-
PC 38:5 [1]	C46H82NO8P	[H][C@@](COC([*])=O)(COP([O-])(=O)OCC[N+](C)(C)C)OC([*])=O	-	807.5778	807.5855	9.5	7.8	-	2	89.4 [7]	-
PE 34:1 [1]	C39H76NO8P	O(P(=O)(OCCN)O)CC(OC(*)=O)COC(*)=O	-	717.5309	717.5324	2.2	7.9	-	2	982 [5]	-
PE 38:3 [1]	C43H80NO8P	O(P(=O)(OCCN)O)CC(OC(*)=O)COC(*)=O	-	769.5622	769.5630	1.1	8.8	-	2	91.8 [7]	-
PE P-40:5 [1]	C45H80NO7P	C(OC[C@H](COP(OCC[NH3+])(=O)[O-])OC(*)=O)=C*	-	777.5672	777.5680	1.0	9.1	-	2	0.1071 [8]	-
Cer d18:1/16:0 [2]	C34H67NO3	CCCCCCCCCCCCCCCC(=O)N[C@@H](CO)[C@H](O)\C=C\CCCCCCCCCCCCC	InChI=1S/C34H67NO3/c1-3-5-7-9-11-13-15-17-19-21-23-25-27-29-33(37)32(31-36)35-34(38)30-28-26-24-22-20-18-16-14-12-10-8-6-4-2/h27,29,32-33,36-37H,3-26,28,30-31H2,1-2H3,(H,35,38)/b29-27+/t32-,33+/m0/s1	537.5121	537.5042	14.7	7.5	0.04	3	-	96.1
PC 30:0 [2]	C38H76NO8P	[H][C@@](COC([*])=O)(COP([O-])(=O)OCC[N+](C)(C)C)OC([*])=O	-	705.5309	705.5234	10.6	7.0	0.02	3	-	100.0
PC 32:0 [2]	C40H80NO8P	[H][C@@](COC([*])=O)(COP([O-])(=O)OCC[N+](C)(C)C)OC([*])=O	-	733.5622	733.5543	10.8	7.9	0.05	3	-	99.2
PC 32:1 [2]	C40H78NO8P	[H][C@@](COC([*])=O)(COP([O-])(=O)OCC[N+](C)(C)C)OC([*])=O	-	731.5465	731.5385	10.9	7.2	0.03	3	-	99.7
PC 32:2 [2]	C40H76NO8P	[H][C@@](COC([*])=O)(COP([O-])(=O)OCC[N+](C)(C)C)OC([*])=O	-	729.5309	729.5236	10.0	6.6	0.01	3	-	94.4
PC 34:0 [2]	C42H84NO8P	[C@](COC(=O)*)(OC(=O)*)([H])COP(OCC[N+](C)(C)C)(=O)[O-]	-	761.5935	761.5857	10.2	8.9	0.06	3	-	99.8
PC 34:1 [2]	C42H82NO8P	[H][C@@](COC(C)=O)(COP([O-])(=O)OCC[N+](C)(C)C)OC(C)=O	-	759.5778	759.5691	11.5	8.2	0.04	3	-	99.3
PC 34:2 [2]	C42H80NO8P	[H][C@@](COC(C)=O)(COP([O-])(=O)OCC[N+](C)(C)C)OC(C)=O	-	757.5622	757.5544	10.3	7.5	0.04	3	-	98.7
PC 34:3 [2]	C42H78NO8P	[H][C@@](COC([*])=O)(COP([O-])(=O)OCC[N+](C)(C)C)OC([*])=O	-	755.5465	755.5378	11.5	6.9	0.11	3	-	99.9
PC 34:4 [2]	C42H76NO8P	[H][C@@](COC([*])=O)(COP([O-])(=O)OCC[N+](C)(C)C)OC([*])=O	-	753.5309	753.5266	5.7	7.3	0.05	3	-	83.2
PC 36:0 [2]	C44H88NO8P	[C@](COC(=O)*)(OC(=O)*)([H])COP(OCC[N+](C)(C)C)(=O)[O-]	-	789.6248	789.6143	13.3	10.0	0.04	3	-	96.4
PC 36:1 [2]	C44H86NO8P	[C@](COC(=O)*)(OC(=O)*)([H])COP(OCC[N+](C)(C)C)(=O)[O-]	-	787.6091	787.6000	11.6	9.2	0.07	3	-	99.6
PC 36:2 [2]	C44H84NO8P	[H][C@@](COC(C)=O)(COP([O-])(=O)OCC[N+](C)(C)C)OC(C)=O	-	785.5935	785.5862	9.3	8.5	0.05	3	-	99.2

Annotation	Formula	SMILES	InChI	Monoisotopic molecular weight	Observed mass	Δppm	Observed retention time [min]	Retention time difference [min] [3]	MSI assignment level [4]	Search engine score (MS/MS)	Profinder score (max)
PC 36:3 [2]	C44H82NO8P	[H][C@@](COC([*])=O)(COP([O-])(=O)OCC[N+](C)(C)C)OC([*])=O	-	783.5778	783.5688	11.5	7.9	0.14	3	-	99.1
PC 36:4 A [2]	C44H80NO8P	[H][C@@](COC(C)=O)(COP([O-])(=O)OCC[N+](C)(C)C)OC(C)=O	-	781.5622	781.5528	12.0	7.5	0.02	3	-	97.5
PC 36:4 B [2]	C44H80NO8P	[H][C@@](COC(C)=O)(COP([O-])(=O)OCC[N+](C)(C)C)OC(C)=O	-	781.5622	781.5530	11.8	7.3	0.18	3	-	99.4
PC 36:5 [2]	C44H78NO8P	[H][C@@](COC(C)=O)(COP([O-])(=O)OCC[N+](C)(C)C)OC(C)=O	-	779.5465	779.5378	11.2	7.0	0.03	3	-	95.9
PC 38:2 [2]	C46H88NO8P	[C@](COC(=O)*)(OC(=O)*)([H])COP(OCC[N+](C)(C)C)(=O)[O-]	-	813.6248	813.6154	11.6	9.1	-0.25	3	-	99.2
PC 38:3 A [2]	C46H86NO8P	[H][C@@](COC(C)=O)(COP([O-])(=O)OCC[N+](C)(C)C)OC(C)=O	-	811.6091	811.6005	10.6	8.9	0.05	3	-	99.7
PC 38:3 B [2]	C46H86NO8P	[H][C@@](COC(C)=O)(COP([O-])(=O)OCC[N+](C)(C)C)OC(C)=O	-	811.6091	811.5988	12.7	8.7	0.08	3	-	99.7
PC 38:4 A [2]	C46H84NO8P	[H][C@@](COC([*])=O)(COP([O-])(=O)OCC[N+](C)(C)C)OC([*])=O	-	809.5935	809.5847	10.9	8.3	0.06	3	-	98.1
PC 38:4 B [2]	C46H84NO8P	[H][C@@](COC([*])=O)(COP([O-])(=O)OCC[N+](C)(C)C)OC([*])=O	-	809.5935	809.5874	7.5	8.5	0.05	3	-	70.9
PC 38:5 A [2]	C46H82NO8P	[H][C@@](COC([*])=O)(COP([O-])(=O)OCC[N+](C)(C)C)OC([*])=O	-	807.5778	807.5685	11.5	7.9	0.18	3	-	98.9
PC 38:5 B [2]	C46H82NO8P	[H][C@@](COC([*])=O)(COP([O-])(=O)OCC[N+](C)(C)C)OC([*])=O	-	807.5778	807.5682	11.9	7.6	0.04	3	-	99.8
PC 38:6 A [2]	C46H80NO8P	[H][C@@](COC(C)=O)(COP([O-])(=O)OCC[N+](C)(C)C)OC(C)=O	-	805.5622	805.5521	12.5	7.3	0.19	3	-	82.5
PC 38:6 B [2]	C46H80NO8P	[H][C@@](COC(C)=O)(COP([O-])(=O)OCC[N+](C)(C)C)OC(C)=O	-	805.5622	805.5530	11.4	7.4	0.03	3	-	82.5
PC 40:5 [2]	C48H86NO8P	[H][C@@](COC([*])=O)(COP([O-])(=O)OCC[N+](C)(C)C)OC([*])=O	-	835.6091	835.5994	11.6	8.6	-0.04	3	-	99.2
PC O-30:1 [2]	C38H76NO7P	C[N+](C)(C)CCOP([O-])(=O)OC[C@@H](CO[*])O[*]	-	689.5359	689.5303	8.1	7.4	-0.08	3	-	77.2
PC O-32:1 [2]	C40H80NO7P	C[N+](C)(C)([CH2-])CCOP(=O)([O-])OC[C@@H](CO[*])O[*]	-	717.5672	717.5612	8.4	8.5	0.06	3	-	70.9
PC O-32:2 [2]	C40H78NO7P	C[N+](C)(C)CCOP([O-])(=O)OC[C@@H](CO[*])O[*]	-	715.5516	715.5472	6.1	7.8	-0.05	3	-	71.3
PC O-34:0 [2]	C42H86NO7P	[H][C@@](CO[*])(COP([O-])(=O)OCC[N+](C)(C)C)O[*]	-	747.6142	747.6032	14.7	9.7	0.07	3	-	98.7
PC O-34:1 [2]	C42H84NO7P	[H][C@@](CO[*])(COP([O-])(=O)OCC[N+](C)(C)C)O[*]	-	745.5985	745.5889	12.9	8.8	0.06	3	-	96.9
PC O-34:2 [2]	C42H82NO7P	[H][C@@](CO[*])(COP([O-])(=O)OCC[N+](C)(C)C)O[*]	-	743.5829	743.5782	6.3	8.8	0.06	3	-	70.5
PC O-34:3 [2]	C42H80NO7P	[H][C@@](CO[*])(COP([O-])(=O)OCC[N+](C)(C)C)O[*]	-	741.5672	741.5604	9.2	8.1	0.05	3	-	71.5
PC O-36:4 [2]	C44H82NO7P	[H][C@@](CO[*])(COP([O-])(=O)OCC[N+](C)(C)C)O[*]	-	767.5829	767.5769	7.8	8.5	0.33	3	-	72.4
PE 38:1 [2]	C43H84NO8P	[NH3+]CCOP([O-])(=O)OC[C@@H](COC([*])=O)OC([*])=O	-	689.4996	689.4997	0.1	7.0	-0.25	3	-	90.4
PE 34:1 [2]	C39H76NO8P	O(P(=O)(OCCN)O)CC(OC(*)=O)COC(*)=O	-	717.5309	717.5308	0.1	7.9	-0.23	3	-	94.0
PE 34:2 [2]	C39H74NO8P	O(P(=O)(OCCN)O)CC(OC(*)=O)COC(*)=O	-	715.5152	715.5146	0.8	7.2	-0.25	3	-	96.1
PE 36:4 [2]	C41H74NO8P	[C@@H](COC(=O)*)(COP(OCCN)(=O)O)OC(=O)*	-	739.5152	739.5063	12.0	7.5	0.01	3	-	91.5
PE 38:4 [2]	C43H78NO8P	[C@@H](COC(=O)*)(COP(OCCN)(=O)O)OC(=O)*	-	767.5465	767.538	11.1	8.5	0.05	3	-	97.9
PE 36:1 [2]	C41H80NO8P	O(P(=O)(OCCN)O)CC(OC(*)=O)COC(*)=O	-	745.5622	745.5533	11.9	9.2	0.06	3	-	98.1
PE 36:2 [2]	C41H78NO8P	O(P(=O)(OCCN)O)CC(OC(*)=O)COC(*)=O	-	743.5465	743.546	0.7	8.2	-0.26	3	-	85.9
PE 36:3 [2]	C41H76NO8P	O(P(=O)(OCCN)O)CC(OC(*)=O)COC(*)=O	-	741.5309	741.5304	0.7	7.5	-0.22	3	-	92.9
PE 38:6 [2]	C43H74NO8P	O(P(=O)(OCCN)O)CC(OC(*)=O)COC(*)=O	-	763.5152	763.5162	1.3	7.0	-0.13	3	-	98.1

Annotation	Formula	SMILES	InChI	Monoisotopic molecular weight	Observed mass	Δppm	Observed retention time [min]	Retention time difference [min] [3]	MSI assignment level [4]	Search engine score (MS/MS)	Profinder score (max)
PE 38:3 [2]	C43H80NO8P	O(P(=O)(OCCN)O)CC(OC(*)=O)COC(*)=O	-	769.5622	769.5564	7.5	9.2	0.10	3	-	89.3
PE P-36:4 [2]	C41H74NO7P	C(OC[C@H](COP(OCC[NH3+])(=O)[O-])OC(*)=O)=C*	-	723.5203	723.5111	12.7	8.1	0.05	3	-	88.4
PE P-38:4 A [2]	C43H78NO7P	C(OC[C@H](COP(OCCN)(=O)O)OC(*)=O)=C*	-	751.5516	751.5432	11.2	9.1	0.38	3	-	84.7
PE P-38:4 B [2]	C43H78NO7P	C(OC[C@H](COP(OCCN)(=O)O)OC(*)=O)=C*	-	751.5516	751.5449	8.9	9.2	0.08	3	-	87.8
SM 34:1 [2]	C39H79N2O6P	C[N+](C)(C)CCOP([O-])(=O)OC[C@H](NC([*])=O)[C@H](O)[*]	-	702.5676	702.5594	11.7	6.9	0.02	3	-	99.7
SM 34:2 [2]	C39H77N2O6P	[H][C@@](O)([*])[C@]([H])(COP([O-])(=O)OCC[N+](C)(C)C)NC([*])=O	-	700.5519	700.5435	12.0	6.3	0.01	3	-	99.8
SM 36:2 [2]	C41H81N2O6P	C[N+](C)(C)CCOP([O-])(=O)OC[C@H](NC([*])=O)[C@H](O)[*]	-	728.5832	728.5729	14.1	7.2	0.03	3	-	98.4
SM 42:1 [2]	C47H95N2O6P	C[N+](C)(C)CCOP([O-])(=O)OC[C@H](NC([*])=O)[C@H](O)[*]	-	814.6928	814.6809	14.6	11.3	0.11	3	-	98.7
SM 42:2 [2]	C47H93N2O6P	C[N+](C)(C)CCOP([O-])(=O)OC[C@H](NC([*])=O)[C@H](O)[*]	-	812.6771	812.6661	13.5	10.2	0.09	3	-	99.7
SM 42:3 [2]	C47H91N2O6P	C[N+](C)(C)CCOP([O-])(=O)OC[C@H](NC([*])=O)[C@H](O)[*]	-	810.6615	810.6514	12.5	9.5	0.08	3	-	97.6
TAG 50:1 [2]	C53H100O6	[*]C(=O)OCC(COC([*])=O)OC([*])=O	-	860.7833	860.7714	13.8	17.4	0.17	3	-	91.4
TAG 50:2 [2]	C53H98O6	[*]C(=O)OCC(COC([*])=O)OC([*])=O	-	830.7363	830.7255	13.0	16.2	0.17	3	-	93.8
TAG 52:2 [2]	C55H102O6	[*]C(=O)OCC(COC([*])=O)OC([*])=O	-	858.7676	858.7549	14.8	16.9	0.17	3	-	93.7
TAG 54:2 [2]	C57H106O6	[*]C(=O)OCC(COC([*])=O)OC([*])=O	-	886.7989	886.7878	12.5	17.6	0.17	3	-	91.4
TAG 54:3 [2]	C57H104O6	[*]C(=O)OCC(COC([*])=O)OC([*])=O	-	884.7833	884.7714	13.4	17.1	0.15	3	-	91.0
TAG 54:4 [2]	C57H102O6	[*]C(=O)OCC(COC([*])=O)OC([*])=O	-	882.7676	882.7578	11.1	16.5	0.14	3	-	97.8
TAG 54:5 [2]	C57H100O6	[*]C(=O)OCC(COC([*])=O)OC([*])=O	-	880.752	880.7415	11.9	16.0	0.17	3	-	94.6

[1] assigned in the proof of concept experiment

[2] assigned via Batch Targeted Feature Extraction in the protocol assessment experiment

[3] compared to reference standard or to previously assigned metabolites (Leuthold et al. Comprehensive Metabolomic and Lipidomic Profiling of Human Kidney Tissue: A Platform Comparison. J. Proteome Res. 2017, 16, 933–944)

[4] Sumner et al. Proposed minimum reporting standards for chemical analysis Chemical Analysis Working Group (CAWG) Metabolomics Standards Initiative (MSI). Metabolomics 2007, 3, 211–221

[5] MassBank of North America

[6] PCDL Manager (Agilent)

[7] Lipid Annotator (Agilent)

[8] CEU Mass Mediator

Cer - ceramide, PC - phosphatidylcholine, PE - phosphatidylethanolamine, SM - sphingomyelin, TAG - triacylglycerol

Supplementary Table S5: Putatively annotated/identified compounds in the RPLC ESI (-) mode

Annotation	Formula	SMILES	InChI	Monoisotopic molecular weight	Observed mass	Δppm	Observed retention time [min]	Retention time difference [min] [3]	MSI assignment level [4]	Search engine score (MS/MS)	Profinder score (max)
Cer d18:1/16:0 [2]	C34H67NO3	CCCCCCCCCCCCCCCC(=O)N[C@@H](CO)[C@H](O)\C=C\CCCCCCCCCCCCC	InChI=1S/C34H67NO3/c1-3-5-7-9-11-13-15-17-19-21-23-25-27-29-33(37)32(31-36)35-34(38)30-28-26-24-22-20-18-16-14-12-10-8-6-4-2/h27,29,32-33,36-37H,3-26,28,30-31H2,1-2H3,(H,35,38)/b29-27+/t32-,33+/m0/s1	537.5121	537.5124	0.6	7.5	0.05	3	-	99.8
Cer d18:1/22:0 [2]	C40H79NO3	CCCCCCCCCCCCCCCCCCCCCC(=O)N[C@@H](CO)[C@H](O)\C=C\CCCCCCCCCCCCC	InChI=1S/C40H79NO3/c1-3-5-7-9-11-13-15-17-18-19-20-21-22-24-26-28-30-32-34-36-40(44)41-38(37-42)39(43)35-33-31-29-27-25-23-16-14-12-10-8-6-4-2/h33,35,38-39,42-43H,3-32,34,36-37H2,1-2H3,(H,41,44)/b35-33+/t38-,39+/m0/s1	621.6060	621.6088	4.5	10.8	0.10	3	-	94.9
Cer d18:1/24:0 [2]	C42H83NO3	CCCCCCCCCCCCCCCCCCCCCCCC(=O)N[C@@H](CO)[C@H](O)\C=C\CCCCCCCCCCCCC	InChI=1S/C42H83NO3/c1-3-5-7-9-11-13-15-17-18-19-20-21-22-23-24-26-28-30-32-34-36-38-42(46)43-40(39-44)41(45)37-35-33-31-29-27-25-16-14-12-10-8-6-4-2/h35,37,40-41,44-45H,3-34,36,38-39H2,1-2H3,(H,43,46)/b37-35+/t40-,41+/m0/s1	649.6373	649.6387	2.2	11.9	0.11	3	-	97.0
Cer d18:1/24:1 [2]	C42H81NO3	CCCCCCCCCCCCC\C=C\[C@@H](O)[C@H](CO)NC(=O)CCCCCCCCCCCCC\C=C/CCCCCCCC	InChI=1S/C42H81NO3/c1-3-5-7-9-11-13-15-17-18-19-20-21-22-23-24-26-28-30-32-34-36-38-42(46)43-40(39-44)41(45)37-35-33-31-29-27-25-16-14-12-10-8-6-4-2/h17-18,35,37,40-41,44-45H,3-16,19-34,36,38-39H2,1-2H3,(H,43,46)/b18-17-,37-35+/t40-,41+/m0/s1	647.6216	647.6240	3.7	10.9	0.09	3	-	94.5
Cholesterol sulfate [2]	C27H46O4S	O(S([O-])(=O)=O)[C@@H]1CC=2[C@](C@]3(CC[C@]4([C@](C@@]3(CC2)[H])(CC[C@@]4([C@H](C)CCCC(C)C)[H])[H])C)[H])(C)CC1	InChI=1S/C27H46O4S/c1-18(2)7-6-8-19(3)23-11-12-24-22-10-9-20-17-21(31-32(28,29)30)13-15-26(20,4)25(22)14-16-27(23,24)5/h9,18-19,21-25H,6-8,10-17H2,1-5H3,(H,28,29,30)/p-1/t19-,21+,22+,23-,24+,25+,26+,27-/m1/s1	466.3117	466.3097	4.3	3.3	0.15	3	-	98.5
HexCer d18:1/16:0 [2]	C40H77NO8	CCCCCCCCCCCCCCCC(=O)N[C@@H](COC1OC(CO)C(O)C(O)C1O)[C@H](O)\C=C\CCCCCCCCCCCCC	InChI=1S/C40H77NO8/c1-3-5-7-9-11-13-15-17-19-21-23-25-27-29-34(43)33(32-48-40-39(47)38(46)37(45)35(31-42)49-40)41-36(44)30-28-26-24-22-20-18-16-14-12-10-8-6-4-2/h27,29,33-35,37-40,42-43,45-47H,3-26,28,30-32H2,1-2H3,(H,41,44)/b29-27+/t33,34+,35?,37?,38?,39?,40?/m0/s1	699.5649	699.5617	4.6	6.9	0.05	3	-	98.1
HexCer d18:1/24:0 [2]	C48H93NO8	O1[C@@H]([C@@H](O)C(O)C(O)[C@@H]1OC[C@H](NC(=O)CCCCCCCCCCCCCCCCCCCCCCC)[C@H](O)/C=C/CCCCCCCCCCCCC)CO	InChI=1S/C48H93NO8/c1-3-5-7-9-11-13-15-17-18-19-20-21-22-23-24-26-28-30-32-34-36-38-44(52)49-41(40-56-48-47(55)46(54)45(53)43(39-50)57-48)42(51)37-35-33-31-29-27-25-16-14-12-10-8-6-4-2/h35,37,41-43,45-48,50-51,53-55H,3-34,36,38-40H2,1-2H3,(H,49,52)/b37-35+/t41,42+,43+,45+,46?,47?,48+/m0/s1	811.6901	811.6916	1.8	11.1	0.10	3	-	96.4

Annotation	Formula	SMILES	InChI	Monoisotopic molecular weight	Observed mass	Δppm	Observed retention time [min]	Retention time difference [min] [3]	MSI assignment level [4]	Search engine score (MS/MS)	Profinder score (max)
HexCer d18:1/24:1 [2]	C48H91NO8	CCCCCCCCCCCCCC\C=C\[C@@H](O)[C@H](CO[C@@H]1O[C@H](CO)[C@H](O)[C@H](O)[C@H]1O)NC(=O)CCCCCCCCCCCCC\C=C/CCCCCCCC	InChI=1S/C48H91NO8/c1-3-5-7-9-11-13-15-17-18-19-20-21-22-23-24-26-28-30-32-34-36-38-44(52)49-42(41(40-56-48-47(55)46(54)45(53)43(39-50)57-48)42(51)37-35-33-31-29-27-25-16-14-12-10-8-6-4-2/h17-18,35,37,41-43,45-48,50-51,53-55H,3-16,19-34,36,38-40H2,1-2H3,(H,49,52)/b18-17-,37-35+/t41-,42+,43+,45-,46-,47+,48+/m0/s1	809.6745	809.6745	0.0	10.1	0.09	3	-	82.9
PC 32:0 [2]	C40H80NO8P	[H][C@@](COC([*])=O)(COP([O-])(=O)OCC[N+](C)(C)C)OC([*])=O	-	733.5622	733.5593	4.0	7.9	0.06	3	-	98.5
PC 32:1 [2]	C40H78NO8P	[H][C@@](COC([*])=O)(COP([O-])(=O)OCC[N+](C)(C)C)OC([*])=O	-	731.5465	731.5475	1.4	7.2	0.04	3	-	94.8
PC 34:0 [2]	C42H84NO8P	[C@](COC(=O)*)(OC(=O)*)([H])COP(OCC[N+](C)(C)C)(=O)[O-]	-	761.5935	761.5877	7.6	8.9	0.07	3	-	98.2
PC 34:1 [2]	C42H82NO8P	[H][C@@](COC(C)=O)(COP([O-])(=O)OCC[N+](C)(C)C)OC(C)=O	-	759.5778	759.5777	0.1	8.2	0.06	3	-	99.5
PC 34:2 [2]	C42H80NO8P	[H][C@@](COC(C)=O)(COP([O-])(=O)OCC[N+](C)(C)C)OC(C)=O	-	757.5622	757.5638	2.1	7.5	0.05	3	-	99.2
PC 34:3 [2]	C42H78NO8P	[H][C@@](COC([*])=O)(COP([O-])(=O)OCC[N+](C)(C)C)OC([*])=O	-	755.5465	755.5536	9.4	6.9	0.12	3	-	98.1
PC 36:1 [2]	C44H86NO8P	[C@](COC(=O)*)(OC(=O)*)([H])COP(OCC[N+](C)(C)C)(=O)[O-]	-	787.6091	787.6090	0.1	9.3	0.07	3	-	99.5
PC 36:2 [2]	C44H84NO8P	[H][C@@](COC(C)=O)(COP([O-])(=O)OCC[N+](C)(C)C)OC(C)=O	-	785.5935	785.5949	1.8	8.5	0.08	3	-	99.2
PC 36:3 [2]	C44H82NO8P	[H][C@@](COC([*])=O)(COP([O-])(=O)OCC[N+](C)(C)C)OC([*])=O	-	783.5778	783.5794	2.0	7.9	0.18	3	-	99.8
PC 36:4 A [2]	C44H80NO8P	[H][C@@](COC(C)=O)(COP([O-])(=O)OCC[N+](C)(C)C)OC(C)=O	-	781.5622	781.5701	10.1	7.5	0.03	3	-	92.2
PC 36:4 B [2]	C44H80NO8P	[H][C@@](COC(C)=O)(COP([O-])(=O)OCC[N+](C)(C)C)OC(C)=O	-	781.5622	781.5703	10.4	7.3	0.20	3	-	97.3
PC 36:5 [2]	C44H78NO8P	[H][C@@](COC(C)=O)(COP([O-])(=O)OCC[N+](C)(C)C)OC(C)=O	-	779.5465	779.5531	8.5	7.0	0.01	3	-	86.8
PC 38:2 [2]	C46H88NO8P	[C@](COC(=O)*)(OC(=O)*)([H])COP(OCC[N+](C)(C)C)(=O)[O-]	-	813.6248	813.6245	0.4	9.1	-0.26	3	-	99.4
PC 38:3 A [2]	C46H86NO8P	[H][C@@](COC(C)=O)(COP([O-])(=O)OCC[N+](C)(C)C)OC(C)=O	-	811.6091	811.6102	1.4	8.9	0.07	3	-	99.3
PC 38:4 A [2]	C46H84NO8P	[H][C@@](COC([*])=O)(COP([O-])(=O)OCC[N+](C)(C)C)OC([*])=O	-	809.5935	809.5938	0.4	8.3	0.06	3	-	97.3
PC 38:4 B [2]	C46H84NO8P	[H][C@@](COC([*])=O)(COP([O-])(=O)OCC[N+](C)(C)C)OC([*])=O	-	809.5935	809.5970	4.3	8.6	0.06	3	-	89.3
PC 38:5 A [2]	C46H82NO8P	[H][C@@](COC([*])=O)(COP([O-])(=O)OCC[N+](C)(C)C)OC([*])=O	-	807.5778	807.5804	3.2	7.9	0.19	3	-	96.4
PC 38:5 B [2]	C46H82NO8P	[H][C@@](COC([*])=O)(COP([O-])(=O)OCC[N+](C)(C)C)OC([*])=O	-	807.5778	807.5788	1.2	7.6	0.04	3	-	97.9
PC 38:6 B [2]	C46H80NO8P	[H][C@@](COC(C)=O)(COP([O-])(=O)OCC[N+](C)(C)C)OC(C)=O	-	805.5622	805.5695	9.1	7.7	0.36	3	-	87.0
PC 40:5 [2]	C48H86NO8P	[H][C@@](COC([*])=O)(COP([O-])(=O)OCC[N+](C)(C)C)OC([*])=O	-	835.6091	835.6095	0.5	8.7	-0.03	3	-	99.1
PC O-34:2 [2]	C42H82NO7P	[H][C@@](CO[*])(COP([O-])(=O)OCC[N+](C)(C)C)O[*]	-	743.5829	743.5862	4.4	8.8	0.07	3	-	71.1
PC O-34:3 [2]	C42H80NO7P	[H][C@@](CO[*])(COP([O-])(=O)OCC[N+](C)(C)C)O[*]	-	741.5672	741.5706	4.6	8.1	0.06	3	-	76.5
PE 38:4 [2]	C43H78NO8P	[C@@H](COC(=O)*)(COP(OCCN)(=O)O)OC(=O)*	-	767.5465	767.5482	2.2	8.6	0.06	3	-	90.3
PE 36:1 [2]	C41H80NO8P	O(P(=O)(OCCN)O)CC(OC(*)=O)COC(*)=O	-	745.5622	745.5615	0.9	9.3	0.07	3	-	99.7

Annotation	Formula	SMILES	InChI	Monoisotopic molecular weight	Observed mass	Δppm	Observed retention time [min]	Retention time difference [min] [3]	MSI assignment level [4]	Search engine score (MS/MS)	Profinder score (max)
PE 36:2 [2]	C41H78NO8P	O(P(=O)(OCCN)O)CC(OC(*)=O)COC(*)=O	-	743.5465	743.5489	3.2	8.5	0.09	3	-	97.4
PE 36:3 [2]	C41H76NO8P	O(P(=O)(OCCN)O)CC(OC(*)=O)COC(*)=O	-	741.5309	741.5369	8.1	7.8	0.04	3	-	71.4
PE 38:3 [2]	C43H80NO8P	O(P(=O)(OCCN)O)CC(OC(*)=O)COC(*)=O	-	769.5622	769.5667	5.8	8.9	-0.26	3	-	98.9
PE P-36:4 [2]	C41H74NO7P	C(OC[C@H](COP(OCC[NH3+])(=O)[O-])OC(*)=O)=C*	-	723.5203	723.5211	1.1	8.1	0.06	3	-	98.3
PI 34:2 [2]	C43H79O13P	[C@@H]1([C@@H]([C@@H]([C@@H]([C@H]([C@@H]1O)O)O)O)OP(OC[C@@H](COC(*)=O)OC(=O)*)(=O)O)O	-	834.5258	834.5156	12.2	5.7	0.19	3	-	91.5
PI 38:3 [2]	C47H85O13P	[C@@H]1([C@@H]([C@@H]([C@@H]([C@H]([C@@H]1O)O)O)O)OP(OC[C@@H](COC(*)=O)OC(=O)*)(=O)O)O	-	888.5728	888.5723	0.6	6.7	0.28	3	-	99.9
PI 38:4 [2]	C47H83O13P	[C@@H]1([C@@H]([C@@H]([C@@H]([C@H]([C@@H]1O)O)O)O)OP(OC[C@@H](COC(*)=O)OC(=O)*)(=O)O)O	-	886.5571	886.5588	1.9	6.5	0.28	3	-	99.7
PI 36:2 [2]	C45H83O13P	[C@@H]1([C@@H]([C@@H]([C@@H]([C@H]([C@@H]1O)O)O)O)OP(OC[C@@H](COC(*)=O)OC(=O)*)(=O)O)O	-	862.5571	862.5560	1.3	6.5	0.25	3	-	99.9
PS 36:1 [2]	C42H80NO10P	[C@@H](COC(=O)*)(COP(OC[C@@H](C(=O)O)O)N)(=O)O)OC(=O)*	-	789.552	789.5549	3.7	7.0	0.02	3	-	99.3
SM 34:1 [2]	C39H79N2O6P	C[N+](C)(C)CCOP([O-])(=O)OC[C@H](NC([*])=O)[C@H](O)[*]	-	702.5676	702.5675	0.1	7.0	0.05	3	-	99.9
SM 42:1 [2]	C47H95N2O6P	C[N+](C)(C)CCOP([O-])(=O)OC[C@H](NC([*])=O)[C@H](O)[*]	-	814.6928	814.6922	0.7	11.3	0.10	3	-	99.6
SM 42:2 [2]	C47H93N2O6P	C[N+](C)(C)CCOP([O-])(=O)OC[C@H](NC([*])=O)[C@H](O)[*]	-	812.6771	812.6782	1.4	10.2	0.09	3	-	95.3

[1] assigned in the proof of concept experiment

[2] assigned via Batch Targeted Feature Extraction in the protocol assessment experiment

[3] compared to reference standard or to previously assigned metabolites (Leuthold et al. Comprehensive Metabolomic and Lipidomic Profiling of Human Kidney Tissue: A Platform Comparison. J. Proteome Res. 2017, 16, 933–944

[4] Sumner et al. Proposed minimum reporting standards for chemical analysis Chemical Analysis Working Group (CAWG) Metabolomics Standards Initiative (MSI). Metabolomics 2007, 3, 211–221

[5] MassBank of North America

[6] PCDL Manager (Agilent)

[7] Lipid Annotator (Agilent)

[8] CEU Mass Mediator

Cer - ceramide, HexCer - hexosylceramide, PC - phosphatidylcholine, PE - phosphatidylethanolamine, SM - sphingomyelin, PI - phosphatidylinositol, PS - phosphatidylserine

Supplementary Table S6: Search result from the accurate mass batch search (CEU mass mediator) of compounds found with higher abundance in ECM blank samples - HILIC ESI (+) mode

Experimental mass	Identifier	Adduct	mz Error (ppm)	Molecular Weight	Name (proposed annotation by CEU Mass Mediator Batch Search)	Formula	CAS	Kegg	HMDB	LipidMaps	Metlin	PubChem
217.1066	153545	M	1	217.1063	N-Acetyl-L-citrulline	C8H15N3O4		C15532				656979
	165180	M	2	217.1063	N-a-Acetylcitrulline	C8H15N3O4	33965-42-3				5819	
	165181	M	2	217.1063	Gamma-glutamyl-Alanine	C8H15N3O4					86034	
	166735	M	2	217.1063	Ala Gly Ala	C8H15N3O4					16009	
	166736	M	2	217.1063	Ala Ala Gly	C8H15N3O4					17382	
	166737	M	2	217.1063	Gly Ala Ala	C8H15N3O4					18391	
	166738	M	2	217.1063	Gln Ala	C8H15N3O4					23736	
	166739	M	2	217.1063	Ala Gln	C8H15N3O4					23902	
	100400	M	2	217.1063	N-a-Acetylcitrulline	C8H15N3O4			HMDB0000856			11506771
	90074	M	2	217.1063	Alanyl-Glutamine	C8H15N3O4			HMDB0028685		85601	542027
	59638	M	2	217.1063	Alanyl-Gamma-glutamate	C8H15N3O4			HMDB0028701		85616	131750731
	147138	M	2	217.1063	Glutaminylalanine	C8H15N3O4			HMDB0028790		85704	9813211
	52438	M	5	217.1076	5-Hydroxysebacate	C10H17O5			HMDB0029189			131750806
136.0385	125526	M	0	136.0385	Allopurinol	C5H4N4O	315-30-0		HMDB0014581		865	2094
	144883	M	0	136.0385	Hypoxanthine	C5H4N4O	68-94-0	C00262	HMDB0000157		83	790
	138754	M	3	136.038	Ethyl isopropyl disulfide	C5H12S2			HMDB0033054		88946	521477
	129402	M	3	136.038	Ethyl propyl disulfide	C5H12S2	30453-31-7		HMDB0033053		88945	35349
	114082	M	3	136.038	1-Pentanesulfenothioic acid	C5H12S2			HMDB0031160		87453	21251947
	64474	M	10	136.0372	L-threonic Acid	C4H8O5	7306-96-9	C01620	HMDB0062620		4244	439535
	116699	M	10	136.0372	Threonic acid	C4H8O5	3909-12-4	C21649	HMDB0000943			151152
	139249	M	10	136.0372	Erythronic acid	C4H8O5	13752-84-6	C21593	HMDB0000613			2781043
	164061	M	10	136.0372	D-threonic acid	C4H8O5					35473	
	164062	M	10	136.0372	DL-erythronic acid	C4H8O5					35474	
	164063	M	10	136.0372	Erythronic acid	C4H8O5					45855	
	164064	M	10	136.0372	Threonic acid	C4H8O5					45859	
71.0736	152914	M	1	71.0735	3-Buten-1-amine	C4H9N		C12244			69390	443732
	88541	M	1	71.0735	Pyrrolidine	C4H9N	123-75-1		HMDB0031641		87832	31268
169.0741	144951	M	1	169.0739	5-Hydroxydopamine	C8H11NO3	1927-04-4		HMDB0004817		7081	114772
	126522	M	1	169.0739	6-Hydroxydopamine	C8H11NO3	1199-18-4		HMDB0001537		6307	4624
	98883	M	1	169.0739	6-Acetyl-2,3-dihydro-2-(hydroxymethyl)-4(1H)-pyridinone	C8H11NO3			HMDB0035178		90505	15847402
	54635	M	1	169.0739	Pyridoxine	C8H11NO3	65-23-6	C00314	HMDB0000239		2202	1054
	123784	M	1	169.0739	L- Norepinephrine	C8H11NO3	51-41-2	C00547	HMDB0000216		63	439260
	50599	M	1	169.0739	xi-Norepinephrine	C8H11NO3			HMDB0037685			951
334.0991	181291	M	1	334.0987	Penicillin	C16H18N2O4S						2349
	72548	M	1	334.0987	Penicillin G	C16H18N2O4S	61-33-6	C05551	HMDB0015186		1735	5904
	155945	M	2	334.0985	Triphenyltetrazolium chloride; 2,3,5-Triphenyltetrazolium chloride	C19H15N4.Cl	298-96-4	C11305			68976	9283
	150023	M	4	334.1006	Aramite	C15H23ClO4S	140-57-8	C19019			72770	8809
	130126	M	6	334.1012	(S)-a-Amino-2,5-dihydro-5-oxo-4-isoxazolepropanoic acid N2-glucoside	C12H18N2O9			HMDB0029404		86247	131750866
495.3326	2628	M	0	495.3325	PC(O-14:0/2:0)	C24H50NO7P				LMGP01020019	40048	
	2981	M	0	495.3325	PC(16:0/0:0)[rac]	C24H50NO7P				LMGP01050113	102768	
	4290	M	0	495.3325	PE(19:0/0:0)	C24H50NO7P				LMGP02050028	77694	
	2969	M	0	495.3325	PC(0:0/16:0)	C24H50NO7P			HMDB0240262	LMGP01050074	40340	
	163400	M	0	495.3325	PC(O-14:0/2:0)[U]	C24H50NO7P					40049	
	163401	M	0	495.3325	PC(16:0/0:0)[S]	C24H50NO7P					40285	
	163402	M	0	495.3325	PC(16:0/0:0)[U]	C24H50NO7P					40286	
	163403	M	0	495.3325	PC(0:0/16:0)[U]	C24H50NO7P					40341	
	2940	M	0	495.3325	PC(16:0/0:0)	C24H50NO7P			HMDB0010382	LMGP01050018	40284	460602
523.3644	4288	M	1	523.3638	PE(21:0/0:0)	C26H54NO7P				LMGP02050026	77692	
	164538	M	1	523.3638	PC(2:0/O-16:0)[U]	C26H54NO7P					40161	
	2641	M	1	523.3638	PC(O-16:0/2:0)	C26H54NO7P			HMDB0062195	LMGP01020046	40075	108156
	163439	M	1	523.3638	PC(O-16:0/2:0)[S]	C26H54NO7P					40076	
	163440	M	1	523.3638	PC(O-16:0/2:0)[U]	C26H54NO7P					40077	
	163441	M	1	523.3638	PC(18:0/0:0)[S]	C26H54NO7P					40293	
	163442	M	1	523.3638	PC(18:0/0:0)[U]	C26H54NO7P					40294	
	163443	M	1	523.3638	PC(0:0/18:0)[S]	C26H54NO7P					40343	

Experimental mass	Identifier	Adduct	mz Error (ppm)	Molecular Weight	Name (proposed annotation by CEU Mass Mediator Batch Search)	Formula	CAS	Kegg	HMDB	LipidMaps	Metlin	PubChem
	163444	M	1	523.3638	PC(0:0/18:0)[U]	C26H54NO7P					40344	
	2944	M	1	523.3638	PC(18:0/0:0)	C26H54NO7P			HMDB0010384	LMGP01050026	40292	497299
	2970	M	1	523.3638	PC(0:0/18:0)	C26H54NO7P			HMDB0011128	LMGP01050076	40342	24779491
	163438	M	1	523.3638	enantio-PAF C-16	C26H54NO7P	117985-57-6				43413	
	165818	M	1	523.3638	PAF C-16	C26H54NO7P	74389-68-7				34488	
56.0626	0	M	0	0	No compounds found for experimental mass 56.0626 and adduct: M							
451.1232	0	M	0	0	No compounds found for experimental mass 451.1232 and adduct: M							
626.158	0	M	0	0	No compounds found for experimental mass 626.158 and adduct: M							
521.3485	2688	M	1	521.3481	PC(O-16:1(11Z)/2:0)	C26H52NO7P				LMGP01020147	40008	
	2945	M	1	521.3481	PC(18:1(6Z)/0:0)	C26H52NO7P				LMGP01050029	40295	
	2946	M	1	521.3481	PC(18:1(9E)/0:0)	C26H52NO7P				LMGP01050030	40296	
	2971	M	1	521.3481	PC(0:0/18:1(6Z))	C26H52NO7P				LMGP01050079	40345	
	2972	M	1	521.3481	PC(0:0/18:1(9E))	C26H52NO7P				LMGP01050080	40346	
	2982	M	1	521.3481	PC(18:1(9Z)/0:0)[rac]	C26H52NO7P				LMGP01050114	102769	
	2798	M	1	521.3481	PC(P-16:0/2:0)	C26H52NO7P				LMGP01030009	40174	
	2973	M	1	521.3481	PC(0:0/18:1(9Z))	C26H52NO7P			HMDB0062651	LMGP01050082	40348	24779494
	163432	M	1	521.3481	PC(18:1(9)/0:0)[U]	C26H52NO7P					40297	
	163433	M	1	521.3481	PC(0:0/18:1(9E))[U]	C26H52NO7P					40347	
	163434	M	1	521.3481	PC(0:0/18:1(9Z))[U]	C26H52NO7P					40349	
	163435	M	1	521.3481	PC(18:1(9E)/0:0)[U]	C26H52NO7P					46689	
	2947	M	1	521.3481	PC(18:1(9Z)/0:0)	C26H52NO7P	3542-29-8		HMDB0002815	LMGP01050032	184	16081932
	2997	M	1	521.3481	LysoPC(18:1(11Z))	C26H52NO7P			HMDB0010385	LMGP01050138	61695	53480465
	163430	M	1	521.3481	PC(O-16:1(9E)/2:0)[U]	C26H52NO7P					40009	
	163431	M	1	521.3481	PC(O-16:1(9Z)/2:0)[U]	C26H52NO7P					40010	
313.0803	0	M	0	0	No compounds found for experimental mass 313.0803 and adduct: M							
164.0475	26318	M	1	164.0473	9-hydroxy-7E-Nonene-3,5-diynoic acid	C9H8O3				LMFA01030721	74318	
	26319	M	1	164.0473	9-hydroxy-7Z-Nonene-3,5-diynoic acid	C9H8O3				LMFA01030722	74319	
	140824	M	1	164.0473	Coumaric acid	C9H8O3	495-79-4	C05838	HMDB0041592		64161	5280841
	54336	M	1	164.0473	cis-p-Coumaric acid	C9H8O3	4501-31-9	C06738	HMDB0030677		87135	1549106
	63571	M	1	164.0473	Enol-phenylpyruvate	C9H8O3		C02763	HMDB0012225		6098	641637
	139373	M	1	164.0473	m-Coumaric acid	C9H8O3	14755-02-3	C12621	HMDB0001713		305	637541
	115347	M	1	164.0473	4-Hydroxycinnamic acid	C9H8O3	7400-08-0	C00811	HMDB0002035		6450	637542
	102319	M	1	164.0473	2-Hydroxycinnamic acid	C9H8O3	614-60-8	C01772	HMDB0002641		306	637540
	142288	M	1	164.0473	Phenylpyruvic acid	C9H8O3	156-06-9	C00166	HMDB0000205		328	997
	104974	M	1	164.0473	3-(4-hydroxyphenyl)prop-2-enoic acid	C9H8O3			HMDB0128076			322
	117263	M	1	164.0473	3-(2,5-dihydroxyphenyl)prop-2-enal	C9H8O3			HMDB0134030			85638857
	99357	M	1	164.0473	3-(2-hydroxyphenyl)prop-2-enoic acid	C9H8O3			HMDB0134028			11968
	148007	M	1	164.0473	Methyl Phenylglyoxalate	C9H8O3	15206-55-0		HMDB0062605			84835
	67885	M	1	164.0473	3-(4-hydroxyphenyl)oxirane-2-carbaldehyde	C9H8O3			HMDB0141768			131839525
	93746	M	1	164.0473	3-(2-hydroxyphenyl)oxirane-2-carbaldehyde	C9H8O3			HMDB0134031			131837795
	86072	M	1	164.0473	3-(2,3-dihydroxyphenyl)prop-2-enal	C9H8O3			HMDB0134029			
	102232	M	1	164.0473	3-(3-hydroxyphenyl)prop-2-enoic acid	C9H8O3			HMDB0125104			11496
	86878	M	1	164.0473	3-phenyloxirane-2-carboxylic acid	C9H8O3			HMDB0126545			415606
	83614	M	1	164.0473	(2E)-3-(3,4-dihydroxyphenyl)prop-2-enal	C9H8O3		C10945	HMDB0141767		64169	5281871
	79776	M	1	164.0473	4-methoxy-1-benzofuran-6-ol	C9H8O3			HMDB0129375			45122636
	156571	M	1	164.0473	3-Oxo-3-phenylpropanoate; Benzoylacetate; 3-Oxo-3-phenylpropionate; 3-Oxo-3-phenylpropionic acid	C9H8O3	614-20-0	C07114			66592	97045
	165104	M	1	164.0473	p-Coumaric acid	C9H8O3	501-98-4				307	
58.0537	0	M	0	0	No compounds found for experimental mass 58.0537 and adduct: M							
129.0421	152200	M	4	129.0426	4-Oxoproline; 4-Oxo-L-proline	C5H7NO3	4347-18-6	C01877			63471	107541
	165047	M	4	129.0426	L-1-Pyrroline-3-hydroxy-5-carboxylate	C5H7NO3					63470	
	61033	M	4	129.0426	(3R,5S)-1-pyrroline-3-hydroxy-5-carboxylic Acid	C5H7NO3		C04281	HMDB0062585			11966267
	100107	M	4	129.0426	Pyrroline hydroxycarboxylic acid	C5H7NO3	22573-88-2		HMDB0001369		284	1059
	71983	M	4	129.0426	Pyrrolidonecarboxylic acid	C5H7NO3	4042-36-8		HMDB0000805		63632	499
	104759	M	4	129.0426	L-Pyroglutamic acid	C5H7NO3	98-79-3	C01879	HMDB0000267		3251	7405

Experimental mass	Identifier	Adduct	mz Error (ppm)	Molecular Weight	Name (proposed annotation by CEU Mass Mediator Batch Search)	Formula	CAS	Kegg	HMDB	LipidMaps	Metlin	PubChem
	101779	M	4	129.0426	1-Pyrroline-4-hydroxy-2-carboxylate	C5H7NO3		C04282	HMDB0002234		63483	440282
	83387	M	4	129.0426	N-Acryloylglycine	C5H7NO3	24599-25-5		HMDB0001843		6343	100321
	117215	M	4	129.0426	dimethadione	C5H7NO3			HMDB0061093			3081
	158656	M	4	129.0426	5-Oxo-D-proline; D-Pyroglutamic acid; D-5-Pyrrolidone-2-carboxylic acid	C5H7NO3		C02237				439685
183.0533	154629	M	1	183.0532	3-Carboxy-4-methoxy-N-methyl-2-pyridone	C8H9NO4		C04447			66184	440344
	165138	M	1	183.0532	Methyl(2-furoylamino)acetic acid	C8H9NO4					5824	
	160537	M	1	183.0532	3-Hydroxy-4-hydroxymethyl-2-methylpyridine-5-carboxylate; 5-Pyridoxate; 5-Pyridoxic acid	C8H9NO4		C04773			63862	440474
	152612	M	1	183.0532	5-Methoxy-3-hydroxyanthranilate; 5-Methoxy-3-hydroxyanthranilic acid	C8H9NO4		C11466			69051	443219
	161324	M	1	183.0532	3,5-Dihydroxy-phenylglycine; L-3,5-Dihydroxyphenylglycine; (S)-3,5-Dihydroxyphenylglycine	C8H9NO4	146255-66-5	C12026			63854	443586
	88910	M	1	183.0532	4-Pyridoxic acid	C8H9NO4	82-82-6	C00847	HMDB0000017		239	6723
596.1869	0	M	0	0	No compounds found for experimental mass 596.1869 and adduct: M							
519.3326	2948	M	0	519.3325	PC(18:2(2E,4E)/0:0)	C26H50NO7P				LMGP01050034	40300	
	100664	M	0	519.3325	2-linoleoyl-sn-glycero-3-phosphocholine	C26H50NO7P			HMDB0062711			
	163429	M	0	519.3325	PC(18:2(9Z,12Z)/0:0)[U]	C26H50NO7P					40302	
	2949	M	0	519.3325	PC(18:2(9Z,12Z)/0:0)	C26H50NO7P			HMDB0010386	LMGP01050035	40301	11005824
844.1646	0	M	0	0	No compounds found for experimental mass 844.1646 and adduct: M							
143.0734	96023	M	1	143.0735	2-Aminonaphthalene	C10H9N	91-59-8	C02227	HMDB0041802		65732	7057
	62287	M	1	143.0735	6-Methylquinoline	C10H9N	91-62-3		HMDB0033115		89006	7059
	114141	M	1	143.0735	Quinaldine	C10H9N	91-63-4		HMDB0042004		96204	7060
	151415	M	1	143.0735	1-Naphthylamine	C10H9N	134-32-7	C14790			70324	8640
260.0633	0	M	0	0	No compounds found for experimental mass 260.0633 and adduct: M							
207.0388	119408	M	2	207.0392	2-Amino-4-hydroxy-6-pteridinecarboxylic acid	C7H5N5O3	948-60-7		HMDB0033136		44527	70361
111.069	89357	M	5	111.0684	4-Ethyl-2-methyloxazole	C6H9NO			HMDB0037838		92646	525785
	80407	M	5	111.0684	N-Acetyl-2,3-dihydro-1H-pyrrole	C6H9NO			HMDB0031163		87456	10909522
	104485	M	5	111.0684	2-Ethyl-4-methyloxazole	C6H9NO			HMDB0037837		92645	528405
	138358	M	5	111.0684	5-Imino-2-methyl-1-cyclopenten-1-ol	C6H9NO			HMDB0039584		94143	12311489
	138388	M	5	111.0684	5-Ethyl-2-methyloxazole	C6H9NO			HMDB0037859		92665	528407
	135838	M	5	111.0684	2-Ethyl-5-methyloxazole	C6H9NO			HMDB0037858		92664	528403
	119717	M	5	111.0684	Trimethyloxazole	C6H9NO	20662-84-4		HMDB0040148		94688	30215
	149691	M	5	111.0684	5-Acetyl-3,4-dihydro-2H-pyrrole	C6H9NO			HMDB0031308		87573	522834
	99015	M	5	111.0684	5-Ethyl-4-methyloxazole	C6H9NO	29584-92-7		HMDB0037863		92669	207286
	150432	M	5	111.0684	N-Vinyl-2-pyrrolidone; 1-Ethenyl-2-pyrrolidinone	C6H9NO	88-12-0	C19548			73224	6917
275.1372	130890	M	1	275.1369	Glutarylcarnitine	C12H21NO6			HMDB0013130			71317118
	32662	M	1	275.1369	Glutarylcarnitine	C12H21NO6				LMFA07070066		
	32687	M	1	275.1369	O-glutarylcarnitine	C12H21NO6				LMFA07070091		
495.3327	2628	M	0	495.3325	PC(O-14:0/2:0)	C24H50NO7P				LMGP01020019	40048	
	2981	M	0	495.3325	PC(16:0/0:0)[rac]	C24H50NO7P				LMGP01050113	102768	
	4290	M	0	495.3325	PE(19:0/0:0)	C24H50NO7P				LMGP02050028	77694	
	2969	M	0	495.3325	PC(0:0/16:0)	C24H50NO7P			HMDB0240262	LMGP01050074	40340	
	163400	M	0	495.3325	PC(O-14:0/2:0)[U]	C24H50NO7P					40049	
	163401	M	0	495.3325	PC(16:0/0:0)[S]	C24H50NO7P					40285	
	163402	M	0	495.3325	PC(16:0/0:0)[U]	C24H50NO7P					40286	
	163403	M	0	495.3325	PC(0:0/16:0)[U]	C24H50NO7P					40341	
	2940	M	0	495.3325	PC(16:0/0:0)	C24H50NO7P			HMDB0010382	LMGP01050018	40284	460602
194.0726	132117	M	3	194.0732	2-Hydroxyphenanthrene	C14H10O			HMDB0059798			69061
	122511	M	3	194.0732	9-Hydroxyphenanthrene	C14H10O		C11430	HMDB0059801		69034	10229
	108757	M	3	194.0732	3-Hydroxyphenanthrene	C14H10O			HMDB0059799			95724
	137463	M	3	194.0732	4-Hydroxyphenanthrene	C14H10O			HMDB0059800			82105
	91133	M	3	194.0732	1-Hydroxyphenanthrene	C14H10O		C11432	HMDB0059797		69036	98490
	150038	M	3	194.0732	Phenanthrene-9,10-oxide	C14H10O	585-08-0	C11429			69033	443196

Experimental mass	Identifier	Adduct	mz Error (ppm)	Molecular Weight	Name (proposed annotation by CEU Mass Mediator Batch Search)	Formula	CAS	Kegg	HMDB	LipidMaps	Metlin	PubChem
	152537	M	3	194.0732	Phenanthrene-1,2-oxide	C14H10O		C11431			69035	443197
480.3945	0	M	0	0	No compounds found for experimental mass 480.3945 and adduct: M							
334.0987	72548	M	0	334.0987	Penicillin G	C16H18N2O4S	61-33-6	C05551	HMDB0015186		1735	5904
	181291	M	0	334.0987	Penicillin	C16H18N2O4S						2349
	155945	M	1	334.0985	Triphenyltetrazolium chloride; 2,3,5-Triphenyltetrazolium chloride	C19H15N4.Cl	298-96-4	C11305			68976	9283
	150023	M	6	334.1006	Aramite	C15H23ClO4S	140-57-8	C19019			72770	8809
	130126	M	8	334.1012	(S)-a-Amino-2,5-dihydro-5-oxo-4-isoxazolepropanoic acid N2-glucoside	C12H18N2O9			HMDB0029404		86247	131750866
	170801	M	10	334.0954	RG-108	C19H14N2O4	48208-26-0				64811	
204.0568	0	M	0	0	No compounds found for experimental mass 204.0568 and adduct: M							
173.9941	0	M	0	0	No compounds found for experimental mass 173.9941 and adduct: M							
223.067	0	M	0	0	No compounds found for experimental mass 223.067 and adduct: M							
470.1374	16428	M	2	470.1366	Didymocalyxin B	C28H22O7				LMPK12120331	52134	
	114477	M	2	470.1366	5-{5-[(E)-2-(3,5-dihydroxyphenyl)ethenyl]-2-(4-hydroxyphenyl)-2,3-dihydro-1-benzofuran-3-yl}benzene-1,2,3-triol	C28H22O7			HMDB0135812			131839307
	126009	M	2	470.1366	3-(3,5-dihydroxyphenyl)-2-(4-hydroxyphenyl)-4-[(E)-2-(4-hydroxyphenyl)ethenyl]-2,3-dihydro-1-benzofuran-5,6-diol	C28H22O7			HMDB0129148			131835431
	130362	M	2	470.1366	5-[(E)-2-[3-(3,5-dihydroxyphenyl)-2-(4-hydroxyphenyl)-2,3-dihydro-1-benzofuran-5-yl]ethenyl]benzene-1,2,3-triol	C28H22O7			HMDB0135813			131839308
	43067	M	2	470.1366	5-[6-hydroxy-2-(4-hydroxyphenyl)-4-[3-(4-hydroxyphenyl)oxiran-2-yl]-2,3-dihydro-1-benzofuran-3-yl]benzene-1,3-diol	C28H22O7			HMDB0129149			131835432
	58209	M	2	470.1366	6-[(E)-2-[3-(3,5-dihydroxyphenyl)-2-(4-hydroxyphenyl)-2,3-dihydro-1-benzofuran-5-yl]ethenyl]benzene-1,2,4-triol	C28H22O7			HMDB0135810			131839305
	121461	M	2	470.1366	4-[3-(3,5-dihydroxyphenyl)-5-[(E)-2-(3,5-dihydroxyphenyl)ethenyl]-2,3-dihydro-1-benzofuran-2-yl]benzene-1,2-diol	C28H22O7			HMDB0135811			131839306
	108667	M	2	470.1366	5-[4-[(E)-2-(3,4-dihydroxyphenyl)ethenyl]-6-hydroxy-2-(4-hydroxyphenyl)-2,3-dihydro-1-benzofuran-3-yl]benzene-1,3-diol	C28H22O7			HMDB0129152			131835434
	96645	M	2	470.1366	5-[6-hydroxy-2-(4-hydroxyphenyl)-4-[(E)-2-(4-hydroxyphenyl)ethenyl]-2,3-dihydro-1-benzofuran-3-yl]benzene-1,2,3-triol	C28H22O7			HMDB0129154			131835436
	72838	M	2	470.1366	5-[4-[(E)-2-(2,4-dihydroxyphenyl)ethenyl]-6-hydroxy-2-(4-hydroxyphenyl)-2,3-dihydro-1-benzofuran-3-yl]benzene-1,3-diol	C28H22O7			HMDB0129153			131835435
	115870	M	2	470.1366	5-[5-[3-(3,5-dihydroxyphenyl)oxiran-2-yl]-2-(4-hydroxyphenyl)-2,3-dihydro-1-benzofuran-3-yl]benzene-1,3-diol	C28H22O7			HMDB0135806			131839302
	103362	M	2	470.1366	5-[5-[(E)-2-(3,5-dihydroxyphenyl)ethenyl]-4-hydroxy-2-(4-hydroxyphenyl)-2,3-dihydro-1-benzofuran-3-yl]benzene-1,3-diol	C28H22O7			HMDB0135808			131839304
	52429	M	2	470.1366	5-[5-[(E)-2-(3,5-dihydroxyphenyl)ethenyl]-7-hydroxy-2-(4-hydroxyphenyl)-2,3-dihydro-1-benzofuran-3-yl]benzene-1,3-diol	C28H22O7			HMDB0135807			131839303
	69328	M	2	470.1366	6-[6-hydroxy-2-(4-hydroxyphenyl)-4-[2-(4-hydroxyphenyl)ethenyl]-2,3-dihydro-1-benzofuran-3-yl]benzene-1,2,4-triol	C28H22O7			HMDB0129150			131835433
	87787	M	2	470.1366	5-[5-[(E)-2-(3,5-dihydroxyphenyl)ethenyl]-6-hydroxy-2-(4-hydroxyphenyl)-2,3-dihydro-1-benzofuran-3-yl]benzene-1,3-diol	C28H22O7			HMDB0135805			131839301
	122860	M	2	470.1366	4-[3-(3,5-dihydroxyphenyl)-6-hydroxy-4-[(E)-2-(4-hydroxyphenyl)ethenyl]-2,3-dihydro-1-benzofuran-2-yl]benzene-1,2-diol	C28H22O7			HMDB0129151			5458896
223.0671	0	M	0	0	No compounds found for experimental mass 223.0671 and adduct: M							
187.0499	150427	M	10	187.0481	(2S,4S)-4-Hydroxy-2,3,4,5-tetrahydrodipicolinate; (2S,4S)-4-Hydroxy-2,3,4,5-tetrahydropyridine-2,6-dicarboxylate; HTPA	C7H9NO5		C20258				
	66773	M	10	187.0481	1-(Malonylamino)cyclopropanecarboxylic acid	C7H9NO5	80550-27-2		HMDB0031700		87876	133503
	152693	M	10	187.0481	2-(Acetamidomethylene)succinate	C7H9NO5		C01215			63871	5280408
83.0374	0	M	0	0	No compounds found for experimental mass 83.0374 and adduct: M							
262.0782	167541	M	7	262.0801	Asp Glu	C9H14N2O7					23953	
	167542	M	7	262.0801	Glu Asp	C9H14N2O7					23962	
	165259	M	7	262.0801	Aspartyl-Glutamate	C9H14N2O7					85667	
	93285	M	7	262.0801	Glutamylaspartic acid	C9H14N2O7	3918-84-1		HMDB0028815		85729	99716
	69458	M	7	262.0801	L-beta-aspartyl-L-glutamic acid	C9H14N2O7			HMDB0011164		62013	25207301
	73966	M	7	262.0801	gamma-Glutamylaspartic acid	C9H14N2O7	16804-55-0		HMDB0030419		86960	161197
239.0885	0	M	0	0	No compounds found for experimental mass 239.0885 and adduct: M							
326.1967	103553	M	8	326.1941	Heptaethylene glycol	C14H30O8	5617-32-3		HMDB0061835			79718

Experimental mass	Identifier	Adduct	mz Error (ppm)	Molecular Weight	Name (proposed annotation by CEU Mass Mediator Batch Search)	Formula	CAS	Kegg	HMDB	LipidMaps	Metlin	PubChem
	156418	M	8	326.1994	Isoajmaline	C20H26N2O2		C09217				6325415
	161590	M	8	326.1994	Ajmaline	C20H26N2O2		C06542				44891335
	67989	M	8	326.1994	Ajmaline	C20H26N2O2	4360-12-7		HMDB0015495		3456	441080
	170257	M	8	326.1994	Hydroquinine	C20H26N2O2	522-66-7				2235	
	152224	M	8	326.1994	Hydroquinidine	C20H26N2O2	1435-55-8	C10696			2221	442912
	162505	M	8	326.1994	(-)-Tortuosamine; Tortuosamine	C20H26N2O2		C12260			69402	443745
278.057	12868	M	3	278.0579	Pongaglabol	C17H10O4				LMPK12110162	48595	
	16734	M	3	278.0579	4-Hydroxyfurano[2",3":6,7]aurone	C17H10O4				LMPK12130024	52439	
	12491	M	3	278.0579	Neorauteen	C17H10O4				LMPK12070144	48232	
255.0622	0	M	0	0	No compounds found for experimental mass 255.0622 and adduct: M							
208.0948	79774	M	1	208.0947	Ethyl beta-D-glucopyranoside	C8H16O6	3198-49-0		HMDB0029968		86625	428040
	75752	M	1	208.0947	Dambonitol	C8H16O6			HMDB0033942		89632	
	166643	M	6	208.096	8-methylcaffeine	C9H12N4O2	832-66-6				84980	
202.0454	0	M	0	0	No compounds found for experimental mass 202.0454 and adduct: M							
509.3481	165812	M	0	509.3481	1-heptadecanoyl-sn-glycero-3-phosphocholine	C25H52NO7P	50930-23-9				24068	
	163415	M	0	509.3481	PC(O-15:0/2:0)[U]	C25H52NO7P					40054	
	163416	M	0	509.3481	PC(16:0/O-1:0)[U]	C25H52NO7P					40158	
	163417	M	0	509.3481	PC(17:0/0:0)[U]	C25H52NO7P					40291	
	163418	M	0	509.3481	PC(16:0/O-1:0)	C25H52NO7P					76587	
	2943	M	0	509.3481	PC(17:0/0:0)	C25H52NO7P			HMDB0012108	LMGP01050024	40290	24779463
	4274	M	0	509.3481	PE(20:0/0:0)	C25H52NO7P			HMDB0011511	LMGP02050012	62296	52925131
	4307	M	0	509.3481	LysoPE(0:0/20:0)	C25H52NO7P			HMDB0011481	LMGP02050045	62269	53480930
	2618	M	0	509.3481	PC(O-1:0/16:0)	C25H52NO7P				LMGP01020004	40033	
	2631	M	0	509.3481	PC(O-15:0/2:0)	C25H52NO7P				LMGP01020024	40053	
	2633	M	0	509.3481	PC(O-16:0/1:0)	C25H52NO7P				LMGP01020028	40057	
145.1104	166013	M	1	145.1103	L-Alanine n-butyl ester	C7H15NO2	2885-02-1				3541	
	166014	M	1	145.1103	2R-aminoheptanoic acid	C7H15NO2					35932	
	166015	M	1	145.1103	2S-aminoheptanoic acid	C7H15NO2					35933	
	166016	M	1	145.1103	2-amino-heptanoic acid	C7H15NO2					35934	
	166017	M	1	145.1103	N2-methyl-L-isoleucine	C7H15NO2	5125-98-8				44542	
	166018	M	1	145.1103	N,N-dimethyl-L-Valine	C7H15NO2	2812-32-0				44985	
	165074	M	1	145.1103	1-nitroheptane	C7H15NO2	693-39-0				85267	
	27387	M	1	145.1103	2R-aminoheptanoic acid	C7H15NO2				LMFA01100013	74866	
	27388	M	1	145.1103	2S-aminoheptanoic acid	C7H15NO2				LMFA01100014	74867	
	107749	M	1	145.1103	3-Dehydroxycarnitine	C7H15NO2			HMDB0006831			725
	27389	M	1	145.1103	2-Aminoheptanoic acid	C7H15NO2	1115-90-8		HMDB0094649	LMFA01100015	74868	227939
	165743	M	1	145.1103	3-Carboxypropyl trimethylammonium	C7H15NO2	6249-56-5				34501	
538.1112	151462	M	0	538.1111	Lithospermic acid	C27H22O12	28831-65-4	C08745			67165	5281302
	106641	M	0	538.1111	Isomelitric acid A	C27H22O12			HMDB0039523		94090	21582559
	60860	M	0	538.1111	Melitric acid A	C27H22O12			HMDB0040681		95156	10459878
431.1936	158094	M	2	431.1944	Fusarin C	C23H29NO7		C19243				6435894
	122621	M	2	431.1944	Fusarin C	C23H29NO7	79748-81-5		HMDB0033337		72964	131751413
	153268	M	5	431.1913	3beta-Chloro-N,N-bis(2-chloroethyl)-androst-5-en-17beta-amine	C23H36Cl3N		C14914			70416	11954081
	151937	M	9	431.1897	Glenvastatin; HR 780	C27H26FNO3	122254-45-9	C11699			69164	5281970
189.0815	73879	M	3	189.0821	Propanoic acid, 2-(methoxyimino)-, trimethylsilyl ester	C7H15NO3Si			HMDB0094703			9601891
	58000	M	4	189.0823	S-Prenyl-L-cysteine	C8H15NO2S	5287-46-7		HMDB0012286		62914	5121218
	165145	M	4	189.0823	Prenyl-L-cysteine	C8H15NO2S					66519	
333.0818	181046	M	9	333.0849	Fumimycin	C16H15NO7						50907655
324.0524	0	M	0	0	No compounds found for experimental mass 324.0524 and adduct: M							
844.1662	0	M	0	0	No compounds found for experimental mass 844.1662 and adduct: M							
572.1973	0	M	0	0	No compounds found for experimental mass 572.1973 and adduct: M							
260.0642	0	M	0	0	No compounds found for experimental mass 260.0642 and adduct: M							
465.3221	115446	M	0	465.3222	TetraHCA	C27H45O6			HMDB0062534			56927964
	3022	M	0	465.3219	PC(P-15:0/0:0)	C23H48NO6P				LMGP01070003	40399	
	4340	M	0	465.3219	PE(O-18:1(9Z)/0:0)	C23H48NO6P				LMGP02060004	46718	
	4345	M	0	465.3219	PE(P-18:0/0:0)	C23H48NO6P				LMGP02070002	46720	

Experimental mass	Identifier	Adduct	mz Error (ppm)	Molecular Weight	Name (proposed annotation by CEU Mass Mediator Batch Search)	Formula	CAS	Kegg	HMDB	LipidMaps	Metlin	PubChem
209.0514	166647	M	2	209.0511	(2R,4R)-2-phenylthiazolidine-4-carboxylic acid	C10H11NO2S					65469	
573.3089	5517	M	4	573.3067	PS(22:4(7Z,10Z,13Z,16Z)/0:0)	C28H48NO9P				LMGP03050014	78841	
330.1008	0	M	0	0	No compounds found for experimental mass 330.1008 and adduct: M							
252.1152	159588	M	1	252.115	cis-Hinokiresinol	C17H16O2	17676-24-3	C10628			68443	5281830
	157890	M	1	252.115	p-(3,4-Dihydro-6-methoxy-2-naphthyl)phenol	C17H16O2		C14897			70400	252381
	128014	M	1	252.115	(1Z,4Z)-1,5-bis(4-hydroxyphenyl)-1,4-pentadiene	C17H16O2			HMDB0033317		89171	131751408
	148758	M	1	252.115	2-Phenylethyl 3-phenyl-2-propenoate	C17H16O2	103-53-7		HMDB0035018		90378	5369459
	125873	M	1	252.115	Cinnamyl phenylacetate	C17H16O2	7492-65-1		HMDB0037707		92530	92468421
	43799	M	2	252.1157	Cimetidine	C10H16N6S	51481-61-9	C06952	HMDB0014644		1755	2756
396.0726	131713	M	8	396.0693	3,4,5-trihydroxy-6-{[2-(4-methoxy-1-benzofuran-5-yl)-2-oxoacetyl]oxy}oxane-2-carboxylic acid	C17H16O11			HMDB0129407			131835657
571.2274	0	M	0	0	No compounds found for experimental mass 571.2274 and adduct: M							
786.6584	34349	M	4	786.6615	SM(d18:1/22:0)	C45H91N2O6P			HMDB0012103	LMSP03010006	41589	44260125
	64250	M	4	786.6615	SM(d18:0/22:1(13Z))	C45H91N2O6P			HMDB0012092			53481362
	34404	M	4	786.6615	SM(d16:1/24:0)	C45H91N2O6P				LMSP03010073	83773	
376.0379	0	M	0	0	No compounds found for experimental mass 376.0379 and adduct: M							
540.1083	74006	M	6	540.1115	6-[2-[3-(3,4-dihydroxy-5-methoxyphenyl)-2-oxopropanoyl]-3,5-dihydroxy-6-methoxyphenoxy}-3,4,5-trihydroxyoxane-2-carboxylic acid	C23H24O15			HMDB0128843			131835140
	129305	M	6	540.1115	6-{[3,7-dihydroxy-2-(1-hydroxy-3-methoxy-4-oxocyclohex-2-en-1-yl)-6-methoxy-4-oxo-4H-chromen-5-yl]oxy}-3,4,5-trihydroxyoxane-2-carboxylic acid	C23H24O15			HMDB0128856			131835153
	149795	M	6	540.1115	6-{[3,5-dihydroxy-2-(1-hydroxy-5-methoxy-4-oxocyclohex-2-en-1-yl)-6-methoxy-4-oxo-4H-chromen-7-yl]oxy}-3,4,5-trihydroxyoxane-2-carboxylic acid	C23H24O15			HMDB0128854			131835151
	88908	M	6	540.1115	6-{[3,5-dihydroxy-2-(1-hydroxy-3-methoxy-4-oxocyclohex-2-en-1-yl)-6-methoxy-4-oxo-4H-chromen-7-yl]oxy}-3,4,5-trihydroxyoxane-2-carboxylic acid	C23H24O15			HMDB0128857			131835154
	98400	M	6	540.1115	6-{4-[2,3-dioxo-3-(2,4,6-trihydroxy-3-methoxyphenyl)propyl]-2-hydroxy-6-methoxyphenoxy}-3,4,5-trihydroxyoxane-2-carboxylic acid	C23H24O15			HMDB0128846			131835143
	85622	M	6	540.1115	6-{[5,7-dihydroxy-2-(1-hydroxy-3-methoxy-4-oxocyclohex-2-en-1-yl)-6-methoxy-4-oxo-4H-chromen-3-yl]oxy}-3,4,5-trihydroxyoxane-2-carboxylic acid	C23H24O15			HMDB0128858			131835155
	106897	M	6	540.1115	6-{4-[3-(3,4-dihydroxy-5-methoxyphenyl)-2-oxopropanoyl]-3,5-dihydroxy-2-methoxyphenoxy}-3,4,5-trihydroxyoxane-2-carboxylic acid	C23H24O15			HMDB0128844			131835141
	78748	M	6	540.1115	6-{2-[3-(3,4-dihydroxy-5-methoxyphenyl)-2-oxopropanoyl]-3,5-dihydroxy-4-methoxyphenoxy}-3,4,5-trihydroxyoxane-2-carboxylic acid	C23H24O15			HMDB0128845			131835142
	50334	M	6	540.1115	6-{[5,7-dihydroxy-2-(1-hydroxy-5-methoxy-4-oxocyclohex-2-en-1-yl)-6-methoxy-4-oxo-4H-chromen-3-yl]oxy}-3,4,5-trihydroxyoxane-2-carboxylic acid	C23H24O15			HMDB0128855			131835152
	96236	M	6	540.1115	6-{[3,7-dihydroxy-2-(1-hydroxy-5-methoxy-4-oxocyclohex-2-en-1-yl)-6-methoxy-4-oxo-4H-chromen-5-yl]oxy}-3,4,5-trihydroxyoxane-2-carboxylic acid	C23H24O15			HMDB0128853			131835150
	102893	M	6	540.1115	6-{5-[2,3-dioxo-3-(2,4,6-trihydroxy-3-methoxyphenyl)propyl]-2-hydroxy-3-methoxyphenoxy}-3,4,5-trihydroxyoxane-2-carboxylic acid	C23H24O15			HMDB0128842			131835139
481.3155	163389	M	3	481.3168	PC(15:0/0:0)[S]	C23H48NO7P					40283	
	163390	M	3	481.3168	PC(15:0/0:0)[U]	C23H48NO7P					40379	
	163391	M	3	481.3168	PC(14:0/O-1:0)	C23H48NO7P					76586	
	163392	M	3	481.3168	PC(7:0/O-8:0)	C23H48NO7P					76591	
	2939	M	3	481.3168	PC(15:0/0:0)	C23H48NO7P			HMDB0010381	LMGP01050016	40282	24779458
	4264	M	3	481.3168	PE(18:0/0:0)	C23H48NO7P		C21484	HMDB0011130	LMGP02050001	40775	9547068
	4300	M	3	481.3168	LysoPE(0:0/18:0)	C23H48NO7P			HMDB0011129	LMGP02050038	61992	53480667
245.1374	97174	M	1	245.1376	Glutaminylvaline	C10H19N3O4			HMDB0028810		85724	57262456
	55576	M	1	245.1376	Asparaginyl-Isoleucine	C10H19N3O4			HMDB0028734		85649	17805101
	84814	M	1	245.1376	Leucyl-Asparagine	C10H19N3O4			HMDB0028924		85828	4128305
	105822	M	1	245.1376	Asparaginyl-Leucine	C10H19N3O4			HMDB0028735		85650	18218182
	50547	M	1	245.1376	Valyl-Glutamine	C10H19N3O4			HMDB0029125		86017	5253209
	139917	M	1	245.1376	Isoleucyl-Asparagine	C10H19N3O4			HMDB0028902		85808	4414300
	51403	M	1	245.1376	Valyl-Gamma-glutamate	C10H19N3O4			HMDB0029141		86033	131750792

Experimental mass	Identifier	Adduct	mz Error (ppm)	Molecular Weight	Name (proposed annotation by CEU Mass Mediator Batch Search)	Formula	CAS	Kegg	HMDB	LipidMaps	Metlin	PubChem
	167168	M	1	245.1376	Asn Ile	C10H19N3O4					23859	
	167169	M	1	245.1376	Leu Asn	C10H19N3O4					23960	
	167170	M	1	245.1376	Ile Asn	C10H19N3O4					24003	
	165218	M	1	245.1376	Gamma-glutamyl-Valine	C10H19N3O4					86054	
	167153	M	1	245.1376	Val Ala Gly	C10H19N3O4					16070	
	167154	M	1	245.1376	Gly Ile Gly	C10H19N3O4					16778	
	167155	M	1	245.1376	Ala Gly Val	C10H19N3O4					17192	
	167156	M	1	245.1376	Gly Gly Leu	C10H19N3O4					17722	
	167157	M	1	245.1376	Gly Val Ala	C10H19N3O4					18620	
	167158	M	1	245.1376	Gly Ala Val	C10H19N3O4					19531	
	167159	M	1	245.1376	Val Gly Ala	C10H19N3O4					19654	
	167160	M	1	245.1376	Leu Gly Gly	C10H19N3O4					19814	
	167161	M	1	245.1376	Ala Val Gly	C10H19N3O4					20508	
	167162	M	1	245.1376	Ile Gly Gly	C10H19N3O4					21047	
	167163	M	1	245.1376	Gly Leu Gly	C10H19N3O4					22420	
	167164	M	1	245.1376	Gly Gly Ile	C10H19N3O4					23054	
	167165	M	1	245.1376	Val Gln	C10H19N3O4					23738	
	167166	M	1	245.1376	Gln Val	C10H19N3O4					23765	
	167167	M	1	245.1376	Asn Leu	C10H19N3O4					23810	
363.1352	0	M	0	0	No compounds found for experimental mass 363.1352 and adduct: M							
204.1625	0	M	0	0	No compounds found for experimental mass 204.1625 and adduct: M							
409.2899	0	M	0	0	No compounds found for experimental mass 409.2899 and adduct: M							
529.0076	0	M	0	0	No compounds found for experimental mass 529.0076 and adduct: M							
346.0751	123160	M	8	346.0722	3-[3,4-dihydroxy-5-(3-methylbut-2-en-1-yl)phenyl]-2-(sulfooxy)propanoic acid	C14H18O8S			HMDB0133287			131837222
	145949	M	8	346.0722	3-{3-[(3,3-dimethyloxiran-2-yl)methyl]-4-(sulfooxy)phenyl}-2-hydroxypropanoic acid	C14H18O8S			HMDB0133281			131837216
	83515	M	8	346.0722	2-hydroxy-3-[3-(4-hydroxy-3-methylbut-2-en-1-yl)-4-(sulfooxy)phenyl]propanoic acid	C14H18O8S			HMDB0133270			
	103995	M	8	346.0722	2-hydroxy-3-[4-hydroxy-3-[3-methyl-4-(sulfooxy)but-2-en-1-yl]phenyl]propanoic acid	C14H18O8S			HMDB0133271			
	75849	M	8	346.0722	3-{3-[(3,3-dimethyloxiran-2-yl)methyl]-4-hydroxyphenyl}-2-(sulfooxy)propanoic acid	C14H18O8S			HMDB0133282			131837217
	137840	M	8	346.0722	2,3-dihydroxy-3-[3-(3-methylbut-2-en-1-yl)-4-(sulfooxy)phenyl]propanoic acid	C14H18O8S			HMDB0133275			131837211
	60826	M	8	346.0722	2-hydroxy-3-[3-hydroxy-5-(3-methylbut-2-en-1-yl)-4-(sulfooxy)phenyl]propanoic acid	C14H18O8S			HMDB0133286			131837221
	125376	M	8	346.0722	3-hydroxy-3-[4-hydroxy-3-(3-methylbut-2-en-1-yl)phenyl]-2-(sulfooxy)propanoic acid	C14H18O8S			HMDB0133277			131837212
	59121	M	8	346.0722	3-[4-hydroxy-3-(4-hydroxy-3-methylbut-2-en-1-yl)phenyl]-2-(sulfooxy)propanoic acid	C14H18O8S			HMDB0133272			
582.1498	181211	M	5	582.1526	Carbonarin A	C33H26O10						15346515
	181212	M	5	582.1526	Carbonarin B	C33H26O10						15346516
601.3409	160816	M	1	601.3403	Lolitrem K	C37H47NO6		C20533				
474.1197	13080	M	7	474.1162	Apigenin 7-(2''-acetylglucoside)	C23H22O11				LMPK12110374	48805	
	13081	M	7	474.1162	Apigenin 7-(6''-acetylglucoside)	C23H22O11				LMPK12110375	48806	
	11865	M	7	474.1162	Fujikinetin 7-O-glucoside	C23H22O11				LMPK12050106	47623	
	13154	M	7	474.1162	Acacetin 7-(6''-methylglucuronide)	C23H22O11				LMPK12110448	48879	
	12909	M	7	474.1162	Apigenin 8-C-(6''-acetylgalactoside)	C23H22O11				LMPK12110203	48634	
	12943	M	7	474.1162	Vitexin 2''-acetate	C23H22O11				LMPK12110237	48668	
	11925	M	7	474.1162	Genistin 6''-O-acetate	C23H22O11				LMPK12050167	47679	
	12980	M	7	474.1162	Isovitexin 6''-O-acetyl	C23H22O11				LMPK12110274	48705	
	12984	M	7	474.1162	Vitexin 3''-O-acetate	C23H22O11				LMPK12110278	48709	
	12985	M	7	474.1162	Vitexin 6''-O-acetate	C23H22O11				LMPK12110279	48710	
	14265	M	7	474.1162	Pongamoside D	C23H22O11				LMPK12111561	49980	
	12988	M	7	474.1162	8-C-beta-D-Glucofuranosylapigenin 2''-O-acetate	C23H22O11				LMPK12110282	48713	
	15555	M	7	474.1162	Viviparum A	C23H22O11				LMPK12112851	51263	
	14030	M	7	474.1162	7-Hydroxy-5,8-dimethoxyflavone 7-glucuronide	C23H22O11				LMPK12111326	49750	

Experimental mass	Identifier	Adduct	mz Error (ppm)	Molecular Weight	Name (proposed annotation by CEU Mass Mediator Batch Search)	Formula	CAS	Kegg	HMDB	LipidMaps	Metlin	PubChem
	14587	M	7	474.1162	Kaempferol 3-(2''-acetylrhamnoside)	C23H22O11				LMPK12111883	50299	
	14588	M	7	474.1162	Kaempferol 3-(3''-acetylrhamnoside)	C23H22O11				LMPK12111884	50300	
	14589	M	7	474.1162	Kaempferol 3-(4''-acetylrhamnoside)	C23H22O11				LMPK12111885	50301	
	13054	M	7	474.1162	Apigenin 7-(6''-ethylglucuronide)	C23H22O11				LMPK12110348	48779	
	59672	M	7	474.1162	Kaempferol 3-(2''-acetylrhamnoside)	C23H22O11			HMDB0039748			14861224
	145218	M	7	474.1162	Apigenin 7-O-(2''-O-acetylglucoside)	C23H22O11			HMDB0037341		92273	73829943
	126314	M	7	474.1162	4''-O-Acetylafzelin	C23H22O11			HMDB0039746		94298	14861229
	84111	M	7	474.1162	Betavulgarin glucoside	C23H22O11			HMDB0041215		95635	131753071
	51130	M	7	474.1162	Apigenin 7-O-(6''-O-acetylglucoside)	C23H22O11			HMDB0037342		92274	14325222
	68285	M	7	474.1162	3''-O-Acetylafzelin	C23H22O11			HMDB0039747		94299	14861226
	59865	M	7	474.1162	6''-O-Acetylgenistin	C23H22O11	73566-30-0		HMDB0029528		86322	22288010
392.1696	175520	M	0	392.1696	Thr Ser Trp	C18H24N4O6					16282	
	175521	M	0	392.1696	Ser Thr Trp	C18H24N4O6					16612	
	175522	M	0	392.1696	Tyr Asn Pro	C18H24N4O6					16705	
	175523	M	0	392.1696	Pro Tyr Asn	C18H24N4O6					17131	
	175524	M	0	392.1696	Ser Trp Thr	C18H24N4O6					17545	
	175525	M	0	392.1696	Pro Asn Tyr	C18H24N4O6					18393	
	175526	M	0	392.1696	Asn Pro Tyr	C18H24N4O6					18397	
	175527	M	0	392.1696	Tyr Pro Asn	C18H24N4O6					19067	
	175528	M	0	392.1696	Thr Trp Ser	C18H24N4O6					19475	
	175529	M	0	392.1696	Trp Thr Ser	C18H24N4O6					20579	
	175530	M	0	392.1696	Trp Ser Thr	C18H24N4O6					21554	
	175531	M	0	392.1696	Asn Tyr Pro	C18H24N4O6					23020	
	175532	M	9	392.173	Met Asp Lys	C15H28N4O6S					16741	
	175533	M	9	392.173	Asp Met Lys	C15H28N4O6S					17188	
	175534	M	9	392.173	Lys Asp Met	C15H28N4O6S					17394	
	175535	M	9	392.173	Asp Lys Met	C15H28N4O6S					20366	
	175536	M	9	392.173	Met Lys Asp	C15H28N4O6S					22663	
	175537	M	9	392.173	Lys Met Asp	C15H28N4O6S					23370	
	121320	M	9	392.166	Sparfloxacin	C19H22F2N4O3	110871-86-8	C07662	HMDB0015339		66707	60464
514.1004	0	M	0	0	No compounds found for experimental mass 514.1004 and adduct: M							
507.3334	2931	M	2	507.3325	PC(17:1(10Z)/0:0)	C25H50NO7P				LMGP01050002	40268	
	2986	M	2	507.3325	PC(17:1(9Z)/0:0)	C25H50NO7P				LMGP01050126	76568	
	4282	M	2	507.3325	PE(20:1(11Z)/0:0)	C25H50NO7P			HMDB0011512	LMGP02050020	62297	52925139
	4308	M	2	507.3325	LysoPE(0:0/20:1(11Z))	C25H50NO7P			HMDB0011482	LMGP02050046	62270	53480931
	83264	M	3	507.3349	Gymnodimine	C32H45NO4	173792-58-0		HMDB0041430		73510	10436276
	154511	M	3	507.3349	Gymnodimine; Gymnodimine A; GYM A	C32H45NO4		C20025				
507.3691	3017	M	0	507.3689	PC(O-18:1(11Z)/0:0)	C26H54NO6P				LMGP01060034	76582	
	3018	M	0	507.3689	PC(O-18:1(9Z)/0:0)	C26H54NO6P				LMGP01060039	76583	
	3026	M	0	507.3689	PC(O-18:1(1E)/0:0)	C26H54NO6P				LMGP01070008	40404	
	163410	M	0	507.3689	PC(O-18:1(9E)/0:0)[S]	C26H54NO6P					40373	
	163411	M	0	507.3689	PC(O-18:1(9Z)/0:0)[S]	C26H54NO6P					40375	
	163412	M	0	507.3689	PC(O-18:1(9Z)/0:0)[U]	C26H54NO6P					40376	
	3027	M	0	507.3689	PC(P-18:0/0:0)	C26H54NO6P			HMDB0013122	LMGP01070009	40405	24779527
500.1918	0	M	0	0	No compounds found for experimental mass 500.1918 and adduct: M							
258.0468	0	M	0	0	No compounds found for experimental mass 258.0468 and adduct: M							
521.9965	0	M	0	0	No compounds found for experimental mass 521.9965 and adduct: M							
126.1037	33888	M	6	126.1045	4,5-Dimethyl-4-hexen-3-one	C8H14O				LMFA12000237	98230	
	30568	M	6	126.1045	2,4-Dimethyl-2E,4E-hexadien-1-ol	C8H14O				LMFA05000114	46067	
	33726	M	6	126.1045	5-Methyl-5E-hepten-2-one	C8H14O				LMFA12000036	98098	
	30925	M	6	126.1045	2-octenal	C8H14O		C21138		LMFA06000029		
	30926	M	6	126.1045	3-octenal	C8H14O				LMFA06000030	75310	
	30927	M	6	126.1045	4-octenal	C8H14O				LMFA06000031	75311	
	30929	M	6	126.1045	6-octenal	C8H14O				LMFA06000033		
	33773	M	6	126.1045	4-Methyl-4E-hepten-3-one	C8H14O				LMFA12000095	98126	
	33774	M	6	126.1045	4S-methyl-1-hepten-3-one	C8H14O				LMFA12000096	98127	

Experimental mass	Identifier	Adduct	mz Error (ppm)	Molecular Weight	Name (proposed annotation by CEU Mass Mediator Batch Search)	Formula	CAS	Kegg	HMDB	LipidMaps	Metlin	PubChem
	33782	M	6	126.1045	4-Methyl-1-hepten-3-one	C8H14O				LMFA12000105	98133	
	33783	M	6	126.1045	4-Methyl-6-hepten-3-one	C8H14O				LMFA12000108	98134	
	33786	M	6	126.1045	6-Methyl-2-hepten-4-one	C8H14O				LMFA12000113	98137	
	30715	M	6	126.1045	1,5Z-Octadien-3-ol	C8H14O				LMFA05000493	96974	
	128770	M	6	126.1045	(E)-2-octenal	C8H14O	2548-87-0		HMDB0013809		75309	16900
	80406	M	6	126.1045	5-Methyl-5-hepten-2-one	C8H14O			HMDB0031591		87791	12663437
	109338	M	6	126.1045	2,5-Octadien-1-ol	C8H14O	83861-75-0		HMDB0040146		94686	92468132
	122140	M	6	126.1045	(2E,4E)-2,4-Octadien-1-ol	C8H14O	18409-20-6		HMDB0040151		94691	12180845
	79942	M	6	126.1045	2-Octenal	C8H14O	2363-89-5		HMDB0030961		87318	6427080
	140110	M	6	126.1045	2-Octen-4-one	C8H14O	4643-27-0		HMDB0031301		87568	12409825
	125532	M	6	126.1045	6-Methyl-3-hepten-2-one, trans-	C8H14O	20859-10-3		HMDB0032403		88427	5462986
	141672	M	6	126.1045	2,4,4-Trimethylcyclopentanone	C8H14O	4694-12-6		HMDB0031197		87486	107324
	48289	M	6	126.1045	5-Octen-2-one	C8H14O			HMDB0035390		90686	5352779
	33699	M	6	126.1045	3E-octen-2-one	C8H14O			HMDB0033547	LMFA12000009	89357	5363229
	66981	M	6	126.1045	(S,E)-Filbertone	C8H14O	122440-59-9		HMDB0035242		90553	89357606
	33701	M	6	126.1045	1-Octen-3-one	C8H14O			HMDB0031309	LMFA12000011	87574	61346
	73387	M	6	126.1045	2-Ethylidenehexanal	C8H14O	25409-08-9		HMDB0037152		92120	5463946
	90301	M	6	126.1045	(3E,5Z)-3,5-Octadien-1-ol	C8H14O			HMDB0040149		94689	87170471
	118462	M	6	126.1045	6-Octenal	C8H14O	63826-25-5		HMDB0039769		75313	21158617
	33729	M	6	126.1045	6-Methyl-5-hepten-2-one	C8H14O		C07287	HMDB0035915	LMFA12000039	44779	9862
	30928	M	6	126.1045	5-octenal	C8H14O			HMDB0039770	LMFA06000032	75312	5283327
	109529	M	6	126.1045	3-Methyl-3-hepten-2-one	C8H14O	39899-08-6		HMDB0031590		87790	5364798
	94445	M	6	126.1045	4-Octen-3-one	C8H14O	14129-48-7		HMDB0032451		88472	5369061
	30710	M	6	126.1045	1,5E-Octadien-3-ol	C8H14O			HMDB0030966	LMFA05000488	87319	6428570
	97787	M	6	126.1045	2-Ethyl-2-hexenal	C8H14O			HMDB0061945			5354264
	54705	M	6	126.1045	trans-3-cis-8,11,14-eicosatetraenoyl-CoA	C8H14O			HMDB0062471			61018
	107026	M	9	126.1026	N(tele)-methylhistaminium	C6H12N3			HMDB0062574			25245502
203.0971	0	M	0	0	No compounds found for experimental mass 203.0971 and adduct: M							
1482.167	0	M	0	0	No compounds found for experimental mass 1482.167 and adduct: M							
412.0762	0	M	0	0	No compounds found for experimental mass 412.0762 and adduct: M							
876.1358	0	M	0	0	No compounds found for experimental mass 876.1358 and adduct: M							
575.2725	0	M	0	0	No compounds found for experimental mass 575.2725 and adduct: M							
523.363	163438	M	1	523.3638	enantio-PAF C-16	C26H54NO7P	117985-57-6				43413	
	165818	M	1	523.3638	PAF C-16	C26H54NO7P	74389-68-7				34488	
	2641	M	2	523.3638	PC(O-16:0/2:0)	C26H54NO7P			HMDB0062195	LMGP01020046	40075	108156
	163439	M	2	523.3638	PC(O-16:0/2:0)[S]	C26H54NO7P					40076	
	163440	M	2	523.3638	PC(O-16:0/2:0)[U]	C26H54NO7P					40077	
	163441	M	2	523.3638	PC(18:0/0:0)[S]	C26H54NO7P					40293	
	163442	M	2	523.3638	PC(18:0/0:0)[U]	C26H54NO7P					40294	
	163443	M	2	523.3638	PC(0:0/18:0)[S]	C26H54NO7P					40343	
	163444	M	2	523.3638	PC(0:0/18:0)[U]	C26H54NO7P					40344	
	2944	M	2	523.3638	PC(18:0/0:0)	C26H54NO7P			HMDB0010384	LMGP01050026	40292	497299
	2970	M	2	523.3638	PC(0:0/18:0)	C26H54NO7P			HMDB0011128	LMGP01050076	40342	24779491
	164538	M	2	523.3638	PC(2:0/O-16:0)[U]	C26H54NO7P					40161	
	4288	M	2	523.3638	PE(21:0/0:0)	C26H54NO7P				LMGP02050026	77692	
542.1064	0	M	0	0	No compounds found for experimental mass 542.1064 and adduct: M							
386.0972	108569	M	8	386.1002	5,7-dihydroxy-2-phenyl-8-(3,4,5-trihydroxyoxan-2-yl)-4H-chromen-4-one	C20H18O8			HMDB0127227			131833592
	148776	M	8	386.1002	Dehydrodiferulic dilactone	C20H18O8			HMDB0033876		89585	3703882
	114009	M	8	386.1002	8-8'-Dehydrodiferulic acid	C20H18O8			HMDB0029277		86149	131750840
	128192	M	8	386.1002	3-[3-Carboxy-2,3-dihydro-2-(4-hydroxy-3-methoxyphenyl)-7-methoxy-5-benzofuranyl]-2-propenoic acid	C20H18O8			HMDB0041277		95691	101088304
	181161	M	8	386.1002	5,6-Dimethoxydihydrosterigmatocystin	C20H18O8						5488181
	15872	M	8	386.1002	Pollenitin 8-butyrate	C20H18O8				LMPK12113168	51580	
	152078	M	8	386.1002	Glucosyloxyanthraquinone	C20H18O8		C03503			65990	440032
	158518	M	8	386.1002	Daphneticin	C20H18O8	83327-22-4	C09924			68014	158341
	12858	M	8	386.1002	Chrysin 5-xyloside	C20H18O8				LMPK12110152	48585	
	15967	M	8	386.1002	Meliternin	C20H18O8				LMPK12113263	51675	
	14185	M	8	386.1002	Linderoflavone B	C20H18O8				LMPK12111481	49903	

Experimental mass	Identifier	Adduct	mz Error (ppm)	Molecular Weight	Name (proposed annotation by CEU Mass Mediator Batch Search)	Formula	CAS	Kegg	HMDB	LipidMaps	Metlin	PubChem
	15728	M	8	386.1002	Melisimplexin	C20H18O8				LMPK12113024	51436	
	12177	M	8	386.1002	Irisflorentin	C20H18O8		C17958		LMPK12050419	47923	170569
	156057	M	8	386.1002	Diferulic acid	C20H18O8		C10446			68330	5281770
	13980	M	8	386.1002	5,6,7,3'-Tetramethoxy-4',5'-methylenedioxyflavone	C20H18O8				LMPK12111276	49700	
	13981	M	8	386.1002	5,3',4',5'-Tetramethoxy-6,7-methylenedioxyflavone	C20H18O8				LMPK12111277	49701	
	12202	M	8	386.1002	5,6,7,8-Tetramethoxy-3',4'-methylenedioxyisoflavone	C20H18O8				LMPK12050444	47948	
	156074	M	8	386.1002	Cleomiscosin A	C20H18O8	76948-72-6	C09922			68012	442510
	155703	M	8	386.1002	Versicolorone	C20H18O8		C20504				
	157245	M	8	386.1002	5'-Oxoaverantin; 1,3,6,8-Tetrahydroxy-2-[(1S)-1-hydroxy-5-oxohexyl]anthracene-9,10-dione	C20H18O8		C20502				
272.0767	97471	M	1	272.077	Pyridine N-oxide glucuronide	C11H14NO7			HMDB0061177			131770061
	167756	M	8	272.0788	Nimustine	C9H13ClN6O2	42471-28-3				44117	
158.0845	161319	M	1	158.0844	1,5-Naphthalenediamine	C10H10N2	2243-62-1	C19463			73157	16720
	150679	M	1	158.0844	Nicotyrine; beta-Nicotyrine	C10H10N2	487-19-4	C10161			68165	10249
	166102	M	1	158.0844	1-Benzylimidazole	C10H10N2	4238-71-5				63058	
90.047	0	M	0	0	No compounds found for experimental mass 90.047 and adduct: M							
337.1102	171022	M	8	337.113	Leu Cys Cys	C12H23N3O4S2					16295	
	171023	M	8	337.113	Gly Met Met	C12H23N3O4S2					16728	
	171024	M	8	337.113	Cys Cys Ile	C12H23N3O4S2					17360	
	171025	M	8	337.113	Cys Ile Cys	C12H23N3O4S2					18168	
	171026	M	8	337.113	Met Gly Met	C12H23N3O4S2					18555	
	171027	M	8	337.113	Met Met Gly	C12H23N3O4S2					20338	
	171028	M	8	337.113	Cys Leu Cys	C12H23N3O4S2					21120	
	171029	M	8	337.113	Ile Cys Cys	C12H23N3O4S2					21205	
	171030	M	8	337.113	Cys Cys Leu	C12H23N3O4S2					21636	
194.092	0	M	0	0	No compounds found for experimental mass 194.092 and adduct: M							
465.1383	0	M	0	0	No compounds found for experimental mass 465.1383 and adduct: M							
603.3014	0	M	0	0	No compounds found for experimental mass 603.3014 and adduct: M							
599.3263	159140	M	3	599.3247	Penitrem E	C37H45NO6	78213-66-8	C20597				
337.0997	34034	M	4	337.1009	(S)-malyl N-acetyl-alpha-D-glucosaminide	C12H19NO10				LMFA13010059		
	65112	M	4	337.0984	Benzyl glycinate 4-methylbenzenesulfonate salt	C16H19NO5S	1738-76-7		HMDB0033374		89217	6451311
541.3169	2957	M	0	541.3168	PC(20:5(5Z,8Z,11Z,14Z,17Z)/0:0)	C28H48NO7P			HMDB0010397	LMGP01050050	40316	11757087
266.0948	67075	M	2	266.0943	(E)-4-[5-(4-Hydroxyphenoxy)-3-penten-1-ynyl]phenol	C17H14O3			HMDB0041447		95843	131753147
	11761	M	2	266.0943	7-Methoxy-2-methylisoflavone	C17H14O3			HMDB0033980	LMPK12050002	47525	354368
	160171	M	2	266.0943	Benzarone; 2-Ethyl-3-(4-hydroxybenzoyl)benzofuran	C17H14O3	1477-19-6	C14474			70089	255968
	167621	M	2	266.0943	Methoxyvone	C17H14O3					43575	
	167622	M	2	266.0943	5-methyl-7-methoxyisoflavone	C17H14O3	82517-12-2				84979	
326.3291	0	M	0	0	No compounds found for experimental mass 326.3291 and adduct: M							
770.4646	0	M	0	0	No compounds found for experimental mass 770.4646 and adduct: M							
252.1165	43799	M	3	252.1157	Cimetidine	C10H16N6S	51481-61-9	C06952	HMDB0014644		1755	2756
	159588	M	6	252.115	cis-Hinokiresinol	C17H16O2	17676-24-3	C10628			68443	5281830
	157890	M	6	252.115	p-(3,4-Dihydro-6-methoxy-2-naphthyl)phenol	C17H16O2		C14897			70400	252381
	128014	M	6	252.115	(1Z,4Z)-1,5-bis(4-hydroxyphenyl)-1,4-pentadiene	C17H16O2			HMDB0033317		89171	131751408
	148758	M	6	252.115	2-Phenylethyl 3-phenyl-2-propenoate	C17H16O2	103-53-7		HMDB0035018		90378	5369459
	125873	M	6	252.115	Cinnamyl phenylacetate	C17H16O2	7492-65-1		HMDB0037707		92530	92468421
888.5636	0	M	0	0	No compounds found for experimental mass 888.5636 and adduct: M							
333.9983	75049	M	7	334.0007	2-Methyl-1,4-naphthalenediol bis(dihydrogen phosphate)	C11H12O8P2	84-98-0		HMDB0032721		88651	8556
453.9817	0	M	0	0	No compounds found for experimental mass 453.9817 and adduct: M							
492.1053	157404	M	3	492.1039	Triflusulfuron-methyl	C17H19F3N6O6S	126535-15-7	C18901			72662	92434
	157121	M	10	492.1006	L-Threonylcarbamoyladenylate; L-Threonylcarbamoyl-AMP; TC-AMP	C15H21N6O11P		C20641				
1587.654	0	M	0	0	No compounds found for experimental mass 1587.654 and adduct: M							
494.3708	0	M	0	0	No compounds found for experimental mass 494.3708 and adduct: M							
319.1522	169880	M	3	319.1532	Pro Gly Phe	C16H21N3O4					18651	
	169881	M	3	319.1532	Phe Gly Pro	C16H21N3O4					19171	

Experimental mass	**Identifier**	**Adduct**	**mz Error (ppm)**	**Molecular Weight**	**Name** (proposed annotation by CEU Mass Mediator Batch Search)	**Formula**	**CAS**	**Kegg**	**HMDB**	**LipidMaps**	**Metlin**	**PubChem**
	169882	M	3	319.1532	Pro Phe Gly	C16H21N3O4					20822	
	169883	M	3	319.1532	Phe Pro Gly	C16H21N3O4					21436	
	169884	M	3	319.1532	Gly Phe Pro	C16H21N3O4					21913	
	169885	M	3	319.1532	Gly Pro Phe	C16H21N3O4					22242	
354.3606	0	M	0	0	No compounds found for experimental mass 354.3606 and adduct: M							
457.1101	0	M	0	0	No compounds found for experimental mass 457.1101 and adduct: M							
455.098	0	M	0	0	No compounds found for experimental mass 455.098 and adduct: M							
962.1399	0	M	0	0	No compounds found for experimental mass 962.1399 and adduct: M							

Supplementary Table S7: Search result from the accurate mass batch search (CEU mass mediator) of compounds found with higher abundance in ECM blank samples - HILIC ESI (-) mode

Experimental mass	Identifier	Adduct	mz Error (ppm)	Molecular Weight	Name (proposed annotation by CEU Mass Mediator Batch Search)	Formula	CAS	Kegg	HMDB	LipidMaps	Metlin	PubChem
135.9032	0	M	0	0	No compounds found for experimental mass 135.9032 and adduct: M							
136.039	125526	M	4	136.0385	Allopurinol	C5H4N4O	315-30-0		HMDB0014581		865	2094
	144883	M	4	136.0385	Hypoxanthine	C5H4N4O	68-94-0	C00262	HMDB0000157		83	790
	138754	M	7	136.038	Ethyl isopropyl disulfide	C5H12S2			HMDB0033C54		88946	521477
	129402	M	7	136.038	Ethyl propyl disulfide	C5H12S2	30453-31-7		HMDB0033C53		88945	35349
	114082	M	7	136.038	1-Pentanesulfenothioic acid	C5H12S2			HMDB0031160		87453	21251947
154.8764	0	M	0	0	No compounds found for experimental mass 154.8764 and adduct: M							
195.913	0	M	0	0	No compounds found for experimental mass 195.913 and adduct: M							
209.9402	147555	M	2	209.9406	1,3,5-Trichloro-2-methoxybenzene	C7H5Cl3O	87-40-1	C11510	HMDB0029643		69083	6884
	151705	M	5	209.9413	Cryolite; Aluminum sodium fluoride	Na3AlF6	15096-52-3	C18816				159692
137.9003	0	M	0	0	No compounds found for experimental mass 137.9003 and adduct: M							
214.8868	0	M	0	0	No compounds found for experimental mass 214.8868 and adduct: M							
156.8734	0	M	0	0	No compounds found for experimental mass 156.8734 and adduct: M							
308.1175	124241	M	5	308.1161	Azacridone A	C18H16N2O3			HMDB0040367		94879	10357912
	114397	M	5	308.1161	C.I. Solvent Red 80	C18H16N2O3	6358-53-8	C19214	HMDB0037521		72938	
	169290	M	5	308.1161	Tyrphostin B44 (-)	C18H16N2O3	133550-32-0				44520	
211.937	0	M	0	0	No compounds found for experimental mass 211.937 and adduct: M							
268.0209	0	M	0	0	No compounds found for experimental mass 268.0209 and adduct: M							
262.8959	0	M	0	0	No compounds found for experimental mass 262.8959 and adduct: M							
368.1103	152924	M	1	368.1107	5-O-Feruloylquinic acid;	C17H20O9		C02572			65790	9799386
	54607	M	1	368.1107	3,4,5-trihydroxy-6-{[2-(hydroxymethyl)-2-methyl-2H-chromen-5-yl]oxy}oxane-2-carboxylic acid	C17H20O9			HMDB0126423			131832842
	132198	M	1	368.1107	3,4,5-trihydroxy-6-{3-[(5-oxooxolan-2-yl)methyl]phenoxy}oxane-2-carboxylic acid	C17H20O9			HMDB0127742			131834071
	110216	M	1	368.1107	3,4,5-trihydroxy-6-[(7-hydroxy-2,2-dimethyl-2H-chromen-5-yl)oxy]oxane-2-carboxylic acid	C17H20O9			HMDB0126419			131832838
	145051	M	1	368.1107	3,4,5-trihydroxy-6-[(6-hydroxy-2,2-dimethyl-2H-chromen-5-yl)oxy]oxane-2-carboxylic acid	C17H20O9			HMDB0126421			131832840
	94630	M	1	368.1107	3,4,5-trihydroxy-6-[(5-hydroxy-2,2-dimethyl-2H-chromen-6-yl)oxy]oxane-2-carboxylic acid	C17H20O9			HMDB0126420			131832839
	50858	M	1	368.1107	3,4,5-trihydroxy-6-[2-methoxy-4-(3-oxobut-1-en-1-yl)phenoxy]oxane-2-carboxylic acid	C17H20O9			HMDB0135673			
	135353	M	1	368.1107	6-({5,5-dimethyl-3,6-dioxatricyclo[5.4.0.0^{2},?]undeca-1(11),7,9-trien-11-yl}oxy)-3,4,5-trihydroxyoxane-2-carboxylic acid	C17H20O9			HMDB0126422			131832841
	63226	M	1	368.1107	3,4,5-trihydroxy-6-[1-(4-methoxy-1-benzofuran-5-yl)ethoxy]oxane-2-carboxylic acid	C17H20O9			HMDB0129399			131835649
	134139	M	1	368.1107	3,4,5-trihydroxy-6-[(5-hydroxy-2,2-dimethyl-2H-chromen-7-yl)oxy]oxane-2-carboxylic acid	C17H20O9			HMDB0126418			131832837
	58119	M	1	368.1107	3-O-Feruloylquinic acid	C17H20O9			HMDB0030669		87130	131751068
	124943	M	1	368.1107	3-O-Caffeoyl-1-O-methylquinic acid	C17H20O9			HMDB0039559		94501	131752768
	46548	M	1	368.1107	3-O-Caffeoyl-4-O-methylquinic acid	C17H20O9			HMDB0039560		94502	131752769
216.8839	0	M	0	0	No compounds found for experimental mass 216.8839 and adduct: M							
308.1182	124241	M	7	308.1161	Azacridone A	C18H16N2O3			HMDB0040367		94879	10357912
	114397	M	7	308.1161	C.I. Solvent Red 80	C18H16N2O3	6358-53-8	C19214	HMDB0037521		72938	
	169290	M	7	308.1161	Tyrphostin B44 (-)	C18H16N2O3	133550-32-0				44520	
630.1497	0	M	0	0	No compounds found for experimental mass 630.1497 and adduct: M							
126.9085	0	M	0	0	No compounds found for experimental mass 126.9085 and adduct: M							
154.8761	0	M	0	0	No compounds found for experimental mass 154.8761 and adduct: M							
214.0223	154325	M	1	214.0226	3,5-Dinitroguaiacol	C7H6N2O6		C17101			71560	14345197
	161844	M	9	214.0242	2-Deoxy-D-ribose 1-phosphate; 2-Deoxy-alpha-D-ribose 1-phosphate	C5H11O7P		C00672				5460448
	150724	M	9	214.0242	2-Deoxy-D-ribose 5-phosphate	C5H11O7P		C00673				439288
	134961	M	9	214.0242	Deoxyribose 5-monophosphate	C5H11O7P			HMDB0059654			49866876
	75604	M	9	214.0242	Deoxyribose 5-phosphate	C5H11O7P			HMDB0001031		63109	45934311
	138139	M	9	214.0242	5-Deoxyribose-1-phosphate	C5H11O7P		C16637	HMDB0060393		71276	24906327

Experimental mass	Identifier	Adduct	mz Error (ppm)	Molecular Weight	Name (proposed annotation by CEU Mass Mediator Batch Search)	Formula	CAS	Kegg	HMDB	LipidMaps	Metlin	PubChem
	134069	M	9	214.0242	Deoxyribose 1-phosphate	C5H11O7P	17210-42-3		HMDB0001351		3348	439287
	129481	M	9	214.0242	1-Deoxy-D-xylulose 5-phosphate	C5H11O7P		C11437	HMDB0001213		6085	443201
	165175	M	9	214.0242	2-Deoxy-D-ribose 5-phosphate	C5H11O7P	7685-50-9				3349	
243.0478	0	M	0	0	No compounds found for experimental mass 243.0478 and adduct: M							
316.9347	0	M	0	0	No compounds found for experimental mass 316.9347 and adduct: M							
314.9373	0	M	0	0	No compounds found for experimental mass 314.9373 and adduct: M							
220.042	152361	M	1	220.0419	Thidiazuron	C9H8N4OS	51707-55-2	C18812			72579	40087
	59974	M	3	220.0414	1-Propenyl 1-(1-propenylthio)propyl disulfide	C9H16S3			HMDB0038967		93576	131752500
318.9324	0	M	0	0	No compounds found for experimental mass 318.9324 and adduct: M							
344.0935	0	M	0	0	No compounds found for experimental mass 344.0935 and adduct: M							
88.0173	0	M	0	0	No compounds found for experimental mass 88.0173 and adduct: M							
298.8716	0	M	0	0	No compounds found for experimental mass 298.8716 and adduct: M							
344.0931	0	M	0	0	No compounds found for experimental mass 344.0931 and adduct: M							
300.8683	0	M	0	0	No compounds found for experimental mass 300.8683 and adduct: M							
294.0159	0	M	0	0	No compounds found for experimental mass 294.0159 and adduct: M							
172.0144	150151	M	4	172.0137	sn-Glycerol 1-phosphate; sn-Gro-1-P; L-Glycerol 1-phosphate	C3H9O6P	5746-57-6	C00623				439276
	151017	M	4	172.0137	DL-Glycerol 1-phosphate; Glycerol 1-phosphate; Glycerol-3-phosphate; rac-Glycerol 1-phosphate; DL-Glyceryl 1-phosphate; DL-Glycerol 3-phosphate	C3H9O6P		C03189			65927	754
	133570	M	4	172.0137	Beta-Glycerophosphoric acid	C3H9O6P	17181-54-3	C02979	HMDB0002520		44760	2526
	88557	M	4	172.0137	Glycerol 3-phosphate	C3H9O6P	17989-41-2	C00093	HMDB0000126		5161	439162
251.9856	156721	M	8	251.9875	Cartilagineal	C10H11Cl3O	53915-35-8	C17102			71561	6385704
425.0341	0	M	0	0	No compounds found for experimental mass 425.0341 and adduct: M							
282.115	27277	M	1	282.1153	3,4-dichloro-tridecanoic acid	C13H24Cl2O2				LMFA01090062	96793	
	160720	M	2	282.1157	2,3-Diphenyl-3-(2-pyridinyl)acrylonitrile	C20H14N2	39077-64-0	C15084			70577	3003768
391.0728	0	M	0	0	No compounds found for experimental mass 391.0728 and adduct: M							
467.1475	0	M	0	0	No compounds found for experimental mass 467.1475 and adduct: M							
435.0237	0	M	0	0	No compounds found for experimental mass 435.0237 and adduct: M							
204.0601	0	M	0	0	No compounds found for experimental mass 204.0601 and adduct: M							
214.0224	154325	M	1	214.0226	3,5-Dinitroguaiacol	C7H6N2O6		C17101			71560	14345197
	161844	M	8	214.0242	2-Deoxy-D-ribose 1-phosphate; 2-Deoxy-alpha-D-ribose 1-phosphate	C5H11O7P		C00672				5460448
	150724	M	8	214.0242	2-Deoxy-D-ribose 5-phosphate	C5H11O7P		C00673				439288
	134961	M	9	214.0242	Deoxyribose 5-monophosphate	C5H11O7P			HMDB0059654			49866876
	75604	M	9	214.0242	Deoxyribose 5-phosphate	C5H11O7P			HMDB0001031		63109	45934311
	138139	M	9	214.0242	5-Deoxyribose-1-phosphate	C5H11O7P		C16637	HMDB0060393		71276	24906327
	134069	M	9	214.0242	Deoxyribose 1-phosphate	C5H11O7P	17210-42-3		HMDB0001351		3348	439287
	129481	M	9	214.0242	1-Deoxy-D-xylulose 5-phosphate	C5H11O7P		C11437	HMDB0001213		6085	443201
	165175	M	9	214.0242	2-Deoxy-D-ribose 5-phosphate	C5H11O7P	7685-50-9				3349	
216.0205	0	M	0	0	No compounds found for experimental mass 216.0205 and adduct: M							
372.1099	173666	M	10	372.1063	N-Dealkylzuclopenthixol sulfoxide	C20H21ClN2OS	21642-95-5				3112	
450.0083	0	M	0	0	No compounds found for experimental mass 450.0083 and adduct: M							
278.0214	110548	M	5	278.02	Fenthion	C10H15O3PS2	55-38-9	C14420	HMDB0033209		44242	3346
488.1776	147531	M	7	488.1741	Fucosyllactose	C18H32O15			HMDB0006620		58498	21771334
	95076	M	7	488.1741	B-Trisaccharide	C18H32O15			HMDB0006601		58484	53477865
	53906	M	7	488.1741	2-Fucosyllactose	C18H32O15	41263-94-9		HMDB0002098		58094	170484
	59368	M	7	488.1741	3-Fucosyllactose	C18H32O15			HMDB0002094		58093	161460
	155050	M	7	488.1741	beta-D-Glc-(1->4)-alpha-L-Rha-(1->3)-D-Glc; beta-D-Glcp-(1->4)-alpha-L-Rhap-(1->3)-D-Glcp	C18H32O15		C19966			73457	
1106.107	78529	M	1	1106.1084	Syzyginin A	C48H34O31			HMDB0030236		86822	131750984
268.0812	42841	M	2	268.0808	Allopurinol riboside	C10H12N4O5	16220-07-8		HMDB0000481		867	
	78981	M	2	268.0808	Arabinosylhypoxanthine	C10H12N4O5	7013-16-3		HMDB0003040		3022	46874582
	80877	M	2	268.0808	Inosine	C10H12N4O5	58-63-9	C00294	HMDB0000195		84	6021

Experimental mass	Identifier	Adduct	mz Error (ppm)	Molecular Weight	Name (proposed annotation by CEU Mass Mediator Batch Search)	Formula	CAS	Kegg	HMDB	LipidMaps	Metlin	PubChem
	72941	M	7	268.0794	3-Deoxy-D-glycero-D-galacto-2-nonulosonic acid	C9H16O9	22594-61-2		HMDB0000425		5414	22833524
	154326	M	7	268.0794	2-O-(alpha-D-Mannosyl)-D-glycerate; alpha-Mannosylglycerate; 2-O-(alpha-D-Mannopyranosyl)-D-glycerate	C9H16O9		C11544			63171	5460194
	155448	M	7	268.0794	3-Deoxy-D-glycero-D-galacto-non-2-ulosonic acid; 2-Keto-3-deoxy-D-glycero-D-galacto-nononic acid; KDN; Deaminated neuraminic acid; Ketodeoxynonulonic acid; 3-Deoxy-D-glycero-D-galacto-non-2-ulopyranosonic acid	C9H16O9		C20934				
	154296	M	7	268.0794	2-O-(alpha-D-Glucopyranosyl)-D-glycerate; (R)-2-(alpha-D-Glucopyranosyloxy)-3-hydroxypropanoate	C9H16O9		C19792				
368.8943	0	M	0	0	No compounds found for experimental mass 368.8943 and adduct: M							
277.9854	0	M	0	0	No compounds found for experimental mass 277.9854 and adduct: M							
252.0232	162579	M	2	252.0237	Thiacloprid	C10H9ClN4S	111988-49-9	C18512			72318	
	156942	M	4	252.0221	3,3'-Dichlorobenzidine	C12H10Cl2N2	91-94-1	C19225			72948	7070
320.9305	0	M	0	0	No compounds found for experimental mass 320.9305 and adduct: M							
251.953	0	M	0	0	No compounds found for experimental mass 251.953 and adduct: M							
224.0324	52483	M	1	224.0321	Dehydrochorismic acid	C10H8O6			HMDB0036314		91459	9920917
346.091	83726	M	3	346.09	Methyl 6-O-galloyl-beta-D-glucopyranoside	C14H18O10			HMDB0039354		93933	78385296
	131977	M	7	346.0884	N1-(2-Hydroxyethyl)flurazepam	C18H16ClFN2O2			HMDB0060853			21498643
289.9249	160785	M	9	289.9224	2,3,5,6-Tetrachlorobiphenyl; PCB 65	C12H6Cl4	33284-54-7	C14363			69998	36402
	150820	M	9	289.9224	2,3,4,4'-Tetrachlorobiphenyl; PCB 60	C12H6Cl4	33025-41-1	C14361			69996	36304
	151588	M	9	289.9224	2,3,4,5-Tetrachlorobiphenyl; PCB 61	C12H6Cl4	33284-53-6	C14362			69997	36401
	155438	M	9	289.9224	2,4,4',6-Tetrachlorobiphenyl; PCB 75	C12H6Cl4	32598-12-2	C14364			69999	63107
	160902	M	9	289.9224	3,4,3',4'-Tetrachlorobiphenyl; PCB 77	C12H6Cl4	32598-13-3	C11057			68802	36187
	155814	M	9	289.9224	2,2',4,5-Tetrachlorobiphenyl; PCB 48	C12H6Cl4	70362-47-9	C14360			69995	51041
	158889	M	9	289.9224	2,2',4,4'-Tetrachlorobiphenyl; PCB 47	C12H6Cl4	2437-79-8	C14247			69908	17097
	161210	M	9	289.9224	3,4,4',5-Tetrachlorobiphenyl; PCB 81	C12H6Cl4	70362-50-4	C18114			72041	51043
	162758	M	9	289.9224	2,2',5,5'-Tetrachlorobiphenyl; 2,2',5,5'-TCB; PCB 52	C12H6Cl4	35693-99-3	C14199			69872	37248
287.9282	0	M	0	0	No compounds found for experimental mass 287.9282 and adduct: M							
294.0159	0	M	0	0	No compounds found for experimental mass 294.0159 and adduct: M							
247.1683	167230	M	1	247.1685	Y-27632	C14H21N3O	129830-38-2				44907	
346.0908	83726	M	2	346.09	Methyl 6-O-galloyl-beta-D-glucopyranoside	C14H18O10			HMDB0039354		93933	78385296
	131977	M	7	346.0884	N1-(2-Hydroxyethyl)flurazepam	C18H16ClFN2O2			HMDB0060853			21498643
256.887	0	M	0	0	No compounds found for experimental mass 256.887 and adduct: M							
253.9498	0	M	0	0	No compounds found for experimental mass 253.9498 and adduct: M							
443.1458	0	M	0	0	No compounds found for experimental mass 443.1458 and adduct: M							
329.0508	79057	M	1	329.0511	Nitisinone	C14H10F3NO5	104206-65-7		HMDB0014492		85368	115355
	119703	M	4	329.0521	Mecarbam	C10H20NO5PS2	2595-54-2	C18661	HMDB0031800		72447	17434
	159189	M	5	329.0525	2',3'-Cyclic AMP	C10H12N5O6P		C02353				101812
	114500	M	5	329.0525	Cyclic AMP	C10H12N5O6P	60-92-4	C00575	HMDB0000058		92	6076
	48378	M	5	329.0525	Adenosine 2',3'-cyclic phosphate	C10H12N5O6P	634-01-5		HMDB0011616		3459	2024
	158806	M	5	329.0525	3',5'-Cyclic dGMP	C10H12N5O6P		C02507			3486	439740
220.0517	71410	M	0	220.0518	N-Acetyl-S-(N-methylcarbamoyl)cysteine	C7H12N2O4S	103974-29-4	C11490	HMDB0041942		69065	108218
	166784	M	0	220.0518	Snap	C7H12N2O4S	67776-06-1				44297	

Experimental mass	Identifier	Adduct	mz Error (ppm)	Molecular Weight	Name (proposed annotation by CEU Mass Mediator Batch Search)	Formula	CAS	Kegg	HMDB	LipidMaps	Metlin	PubChem
	181277	M	7	220.0502	8-chloro-9-hydroxy-8,9-deoxyasperlactone	C9H13ClO4						10998579
238.099	58883	M	1	238.0987	HEPES	C8H18N2O4S	7365-45-9		HMDB0062295			23830
	140617	M	2	238.0994	Cinnamyl benzoate	C16H14O2	50555-04-9		HMDB0029700		86431	5705112
	16286	M	2	238.0994	4'-Methoxychalcone	C16H14O2			HMDB0032585	LMPK12120188		641818
	64689	M	2	238.0994	Benzyl cinnamate	C16H14O2	103-41-3		HMDB0040286		94811	15558051
	167047	M	2	238.0994	4'-Methoxychalcone	C16H14O2	959-33-1				44091	
376.1011	174135	M	0	376.1012	Capsazepine	C19H21ClN2O2S	138977-28-3				45065	
	94059	M	1	376.1006	Furaneol 4-(6-malonylglucoside)	C15H20O11			HMDB0029778		86485	131750900
	27334	M	7	376.1038	Ethyl 18-bromooctadec-17-en-5,7,15-triynoate	C20H25BrO2				LMFA01090119	96846	
	87735	M	8	376.0981	{4-[(E)-2-{3,5-dihydroxy-4-[(1E)-3-methylbut-1-en-1-yl]phenyl}ethenyl]phenyl}oxidanesulfonic acid	C19H20O6S			HMDB0128896			131835282
557.3121	1670	M	1	557.3118	PC(6:2(3E,5E)/14:2(11E,13E))	C28H48NO8P				LMGP01011236	39970	
	163496	M	1	557.3118	PC(10:2(2E,4E)/10:2(2E,4E))[S]	C28H48NO8P					39147	
506.0903	0	M	0	0	No compounds found for experimental mass 506.0903 and adduct: M							
399.1093	176015	M	2	399.11	Asp Cys Tyr	C16H21N3O7S					16258	
	176016	M	2	399.11	Cys Asp Tyr	C16H21N3O7S					19400	
	176017	M	2	399.11	Cys Tyr Asp	C16H21N3O7S					19641	
	176018	M	2	399.11	Tyr Cys Asp	C16H21N3O7S					21048	
	176019	M	2	399.11	Tyr Asp Cys	C16H21N3O7S					21231	
	176020	M	2	399.11	Asp Tyr Cys	C16H21N3O7S					22293	
	119053	M	5	399.1074	6-[(6-carboxy-3,4,5-trihydroxyoxan-2-yl)oxy]-2-phenyl-1??-chromen-1-ylium	C21H19O8			HMDB0133416			131837323
	62481	M	5	399.1074	5-[(6-carboxy-3,4,5-trihydroxyoxan-2-yl)oxy]-2-phenyl-1??-chromen-1-ylium	C21H19O8			HMDB0133423			131837330
	48412	M	5	399.1074	2-{2-[(6-carboxy-3,4,5-trihydroxyoxan-2-yl)oxy]phenyl}-1??-chromen-1-ylium	C21H19O8			HMDB0133415			131837322
	64578	M	5	399.1074	8-[(6-carboxy-3,4,5-trihydroxyoxan-2-yl)oxy]-2-phenyl-1??-chromen-1-ylium	C21H19O8			HMDB0133422			131837329
	140646	M	5	399.1074	(6-carboxy-3,4,5-trihydroxyoxan-2-yl)[4-(2H-chromen-2-ylidene)cyclohexa-2,5-dien-1-ylidene]oxidanium	C21H19O8			HMDB0133420			131837328
	138697	M	5	399.1074	2-{3-[(6-carboxy-3,4,5-trihydroxyoxan-2-yl)oxy]phenyl}-1??-chromen-1-ylium	C21H19O8			HMDB0133418			131837325
	63210	M	5	399.1074	7-[(6-carboxy-3,4,5-trihydroxyoxan-2-yl)oxy]-2-phenyl-1??-chromen-1-ylium	C21H19O8			HMDB0133417			131837324
	161828	M	7	399.1067	Nocardicin E	C19H17N3O7	63555-59-9	C01739			65640	
	160642	M	7	399.1067	Nocardicin F	C19H17N3O7	63598-46-9	C17354			71628	
174.0113	0	M	0	0	No compounds found for experimental mass 174.0113 and adduct: M							
340.0393	0	M	0	0	No compounds found for experimental mass 340.0393 and adduct: M							
395.9974	0	M	0	0	No compounds found for experimental mass 395.9974 and adduct: M							
318.0275	0	M	0	0	No compounds found for experimental mass 318.0275 and adduct: M							
277.0643	0	M	0	0	No compounds found for experimental mass 277.0643 and adduct: M							
374.1077	165400	M	10	374.1114	Portulacaxanthin II	C18H18N2O7	135545-98-1				64473	
	173858	M	10	374.1114	Tyr-Ala-OH	C18H18N2O7					64984	
	173859	M	10	374.1114	Ser-Phe-OH	C18H18N2O7					65017	
	173860	M	10	374.1114	TyrMe-Gly-OH	C18H18N2O7					65080	
	173861	M	10	374.1114	Ala-TyrMe-OH	C18H18N2O7					65091	
	173862	M	10	374.1114	Phe-Thr-OH	C18H18N2O7					65109	
	173863	M	10	374.1114	HoPhe-Ser-OH	C18H18N2O7					65154	
	173864	M	10	374.1114	Abu-Tyr-OH	C18H18N2O7					65170	
	162998	M	10	374.1114	Portulacaxanthin II	C18H18N2O7		C08565				
	96310	M	10	374.1114	Portulacaxanthin II	C18H18N2O7			HMDB0012281			
586.0462	0	M	0	0	No compounds found for experimental mass 586.0462 and adduct: M							
450.0093	0	M	0	0	No compounds found for experimental mass 450.0093 and adduct: M							
325.9175	0	M	0	0	No compounds found for experimental mass 325.9175 and adduct: M							
492.11	0	M	0	0	No compounds found for experimental mass 492.11 and adduct: M							
250.9287	0	M	0	0	No compounds found for experimental mass 250.9287 and adduct: M							
435.024	0	M	0	0	No compounds found for experimental mass 435.024 and adduct: M							

Experimental mass	Identifier	Adduct	mz Error (ppm)	Molecular Weight	Name (proposed annotation by CEU Mass Mediator Batch Search)	Formula	CAS	Kegg	HMDB	LipidMaps	Metlin	PubChem
335.9392	0	M	0	0	No compounds found for experimental mass 335.9392 and adduct: M							
499.1724	156519	M	7	499.169	5-O-(Indol-3-ylacetyl-myo-inositol) D-galactoside	C22H29NO12		C04695			66241	
230.1419	162108	M	0	230.1419	Camoensine	C14H18N2O		C10758			68555	
	68110	M	0	230.1419	Ibudilast	C14H18N2O	50847-11-5		HMDB0015614		85552	3671
533.2945	0	M	0	0	No compounds found for experimental mass 533.2945 and adduct: M							
274.1499	167824	M	3	274.1507	trans-trismethoxy Resveratrol-d4	C17H14D4O3					96499	
246.067	117152	M	7	246.0652	5'-Deoxy-5-fluorouridine	C9H11FN2O5		C12739	HMDB0060406		44123	18343
	65729	M	7	246.0652	Floxuridine	C9H11FN2O5	50-91-9	C11736	HMDB0014467		4028	5790
201.9941	161302	M	3	201.9936	4-Sulfobenzoate; 4-Sulfobenzoic acid	C7H6O5S	636-78-2	C02236			65735	69469
373.9645	0	M	0	0	No compounds found for experimental mass 373.9645 and adduct: M							
470.1454	179372	M	5	470.1478	Nap-Phe-OH	C27H22N2O6					65011	
	179373	M	5	470.1478	Phe-Nap-OH	C27H22N2O6					65335	
	154564	M	6	470.1424	Plumieride	C21H26O12	511-89-7	C09797			67941	72319
451.1187	0	M	0	0	No compounds found for experimental mass 451.1187 and adduct: M							
541.1811	0	M	0	0	No compounds found for experimental mass 541.1811 and adduct: M							
760.0736	0	M	0	0	No compounds found for experimental mass 760.0736 and adduct: M							
565.3245	0	M	0	0	No compounds found for experimental mass 565.3245 and adduct: M							
588.0425	0	M	0	0	No compounds found for experimental mass 588.0425 and adduct: M							
303.1111	0	M	0	0	No compounds found for experimental mass 303.1111 and adduct: M							
410.0497	0	M	0	0	No compounds found for experimental mass 410.0497 and adduct: M							
550.071	0	M	0	0	No compounds found for experimental mass 550.071 and adduct: M							
1106.6089	10562	M	8	1106.6002	PIM2(16:0/14:0)	C51H95O23P				LMGP15010050		
403.0041	0	M	0	0	No compounds found for experimental mass 403.0041 and adduct: M							
483.9211	0	M	0	0	No compounds found for experimental mass 483.9211 and adduct: M							
555.2978	0	M	0	0	No compounds found for experimental mass 555.2978 and adduct: M							
696.167	0	M	0	0	No compounds found for experimental mass 696.167 and adduct: M							
298.0541	157379	M	0	298.0541	Quinalphos	C12H15N2O3PS	13593-03-8	C11030			68785	26124
	159226	M	0	298.0541	Phoxim	C12H15N2O3PS	14816-18-3	C18757			72530	9570290
808.0764	0	M	0	0	No compounds found for experimental mass 808.0764 and adduct: M							
516.1195	0	M	0	0	No compounds found for experimental mass 516.1195 and adduct: M							
445.1423	0	M	0	0	No compounds found for experimental mass 445.1423 and adduct: M							
496.9296	0	M	0	0	No compounds found for experimental mass 496.9296 and adduct: M							
494.9323	0	M	0	0	No compounds found for experimental mass 494.9323 and adduct: M							
539.1493	161271	M	8	539.1451	Piperacillin sodium; Pipracil	C23H26N5O7S.Na	59703-84-3	C07361				23666879
401.1081	162833	M	1	401.1087	Salbostatin 6'-phosphate	C13H24NO11P		C21211				
	59981	M	9	401.1045	Oxacillin	C19H19N3O5S	66-79-5	C07334	HMDB0014851		43286	6196
608.112	91775	M	8	608.1166	Prodelphinidin A1	C30H24O14			HMDB0036336		91480	14521015
1142.1776	0	M	0	0	No compounds found for experimental mass 1142.1776 and adduct: M							
481.9239	0	M	0	0	No compounds found for experimental mass 481.9239 and adduct: M							
724.2117	0	M	0	0	No compounds found for experimental mass 724.2117 and adduct: M							
776.5878	6672	M	7	776.5931	PG(P-20:0/17:0)	C43H85O9P				LMGP04030064	79968	
	6548	M	7	776.5931	PG(O-18:0/19:1(9Z))	C43H85O9P				LMGP04020033	79844	
	6564	M	7	776.5931	PG(O-20:0/17:1(9Z))	C43H85O9P				LMGP04020049	79860	
	6631	M	7	776.5931	PG(P-16:0/21:0)	C43H85O9P				LMGP04030023	79927	
	6652	M	7	776.5931	PG(P-18:0/19:0)	C43H85O9P				LMGP04030044	79948	
1104.1907	0	M	0	0	No compounds found for experimental mass 1104.1907 and adduct: M							
778.225	0	M	0	0	No compounds found for experimental mass 778.225 and adduct: M							

Supplementary Table S8: Search result from the accurate mass batch search (CEU mass mediator) of compounds found with higher abundance in ECM blank samples - RPLC ESI (+) mode

Experimental mass	Identifier	Adduct	mz Error (ppm)	Molecular Weight	Name (proposed annotation by CEU Mass Mediator Batch Search)	Formula	CAS	Kegg	HMDB	LipidMaps	Metlin	PubChem
472.3969	0	M	0	0	No compounds found for experimental mass 472.3969 and adduct: M							
106.0429	50140	M	10	106.0419	Benzaldehyde	C7H6O	100-52-7	C00193	HMDB0006115		58358	240
588.5283	0	M	0	0	No compounds found for experimental mass 588.5283 and adduct: M							
530.4495	0	M	0	0	No compounds found for experimental mass 530.4495 and adduct: M							
495.3371	2628	M	9	495.3325	PC(O-14:0/2:0)	C24H50NO7P				LMGP01020019	40048	
	2981	M	9	495.3325	PC(16:0/0:0)[rac]	C24H50NO7P				LMGP01050113	102768	
	4290	M	9	495.3325	PE(19:0/0:0)	C24H50NO7P				LMGP02050028	77694	
	2969	M	9	495.3325	PC(0:0/16:0)	C24H50NO7P			HMDB0240262	LMGP01050074	40340	
	163400	M	9	495.3325	PC(O-14:0/2:0)[U]	C24H50NO7P					40049	
	163401	M	9	495.3325	PC(16:0/0:0)[S]	C24H50NO7P					40285	
	163402	M	9	495.3325	PC(16:0/0:0)[U]	C24H50NO7P					40286	
	163403	M	9	495.3325	PC(0:0/16:0)[U]	C24H50NO7P					40341	
	2940	M	9	495.3325	PC(16:0/0:0)	C24H50NO7P			HMDB0010382	LMGP01050018	40284	460602
474.4127	0	M	0	0	No compounds found for experimental mass 474.4127 and adduct: M							
523.3681	4288	M	8	523.3638	PE(21:0/0:0)	C26H54NO7P				LMGP02050026	77692	
	164538	M	8	523.3638	PC(2:0/O-16:0)[U]	C26H54NO7P					40161	
	2641	M	8	523.3638	PC(O-16:0/2:0)	C26H54NO7P			HMDB0062195	LMGP01020046	40075	108156
	163439	M	8	523.3638	PC(O-16:0/2:0)[S]	C26H54NO7P					40076	
	163440	M	8	523.3638	PC(O-16:0/2:0)[U]	C26H54NO7P					40077	
	163441	M	8	523.3638	PC(18:0/0:0)[S]	C26H54NO7P					40293	
	163442	M	8	523.3638	PC(18:0/0:0)[U]	C26H54NO7P					40294	
	163443	M	8	523.3638	PC(0:0/18:0)[S]	C26H54NO7P					40343	
	163444	M	8	523.3638	PC(0:0/18:0)[U]	C26H54NO7P					40344	
	2944	M	8	523.3638	PC(18:0/0:0)	C26H54NO7P			HMDB0010384	LMGP01050026	40292	497299
	2970	M	8	523.3638	PC(0:0/18:0)	C26H54NO7P			HMDB0011128	LMGP01050076	40342	24779491
	163438	M	8	523.3638	enantio-PAF C-16	C26H54NO7P	117985-57-6				43413	
	165818	M	8	523.3638	PAF C-16	C26H54NO7P	74389-68-7				34488	
418.35	0	M	0	0	No compounds found for experimental mass 418.35 and adduct: M							
269.2054	167707	M	5	269.2039	dinor-12-oxo Phytodienoic Acid-d5	C16H19D5O3					96439	
429.3778	0	M	0	0	No compounds found for experimental mass 429.3778 and adduct: M							
474.4109	0	M	0	0	No compounds found for experimental mass 474.4109 and adduct: M							
462.3749	40290	M	9	462.3709	2alpha-(3-Hydroxypropyl)-1alpha,25-dihydroxy-19-norvitamin D3	C29H50O4				LMST03020627	42553	
	123016	M	9	462.3709	(3beta,22R,23R,24S)-3,22,23-Trihydroxystigmastan-6-one	C29H50O4			HMDB0039713		94268	73834440
	117689	M	9	462.3709	6-Deoxohomodolichosterone	C29H50O4			HMDB0034430		89932	13870434
164.0859	0	M	0	0	No compounds found for experimental mass 164.0859 and adduct: M							
148.0535	154485	M	7	148.0524	3-Hydroxy-1-indanone	C9H8O2	26976-59-0	C07720			66724	176448
	160196	M	7	148.0524	3-Isochromanone; 1,4-Dihydro-3H-2-benzopyran-3-one	C9H8O2	4385-35-7	C07728			44717	78092
	140583	M	7	148.0524	1-Phenyl-1,2-propanedione	C9H8O2	579-07-7	C17268	HMDB0035243		63534	11363
	43331	M	7	148.0524	Cinnamic acid	C9H8O2	621-82-9		HMDB0000567		310	5372954
	47243	M	7	148.0524	Di-2-furanylmethane	C9H8O2	1197-40-6		HMDB0032947		88849	70972
	140691	M	7	148.0524	trans-Cinnamic acid	C9H8O2	140-10-3	C00423	HMDB0000930		63104	444539
	106647	M	7	148.0524	(E)-3-(4-Hydroxyphenyl)-2-propenal	C9H8O2		C05608	HMDB0040986		44643	641301
	122277	M	7	148.0524	(E)-3-(2-Hydroxyphenyl)-2-propenal	C9H8O2			HMDB0031725		87897	5318169
	64249	M	7	148.0524	3,4-Dihydro-2H-1-benzopyran-2-one	C9H8O2	119-84-6	C02274	HMDB0036626		65745	660
	99592	M	7	148.0524	(2E)-3-(3-hydroxyphenyl)prop-2-enal	C9H8O2			HMDB0135274			6538957
	92456	M	7	148.0524	3-(2-hydroxyphenyl)prop-2-enal	C9H8O2			HMDB0134039			98373
	147513	M	7	148.0524	3-phenylprop-2-enoic acid	C9H8O2			HMDB0128078			8784
	83814	M	7	148.0524	3-phenyloxirane-2-carbaldehyde	C9H8O2			HMDB0135275			11194419
	89200	M	7	148.0524	(2Z)-2-hydroxy-3-phenylprop-2-enal	C9H8O2			HMDB0135273			13170418
	144544	M	7	148.0524	3-(4-hydroxyphenyl)prop-2-enal	C9H8O2			HMDB0135648			440733
	180755	M	7	148.0524	C9:5	C9H8O2						
467.3833	159033	M	9	467.3876	Lucidine B; Serratanine	C30H49N3O	71384-23-1	C09869			67977	442479
406.3306	0	M	0	0	No compounds found for experimental mass 406.3306 and adduct: M							
511.4097	0	M	0	0	No compounds found for experimental mass 511.4097 and adduct: M							

Experimental mass	Identifier	Adduct	mz Error (ppm)	Molecular Weight	Name (proposed annotation by CEU Mass Mediator Batch Search)	Formula	CAS	Kegg	HMDB	LipidMaps	Metlin	PubChem
599.4638	34053	M	9	599.4583	N-(3E-hexadecenoyl)-deoxysphing-4-enine-1-sulfonate	C34H65NO5S				LMSP00000003	53896	
773.2827	0	M	0	0	No compounds found for experimental mass 773.2827 and adduct: M							
687.5172	138062	M	4	687.5203	PE(15:0/P-18:1(11Z))	C38H74NO7P			HMDB0008918		60361	53479585
	111962	M	4	687.5203	PC(14:1(9Z)/P-16:0)	C38H74NO7P			HMDB0007928		59378	53478639
	93813	M	4	687.5203	PC(o-16:1(9Z)/14:1(9Z))	C38H74NO7P			HMDB0013410			53481703
	111515	M	4	687.5203	PE(15:0/P-18:1(9Z))	C38H74NO7P			HMDB0008919		60362	53479586
	132026	M	4	687.5203	PE(P-18:1(11Z)/15:0)	C38H74NO7P			HMDB0011403		62202	53480863
	141304	M	4	687.5203	PE(P-18:1(9Z)/15:0)	C38H74NO7P			HMDB0011436		62231	53480892
	2811	M	4	687.5203	PC(P-16:0/14:1(9Z))	C38H74NO7P			HMDB0011204	LMGP01030022	62034	52923876
	4177	M	4	687.5203	PE(P-16:0/17:1(9Z))	C38H74NO7P				LMGP02030016	77594	
	4200	M	4	687.5203	PE(P-18:0/15:1(9Z))	C38H74NO7P				LMGP02030039	77617	
	4087	M	4	687.5203	PE(O-16:0/17:2(9Z,12Z))	C38H74NO7P				LMGP02020029	77508	
606.3894	0	M	0	0	No compounds found for experimental mass 606.3894 and adduct: M							
736.6175	160286	M	2	736.6158	2-Methyl-6-solanyl-1,4-benzoquinol; 2-Methyl-6-nonaprenyl-benzene-1,4-diol; 2-Methyl-6-all-trans-nonaprenylbenzene-1,4-diol; 2-Methyl-6-solanesylbenzene-1,4-diol; MSBQ	C52H80O2		C17570			64000	44237185
700.549	34372	M	4	700.5519	SM(d16:1/18:1)	C39H77N2O6P				LMSP03010040	83741	
	34373	M	4	700.5519	SM(d18:1/16:1)	C39H77N2O6P				LMSP03010041	83742	
	34421	M	4	700.5519	SM(d18:2/16:0)	C39H77N2O6P				LMSP03010090	83790	
	34466	M	4	700.5519	PE-Cer(d14:2(4E,6E)/23:0)	C39H77N2O6P				LMSP03020041	103080	
	34470	M	4	700.5519	PE-Cer(d15:2(4E,6E)/22:0)	C39H77N2O6P				LMSP03020045	103084	
	34482	M	4	700.5519	PE-Cer(d16:2(4E,6E)/21:0)	C39H77N2O6P				LMSP03020057	103096	
292.2074	0	M	0	0	No compounds found for experimental mass 292.2074 and adduct: M							
490.2883	157995	M	10	490.293	Hemibrevetoxin B	C28H42O7	122271-91-4	C20016			73501	
	77140	M	10	490.2931	Macrocarpal I	C28H42O7	179388-54-6		HMDB0041587		95967	56776316
	41212	M	10	490.2931	Ximaosteroid D	C28H42O7				LMST05050007	84927	

Supplementary Table S9: Search result from the accurate mass batch search (CEU mass mediator) of compounds found with higher abundance in ECM blank samples - RPLC ESI (-) mode

Experimental mass	Identifier	Adduct	mz Error (ppm)	Molecular Weight	Name (proposed annotation by CEU Mass Mediator Batch Search)	Formula	CAS	Kegg	HMDB	LipidMaps	Metlin	PubChem
282.2589	0	M	0	0	No compounds found for experimental mass 282.2589 and adduct: M							
280.2444	0	M	0	0	No compounds found for experimental mass 280.2444 and adduct: M							
217.1082	52438	M	3	217.1076	5-Hydroxysebacate	C10H17O5			HMDB0029189			131750806
	153545	M	9	217.1063	N-Acetyl-L-citrulline	C8H15N3O4		C15532				656979
	165180	M	9	217.1063	N-a-Acetylcitrulline	C8H15N3O4	33965-42-3				5819	
	165181	M	9	217.1063	Gamma-glutamyl-Alanine	C8H15N3O4					86034	
	166735	M	9	217.1063	Ala Gly Ala	C8H15N3O4					16009	
	166736	M	9	217.1063	Ala Ala Gly	C8H15N3O4					17382	
	166737	M	9	217.1063	Gly Ala Ala	C8H15N3O4					18391	
	166738	M	9	217.1063	Gln Ala	C8H15N3O4					23736	
	166739	M	9	217.1063	Ala Gln	C8H15N3O4					23902	
	100400	M	9	217.1063	N-a-Acetylcitrulline	C8H15N3O4			HMDB0000856			11506771
	90074	M	9	217.1063	Alanyl-Glutamine	C8H15N3O4			HMDB0028685		85601	542027
	59638	M	9	217.1063	Alanyl-Gamma-glutamate	C8H15N3O4			HMDB0028701		85616	131750731
	147138	M	9	217.1063	Glutaminylalanine	C8H15N3O4			HMDB0028790		85704	9813211
	45418	M	10	217.1103	Glutethimide	C13H15NO2	77-21-4	C07489	HMDB0015505		66661	3487
	111595	M	10	217.1103	N-desisopropylpropranolol	C13H15NO2			HMDB0060961			159899
	153060	M	10	217.1103	Pyracarbolid	C13H15NO2	24691-76-7	C18914			72675	32597
	157421	M	10	217.1103	Securinine	C13H15NO2	5610-40-2	C10614			43991	442872
855.3034	0	M	0	0	No compounds found for experimental mass 855.3034 and adduct: M							
278.2271	31501	M	9	278.2246	10E,12E,14E-Hexadecatrienyl acetate	C18H30O2				LMFA07010350	46349	
	31503	M	9	278.2246	10E,12E,14Z-Hexadecatrienyl acetate	C18H30O2				LMFA07010352	46351	
	31504	M	9	278.2246	4E,6E,10Z-Hexadecatrienyl acetate	C18H30O2				LMFA07010353	46352	
	31505	M	9	278.2246	4E,6E,11Z-Hexadecatrienyl acetate	C18H30O2				LMFA07010354	46353	
	31511	M	9	278.2246	4E,6Z,10Z-Hexadecatrienyl acetate	C18H30O2				LMFA07010360	46359	
	31515	M	9	278.2246	13Z-Hexadecen-11-ynyl acetate	C18H30O2				LMFA07010364	46363	
	26399	M	9	278.2246	Columbinic acid	C18H30O2				LMFA01030815	45817	
	31521	M	9	278.2246	11Z,13E,15-Hexadecatrienyl acetate	C18H30O2				LMFA07010370	46369	
	27946	M	9	278.2246	Rumelenic acid	C18H30O2				LMFA02000299		
	27459	M	9	278.2246	Gorlic acid	C18H30O2				LMFA01140020	45900	
	26467	M	9	278.2246	Catalpic acid	C18H30O2				LMFA01030883	74419	
	26217	M	9	278.2246	Ximenynic acid	C18H30O2				LMFA01030560	74217	
	26218	M	9	278.2246	11Z-octadecen-9-ynoic acid	C18H30O2				LMFA01030561	74218	
	26219	M	9	278.2246	17-octadecen-9-ynoic acid	C18H30O2				LMFA01030562	74219	
	26004	M	9	278.2246	2E,9Z,12Z-octadecatrienoic acid	C18H30O2				LMFA01030339	74011	
	26005	M	9	278.2246	5,8,11-octadecatrienoic acid	C18H30O2				LMFA01030341	74012	
	26006	M	9	278.2246	5,9,12-octadecatrienoic acid	C18H30O2				LMFA01030342	74013	
	26007	M	9	278.2246	5Z,9Z,12E-octadecatrienoic acid	C18H30O2				LMFA01030343	74014	
	26008	M	9	278.2246	Pinolenic acid	C18H30O2				LMFA01030344		
	26009	M	9	278.2246	7E,9Z,12Z-octadecatrienoic acid	C18H30O2				LMFA01030345	74016	
	26010	M	9	278.2246	7Z,9Z,12Z-octadecatrienoic acid	C18H30O2				LMFA01030346	74017	
	25499	M	9	278.2246	16-methyl-6Z,9Z,12Z-heptadecatrienoic acid	C18H30O2				LMFA01020209	73655	
	26011	M	9	278.2246	9E,11Z,13Z-octadecatrienoic acid	C18H30O2				LMFA01030347	74018	
	26012	M	9	278.2246	9E,12E,15Z-octadecatrienoic acid	C18H30O2				LMFA01030348	74019	
	26013	M	9	278.2246	9E,12Z,15E-octadecatrienoic acid	C18H30O2				LMFA01030349	74020	
	26014	M	9	278.2246	9E,12Z,15Z-octadecatrienoic acid	C18H30O2				LMFA01030350	74021	
	26015	M	9	278.2246	9Z,12E,15E-octadecatrienoic acid	C18H30O2				LMFA01030351	74022	
	26016	M	9	278.2246	9Z,12E,15Z-octadecatrienoic acid	C18H30O2				LMFA01030352	74023	
	26017	M	9	278.2246	9Z,12Z,15E-octadecatrienoic acid	C18H30O2				LMFA01030353	74024	
	31692	M	9	278.2246	(E,E)-3,7,11-Trimethyl-2,6,10-dodecatrienyl propionate	C18H30O2				LMFA07010541	97247	
	25819	M	9	278.2246	Caleic acid	C18H30O2				LMFA01030140	73848	
	26331	M	9	278.2246	9E-Octadecen-12-ynoic acid	C18H30O2				LMFA01030741	74331	
	26332	M	9	278.2246	Crepenynic acid	C18H30O2		C07289		LMFA01030742	35331	5281024
	25821	M	9	278.2246	6,10,14-octadecatrienoic acid	C18H30O2				LMFA01030142	73849	
	25822	M	9	278.2246	Jacaric acid	C18H30O2				LMFA01030143	73850	
	39390	M	9	278.2246	estrane-3alpha,17alpha-diol	C18H30O2				LMST02010019	84283	

Experimental mass	Identifier	Adduct	mz Error (ppm)	Molecular Weight	Name (proposed annotation by CEU Mass Mediator Batch Search)	Formula	CAS	Kegg	HMDB	LipidMaps	Metlin	PubChem
	25824	M	9	278.2246	beta-calendic acid	C18H30O2				LMFA01030145	34819	
	25825	M	9	278.2246	Punicic acid	C18H30O2		C08364		LMFA01030146	34820	5281126
	25826	M	9	278.2246	alpha-eleostearic acid	C18H30O2		C08315		LMFA01030147	34821	5281115
	25827	M	9	278.2246	beta-eleostearic acid	C18H30O2				LMFA01030148	34822	
	25828	M	9	278.2246	9,12,14-octadecatrienoic acid	C18H30O2				LMFA01030151	73851	
	25830	M	9	278.2246	Elaidolinolenic acid	C18H30O2				LMFA01030153	34824	
	25831	M	9	278.2246	10,12,14-octadecatrienoic acid	C18H30O2				LMFA01030154	96766	
	25832	M	9	278.2246	Pseudoeleostearic acid	C18H30O2				LMFA01030155	96767	
	25833	M	9	278.2246	10,12,15-octadecatrienoic acid	C18H30O2				LMFA01030156	73852	
	26359	M	9	278.2246	octadeca-9Z,11E,14Z-trienoic acid	C18H30O2				LMFA01030773	45782	
	26361	M	9	278.2246	(R)-lamenallenic acid	C18H30O2				LMFA01030775	74349	
	26362	M	9	278.2246	(S)-lamenallenic acid	C18H30O2				LMFA01030776	74350	
	26363	M	9	278.2246	octadeca-11E,13E,15Z-trienoic acid	C18H30O2				LMFA01030777	45783	
	104503	M	9	278.2246	Linolenelaidic acid	C18H30O2	28290-79-1		HMDB0030964			860
	26504	M	9	278.2246	9E,11Z,13E-octadecatrienoic acid	C18H30O2			HMDB0030963	LMFA01030923		12309425
	25820	M	9	278.2246	gamma-Linolenic acid	C18H30O2		C06426	HMDB0003073	LMFA01030141	386	5280933
	25823	M	9	278.2246	alpha-calendic acid	C18H30O2			HMDB0030962	LMFA01030144	34818	5282818
	25829	M	9	278.2246	alpha-Linolenic acid	C18H30O2		C06427	HMDB0001388	LMFA01030152	192	5280934
	180701	M	9	278.2246	C18:3	C18H30O2						
	27945	M	9	278.2246	Isorumelenic acid	C18H30O2				LMFA02000298		
	27966	M	9	278.2246	3Z,6Z,9Z-Octadecatrienoic acid	C18H30O2				LMFA02000319		
	168002	M	9	278.2246	3E,9Z,12Z-Octadecatrienoic acid	C18H30O2					34815	
	168003	M	9	278.2246	6,10,14-Octadecatrienoic acid	C18H30O2					34816	
	168004	M	9	278.2246	8Z,10E,12Z-Octadecatrienoic acid	C18H30O2					34817	
	168005	M	9	278.2246	9,12,14-Octadecatrienoic acid	C18H30O2					34823	
	168006	M	9	278.2246	10,12,15-Octadecatrienoic acid	C18H30O2					34826	
	168007	M	9	278.2246	2E,9Z,12Z-octadecatrienoic acid	C18H30O2					35003	
	168008	M	9	278.2246	5,8,11-octadecatrienoic acid	C18H30O2					35005	
	168009	M	9	278.2246	5,9,12-octadecatrienoic acid	C18H30O2					35006	
	168010	M	9	278.2246	5Z,9Z,12E-octadecatrienoic acid	C18H30O2					35007	
	168011	M	9	278.2246	Pinolenic Acid	C18H30O2	16833-54-8				35008	
	168012	M	9	278.2246	7E,9Z,12Z-octadecatrienoic acid	C18H30O2					35009	
	168013	M	9	278.2246	7Z,9Z,12Z-octadecatrienoic acid	C18H30O2					35010	
	168014	M	9	278.2246	9E,11Z,13Z-octadecatrienoic acid	C18H30O2					35011	
	168015	M	9	278.2246	9E,12E,15Z-octadecatrienoic acid	C18H30O2					35012	
	168016	M	9	278.2246	9E,12Z,15E-octadecatrienoic acid	C18H30O2					35013	
	27473	M	9	278.2246	Isogorlic acid	C18H30O2				LMFA01140035		
	168017	M	9	278.2246	9E,12Z,15Z-octadecatrienoic acid	C18H30O2					35014	
	168018	M	9	278.2246	9Z,12E,15E-octadecatrienoic acid	C18H30O2					35015	
	168019	M	9	278.2246	9Z,12E,15Z-octadecatrienoic acid	C18H30O2					35016	
	168020	M	9	278.2246	9Z,12Z,15E-octadecatrienoic acid	C18H30O2					35017	
	168021	M	9	278.2246	11E-octadecen-9-ynoic acid	C18H30O2					35214	
	168022	M	9	278.2246	11Z-octadecen-9-ynoic acid	C18H30O2					35215	
	168023	M	9	278.2246	17-octadecen-9-ynoic acid	C18H30O2					35216	
	27480	M	9	278.2246	13-(2-Cyclopentenyl)-9Z-tridecenoic acid	C18H30O2				LMFA01140042		
	168024	M	9	278.2246	9E-Octadecen-12-ynoic acid	C18H30O2					35330	
	168025	M	9	278.2246	8-Hydroxy-15,16-Bisnor-11-Labden-13-One	C18H30O2					43976	
	27500	M	9	278.2246	2-(1,2-tetra-decadienyl)-cyclopropanecarboxylic acid	C18H30O2				LMFA01140062		
	164247	M	9	278.2246	octadeca-5S,6,16E-trienoic acid	C18H30O2					35004	
	164248	M	9	278.2246	octadeca-9Z,11E,15Z-trienoic acid	C18H30O2					45784	
	26556	M	9	278.2246	Alvaradoic acid	C18H30O2				LMFA01031029		
	26557	M	9	278.2246	Alvaradonic acid	C18H30O2				LMFA01031030		
	154052	M	9	278.2246	5beta-Estrane-3alpha,17beta-diol; 19-Nor-5beta-androstane-3alpha,17beta-diol	C18H30O2		C15201			41821	255697
	26566	M	9	278.2246	Xionenynic acid	C18H30O2				LMFA01031039		
	26574	M	9	278.2246	7E-Octadecen-9-ynoic acid	C18H30O2				LMFA01031047		
	26582	M	9	278.2246	3Z,9Z,12Z-Octadecatrienoic acid	C18H30O2				LMFA01031055		
254.2268	26392	M	9	254.2246	Hypogeic acid	C16H30O2				LMFA01030808	45810	

Experimental mass	Identifier	Adduct	mz Error (ppm)	Molecular Weight	Name (proposed annotation by CEU Mass Mediator Batch Search)	Formula	CAS	Kegg	HMDB	LipidMaps	Metlin	PubChem
	26438	M	9	254.2246	16:1(5Z)	C16H30O2				LMFA01030854	74390	
	25927	M	9	254.2246	10-hexadecenoic acid	C16H30O2				LMFA01030260	73935	
	25929	M	9	254.2246	cis-Palmitvaccenic acid	C16H30O2				LMFA01030262	73937	
	25930	M	9	254.2246	13-hexadecenoic acid	C16H30O2				LMFA01030263	73938	
	25932	M	9	254.2246	2Z-hexadecenoic acid	C16H30O2				LMFA01030265	34929	
	25933	M	9	254.2246	3E-hexadecenoic acid	C16H30O2				LMFA01030266	73941	
	25934	M	9	254.2246	Sapienic acid	C16H30O2				LMFA01030267	73942	
	25428	M	9	254.2246	2,4-dimethyl-2E-tetradecenoic acid	C16H30O2				LMFA01020133	73589	
	25434	M	9	254.2246	14-methyl-4-pentadecenoic acid	C16H30O2				LMFA01020140	73595	
	25435	M	9	254.2246	2-hexyl-2-decenoic acid	C16H30O2				LMFA01020141	73596	
	25436	M	9	254.2246	6-isopentyl-9-methyl-5-decenoic acic	C16H30O2				LMFA01020142	73597	
	26477	M	9	254.2246	15:1(4)(13Me)	C16H30O2				LMFA01030893	74429	
	26478	M	9	254.2246	16:1(4)	C16H30O2				LMFA01030894	74430	
	25739	M	9	254.2246	cis-10-palmitoleic acid	C16H30O2				LMFA01030058	34745	
	31642	M	9	254.2246	ethyl 7E-tetradecenoate	C16H30O2				LMFA07010491	97213	
	31643	M	9	254.2246	ethyl 9E-tetradecenoate	C16H30O2				LMFA07010492	97214	
	31645	M	9	254.2246	ethyl 9Z-tetradecenoate	C16H30O2				LMFA07010494	97215	
	31666	M	9	254.2246	dodecyl 2E-butenoate	C16H30O2				LMFA07010515	97225	
	31688	M	9	254.2246	(Z)-7-Dodecenyl butyrate	C16H30O2				LMFA07010537	97243	
	31434	M	9	254.2246	10E-Tetradecenyl acetate	C16H30O2				LMFA07010283	46282	
	31436	M	9	254.2246	11E-Tetradecenyl acetate	C16H30O2				LMFA07010285	46284	
	31437	M	9	254.2246	12E-Tetradecenyl acetate	C16H30O2				LMFA07010286	46285	
	31438	M	9	254.2246	3E-Tetradecenyl acetate	C16H30O2				LMFA07010287	46286	
	31439	M	9	254.2246	5E-Tetradecenyl acetate	C16H30O2				LMFA07010288	46287	
	31440	M	9	254.2246	6E-Tetradecenyl acetate	C16H30O2				LMFA07010289	46288	
	31441	M	9	254.2246	7E-Tetradecenyl acetate	C16H30O2				LMFA07010290	46289	
	31442	M	9	254.2246	8E-Tetradecenyl acetate	C16H30O2				LMFA07010291	46290	
	31444	M	9	254.2246	9E-Tetradecenyl acetate	C16H30O2				LMFA07010293	46292	
	32221	M	9	254.2246	Vittatalactone	C16H30O2				LMFA07040032	97389	
	31458	M	9	254.2246	10Z-Tetradecenyl acetate	C16H30O2				LMFA07010307	46306	
	31460	M	9	254.2246	11Z-Tetradecenyl acetate	C16H30O2				LMFA07010309	46308	
	31461	M	9	254.2246	12Z-Tetradecenyl acetate	C16H30O2				LMFA07010310	46309	
	31462	M	9	254.2246	3Z-Tetradecenyl acetate	C16H30O2				LMFA07010311	46310	
	31463	M	9	254.2246	5Z-Tetradecenyl acetate	C16H30O2				LMFA07010312	46311	
	31464	M	9	254.2246	6Z-Tetradecenyl acetate	C16H30O2				LMFA07010313	46312	
	31465	M	9	254.2246	7Z-Tetradecenyl acetate	C16H30O2				LMFA07010314	46313	
	31466	M	9	254.2246	8Z-Tetradecenyl acetate	C16H30O2				LMFA07010315	46314	
	31467	M	9	254.2246	9Z-Tetradecenyl acetate	C16H30O2				LMFA07010316	46315	
	32241	M	9	254.2246	15R-Hexadecanolide	C16H30O2				LMFA07040052	97405	
	32243	M	9	254.2246	16-Hexadecanolide	C16H30O2				LMFA07040054	97407	
	32244	M	9	254.2246	delta-hexadecalactone	C16H30O2				LMFA07040055	97408	
	25928	M	9	254.2246	Lycopodic acid	C16H30O2			HMDB0037647	LMFA01030261	73936	5312413
	25931	M	9	254.2246	13Z-hexadecenoic acid	C16H30O2			HMDB0035877	LMFA01030264	73939	5312416
	75875	M	9	254.2246	5-Dodecyldihydro-2(3H)-furanone	C16H30O2	730-46-1		HMDB0031145		87443	97747
	25735	M	9	254.2246	Gaidic acid	C16H30O2			HMDB0010735	LMFA01030054	34742	5282743
	25736	M	9	254.2246	7Z-palmitoleic acid	C16H30O2			HMDB0002186	LMFA01030055	34743	5318393
	25737	M	9	254.2246	cis-9-palmitoleic acid	C16H30O2		C08362	HMDB0003229	LMFA01030056	188	445638
	25738	M	9	254.2246	trans-9-palmitoleic acid	C16H30O2			HMDB0012328	LMFA01030057	34744	5282745
	31924	M	9	254.2246	Citronellyl hexanoate	C16H30O2			HMDB0038958	LMFA07010816	93569	114416
	111800	M	9	254.2246	15-Hexadecanolide	C16H30O2			HMDB0031711		87885	543385
	94922	M	9	254.2246	(Z)-5-Hexadecenoic acid	C16H30O2			HMDB0032638		88581	13105359
	107503	M	9	254.2246	(Z)-14-Methyl-6-pentadecenoic acid	C16H30O2			HMDB0041422		95819	87508980
	26609	M	9	254.2246	6E-Hexadecenoic acid	C16H30O2			HMDB0031053	LMFA01031082		5282744
	147443	M	9	254.2246	(E)-3-Hexadecenoic acid	C16H30O2			HMDB0033791		89535	5355370
	180632	M	9	254.2246	C16:1	C16H30O2						
	27482	M	9	254.2246	6,7-methylene-pentadecanoic acid	C16H30O2				LMFA01140044		
	164214	M	9	254.2246	hexadec-7Z-enoic acid	C16H30O2					74346	
	167369	M	9	254.2246	10-Hexadecenoic acid	C16H30O2					34924	

Experimental mass	Identifier	Adduct	mz Error (ppm)	Molecular Weight	Name (proposed annotation by CEU Mass Mediator Batch Search)	Formula	CAS	Kegg	HMDB	LipidMaps	Metlin	PubChem
	167370	M	9	254.2246	11-Hexadecenoic acid	C16H30O2					34925	
	167371	M	9	254.2246	11Z-Hexadecenoic acid	C16H30O2					34926	
	167372	M	9	254.2246	13-Hexadecenoic acid	C16H30O2					34927	
	167373	M	9	254.2246	13Z-Hexadecenoic acid	C16H30O2					34928	
	167374	M	9	254.2246	3E-Hexadecenoic acid	C16H30O2					34930	
	167375	M	9	254.2246	6Z-Hexadecenoic acid	C16H30O2					34931	
	167376	M	9	254.2246	cis-7-Hexadecenoic Acid	C16H30O2	2416-19-5				45058	
	167377	M	9	254.2246	?2-trans-Hexadecenoic Acid	C16H30O2	929-79-3				96484	
	167378	M	9	254.2246	?2-cis-Hexadecenoic Acid	C16H30O2	2825-68-5				96485	
	26608	M	9	254.2246	8Z-Hexadecenoic acid	C16H30O2				LMFA01031081		
304.2431	39429	M	9	304.2402	Methandriol	C20H32O2		C14493		LMST02020012	41839	229021
	39438	M	9	304.2402	Mestanolone	C20H32O2				LMST02020027	41846	
	26400	M	9	304.2402	2E,8Z,11Z,14Z-Eicosatetraenoic acid	C20H32O2				LMFA01030816	74352	
	26401	M	9	304.2402	5(E)-Arachidonic acid	C20H32O2				LMFA01030817	74353	
	25635	M	9	304.2402	16:3(2E,10E,12E)(3Me,5Me[R],7My,15Me)	C20H32O2				LMFA01020367	73777	
	25648	M	9	304.2402	17:4(2E,4E,9E,11E)(8Me[R],10Me,15Me[R])	C20H32O2				LMFA01020381	73790	
	27445	M	9	304.2402	8-[3]-ladderane-octanoic acid	C20H32O2				LMFA01140006	74893	
	590	M	9	304.2402	(+)-Serradiol	C20H32O2				LMPR0104150006	53642	
	26455	M	9	304.2402	20:4(5Z,13Z,16Z,19Z)	C20H32O2				LMFA01030871	74407	
	26488	M	9	304.2402	17:4(2E,4E,9E,11E)(7Me[R],10Me,13Me[S])	C20H32O2				LMFA01030905	74440	
	26489	M	9	304.2402	16:3(2E,9E,11E)(3Me,5Me[S],7My,15Me)	C20H32O2				LMFA01030906	74441	
	636	M	9	304.2402	(-)-Cladiella||ine	C20H32O2				LMPR0104210003	53661	
	646	M	9	304.2402	(-)-Amijiol	C20H32O2				LMPR0104250001	53671	
	647	M	9	304.2402	(-)-Isoamijiol	C20H32O2				LMPR0104250002	53672	
	678	M	9	304.2402	Taxa-4(20),11(12)-dien-5alpha,13alpha-diol	C20H32O2		C11897		LMPR0104390005	41259	443487
	25512	M	9	304.2402	18-methyl-5Z,8Z,11Z,14Z-nonadecatetraenoic acid	C20H32O2				LMFA01020222	73668	
	682	M	9	304.2402	Isotrinervidiol	C20H32O2				LMPR0104400003	53699	
	26288	M	9	304.2402	7,13-Eicosadiynoic acid	C20H32O2				LMFA01030687	74288	
	26289	M	9	304.2402	8,11-Eicosadiynoic acid	C20H32O2				LMFA01030688	24087	
	26290	M	9	304.2402	10,13-Eicosadiynoic acid	C20H32O2				LMFA01030689	74290	
	696	M	9	304.2402	Acutilol A	C20H32O2		C09057		LMPR0104470001	53713	441999
	706	M	9	304.2402	(-)-Reiswigin A	C20H32O2				LMPR0104530002	53723	
	26052	M	9	304.2402	4,7,10,13-Eicosatetraenoic acid	C20H32O2				LMFA01030389	74056	
	26053	M	9	304.2402	4Z,7Z,10Z,13Z-eicosatetraenoic acid	C20H32O2				LMFA01030390	74057	
	26054	M	9	304.2402	4Z,8Z,11Z,14Z-eicosatetraenoic acid	C20H32O2				LMFA01030391	74058	
	26055	M	9	304.2402	5,11,14,17-Eicosatetraenoic acid	C20H32O2				LMFA01030392	74059	
	26056	M	9	304.2402	5,8,11,14-eicosatetraenoic acid	C20H32O2				LMFA01030393	74060	
	26057	M	9	304.2402	Juniperonic acid	C20H32O2				LMFA01030394	74061	
	26058	M	9	304.2402	8Z,11Z,14Z,18Z-eicosatetraenoic acid	C20H32O2				LMFA01030395	74062	
	25847	M	9	304.2402	4,8,12,16-eicosatetraenoic acid	C20H32O2				LMFA01030173	73864	
	25848	M	9	304.2402	6,10,14,18-eicosatetraenoic acid	C20H32O2				LMFA01030175	73865	
	25849	M	9	304.2402	8,11,14,17-eicosatetraenoic acid	C20H32O2				LMFA01030176		
	79374	M	9	304.2402	Sideridiol	C20H32O2			HMDB0036702		91734	12315540
	83987	M	9	304.2402	Drostanolone	C20H32O2	58-19-5	C14605	HMDB0014996		70197	6011
	93716	M	9	304.2402	Junicedral	C20H32O2			HMDB0036830		91843	131752060
	26402	M	9	304.2402	omega-3-Arachidonic acid	C20H32O2			HMDB0002177	LMFA01030818	74354	11722594
	43320	M	9	304.2402	Yucalexin P21	C20H32O2			HMDB0036754		91781	14191208
	39494	M	9	304.2402	Mesterolone	C20H32O2			HMDB0006036	LMST02020107	57837	15020
	115274	M	9	304.2402	Oryzalexin S	C20H32O2			HMDB0039687		94242	131752705
	25683	M	9	304.2402	Arachidonic acid	C20H32O2		C00219	HMDB0001043	LMFA01030001	193	444899

Experimental mass	Identifier	Adduct	mz Error (ppm)	Molecular Weight	Name (proposed annotation by CEU Mass Mediator Batch Search)	Formula	CAS	Kegg	HMDB	LipidMaps	Metlin	PubChem
	101717	M	9	304.2402	Oryzalexin E	C20H32O2		C21561	HMDB0039702		94257	86289490
	146831	M	9	304.2402	Copalic acid	C20H32O2	20257-75-4		HMDB0036829		91842	131752059
	62411	M	9	304.2402	ent-17-Hydroxy-16beta-kauran-19-al	C20H32O2			HMDB0036721		91751	3481851
	46288	M	9	304.2402	7,13-Eperudien-15-oic acid	C20H32O2			HMDB0037824		92634	131752241
	180735	M	9	304.2402	C20:4	C20H32O2						
	151303	M	9	304.2402	17-Methyl-5alpha-androst-2-ene-1alpha,17beta-diol	C20H32O2		C15176			70666	254634
	161596	M	9	304.2402	2-Ketoepimanool	C20H32O2		C09124			67447	442052
	151377	M	9	304.2402	3beta-Methoxyandrost-5-en-16beta-ol	C20H32O2		C15367			70839	234498
	161138	M	9	304.2402	17beta-Hydroxy-4alpha-methyl-5alpha-androstan-3-one; 4,5alpha-Dihydro-4alpha-methyltestosterone	C20H32O2		C15252			70729	11954137
	169103	M	9	304.2402	4,8,12,16-Eicosatetraenoic acid	C20H32O2					34842	
	169104	M	9	304.2402	6,10,14,18-Eicosatetraenoic acid	C20H32O2					34843	
	169105	M	9	304.2402	8,11,14,17-Eicosatetraenoic acid	C20H32O2					34844	
	169106	M	9	304.2402	4,7,10,13-Eicosatetraenoic acid	C20H32O2					35052	
	169107	M	9	304.2402	4Z,7Z,10Z,13Z-eicosatetraenoic acid	C20H32O2					35053	
	169108	M	9	304.2402	4Z,8Z,11Z,14Z-eicosatetraenoic acid	C20H32O2					35054	
	169109	M	9	304.2402	5,11,14,17-Eicosatetraenoic acid	C20H32O2					35055	
	169110	M	9	304.2402	5,8,11,14-Eicosatetraenoic acid / 5,8,11,14-icosatetraenoic acid	C20H32O2					35056	
	169111	M	9	304.2402	5Z,11Z,14Z,17Z-eicosatetraenoic acid	C20H32O2					35057	
	169112	M	9	304.2402	8Z,11Z,14Z,18Z-eicosatetraenoic acid	C20H32O2					35058	
	169113	M	9	304.2402	Stearidonic Acid ethyl ester	C20H32O2	119798-44-6				44955	
	169114	M	9	304.2402	omega-3 Arachidonic Acid	C20H32O2	24880-40-8				62952	
	158369	M	9	304.2402	3alpha-Hydroxy-2alpha-methyl-5alpha-androstan-17-one; 2alpha-Methylandrosterone	C20H32O2		C14956			70455	247863
	164284	M	9	304.2402	8, 11, 14, 17-icosatetraenoic acid C20:4n-3,6,9,12	C20H32O2					73866	
	154072	M	9	304.2402	Dihydroabietic acid	C20H32O2	19407-37-5	C17920			71945	44150026
	26596	M	9	304.2402	7Z,11Z,14Z,17Z-Eicosatetraenoic acid	C20H32O2				LMFA01031069		
	161823	M	10	304.2402	ent-2alpha,3alpha-Dihydroxyisokaurene	C20H32O2		C21831				
	150105	M	10	304.2402	Abieta-7,13-dien-18,18-diol	C20H32O2		C20329				
	157869	M	10	304.2402	ent-Cassa-12,15-diene-2beta,3beta-diol	C20H32O2		C21829				
	160998	M	10	304.2402	Oryzalexin D; ent-Sandaracopimaradiene-3beta,7alpha-diol	C20H32O2	110268-98-9	C21562				
635.3081	63112	M	3	635.3101	Glycylserylprolylmethionylphenylalanylvalinamide	C29H45N7O7S			HMDB0033242		89109	71338674
769.3248	0	M	0	0	No compounds found for experimental mass 769.3248 and adduct: M							
955.2965	0	M	0	0	No compounds found for experimental mass 955.2965 and adduct: M							
801.3306	0	M	0	0	No compounds found for experimental mass 801.3306 and adduct: M							
330.2585	152125	M	8	330.2559	Ethyl icosapentate; Eicosapentaenoic acid, ethyl ester	C22H34O2	73310-10-8	C13364				
	25856	M	8	330.2559	7,10,13,16,19-docosapentaenoic acid	C22H34O2				LMFA01030184	73872	
	39683	M	8	330.2559	1alpha-hydroxy-23,24,25,26,27-pentanorvitamin D3 / 1alpha-hydroxy-23,24,25,26,27-pentanorcholecalciferol	C22H34O2				LMST03020009	41950	
	39684	M	8	330.2559	22-hydroxy-23,24,25,26,27-pentanorvitamin D3 / 22-hydroxy-23,24,25,26,27-pentanorcholecalciferol	C22H34O2				LMST03020010	41951	
	27452	M	8	330.2559	10-[5]-ladderane-decanoic acid	C22H34O2				LMFA01140013	45895	
	677	M	8	330.2559	Taxa-4(20),11(12)-dien-5alpha-yl acetate	C22H34O2		C11896		LMPR0104390004	41258	443486
	29359	M	8	330.2559	docosapentaenoic acid	C22H34O2				LMFA04000049	46021	
	25854	M	8	330.2559	4,7,10,13,16-docosapentaenoic acid	C22H34O2				LMFA01030182	73870	
	25855	M	8	330.2559	4,8,12,15,19-docosapentaenoic acid	C22H34O2				LMFA01030183	73871	
	79885	M	8	330.2559	Ethyl abietate	C22H34O2	631-71-0		HMDB0032257		88305	61182
	121613	M	8	330.2559	4,8,12,15,19-Docosapentaenoic acid	C22H34O2	2548-85-8		HMDB0039133		194	102281
	114984	M	8	330.2559	1-Phenyl-1,3-hexadecanedione	C22H34O2			HMDB0035581		90861	19900903
	96073	M	8	330.2559	ent-16-Kauren-19-ol acetate	C22H34O2			HMDB0035024		90383	537596
	29358	M	8	330.2559	DPA	C22H34O2		C16513	HMDB0006528	LMFA04000044	24096	5497182
	29373	M	8	330.2559	22:5(4Z,7Z,10Z,13Z,16Z)	C22H34O2			HMDB0001976	LMFA04000064	75223	6441454
	31971	M	8	330.2559	Ethyl icosapentate	C22H34O2		C16184	HMDB0039530	LMFA07010877	45153	9831415
	57595	M	8	330.2559	2-Methyl-5-(8,11-pentadecadienyl)-1,3-benzenediol	C22H34O2			HMDB0038909		93522	131752491
	180768	M	8	330.2559	C22:5	C22H34O2						

Experimental mass	Identifier	Adduct	mz Error (ppm)	Molecular Weight	Name (proposed annotation by CEU Mass Mediator Batch Search)	Formula	CAS	Kegg	HMDB	LipidMaps	Metlin	PubChem
	153007	M	8	330.2559	17beta-Hydroxy-4,4,17-trimethylandrost-5-en-3-one	C22H34O2		C15413			70882	225742
	29384	M	8	330.2559	Clupadonic acid	C22H34O2				LMFA04000082		
	170486	M	8	330.2559	4,7,10,13,16-Docosapentaenoic acid	C22H34O2					34850	
	170487	M	8	330.2559	4,8,12,15,19-Docosapentaenoic acid	C22H34O2					34851	
	170488	M	8	330.2559	7,10,13,16,19-Docosapentaenoic acid	C22H34O2					34852	
	155134	M	8	330.2559	2-Methyl-5alpha-androst-2-en-17beta-ol acetate	C22H34O2		C15421			70890	249474
461.295	179157	M	4	461.293	AMC Arachidonoyl Amide	C30H39NO3					45116	

Supplementary Table S10: Significantly and relevantly regulated features detected upon 5-flurouracil treatment - all modes

Experiment	Analytical mode	Observed mass [1)]	Retention time (min)	Spearman correlation coefficient	p-value	BH adjusted p-value	Fold change (control sample vs. blank)	Assignment [2)]
1	HILIC ESI (+)	257.1015	3.19	0.81	3.12E-05	1.21E-03	41.0	2'-O-Metylcytidine
1	HILIC ESI (+)	203.1161	7.61	-0.91	9.83E-08	1.53E-05	225.5	Acetylcarnitine
1	HILIC ESI (+)	315.2420	3.35	0.73	3.53E-04	4.77E-03	43.1	Acylcarnitine 10:0
1	HILIC ESI (+)	399.3355	2.61	0.87	1.36E-06	1.06E-04	1.9	Acylcarnitine 16:0
1	HILIC ESI (+)	231.1465	5.95	-0.91	9.83E-08	1.53E-05	245.9	Acylcarnitine 4:0
1	HILIC ESI (+)	287.2098	3.90	0.74	2.72E-04	4.45E-03	33.0	Acylcarnitine 8:0
1	HILIC ESI (+)	111.0438	3.19	0.81	2.15E-05	1.11E-03	25.2	Cytosine, in-source fragment of 2'-O-methylcytidine
1	HILIC ESI (+)	251.1015	2.42	-0.84	5.35E-06	3.33E-04	91.1	2'-Deoxyadenosine
1	HILIC ESI (+)	268.0830	4.91	0.73	4.21E-04	5.23E-03	33.5	Inosine
1	HILIC ESI (+)	633.4745	3.82	-0.80	4.00E-05	1.38E-03	8.8	LysoPC 26:1
1	HILIC ESI (+)	259.1771	4.91	0.88	7.64E-07	7.92E-05	3.8	na
1	HILIC ESI (+)	301.2968	2.37	-0.74	2.72E-04	4.45E-03	3.7	na
1	HILIC ESI (+)	467.3002	5.08	-0.71	7.10E-04	7.79E-03	2.1	na
1	HILIC ESI (+)	481.3174	5.28	-0.73	3.53E-04	4.77E-03	8.9	na
1	HILIC ESI (+)	607.3818	2.83	-0.73	3.90E-04	5.06E-03	8.7	na
1	HILIC ESI (+)	607.4553	3.88	-0.77	1.00E-04	2.79E-03	9.2	na
1	HILIC ESI (+)	649.4659	2.23	-0.79	5.83E-05	1.81E-03	9.0	na
1	HILIC ESI (+)	663.4956	7.40	-0.72	4.53E-04	5.42E-03	66.1	na
1	HILIC ESI (+)	705.4915	2.32	0.76	1.57E-04	3.04E-03	1.7	na
1	HILIC ESI (+)	705.4932	2.32	0.76	1.57E-04	3.04E-03	1.7	na
1	HILIC ESI (+)	737.4976	2.22	-0.73	3.53E-04	4.77E-03	67.8	na
1	HILIC ESI (+)	748.5363	3.53	0.81	2.50E-05	1.11E-03	3.0	na
1	HILIC ESI (+)	779.5651	2.07	0.74	3.02E-04	4.70E-03	15.0	na
1	HILIC ESI (+)	301.1895	3.49	0.76	1.57E-04	3.04E-03	1.8	na
1	HILIC ESI (+)	677.4972	2.14	-0.77	1.17E-04	2.79E-03	314.9	PC 28:0
1	HILIC ESI (+)	687.4865	2.37	-0.77	1.17E-04	2.79E-03	11.9	PC 29:2
1	HILIC ESI (+)	689.4963	2.35	-0.72	5.76E-04	6.63E-03	61.4	PE 32:1
1	HILIC ESI (+)	717.5288	2.29	-0.74	2.72E-04	4.45E-03	22.1	PE 34:1
1	HILIC ESI (+)	713.5029	2.33	-0.71	7.26E-04	7.79E-03	35.8	PE 34:3
2	HILIC ESI (+)	257.1024	3.27	0.93	2.72E-09	2.28E-07	52.6	2'-O-Metylcytidine
2	HILIC ESI (+)	165.0648	3.65	0.73	2.66E-04	7.42E-03	105.9	7-Methylguanine
2	HILIC ESI (+)	217.1318	6.79	-0.85	2.70E-06	1.00E-04	52.5	Acylcarnitine 3:0
2	HILIC ESI (+)	231.1471	5.94	-0.93	2.72E-09	2.28E-07	219.2	Acylcarnitine 4:0
2	HILIC ESI (+)	231.1474	6.14	-0.88	2.33E-07	1.11E-05	12.2	na
2	HILIC ESI (+)	111.0435	3.27	0.92	6.88E-09	4.61E-07	39.5	Cytosine, in-source fragment of 2'-O-methylcytidine
2	HILIC ESI (+)	251.1040	2.45	-0.94	9.64E-10	1.61E-07	803.6	2'-Deoxyadenosine
2	HILIC ESI (+)	633.4732	3.73	-0.71	5.07E-04	1.21E-02	11.4	LysoPC 26:1
2	HILIC ESI (+)	281.1115	7.92	0.74	1.66E-04	5.07E-03	6.5	1-Methyladenosine
2	HILIC ESI (+)	118.0288	2.45	-0.94	9.64E-10	1.61E-07	8.9	na
2	HILIC ESI (+)	304.0793	2.61	0.92	1.58E-08	8.84E-07	21.7	na
2	HILIC ESI (+)	635.4869	3.65	-0.71	4.12E-04	1.06E-02	7.8	na
2	HILIC ESI (+)	702.5661	2.89	-0.85	2.70E-06	1.00E-04	9.7	na
2	HILIC ESI (+)	243.1473	5.82	-0.76	1.01E-04	3.38E-03	40.9	Tiglylcarnitine
3	HILIC ESI (+)	257.1027	3.16	0.81	1.74E-05	8.67E-04	30.6	2'-O-Metylcytidine
3	HILIC ESI (+)	111.0434	3.16	0.78	4.41E-05	1.47E-03	72.1	Cytosine, in-source fragment of 2'-O-methylcytidine
3	HILIC ESI (+)	111.0431	4.41	-0.83	6.01E-06	5.14E-04	214.9	Cytosine, in-source fragment of deoxycytidine
3	HILIC ESI (+)	251.1024	2.40	-0.83	6.01E-06	5.14E-04	165.8	2'-Deoxyadenosine
3	HILIC ESI (+)	227.0898	4.41	-0.83	6.01E-06	5.14E-04	18.4	Deoxycytidine
3	HILIC ESI (+)	268.0826	4.87	0.88	4.05E-07	1.21E-04	13.9	Inosine
3	HILIC ESI (+)	281.1114	7.87	0.83	6.01E-06	5.14E-04	25.8	1-Methyladenosine
3	HILIC ESI (+)	113.0728	2.40	-0.79	3.28E-05	1.15E-03	6.2	na
3	HILIC ESI (+)	136.0383	2.55	0.80	2.41E-05	9.59E-04	15.4	na
3	HILIC ESI (+)	225.0988	7.63	-0.74	2.11E-04	5.05E-03	66.0	na
3	HILIC ESI (+)	229.1786	6.57	0.82	8.71E-06	5.79E-04	31.6	na
3	HILIC ESI (+)	282.0977	2.55	0.82	8.71E-06	5.79E-04	201.8	na
3	HILIC ESI (+)	285.1939	4.19	0.92	1.58E-08	9.47E-06	5.4	na
3	HILIC ESI (+)	293.0871	7.65	-0.77	7.73E-05	2.31E-03	25.7	na
3	HILIC ESI (+)	319.0928	4.28	0.79	3.28E-05	1.15E-03	29.5	na
3	HILIC ESI (+)	511.4590	2.22	0.80	2.41E-05	9.59E-04	3.3	na
3	HILIC ESI (+)	537.4747	2.19	0.81	1.74E-05	8.67E-04	31.6	na
3	HILIC ESI (+)	539.4897	2.15	0.77	7.73E-05	2.31E-03	13.5	na
3	HILIC ESI (+)	590.2098	2.54	0.81	1.24E-05	7.42E-04	10.2	na
3	HILIC ESI (+)	591.1970	3.15	0.74	2.11E-04	5.05E-03	12.0	na
3	HILIC ESI (+)	605.4426	3.96	-0.72	3.32E-04	7.35E-03	3.4	na
3	HILIC ESI (+)	631.4581	3.88	-0.73	2.66E-04	6.11E-03	13.3	na

Experiment	Analytical mode	Observed mass [1)]	Retention time (min)	Spearman correlation coefficient	p-value	BH adjusted p-value	Fold change (control sample vs. blank)	Assignment [2)]
3	HILIC ESI (+)	719.5585	2.34	-0.71	4.12E-04	8.79E-03	7.3	na
3	HILIC ESI (+)	765.6260	2.11	0.80	2.41E-05	9.59E-04	5.8	na
3	HILIC ESI (+)	813.6211	2.12	0.76	1.01E-04	2.87E-03	8.2	na
3	HILIC ESI (+)	834.5270	5.96	-0.83	6.01E-06	5.14E-04	53.5	na
3	HILIC ESI (+)	1389.0732	2.09	-0.74	2.11E-04	5.05E-03	191.6	na
3	HILIC ESI (+)	1433.0547	2.09	-0.74	2.11E-04	5.05E-03	31.1	na
1	HILIC ESI (-)	228.0710	2.13	0.86	2.21E-06	3.30E-04	5.6	2'-Deoxyuridine
1	HILIC ESI (-)	133.0218	2.13	0.87	1.44E-06	3.30E-04	2.5	na
1	HILIC ESI (-)	536.1845	2.17	0.78	7.56E-05	4.52E-03	7.3	na
1	HILIC ESI (-)	553.2678	3.31	0.72	5.62E-04	2.80E-02	3.7	na
1	HILIC ESI (-)	291.0671	2.13	0.84	8.39E-06	8.36E-04	14.0	na
1	HILIC ESI (-)	264.0481	2.13	0.83	1.23E-05	9.19E-04	21.3	related to uracil -> Fragment 111.0211
2	HILIC ESI (-)	228.0733	2.12	0.85	2.70E-06	4.20E-04	10.3	2'-Deoxyuridine
2	HILIC ESI (-)	536.1939	2.17	0.84	4.07E-06	4.22E-04	3.3	na
2	HILIC ESI (-)	264.0518	2.12	0.85	1.75E-06	4.20E-04	2.2	related to uracil -> Fragment 111.0211
3	HILIC ESI (-)	228.0751	2.12	0.78	1.50E-04	2.58E-02	20.7	2'-Deoxyuridine
3	HILIC ESI (-)	297.1078	4.27	0.74	4.66E-04	2.58E-02	29.5	na
3	HILIC ESI (-)	281.1127	7.85	0.73	6.53E-04	2.84E-02	9.8	1-Methyladenosine
3	HILIC ESI (-)	137.9986	2.12	0.75	2.98E-04	2.58E-02	2.1	na
3	HILIC ESI (-)	146.0223	3.05	0.73	6.36E-04	2.84E-02	2.3	na
3	HILIC ESI (-)	304.0593	4.87	0.80	7.79E-05	2.37E-02	2.3	na
3	HILIC ESI (-)	312.1329	2.10	0.74	5.08E-04	2.58E-02	4.7	na
3	HILIC ESI (-)	318.1796	2.09	0.74	4.66E-04	2.58E-02	16.1	na
3	HILIC ESI (-)	514.0662	2.36	0.74	4.94E-04	2.58E-02	2.1	na
3	HILIC ESI (-)	658.2132	3.11	-0.82	3.46E-05	2.11E-02	1.5	na
3	HILIC ESI (-)	757.4781	2.16	0.76	2.31E-04	2.58E-02	79.3	na
3	HILIC ESI (-)	834.5261	5.95	-0.74	4.03E-04	2.58E-02	7.3	na
3	HILIC ESI (-)	868.1227	2.36	0.74	4.27E-04	2.58E-02	16.6	na
3	HILIC ESI (-)	926.0830	2.37	0.77	1.96E-04	2.58E-02	7.5	na
3	HILIC ESI (-)	264.0521	2.11	0.71	9.97E-04	3.79E-02	9.9	related to uracil -> Fragment 111.0211
3	HILIC ESI (-)	112.0260	2.12	0.71	9.97E-04	3.79E-02	4.9	Uracil, in-source fragment of 2'-deoxyuridine
1	RPLC ESI (+)	691.5586	7.42	-0.74	2.72E-04	8.11E-03	8.6	na
1	RPLC ESI (+)	677.5040	5.97	-0.81	2.15E-05	3.20E-03	54.8	PC 28:0
1	RPLC ESI (+)	705.5382	6.81	-0.72	5.76E-04	9.53E-03	58.6	PC 30:0
1	RPLC ESI (+)	729.5382	6.45	-0.72	5.62E-04	9.53E-03	33.4	PC 32:2
1	RPLC ESI (+)	703.5198	6.33	-0.77	1.10E-04	5.46E-03	93.2	PC 33:4
1	RPLC ESI (+)	703.5203	6.20	-0.76	1.48E-04	5.51E-03	96.4	PC 33:4
1	RPLC ESI (+)	809.6006	7.94	0.73	3.53E-04	8.76E-03	47.2	PC 38:4
1	RPLC ESI (+)	807.5855	7.76	0.73	4.42E-04	9.41E-03	11.3	PC 38:5
1	RPLC ESI (+)	777.5680	9.05	0.78	7.32E-05	5.46E-03	37.8	PE (P-18:0/22:5)
2	RPLC ESI (+)	755.5465	7.01	-0.75	1.30E-04	8.30E-03	26.9	na
2	RPLC ESI (+)	789.5285	9.11	-0.74	2.11E-04	8.30E-03	10.1	na
2	RPLC ESI (+)	865.5346	8.37	0.71	4.12E-04	8.30E-03	7.9	na
2	RPLC ESI (+)	729.5312	6.50	-0.74	2.11E-04	8.30E-03	17.6	PC 32:2
2	RPLC ESI (+)	783.5790	7.67	0.71	4.12E-04	8.30E-03	25.7	PC 36:3
2	RPLC ESI (+)	769.5630	8.75	-0.72	3.32E-04	8.30E-03	51.8	PE 38:3
3	RPLC ESI (+)	170.1414	1.11	0.71	5.07E-04	7.22E-03	19.4	na
3	RPLC ESI (+)	691.5140	7.59	-0.85	2.70E-06	2.50E-04	5.0	na
3	RPLC ESI (+)	691.5494	7.27	-0.74	2.11E-04	3.91E-03	21.4	na
3	RPLC ESI (+)	771.6125	8.75	0.74	1.66E-04	3.85E-03	22.3	na
3	RPLC ESI (+)	791.6121	7.58	-0.74	2.11E-04	3.91E-03	7.7	na
3	RPLC ESI (+)	801.6592	10.62	0.74	1.66E-04	3.85E-03	5.6	na
3	RPLC ESI (+)	823.6790	8.87	0.71	5.07E-04	7.22E-03	8.5	na
3	RPLC ESI (+)	855.7062	11.78	0.74	1.66E-04	3.85E-03	11.3	na
3	RPLC ESI (+)	869.6628	8.50	0.80	2.41E-05	1.11E-03	8.9	na
3	RPLC ESI (+)	705.5299	6.68	-0.82	8.71E-06	5.37E-04	102.7	PC 30:0
3	RPLC ESI (+)	733.5596	7.58	-0.85	2.70E-06	2.50E-04	6.9	PC 32:0
3	RPLC ESI (+)	785.5901	8.13	0.74	1.66E-04	3.85E-03	24.5	PC 36:2
3	RPLC ESI (+)	717.5324	7.86	-0.72	3.32E-04	5.58E-03	30.8	PE 34:1

[1)] nonunique features reported by the batch recursive feature extraction preprocessing workflow
[2)] for annotation details see Supplementary Tables S2-S5
na, not assigned; PC, phosphatidylcholine; PE, phosphatidylethanolamine

Supplementary Table S11: Used chemicals and reagents

Chemical/reagent/ingredient	Manufacturer	Article number
Acetonitrile	Carl Roth GmbH & Co KG	HN40.1
Methanol	Carl Roth GmbH & Co KG	HN41.1
Methyl tert-butyl ether	Sigma-Aldrich	650560-1L
2-Propanol	Sigma-Aldrich	34965-1L
Formic acid (distilled in glasware prior to use)	Sigma-Aldrich	27001-M
Ammonium acetate	Sigma-Aldrich	73594-100G-F
5-Fluorouracil	Sigma-Aldrich	F-6627
Advanced DMEM/F-12	Fisher Scientific GmbH	12634028
GlutaMAX™ Supplement	Fisher Scientific GmbH	35050061
PEN STREP,10000UNITS	Fisher Scientific GmbH	15140122
B-27 supplement serumfree (50x)	Fisher Scientific GmbH	17504044
N-2 supplement (100x)	Fisher Scientific GmbH	17502048
N-Acetyl-L-cysteine	SIGMA-Aldrich GmbH	A7250-50G
Animal-Free Recombinant Human EGF	PeproTech GmbH	AF-100-15
Y-27632 2HCl	Absource Diagnostics GmbH	S1049
Amphotericin B solution	Sigma-Aldrich	A2942
HEPES	Carl Roth GmbH & Co KG	9105.3
TrypLE™ Express Enzyme (1X), no phenol red	Thermo Fisher Scientific	12604013
Corning™ Matrigel™ Growth Factor Reduced, Basement Membrane Matrix, Phenol Red-free, LDEV-free	Corning B.V.	356231
CellTiter-Glo 3D cell viability assay	Promega	G9681
NucRed™ Dead 647 ReadyProbes™ Reagent	Thermo Fisher Scientific	R37113

6.2. Manuskript in Vorbereitung

Performance comparison of narrow-bore and capillary liquid-chromatography for non-targeted metabolomics profiling of small sample amounts by LC-QTOF-MS

Sylvia K. Neef [1], Stefan Winter [1], Ute Hofmann [1], Thomas E. Mürdter [1], Matthias Schwab [1,2,3] and Mathias Haag [1]

[1] *Dr. Margarete Fischer-Bosch-Institute of Clinical Pharmacology, Stuttgart, Germany and University of Tuebingen, Tuebingen, Germany*
[2] *Departments of Clinical Pharmacology, and of Pharmacy and Biochemistry, University of Tuebingen, Tuebingen, Germany*
[3] *Cluster of Excellence iFIT (EXC 2180) „Image-Guided and Functionally Instructed Tumor Therapies“, University of Tuebingen, Germany*

Short Communication

Performance comparison of narrow-bore and capillary liquid-chromatography for non-targeted metabolomics profiling of small sample amounts by LC-QTOF-MS

Sylvia K. Neef [1], Stefan Winter [1], Ute Hofmann 1, Thomas E. Mürdter [1], Matthias Schwab [1,2,3] and Mathias Haag [1,*]

[1] Dr. Margarete Fischer-Bosch-Institute of Clinical Pharmacology, Stuttgart, Germany and University of Tuebingen, Tuebingen, Germany
[2] Departments of Clinical Pharmacology, and of Pharmacy and Biochemistry, University of Tuebingen, Tuebingen, Germany
[3] Cluster of Excellence iFIT (EXC 2180) „Image-Guided and Functionally Instructed Tumor Therapies", University of Tuebingen, Germany

*Corresponding Author:
Dr. rer. nat. Mathias Haag
Dr. Margarete Fischer-Bosch-Institute of Clinical Pharmacology
Auerbachstr. 112
70376 Stuttgart, Germany
Phone +49 (0)711 / 8101-5429
Fax +49 (0)711 / 85 92 95
Mail: mathias.haag@ikp-stuttgart.de

Abstract

Liquid chromatography quadrupole time-of-flight mass spectrometry (LC-QTOF-MS) is a powerful tool for metabolic phenotyping of clinical samples and is increasingly used to find diagnostic or prognostic biomarkers. In this context, the samples used for analysis are often available in limited quantities, and therefore metabolomics studies could benefit from the use of highly sensitive systems with reduced column inner diameters and low flow rates, such as capillary liquid chromatography (CapLC), to examine rare clinical samples. In the present work, the suitability of a new CapLC system for non-targeted metabolomics analysis of small sample amounts was evaluated based on extracts of porcine formalin-fixed, paraffin-embedded (FFPE) tissue samples. The performance was assessed with respect to the number of features as well as the analytical repeatability, the signal-to-noise ratio and the signal intensity of 16 annotated metabolites. The results were compared with a well established narrow-bore LC system. No meaningful difference in the number of detected features could be observed between the systems. Further, while the signal areas of all evaluated metabolites were increased (max. 18-fold increase) by using CapLC, the signal-to-noise ratio was only improved in 50% of the metabolites. In addition, the analytical repeatability (median CV = 11.8%) was poor for the CapLC system compared to narrow-bore LC (median CV = 2.9%) when FFPE tissue extracts were analyzed. In contrast, significantly better reproducibility (median CV = 5.2%) and up to 80-fold increase in signal intensity were observed in the analysis of pure bile acid standard solutions. Even if the observed improvement for specific bile acids (e.g. taurocholic acid) must be evaluated in biological matrix, the platform comparison indicate, that the tested CapLC system is more suitable for specific targeted analyses than for non-targeted metabolomics of rare clinical samples.

Introduction

In the field of chromatography technology, miniaturized systems have been increasingly developed in the last decades, which are mainly used in combination with electrospray ionization mass spectrometry (ESI-MS) [1]. By reducing the inner diameter (i.d.) of the chromatographic column, a lower flow rate is required for the mobile phase. This causes less dilution of the injected sample band, resulting in an increase of the concentration in the ion source of the MS and thus an increase of the sensitivity [2,3]. Other advantages include a potential improvement in chromatographic efficiency and resolution [2,4], as well as much lower consumption of solvents, reducing the cost of their purchase and disposal. Therefore, liquid chromatography (LC) systems with reduced flow rates are a valuable tool for trace level applications [5] or when only small amounts of sample are available [6]. Non-targeted metabolomics studies for the discovery of potential prognostic and diagnostic biomarkers are often based on rare clinical samples. In some applications, e.g., working with tumor organoid cultures [7], laser-microdissected tissue [8] or slices of formalin-fixed, paraffin-embedded (FFPE) material [9], only a limited number of cells are available for analysis. In this context, the application of low-flow chromatographic systems such as capillary liquid chromatography (CapLC) is desirable.

In this work, we used a new LC system, which consisted of a Zirconium™ CUBE Autosampler (Prolab, Reinach, Switzerland), a Zirconium™ Ultra Nano- and Micro-UHPLC Pump (Prolab) as well as a custom-made micro-ESI interface (Prolab), and compared its performance for non-targeted metabolomics of small sample amounts by LC-QTOF-MS to a well-established narrow-bore LC platform [7,10,11]. The quality of the analyses was evaluated based on a porcine FFPE kidney tissue extract with regard to the following parameters: the numbers of detected features; the S/N ratios (as commonly accepted measure for analytical

sensitivity [12]); the peak area and height, (as measure for signal intensity [13]); as well as the analytical repeatability. The latter four parameters were evaluated based on 16 annotated metabolites belonging to the classes of lysophosphatidylethanolamines (LysoPE), amino acids, purine derivatives, nucleosides and organic acids.

Furthermore, in independent experiments, the influence of the chromatographic gradient (ratio of solvents A and B) on the CapLC-QTOF-MS analysis of bile acid reference substances was investigated.

Materials and Methods

Chemicals and Reagents

Ultra LC−MS grade acetonitrile (ACN) and methanol (MeOH) were purchased from Carl Roth GmbH & Co KG (Karlsruhe, Germany). Formic acid (FA) and ammonium acetate (AmAc) were purchased from Sigma-Aldrich (Taufkirchen, Germany). Pure water was in-house produced by a Milli-Q system (Millipore, Billerica, MA, USA) and used for the preparation of aqueous solvents. Glycocholic acid (GCA), glycolithocholic acid (GLCA), taurocholic acid (TCA) and taurolithocholic acid (TLCA) were purchased from Sigma-Aldrich (Taufkirchen, Germany).

Sample Preparation

For CapLC method optimization, bile acid working solutions were prepared as described [14] and diluted with ACN/water (95:5, *v*/*v*) to obtain the following final concentrations [pmol/µl]: GCA, 0.5; GLCA, 0.06; TCA, 0.1; TLCA, 0.06. FFPE tissue samples were prepared from porcine kidney as previously described using porcine FFPE kidney tissue samples fixed for 120 days in formalin [11].

95 **CapLC- QTOF-MS Analysis**

96 The CapLC setup consisted of a Zirconium™ CUBE Autosampler (Prolab, Reinach,
97 Switzerland) and a Zirconium™ Ultra Nano- and Micro-UHPLC System (Prolab) connected to
98 a 6550 iFunnel QTOF mass spectrometer (Agilent Technologies, Waldbronn, Germany)
99 equipped with a customized prototype micro-ESI interface (Prolab). A custom-packed
100 analytical HILIC column (0.3 mm x 150 mm) prepared by Dr. Maisch GmbH (Ammerbuch,
101 Germany) from a commercially available HILIC column (Acquity UPLC BEH Amide Column,
102 1.7 µm, 2.1 mm × 150 mm Waters, Eschborn, Germany) was used.

103 Gradient elution at a flow rate of 5 µL/min with a total run time of 30 min per sample, was
104 applied (mobile phase A: 5 mM AmAc and 0.06% FA in water:ACN 5:95, v/v; mobile phase
105 B: 5 mM AmAc and 0.06% FA in water:ACN 1:1, v/v) as follows: 0−3 min, 5% B; 3−18 min,
106 5−95% B; 18−30 min, 95% B. Column equilibration time was set to 5 min. Separation was
107 performed at ambient temperature. The autosampler was operated at 6 °C and ACN/water (95:5,
108 *v*/*v*) was used for both wash channels. The injection volume was set to 1 µL. To this end, the
109 "shift volume" of the injector was manually adjusted (tested range: 2−4 µL) and set to 3.5 µL
110 to obtain a maximum peak area. Glass vials (2 mL) containing 250 µL glass inserts with
111 polymer feets (Agilent Technologies, Waldbronn, Germany), covered with preslit
112 polytetrafluoroethylene (PTFE)/silicone screw caps (Agilent Technologies, Waldbronn,
113 Germany) were used for injection of samples.

114 The QTOF mass spectrometer was operated by the Mass Hunter Data Acquisition Software
115 (version B.08.00). Electrospray parameters were as follows: gas temperature, 150 °C; drying
116 gas flow, 11 L/min; nebulizer pressure, 40 psig; VCap voltage, 2800 V. Further QTOF
117 operation parameters in MS and MS/MS mode were set as described [10] and negative
118 ionization mode was used. Prior analysis, the axially aligned position of the micro-ESI

119 interface, in front of the spray shield, was manually optimized. Therefore a syringe-pump (flow
120 rate of 5 µL bile acid standard solution/min, see section Sample Preparation) was directly
121 connected to the ESI spray unit and the position was adjusted to achieve maximum signal
122 intensity.

123 **Narrow-bore LC-QTOF-MS Analysis**

124 The narrow-bore LC-QTOF-MS analysis in negative ionization mode was performed as
125 described [10], with slightly adjusted modifier concentrations of the chromatographic solvents
126 [7]. The injection volume was set to 1 µL.

127 **Data Preprocessing and Analysis**

128 Data preprocessing was carried out by using the Mass Hunter Profinder Software (version
129 B.08.00, Agilent Technologies).

130 Non-targeted feature extraction by Batch Recursive Feature Extraction was applied as
131 described [7]. The intensity threshold was set to 500 counts. For protocol assessment based on
132 annotated metabolites, Batch Targeted Feature Extraction on the basis of structurally assigned
133 metabolites [10] was used as described [7]. With respect to CapLC data, Batch Targeted Feature
134 Extraction based on molecular formulas was performed without retention time matching.

135 The signal-to-noise (S/N) ratio was automatically calculated for a single representative
136 sample using the Qualitative Analysis Software (version B. 07.00, Agilent Technologies). The
137 signal was defined to the height and noise definition was set to peak-to-peak (the noise value
138 for each noise range is computed as the difference between the highest and lowest abundance
139 values in that noise region and the largest of those noise values is then reported as the overall
140 noise value). The noise region with a desired length of 1 min and a minimum length of 0.1 min
141 was automatically detected. Calculations were performed using Microsoft Excel 2016.

142 **Metabolite Identification and Annotation**

143 Metabolite annotation was performed as described [7]. With respect to CapLC, for targeted
144 matching score calculation, the following weightings were used: mass score: 100%; isotope
145 abundance score: 60%; isotope spacing score: 50% and retention time score: 0%. In addition,
146 available fragment spectra (acquired in the porcine FFPE sample extract used for performance
147 evaluation) were matched to reference spectra present in the MassBank of North America
148 MS/MS Similarity Search (https://mona.fiehnlab.ucdavis.edu/), the CEU Mass Mediator
149 MS/MS Search [15,16] or in the METLIN Metabolite PCDL (Version B.07.00, Agilent
150 Technologies). Annotated metabolites with retention time information and assignment levels
151 proposed by the Metabolomics Standard Initiative (MSI) [17] are provided in Supplementary
152 Table 1.

153 ## Results and Discussion

154 To achieve the best possible comparability of the two LC systems used, both systems were
155 operated with columns of the same length (150 mm) and the identical stationary phase (BEH
156 Amide HILIC material, particle size: 1.7 µm, manufactured by Waters). In addition, the same
157 amount of sample extract was injected (1 µL) and the flow gradient as well as the QTOF-MS
158 analysis were designed as similarly as possible.

159 Figure 1 A displays typical total ion chromatograms (TICs) obtained after the analysis of
160 porcine FFPE kidney tissue extracts by narrow-bore or CapLC-QTOF-MS. It is evident that the
161 total intensity is much higher in the TIC obtained for narrow-bore LC (blue line, ~ 1.3 x 10^7
162 counts) than in the CapLC TIC (black line, ~ 0.3 x 10^7 counts). However, the difference in the
163 TICs of the methods did not result in a meaningful difference in the number of detected features.
164 Thus, 140 features could be detected using the CapLC and 141 using the narrow-bore LC.

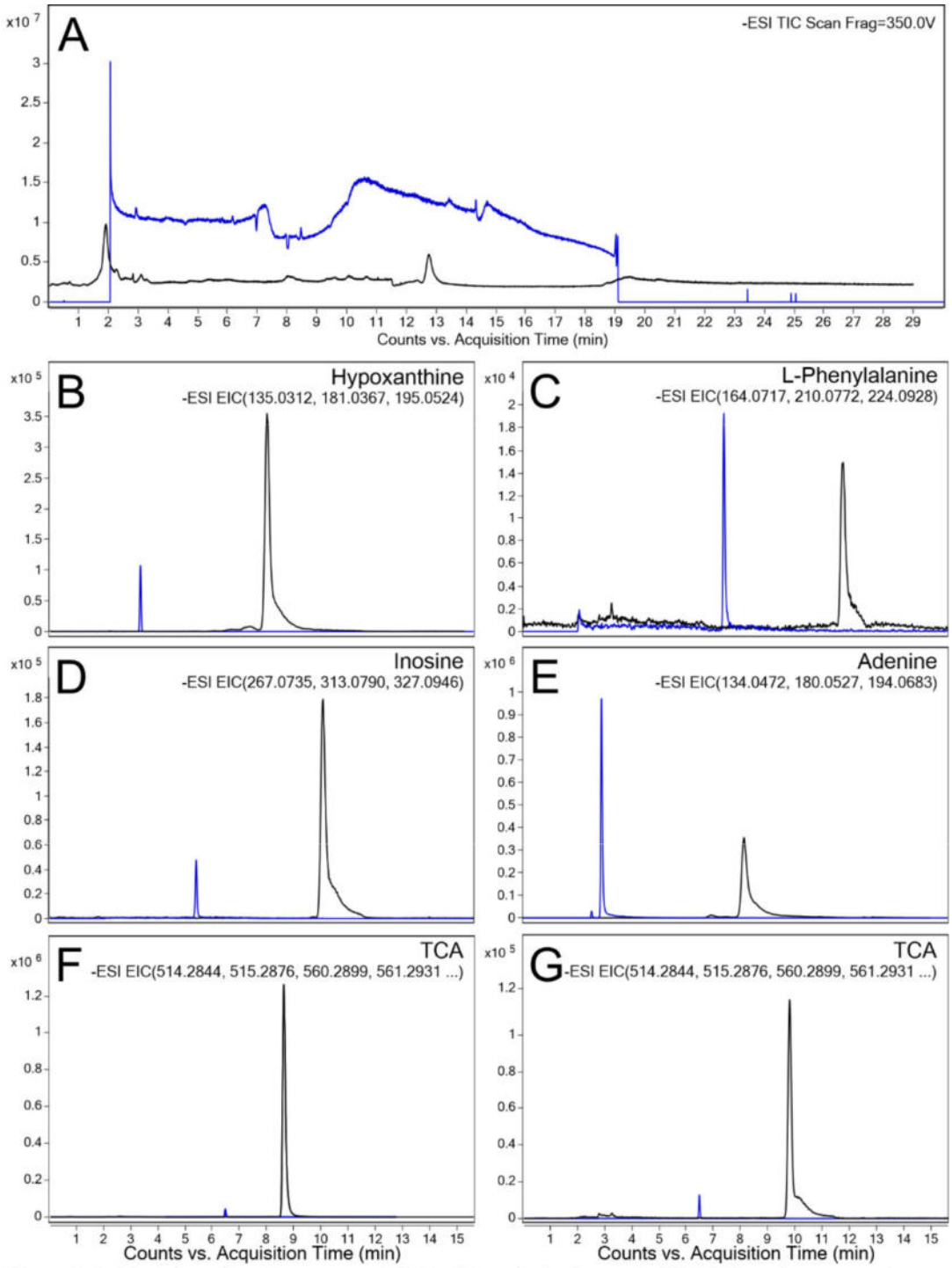

Figure 1. (A) Typical total ion chromatogram (TICs) of the analysis of a porcine FFPE kidney tissue extract by narrow-bore LC-QTOF-MS (blue) and CapLC-QTOF-MS (black) in ESI (−) mode, as well as typical extracted ion chromatograms (EICs) of (B) hypoxanthine, (C) L-phenylalanine, (D) inosine and (E) adenine. Further EICs from narrow-bore LC-QTOF-MS (blue) and CapLC-QTOF-MS (black) analysis in ESI (−) mode: (F) a standard solution containing 0.2 pmol TCA/µl analyzed using the same conditions as described in the methods section with an adjusted gradient elution (0-3 min, 2% B; 3-10 min, 2-95% B; 10-30 min, 95% B) used for CapLC; (G) a standard solution containing 0.1 pmol TCA/µl using the same conditions as described in the methods section (CapLC gradient: 0–3 min, 5% B; 3–18 min, 5–95% B; 18–30 min, 95% B).

For this comparison, all detectable metabolites eluting between D-pantothenic acid (early elution, see Table 1) and L-carnitine (late elution, see Table 1) were used. This was done as in the narrow-bore LC measurements (see Figure 1 A, blue line) the flow was directed into the solvent waste during the first 2 min, as well as from minute 19 onwards, which is a method to protect the analytical column and the ion source from contamination by unwanted matrix components and is commonly used in LC-MS based analysis of complex samples [18,19]. With the Cap LC system used, it is technically not possible to discharge the LC flow into waste.

Table 1. Results for signal intensity (area ratio and height ratio), sensitivity (S/N ratio) and analytical repeatability of annotated metabolites analyzed in porcine FFPE tissue extracts by narrow-bore LC and CapLC-QTOF-MS

Metabolite	**Narrow-bore LC**			**Cap LC**			**System Comparison Parameters**		
	RT [min]	CV[1] [%]	S/N ratio	RT [min]	CV[1] [%]	S/N ratio	Area Ratio[2]	Height Ratio[3]	Fold Change[4] of S/N Ratios
Adenine	2.9	1.7	462	8.2	8.9	9	2	0.4	1
Adenosine	3.3	2.1	9	8.4	8.3	8	9	2	3
D-Pantothenic acid	3.1	2.4	30	5.4	11.5	12	3	0.6	1
Guanosine	7.3	4.3	12	11.8	9.4	9	9	2	3
Hypoxanthine	3.4	1.3	77	8.0	8.9	9	16	3	1
Inosine	5.4	1.8	24	10.1	11.8	12	18	4	5
Lactate	4.0	10.9	34	8.0	18.6	19	3	2	0.4
L-Carnitine	8.9	14.0	4	13.5	20.2	20	7	2	2
L-Isoleucine	7.7	8.2	10	12.2	27.1	27	5	3	1
L-Leucine	7.4	6.3	20	11.9	19.4	19	3	0.4	2
L-Phenylalanine	7.4	5.2	23	11.8	20.7	21	3	0.8	1
LysoPE 16:0	6.0	3.5	15	9.5	22.0	22	7	1	2
LysoPE 18:0	5.6	2.1	77	9.3	11.8	12	10	2	1
LysoPE 20:4	5.8	1.2	96	9.4	21.6	22	8	1	1
Succinate	3.4	7.6	6	4.9	11.0	11	8	2	4
Uridine	3.3	1.7	7	7.9	8.4	8	15	3	3

[1] Coefficients of variation of areas across repeated injections ($n = 4$)
[2] (Mean area CapLC/Mean area narrow-bore LC), mean determined across four sample injections each
[3] (Mean height CapLC/Mean height narrow-bore LC), mean determined across four sample injections each
[4] (S/N ratio CapLC/ S/N ratio narrow-bore LC), determined across one sample injection each
RT, retention time; S/N, signal-to-noise ratio, CV, coefficient of variation

As demonstrated by the fold change between the S/N ratios (see Table 1) the sensitivity was improved for 50% of the metabolites. The strongest effect was observed for the nucleosides adenosine, guanosine, uridine and inosine (3 to 5-fold increase in the S/N ratio) and for

191 succinate (4-fold increase in the S/N ratio). For the metabolites belonging to the lysoPEs, amino
192 acids and organic acids, no or only a slight improvement in sensitivity could be achieved in the
193 CapLC analysis (quotient of S/N ratios = 1–2, see Table 1). Lactate, whose S/N ratio was
194 reduced (quotient of S/N ratios = 0.4), is an exception here.
195 In terms of signal intensity, the peak area of all metabolites was increased compared to the
196 narrow-bore LC as displayed by the area ratio calculated between the mean areas of four
197 repeated injections of the porcine FFPE kidney tissue extract (see Table 1). However signal
198 height was reduced for four metabolites (adenine, D-pantothenic acid, L-leucin and L-
199 phenylalanine) as indicated by height ratios <1 (see Table 1 and Figure 1 C and E).
200 The partially reduced height can be attributed to the relatively poor peak shape (broad peaks
201 and tailing). The peak height represents the maximum signal intensity (maximum ion count
202 achieved in the ion source at one time point), while the area sums up all achieved intensities
203 over the time of compound elution. As the area of all metabolites used for intensity evaluation
204 is higher by using CapLC, signal height would also be increased after optimization of
205 chromatographic conditions (e.g., gradient or column material).

206 The effect of adjusting the gradient on signal intensity was investigated in independent
207 experiments by analyzing bile acid reference solutions. Using a steeper flow gradient (0–3 min,
208 2% B; 3–10 min, 2–95% B; 10–30 min, 95% B), an up to 79-fold increase in signal intensity
209 (determined by the area ratio, $n = 1$, see Figure 1 F) was obtained for TCA. In comparison, the
210 flatter gradient (0–3 min, 5% B; 3–18 min, 5–95% B; 18–30 min, 95% B), which was also used
211 in the analysis of porcine FFPE tissue samples, achieved an area quotient ($n = 1$; see Figure 1
212 G) of 33. The adjustment of the chromatographic conditions also led to a significant
213 improvement of the peak shape and a reduction of the observed tailing (compare Figure 1 F
214 with Figure 1 G). Even though this increase in intensity was accompanied by a slight decrease
215 in the S/N ratio from 86 (narrow-bore LC) to 79 (CapLC), this result shows that under more

optimal chromatographic conditions a remarkable increase in the signal intensity of certain metabolites is possible by using the CapLC system tested here.

In this context it should be mentioned, that the customized ESI-interface used did not allow the use of the column oven. The temperature is an important parameter in the optimization of HILIC methods [20]. Therefore, after a technical optimization of the ESI interface, the influence of the temperature on the peak shape and thus on the signal intensity and S/N ratio should be evaluated.

However, our experiments show that the performance of CapLC analysis, in terms of signal intensity and sensitivity, varies between different metabolite classes. With the exception of adenine, a clear increase in signal intensity was observed for all metabolites belonging to the purines and nucleosides (adenosine, guanosine, hypoxanthine, inosine and uridine), although the S/N ratio of hypoxanthine (see Figure 1 B) was not improved. The analysis of the lysoPE species showed a rather moderate improvement of signal intensity and S/N ratio. In contrast, the evaluated parameters were in the case of amino acids and organic acids only slightly or not improved (see exemplary Figure 1 C). Overall, the strongest improvement in S/N ratio and signal intensity was observed for inosine (see Figure 1 D) while the least favorable was observed for adenine (see Figure 1 E).

In terms of analytical repeatability, for each of the 16 metabolites assessed, the variation in the CapLC (median CV = 11.8%) was stronger compared to the narrow-bore LC (median CV = 2.9%, see Table 1). In the case of five metabolites (31%), a CV > 20% was determined, whereas all CVs were < 15% when using the narrow-bore LC system. Nevertheless, the CVs determined were largely within an acceptable range of CV < 20% for non-targeted metabolomics analyses [21]. In this context it should be mentioned, that the analytical precision in the field of non-targeted metabolomics is typically determined by repeated injections of a

240 pooled QC sample at regular intervals over the analytical batch. However, in the course of the
241 comparative measurements carried out here, it was found that the current software version of
242 the CapLC system does not allow a return to a previously measured sample within the analytical
243 batch.

244 However, by analyzing bile acid standard solutions better analytical repeatability (median
245 CV [%]: GCA, 4.2; GLCA, 6.2; TCA, 4.0; TLCA, 7.1, median, 5.2) was observed. It remains
246 to be verified whether the analytical repeatability, satisfactory in our experiments for bile acid
247 standard solutions, can also be reproduced in biological matrix. In addition, it must be verified
248 whether the analytical repeatability for other metabolites can be improved by adapting the
249 method (e.g. modifiers in the mobile phase [22]) or instrumentation used (e.g. equipping the
250 customized ESI-interface by ACN enriched nitrogen gas supply to enhance ionization
251 efficiency and spray stability [23]).

252 ## Conclusion

253 In summary, it can be concluded that by using the CapLC system evaluated here for
254 individual metabolites (e.g. nucleosides), a significant increase in signal intensity and an
255 improvement in the S/N ratios could be achieved. In addition, the analysis of certain metabolites
256 (e.g. adenosine and uridine in porcine FFPE tissue extracts as well as the bile acids GCA,
257 GLCA, TCA and TLCA in reference solutions) is possible with satisfactory analytical
258 precision. However, a significant disadvantage of the tested CapLC system is the fact that the
259 current software does not offer the possibility to repeatedly inject from one and the same vial
260 over the course of a analytical batch. Since for non-targeted metabolomics the repeated injection
261 of QC samples is a core element for monitoring analytical precision (and also correction of
262 signal fluctuations in the course of the measurement series), the system tested here can only be
263 used if there is enough sample to fill a separate vial for each QC injection. For this reason, the

tested system in the current software configuration seems to be suitable for non-targeted metabolomics analyses only in a limited way.

However, the results of this study indicate that the CapLC system used could be suitable for specific targeted metabolomics approaches. For example, the targeted analysis of metabolites with particularly low concentrations, such as oxylipins in plasma and platelets [5], supported by stable isotope-labelled internal standards, would be a conceivable application. Furthermore, the targeted analysis of specific classes of metabolites (e.g. lysophosphatidylcholines and sphingomyelins) previously identified as differential metabolites between the renal tumor subtypes of clear cell and chromophobe renal cell carcinoma [24], in combination with imaging mass spectrometry and laser capture microdissection of defined regions from FFPE tissue sections, could be a useful approach for spatially resolved biomarker discovery supporting clinical tumor subtype classification.

Nevertheless, for a final assessment of a possible implementation to the proposed applications, a detailed evaluation of the CapLC system used here with regard to its suitability for the targeted, quantitative analysis of metabolites is still pending.

References

[1] K.L. Sanders, J.L. Edwards, Nano-liquid chromatography-mass spectrometry and recent applications in omics investigations, Anal. Methods 12 (36) (2020) 4404–4417. https://doi.org/10.1039/d0ay01194k.

[2] M. Asensio-Ramos, C. Fanali, G. D'Orazio, S. Fanali, Nano-liquid chromatography, in: Liquid Chromatography, Elsevier, 2017, pp. 637–695.

[3] N.W. Smith, C. Legido-Quigley, N.D. Marlin, V. Melin, I. Mutton, Capillary and Micro High Performance Liquid Chromatography, in: Reference Module in Chemistry, Molecular Sciences and Chemical Engineering, Elsevier, 2013.

[4] J. Abian, M. Carrascal, Quantitative Peptide Determination Using Column-Switching Capillary Chromatography Interfaced with Mass Spectrometry, in: Emerging technologies in protein and genomic material analysis, Elsevier, 2003, pp. 39–73.

[5] M. Cebo, X. Fu, M. Gawaz, M. Chatterjee, M. Lämmerhofer, Micro-UHPLC-MS/MS method for analysis of oxylipins in plasma and platelets, J. Pharm. Biomed. Anal. 189 (2020) 113426. https://doi.org/10.1016/j.jpba.2020.113426.

[6] X. Luo, L. Li, Metabolomics of Small Numbers of Cells: Metabolomic Profiling of 100, 1000, and 10000 Human Breast Cancer Cells, Anal. Chem. 89 (21) (2017) 11664–11671. https://doi.org/10.1021/acs.analchem.7b03100.

[7] S.K. Neef, N. Janssen, S. Winter, S.K. Wallisch, U. Hofmann, M.H. Dahlke, M. Schwab, T.E. Mürdter, M. Haag, Metabolic Drug Response Phenotyping in Colorectal Cancer Organoids by LC-QTOF-MS, Metabolites 10 (12) (2020) 494. https://doi.org/10.3390/metabo10120494.

[8] O. Knittelfelder, S. Traikov, O. Vvedenskaya, A. Schuhmann, S. Segeletz, A. Shevchenko, A. Shevchenko, Shotgun Lipidomics Combined with Laser Capture Microdissection: A Tool To Analyze Histological Zones in Cryosections of Tissues, Anal. Chem. 90 (16) (2018) 9868–9878. https://doi.org/10.1021/acs.analchem.8b02004.

[9] S. Cacciatore, G. Zadra, C. Bango, K.L. Penney, S. Tyekucheva, O. Yanes, M. Loda, Metabolic Profiling in Formalin-Fixed and Paraffin-Embedded Prostate Cancer Tissues, Mol. Cancer Res. 15 (4) (2017) 439–447. https://doi.org/10.1158/1541-7786.MCR-16-0262.

[10] P. Leuthold, E. Schaeffeler, S. Winter, F. Buttner, U. Hofmann, T.E. Murdter, S. Rausch, D. Sonntag, J. Wahrheit, F. Fend, J. Hennenlotter, J. Bedke, M. Schwab, M. Haag, Comprehensive Metabolomic and Lipidomic Profiling of Human Kidney Tissue: A Platform Comparison, J. Proteome Res. 16 (2) (2017) 933–944. https://doi.org/10.1021/acs.jproteome.6b00875.

[11] S.K. Neef, S. Winter, U. Hofmann, T.E. Mürdter, E. Schaeffeler, H. Horn, A. Buck, A. Walch, J. Hennenlotter, G. Ott, F. Fend, J. Bedke, M. Schwab, M. Haag, Optimized protocol for metabolomic and lipidomic profiling in formalin-fixed paraffin-embedded kidney tissue by LC-MS, Analytica Chimica Acta 1134 (2020) 125–135. https://doi.org/10.1016/j.aca.2020.08.005.

[12] M. Li, Y. Alnouti, R. Leverence, H. Bi, A.I. Gusev, Increase of the LC-MS/MS sensitivity and detection limits using on-line sample preparation with large volume plasma injection,

321 J. Chromatogr. B Analyt. Technol. Biomed. Life Sci. 825 (2) (2005) 152–160.
322 https://doi.org/10.1016/j.jchromb.2005.03.047.
323 [13] J.H.Y. Galani, M. Houbraken, M. van Hulle, P. Spanoghe, Comparison of electrospray and
324 UniSpray, a novel atmospheric pressure ionization interface, for LC-MS/MS analysis of
325 81 pesticide residues in food and water matrices, Anal. Bioanal. Chem. 411 (20) (2019)
326 5099–5113. https://doi.org/10.1007/s00216-019-01886-z.
327 [14] M. Haag, U. Hofmann, T.E. Mürdter, G. Heinkele, P. Leuthold, A. Blank, W.E. Haefeli,
328 A. Alexandrov, S. Urban, M. Schwab, Quantitative bile acid profiling by liquid
329 chromatography quadrupole time-of-flight mass spectrometry: Monitoring hepatitis B
330 therapy by a novel Na(+)-taurocholate cotransporting polypeptide inhibitor, Anal. Bioanal.
331 Chem. 407 (22) (2015) 6815–6825. https://doi.org/10.1007/s00216-015-8853-5.
332 [15] Gil de la Fuente, Alberto, J. Godzien, M. Fernández López, F.J. Rupérez, C. Barbas, A.
333 Otero, Knowledge-based metabolite annotation tool: CEU Mass Mediator, J. Pharm.
334 Biomed. Anal. 154 (2018) 138–149. https://doi.org/10.1016/j.jpba.2018.02.046.
335 [16] A. Gil-de-la-Fuente, J. Godzien, S. Saugar, R. Garcia-Carmona, H. Badran, D.S. Wishart,
336 C. Barbas, A. Otero, CEU Mass Mediator 3.0: A Metabolite Annotation Tool, J. Proteome
337 Res. 18 (2) (2019) 797–802. https://doi.org/10.1021/acs.jproteome.8b00720.
338 [17] L.W. Sumner, A. Amberg, D. Barrett, M.H. Beale, R. Beger, C.A. Daykin, T.W.-M. Fan,
339 O. Fiehn, R. Goodacre, J.L. Griffin, T. Hankemeier, N. Hardy, J. Harnly, R. Higashi, J.
340 Kopka, A.N. Lane, J.C. Lindon, P. Marriott, A.W. Nicholls, M.D. Reily, J.J. Thaden, M.R.
341 Viant, Proposed minimum reporting standards for chemical analysis Chemical Analysis
342 Working Group (CAWG) Metabolomics Standards Initiative (MSI), Metabolomics 3 (3)
343 (2007) 211–221. https://doi.org/10.1007/s11306-007-0082-2.
344 [18] J.-D. Berset, R. Brenneisen, C. Mathieu, Analysis of llicit and illicit drugs in waste, surface
345 and lake water samples using large volume direct injection high performance liquid
346 chromatography--electrospray tandem mass spectrometry (HPLC-MS/MS), Chemosphere
347 81 (7) (2010) 859–866. https://doi.org/10.1016/j.chemosphere.2010.08.011.
348 [19] L. Gao, W. Chiou, H. Tang, X. Cheng, H.S. Camp, D.J. Burns, Simultaneous quantification
349 of malonyl-CoA and several other short-chain acyl-CoAs in animal tissues by ion-pairing
350 reversed-phase HPLC/MS, J. Chromatogr. B Analyt. Technol. Biomed. Life Sci. 853 (1-
351 2) (2007) 303–313. https://doi.org/10.1016/j.jchromb.2007.03.029.

352 [20] A. Kumar, J.C. Heaton, D.V. McCalley, Practical investigation of the factors that affect
353 the selectivity in hydrophilic interaction chromatography, J. Chromatogr. A 1276 (2013)
354 33–46. https://doi.org/10.1016/j.chroma.2012.12.037.
355 [21] W.B. Dunn, D. Broadhurst, P. Begley, E. Zelena, S. Francis-McIntyre, N. Anderson, M.
356 Brown, J.D. Knowles, A. Halsall, J.N. Haselden, A.W. Nicholls, I.D. Wilson, D.B. Kell,
357 R. Goodacre, Procedures for large-scale metabolic profiling of serum and plasma using
358 gas chromatography and liquid chromatography coupled to mass spectrometry, Nat.
359 Protoc. 6 (7) (2011) 1060–1083. https://doi.org/10.1038/nprot.2011.335.
360 [22] P.M. van Midwoud, L. Rieux, R. Bischoff, E. Verpoorte, H.A.G. Niederländer,
361 Improvement of recovery and repeatability in liquid chromatography-mass spectrometry
362 analysis of peptides, J. Proteome Res. 6 (2) (2007) 781–791.
363 https://doi.org/10.1021/pr0604099.
364 [23] G.S.M. Kammeijer, I. Kohler, B.C. Jansen, P.J. Hensbergen, O.A. Mayboroda, D. Falck,
365 M. Wuhrer, Dopant Enriched Nitrogen Gas Combined with Sheathless Capillary
366 Electrophoresis-Electrospray Ionization-Mass Spectrometry for Improved Sensitivity and
367 Repeatability in Glycopeptide Analysis, Anal. Chem. 88 (11) (2016) 5849–5856.
368 https://doi.org/10.1021/acs.analchem.6b00479.
369 [24] E. Schaeffeler, F. Büttner, A. Reustle, V. Klumpp, S. Winter, S. Rausch, P. Fisel, J.
370 Hennenlotter, S. Kruck, A. Stenzl, J. Wahrheit, D. Sonntag, M. Scharpf, F. Fend, A.
371 Agaimy, A. Hartmann, J. Bedke, M. Schwab, Metabolic and Lipidomic Reprogramming
372 in Renal Cell Carcinoma Subtypes Reflects Regions of Tumor Origin, Eur. Urol. Focus
373 (2018). https://doi.org/10.1016/j.euf.2018.01.016.
374

Supplementary Materials

Performance comparison of narrow-bore and capillary liquid-chromatography for non-targeted metabolomics profiling of small sample amounts by LC-QTOF-MS

Sylvia K. Neef [1], Stefan Winter [1], Ute Hofmann 1, Thomas E. Mürdter [1], Matthias Schwab [1,2,3] and Mathias Haag [1,*]

Supplementary Table S 1. Putatively annotated/identified compounds in the HILIC ESI (-) mode

Metabolite	Narrow-bore LC				Cap LC			
	RT [min]	MSI[1]	Score	Search engine	RT [min]	MSI[1]	Score	Search engine
Adenine	2.9	2	97.65	AMRT[3]	8.2	2	99.71	AMRT[3]
Adenosine	3.3		86.71	P[2]	8.4	3	98.45	P[2]
D-Pantothenic acid	3.1	2	0.01	CEU[3]	5.4	3	97.30	P[2]
Guanosine	7.3	3	91.88	P[2]	11.8	3	95.64	P[2]
Hypoxanthine	3.4	3	86.26	P[2]	8.0	2	96.52	AMRT[3]
Inosine	5.4	2	94.18	AMRT[3]	10.1	2	95.01	AMRT[3]
Lactate	4.0	3	87.81	P[2]	8.0	3	87.87	P[2]
L-Carnitine	8.9	3	81.50	P[2]	13.5	3	79.10	P[2]
L-Isoleucine	7.7	3	84.66	P[2]	12.2	3	87.77	P[2]
L-Leucine	7.4	3	95.44	P[2]	11.9	3	99.98	P[2]
L-Phenylalanine	7.4	3	93.38	P[2]	11.8	3	99.78	P[2]
LysoPE 16:0	6.0	3	99.47	P[2]	9.5	3	99.24	P[2]
LysoPE 18:0	5.6	3	99.29	P[2]	9.3	3	99.39	P[2]
LysoPE 20:4	5.8	2	99.48	MoNA[3]	9.4	3	97.59	P[2]
Succinate	3.4	3	910	P[2]	4.9	2	99.20	AMRT[3]
Uridine	3.3	3	90.81	P[2]	7.9	3	96.53	P[2]

[1] Assignment level according to: Sumner et al. Proposed minimum reporting standards for chemical analysis Chemical Analysis Working Group (CAWG) Metabolomics Standards Initiative (MSI). Metabolomics 2007, 3, 211–221

[2] Targeted score (formula matching score reported by Profinder)

[3] MS/MS assignment score

AMRT, METLIN Metabolite PCDL (Agilent); P, Profinder (Agilent); CEU, the CEU Mass Mediator MS/MS Search; MoNA, MassBank of North America MS/MS Similarity Search.